“From Straw to Oil
A Biological Upcycling Process”

Zur Erlangung des akademischen Grades eines

DOKTORS DER NATURWISSENSCHAFTEN

von der KIT-Fakultät für Chemieingenieurwesen und Verfahrenstechnik des
Karlsruher Instituts für Technologie (KIT)
genehmigte

DISSERTATION

von

(M.Sc.) Kevin Edward Schulz
aus Karlsruhe

Tag der mündlichen Prüfung: 14.10.2026

Erstgutachter: Prof. Dr. Christoph Syldatk

Zweitgutachter: Prof. Dr. Nicolaus Dahmen

KIT-Associate Fellow: Dr. Anke Neumann

Some people travel the world, while others carry the whole world within their minds. This journey is my own, a voyage into new lands and unknown territory, laying a foundation for the future

Preamble

This dissertation implements an upcycling process of hemi- and lignocellulosic materials. In addition to investigating the biotechnological applications of anaerobic fungi from the phylum *Neocallimastigomycota* as key species in the breakdown of hemicellulosic materials, oleaginous yeasts are being utilized and extensively examined for their potential in lipid production. Certain portions of this text have undergone evaluation through the peer review process and have either been published as research articles or are presently under consideration by publishers. These sections will be clearly identified, and their content mirror that of the corresponding published work.

Chapter 1 describes the metabolic and physiological analysis of several anaerobic gut fungi used in this dissertation under different cultivation conditions, including variations in temperature, carbon sources, substrate particle sizes, and cultivation strategies. The study provides insights into strain-specific metabolic responses, evaluates the robustness of anaerobic fungal cultivation for biotechnological applications and is fundamental for biotechnological application of anaerobic gut fungi.

The results have been published as:
“Anaerobic gut fungi as biocatalysts: metabolic and physiological analysis of anaerobic gut fungi under diverse cultivation conditions” by Kevin Edward Schulz, Dominik Scholz, Anto Rafael Sikirić, Daniela Rambow, Anke Neumann and Katrin Ochsenreither in Frontiers in Microbiology 2025, 16, 1662047, https://doi.org/10.3389/fmicb.2025.1662047”.

Chapter 2 builds upon the metabolic analysis of anaerobic gut fungi presented in Chapter 1. The evaluation of fermentation datasets revealed a systematic decline in electron recovery with increasing substrate concentrations, indicating that a fraction of reducing equivalents could not be accounted for by the quantified fermentation products. Since medium-derived redox-active compounds were insufficient to explain this discrepancy, the possibility arose that anaerobic gut fungi might channel electrons toward previously unrecognized sinks.
To investigate whether part of the missing electrons could be transferred to extracellular acceptors, an electrobiotechnological approach was employed. Using an eCuvette-based platform that enables electrochemical measurements under strict anaerobic conditions, the extracellular electron transfer (EET) capabilities of *Neocallimastix cameroonii* were systematically assessed in the presence of different redox mediators. This work represents the first experimental investigation of electrochemical activity in anaerobic gut fungi and aims to determine whether these early-branching eukaryotes are capable of interacting with external electron acceptors.

The results of this study are submitted to FEMS Microbiology letters for publication as:
“Ferricyanide-dependent current production by *Neocallimastix cameroonii* G341 in a miniaturized anaerobic bioelectrochemical system” by Kevin Edward Schulz, Daniel Baron Diaz and Dirk Holtmann.

Chapter 3 builds on the findings of the preceding chapters by moving from carbon-source-dependent metabolic profiling and electron-balance considerations toward the establishment of a cultivation framework that is suitable for reproducible biotechnological work with anaerobic gut fungi. While carbon availability strongly shapes product spectra, conventional serum-bottle cultivation intrinsically couples the carbon source with key physicochemical parameters, most notably buffering chemistry and headspace composition, through the CO_2/HCO_3^-/carbonate equilibrium. This coupling complicates mechanistic interpretation and limits transferability of results across setups.
To decouple these effects, Chapter 3 systematically evaluates the influence of the buffering system and the gas phase while independently controlling external pH and inorganic carbon availability. In parallel, a transferable biomass quantification strategy is established to enable robust growth assessment despite the filamentous morphology of anaerobic gut fungi. Together, these methodological advances provide the basis for interpreting metabolic shifts in a mechanistically meaningful way and for designing scalable cultivation strategies.

The results of this study are submitted to Fungal Biology and Biotechnology as:
“Beyond Carbon Dioxide: Decoupling Headspace and Buffering Reveals a Bicarbonate Requirement for Anaerobic Gut Fungi Growth” by Kevin Edward Schulz, Alisa Pfau, Tuba Tarhan, Charlotte van Almsick, Dominik Scholz, Anto Rafael Sikirić, Anke Neumann and Katrin Ochsenreither.

To integrate the anaerobic gut fungal conversion of hemi- and lignocellulosic substrates with downstream single-cell oil (SCO) production in oleaginous yeasts, understanding the fungal platform alone is not sufficient. A future coupling concept, particularly one aimed at valorizing nitrogen-rich residual streams, also requires reactor-scale process knowledge of oleaginous yeasts as the second biological platform. This is especially relevant because conventional lipid induction by nitrogen limitation relies on nitrogen depletion and high C/N ratios, making it poorly aligned with nitrogen-rich feedstocks. **Chapter 4** therefore uses controlled stirred-tank cultivations to evaluate phosphate limitation as an alternative lipid-induction strategy for feedstock-flexible SCO production.
Chapter 4 compares nitrogen limitation and phosphate limitation at bioreactor scale to establish a process-relevant foundation for future coupling concepts and for the utilization of industrial side streams. Four oleaginous yeasts, *Cutaneotrichosporon oleaginosum* ATCC 20509, *Saitozyma podzolica* DSM 27192, *Scheffersomyces segobiensis* DSM 27193, and *Apiotrichum porosum* DSM 27194, were cultivated in 2.5-L stirred-tank reactors under nitrogen-limited, phosphate-limited, and nutrient-replete conditions using standardized media and identical process parameters. Biomass formation, lipid titres, specific lipid production rates, biomass composition, and fatty acid profiles were systematically compared to derive rate-based and scalable performance metrics beyond final titres alone.

The results have been published as:
“Phosphate Versus Nitrogen Limitation: A Reactor-Scale Process Comparison for Single-Cell Oil Production in Oleaginous Yeasts” by Kevin Edward Schulz, Paula Hegmann, Bastian Dreher, Lena Regenauer, Carlota Delso Muniesa, Wolfgang Frey, Katrin Ochsenreither and Anke Neumann in MDPI Fermentation 2026, Volume 12, Issue 4, https://doi.org/10.3390/fermentation12040172”.

Chapter 5 addresses the utilization of industrial residual streams as carbon sources for single-cell oil production. While the reactor-scale benchmark in Chapter 4 established nutrient-limitation strategies as a key lever for lipid induction, a future biotechnological coupling concept also requires feedstock-flexible processes that can operate on low-value, heterogeneous side streams. Among the tested residues, crude glycerol, an abundant byproduct of biodiesel production, emerged as the only substrate with clear potential to support growth and lipid accumulation under nitrogen-limited conditions. However, crude glycerol typically contains variable impurity loads (e.g., methanol, soaps, salts, and catalyst residues) that can cause severe growth inhibition and render direct batch cultivation unreliable.
Chapter 5 therefore investigates the bioprocessing of untreated industrial crude glycerol using *Cutaneotrichosporon oleaginosum* ATCC 20509. To overcome early-phase inhibition without detoxification or sterilization, adapted stepwise feeding strategies were established that reduce the inhibitor-to-biomass ratio during the initial growth phase. The approach was developed in 2.5-L stirred-tank fermentations and subsequently validated in transition scale (19 L) using repeated-batch operation to assess process robustness over extended runtimes and across different crude glycerol batches.

The results have been published as:
“Adapted Feeding Strategies Enable Efficient Growth and Lipid Accumulation Using Untreated Crude Glycerol in Transition Scale with *Cutaneotrichosporon oleaginosum* ATCC 20509” by Kevin Edward Schulz, Paula Hegmann, Bastian Dreher, Marina Schreidl, Katrin Ochsenreither and Anke Neumann in MDPI Fermenation 2026, Volume 12, Issue 3, https://doi.org/10.3390/fermentation12030154.

Chapter 6 focuses on adapting the oleaginous yeast *Cutaneotrichosporon oleaginosum* ATCC 20509 to the metabolite spectrum generated by anaerobic gut fungi, thereby establishing a key prerequisite for a future two-stage coupling process. While anaerobic fungi can convert untreated lignocellulosic biomass into reduced fermentation intermediates such as ethanol, acetate, lactate, succinate, and formate, efficient downstream lipid production requires that the yeast can tolerate and utilize these complex, inhibitor-rich mixtures. In preliminary experiments, the wild-type strain exhibited strongly impaired growth on representative metabolite blends, with formate causing complete growth arrest under the tested conditions, highlighting the need for strain-level adaptation.
To address this limitation without genetic engineering, Chapter 6 applies adaptive laboratory evolution (ALE) using a microfluidic evo.S platform that enables accelerated selection under defined concentration gradients. Two gradient regimes, smooth and steep, were implemented to evolve the yeast under increasing concentrations of key anaerobic fungal metabolites supplemented with crude glycerol as a low-cost co-carbon source. The resulting isolates showed improved growth relative to the wild type, with the smooth-gradient lineage yielding the strongest and most stable improvements in planktonic cultivation. Follow-up cultivation and metabolite analyses confirmed significantly enhanced uptake of ethanol, lactate, and formate in the best-performing isolate, demonstrating that microfluidic ALE can rapidly generate non-GMO yeast strains with improved robustness and substrate utilization on anaerobic fungal fermentation intermediates.

The results of this study are submitted to Applied Microbiology and Biotechnology as:
“Microfluidic adaptive laboratory evolution of the oleaginous yeast *Cutaneotrichosporon oleaginosum*” by Kevin Edward Schulz, Camilla Stolle, Anne Rosa Maria Schwendemann, Dirk Holtmann and Kersten Stefan Rabe.

Chapter 7 evaluates the practical feasibility of integrating anaerobic gut fungi with oleaginous yeasts by systematically testing the interface between both biological platforms. As a first step, six anaerobic gut fungal strains were cultivated not only as monocultures but also in defined mixed-strain consortia, covering 63 mono- and multi-strain configurations, to determine how strain composition affects fermentation performance and the formation of yeast-relevant metabolites. Based on this screening, the two-strain consortium AG, consisting of *Aestipascuomyces dupliciliberans* A252 and *Neocallimastix cameroonii* G341, was selected as a biologically tractable upstream culture with comparatively high product formation and a balanced metabolite profile. The resulting fungal broth was then transferred to downstream cultivation with *Cutaneotrichosporon oleaginosum*, including both the non-adapted wild type and the microfluidic-ALE-adapted Smooth 3 lineage described in Chapter 6, to assess whether yeast performance can be improved on authentic and chemically complex AGF fermentation broths.

The results are monographically integrated in the flow of the dissertation.

Acknowledgements

At this point, I would like to express my sincere gratitude to all those who contributed to the successful completion of my doctoral studies through administrative, scientific, social, and emotional support.

First and foremost, I would like to thank Prof. Dr. rer. nat. Christoph Syldatk, Dr. rer. nat. Anke Neumann and Prof. Dr.-Ing. Katrin Ochsenreither for welcoming me into the field of Technical Biology. What originally began as a project on hydrogen production with anaerobic gut fungi evolved, through the integration of oil-producing yeasts, into a completely new research direction. Despite numerous challenges, this project never became dull and ultimately proved to be both intellectually stimulating and deeply fulfilling. I am particularly grateful for the constant scientific engagement, the willingness to discuss ideas, and the unwavering support that all three of you provided throughout my doctoral journey.
In our discussions, Prof. Dr. rer. nat. Christoph Syldatk was always someone who could enthusiastically share his passion for biotechnology, but also for personal topics such as Kashubia, thereby inspiring my own curiosity and interest in these areas.
Dr. rer. nat. Anke Neumann and Prof. Dr.-Ing. Katrin Ochsenreither, who served as my co-supervisors, always made time whenever I needed guidance. They consistently helped me refocus on what truly mattered and provided valuable scientific advice.

I would also like to thank Prof. Dr.-Ing. Dirk Holtmann, who transformed Technical Biology into Electrobiotechnology. Prof. Dr.-Ing. Holtmann, also known simply as Dirk, was always open to constructive discussions and created a friendly and supportive atmosphere. In addition to helping refine scientific texts and formulations, he constantly encouraged us to push beyond our limits and grow both scientifically and personally. His remarkable attention to detail repeatedly helped me improve my writing, refine evaluation criteria, and significantly enhance the quality of my work. If one were to describe him, it would not only be as an outstanding scientist but also as a kind of “father of the research group,” someone who was always willing to offer advice even on personal matters and who genuinely aimed for the best outcome for everyone involved. Among many things, he also supported my highly professional wine production and enabled the purchase of an oven system that was originally acquired at my request and kindly secured by Lukas Hartmann.

I would also like to express my special thanks to those who accompanied me closely during my doctoral journey: Dr.-Ing. André Delavault, Dr. Jens Rudat, and Dr. Habibu Aliyu. Their passion for science, their willingness to share knowledge, and their constant support greatly contributed to my scientific development. Even after they had left the institute, they remained approachable and supportive.
Dr.-Ing. André Delavault was my first long-term office neighbor, and I had the privilege of experiencing him as a helpful, friendly, communicative, and open colleague who never made me feel alone during my time in Technical Biology. Dr. Habibu Aliyu, on the other hand, was my partner in “illegal activities”, a knight of late-night work sessions, cryptologist, and chief geneticist. His enthusiasm, critical thinking, and deeply scientific perspective often inspired me and transformed long working days into something genuinely enjoyable.
Dr. Jens Rudat was my mentor during the microbiology practical course, a role model in microscopy, and the undisputed champion of Gorgonzola cake. He was always ready for humor, even though sweets were sometimes avoided because he still had to drive home.

I would also like to thank my fellow PhD candidates in Technical Biology, Christin Kubisch, Aline Kövilein, Flávio Baleeiro, Fei Peng, Alberto Robazza, Magda Ardila, and Nebyat Abdu Seid, for welcoming me warmly into the group. Whether during collaborative research, lunches at the Oxford Café, movie nights, or discussions about scientific questions, each of you contributed valuable ideas and support. Christin and Aline served as my first advisors and tutors, while Alberto introduced me to numerous conceptual approaches, including the philosophy of e-mol. Magda, who also became a good friend of mine, always ensured that the group remained organized and well supplied, while Nebyat taught me the art of permanently reserving calendar slots and mastering HPLC analytics. From melted bags during my first autoclave training to the initial testing of my fermenters, you were always willing to help.

I would also like to thank Lukas Hartmann, who joined our group shortly before the era of Electrobiotechnology began. In addition to many scientific discussions on fermentation processes, Lukas was my regular companion in the university cafeteria, my first point of contact during difficult moments, and someone who never hesitated to help, even on weekends. As doctoral students belonging to the “second salary class”, we shared a unique dynamic. Even holiday shifts could turn into foam parties thanks to our sense of humor. As ironic rivals in Room 118, Lukas’s students unfortunately often lost, but Lukas, being highly empathetic, was always able to comfort them.

My sincere thanks also go to my fellow PhD candidates and postdoctoral fellows in Electrobiotechnology, Jakub Gizewski, Lea Maerz, Björn Sabel-Becker, Sera Bolat, Niklas Teetz, Lisa van Sande, Anna-Lena Drommershausen, Daniel Baron Diaz, Emely Sarah Fuderer, Selina Lang, Emily Schepp, Sonja Schönrock, Michael Abt, Lukas Platz and Arabi Sivanesapillai. Through barbecues with collapsing tables, summer and Christmas celebrations, game nights, and private gatherings, you contributed greatly to the vibrant social life of the institute. Lea and later Selina jointly organized the institute seminar with me, while Jakub assisted with numerous construction projects and supplied me with enough Cola Zero to prevent me from falling asleep multiple times a day. Daniel, Lisa, Emily, and later Emely were next to Lukas Hartmann my office neighbors, and filled our room not only with plants but also with discussions about simulations, residual streams, design of experiments (DoE), and electro biotechnology. I would particularly like to thank Lisa for her pioneering role as a running expert and for inspiring my own athletic development.

I am also deeply grateful to the technical staff, Pascal Gorenflo, Marvin Siedler, Daniela Rambow, Sandra Baumann, Birte Fahn, Michaela Kugel, Delphine Muller, and Laura Krämer. Without their help in commissioning and repairing equipment, ordering chemicals, training me on reactor systems, organizing laboratory duties, maintaining microbial strain collections, and replacing gas cylinders, this work would not have been possible. I would particularly like to emphasize the outstanding contribution of Daniela Rambow, whose maintenance of microbial strains undoubtedly prevented my project from reaching an early and unfortunate end, and Sandra Baumann, who provided essential support during the final phase of the project.

My thanks also go to Simon Marangoz, Thomas Uhl, and Philipp Kienzle for their invaluable assistance with information technology. Without their support, my computer would probably still be somewhere in procurement, poorly configured, lacking RAM, or missing essential software.

I am equally grateful to Susanne Warth and Beate Saito (previously known as Skolik). From the very beginning of my enrollment at the faculty, they were my primary contacts for overcoming bureaucratic challenges. Without them, I would certainly have lost a considerable number of nerves and health. Beate also proved to be an exceptional detective and lock-picking expert, capable of solving even the most complicated cases. I would also like to thank Susanne for her excellent cake recipes.

My greatest thanks go to my students Anto Rafael Sikirić, Tuba Tarhan, Alisa Pfau, Dominik Scholz, Bastian Dreher, Paula Hegmann, Lena Regenauer, Charlotte van Almsick, Anne Rosa Maria Schwendemann, and David Fischbach. Without the ten of you, this work would not have been possible. Your enthusiasm, curiosity, diligence, and individual personalities made working together a constant source of joy (and provided a good excuse to buy a whole truck load of sweets). Whether building reactor systems, developing unexpected gambling addictions, enjoying food at Christmas markets, falling off climbing walls, or experiencing the ups and downs of roller coasters, there was never a dull moment. Team 120 repeatedly proved itself superior to its rivals in Room 118. You were not only my students but also my partners in the laboratory and in scientific publications. It was truly an honor to work with such an exceptional group of people.

I would like to additionally express my particular gratitude to Paula Hegmann, Bastian Dreher, Marina Schreidl and David Fischbach whom were/ also were my student assistants. Through their dedicated work, they supported not only me but also the entire Technical Biology and Electrobiotechnology group. Their contributions were essential for maintaining smooth fermentation processes and reliable experimental workflows, thereby allowing me to focus on other scientific and organizational responsibilities. Paula provided invaluable emotional support throughout the project, whether after an exploding vortex mixer accompanied by flash flames, after failed experiments, or during periods of intense time pressure. Bastian demonstrated an impressive engineering-oriented mindset that strongly influenced my own way of approaching technical challenges and experimental setups. Marina and David also made valuable contributions through their reliability, dedication, and practical support in the laboratory, particularly by assisting with the operation and monitoring of the 19-L fermentation experiments. I would also like to thank Annina Müller, who temporarily assisted with conductivity measurements and ultimately played a role in the acquisition of a new balance that I had long advocated for.

Beyond the people at my institute, I would also like to thank the entire Biochemical Engineering and Biotechnology (BLT) community for stimulating scientific discussions during the large group seminar (For Dirk: institute seminar). In particular, I would like to thank the team from µBVT for enabling the use of the 19-liter reactor system and for maintaining their sense of humor even during exam reviews. I would especially like to acknowledge Prof. Dr.-Ing. Grünberger, who even used my research topic as an example of a bioprocess cascade in his lecture, Christian Steinweg for supervising my scale-up experiments, and Laura Krämer for ensuring access to clean water when our own systems failed.

I am also grateful to my collaborators in the ELEGANT project, especially the colleagues from the Institute for Pulsed Power and Microwave Technology (IHM) at KIT Campus North, Dr. Wolfgang Frey, Dr. Aude Silve, Rüdiger Wüstner, Natalja Nazarova, Steven Kopp, and Dr. Carlota Muniesa Delso, for their cooperative and motivating collaboration.
Furthermore, I would like to thank the Bundesministerium für Landwirtschaft, Ernährung und Heimat (BMLEH) for their financial support as well as Südzucker AG and Hydroxy Energy GmbH for their material support, which made the analysis of residual streams and this project possible.

I would also like to thank my collaborators from the Institute of Biological and Chemical Systems – Biological Information Processing (IBG) at KIT Campus North. What initially began as a small excursion into adaptive evolution, initiated by Kersten Rabe, ultimately enabled the first microfluidic on-chip adaptation of fungi. I would particularly like to highlight the important role of Camilla Stolle, whose communicative nature and technical expertise greatly facilitated these experiments and contributed significantly to their success.

Finally, I would like to thank my friends and companions, whose support, encouragement, and presence enriched my life far beyond the laboratory. Throughout the many years of studying and conducting my doctoral research, you reminded me that life extends beyond experiments, deadlines, and publications. The laughter, conversations, shared experiences, and occasional nonsense we shared provided the balance and perspective that helped me navigate the challenges of academic life. My deepest gratitude goes to Desiree Steuernagel, better known as Daisy, my best friend, who has accompanied me through many stages of my life. Her loyalty, humor, and unwavering presence ensured that there was never a shortage of laughter, even during the most demanding phases of this journey. I am equally grateful to Manuel Müller, a companion in countless ridiculous bets and memorable moments, whose openness and sociability have always been inspiring and whose outlook on life often reminded me to take things a little less seriously. My sincere thanks also go to Vanessa “Brain” Lindörfer, whose remarkable trust and friendship have meant a great deal to me over the years, and to Maria Consiglio, whose creativity and open-hearted nature consistently brought warmth and positivity. A particularly heartfelt thank-you goes to Linda Kozdon, who has been part of my life for more than half of it. Her unwavering support throughout my studies, and every shared round of Stardew Valley, made even the more difficult days easier. I would also like to thank Silke Notter for her thoughtful advice during important professional decisions. I am also grateful to Noah Nepstad, with whom I regularly train and who helped me maintain balance outside of academic life, as well as to my cousin Marcel Schmaling for the many relaxing gaming sessions that provided a welcome escape from everyday research stress. My thanks also go to Celine Maier for her steady support and her ability to bring me back down to earth whenever needed. Further thanks go to Max Oebel, with whom I can simply switch off and relax (and eat a ton of food), and to Ferdinand Betting, whose perspective as a dedicated ecologist and person of faith often added thoughtful and refreshing insights to many conversations. I am also grateful to Sascha Wünsch aka Knutschii who shared my enthusiasm for streaming and patiently endured countless ARAM matches, and to Lara Goldkuhle, with whom I discovered Min Ramen as something of a second home and who never hesitates to join me for the most wonderfully bizarre films. Finally, I would like to acknowledge the two feline companions Ori and Maunz, whose “quiet” presence and insistence on timely breaks provided small but meaningful moments of comfort during this journey. There are many more friends and companions who have shaped my life in ways both large and small. Even if not, everyone can be mentioned individually here, please know that your friendship and encouragement have been an important part of this journey.

Above all, I would like to express my deepest gratitude to my family. Your unconditional support, patience, and encouragement have accompanied me throughout every stage of my life and made this journey possible in the first place. You have always believed in me, even during times when the path ahead seemed uncertain, and your trust has given me the strength and confidence to continue moving forward. Your support extended far beyond words of encouragement. Through your understanding, advice, and constant presence, you provided the foundation that allowed me to pursue my academic goals with determination and curiosity. Knowing that I could always rely on you gave me the stability and reassurance necessary to face the many challenges that come with a doctoral journey. For everything you have done for me, and for always standing by my side, I am deeply grateful.

As this acknowledgement illustrates, this dissertation was shaped, influenced, and improved by many people. Each of you contributed in your own way, not only to this work but also to my development as a scientist and as a person. I would therefore like to thank everyone who may not have been mentioned by name but who nevertheless played an important role in my journey.

I would also like to remember those who are no longer with us and cannot celebrate this milestone with me. You will always remain a part of me.

Thank you all very much, and Vergelt’s Gott!

Abstract

Utilization of hemi- and lignocellulosic side streams will be essential for the transition from a fossil-based to a circular bioeconomy. However, the direct biotechnological use of such materials remains limited by structural recalcitrance, the need for energy-intensive pretreatment, and the low economic robustness of many downstream conversion routes.

This dissertation addresses these limitations by investigating a two-stage upcycling concept in which anaerobic gut fungi (AGF) first convert untreated plant biomass into hydrogen and reduced fermentation intermediates, which are subsequently upgraded to microbial lipids by oleaginous yeasts. To establish the upstream platform, six AGF strains, *Aestipascuomyces dupliciliberans*, *Caecomyces churrovis*, *Khoyollomyces ramosus*, *Orpinomyces joyonii*, *Pecoramyces ruminantium*, and *Neocallimastix cameroonii*, were systematically characterized with respect to cultivation robustness, substrate utilization, and metabolic output. Across strains, overall activity was generally highest around 39 °C, whereas hydrogen production optima were strain-specific and reached up to 41 °C. Larger wheat straw particles partly enhanced hydrogen formation, while glucose and cellobiose were readily metabolized. By contrast, xylose induced stress-associated responses and poor hydrogen production in several strains. Increasing sugar concentrations triggered a reproducible shift toward overflow metabolism, reflected in elevated lactate and formate formation, whereas fed-batch cultivation did not improve total metabolite formation, indicating that process performance was constrained by physiological rather than simple substrate-supply limitations. In addition, several low-value biowastes, particularly cucumber, carrot, and potato peel residues, supported efficient growth and degradation, and a previously undescribed stress-associated growth form of *O. joyonii* was observed under prolonged cultivation on soluble substrates. To clarify fundamental cultivation requirements, the classical CO_2/HCO_3^- buffer system was deconvoluted by independently varying gas atmosphere, buffering chemistry, bicarbonate supply, pH, and nitrogen availability. Replacement of CO_2 with N_2 increased hydrogen production, whereas bicarbonate-free media failed to sustain growth despite stable external pH, demonstrating that bicarbonate is required beyond its function as an extracellular buffer. Reintroduction of $NaHCO_3$ restored growth at low, strain-specific threshold concentrations, alternative carboxylic acids did not substitute for bicarbonate, and maximal activity under defined conditions was observed at pH 6.4. An OD_{750}-based biomass quantification method further enabled transferable growth assessment in filamentous cultures. Bioelectrochemical screening revealed that historical electron-recovery deficits in AGF fermentations cannot be explained by medium-derived redox-active compounds alone; ferricyanide supported reproducible fungus-dependent current generation, providing the first experimental evidence for mediated extracellular electron transfer in an anaerobic gut fungus. Together, these results define the cultivation and metabolic framework required to use AGF as robust primary biocatalysts for lignocellulosic conversion.

To establish the downstream upgrading platform, four oleaginous yeasts, *Cutaneotrichosporon oleaginosum*, *Saitozyma podzolica*, *Scheffersomyces segobiensis*, and *Apiotrichum porosum,* were benchmarked in 2.5 L stirred-tank reactors under nitrogen-limited, phosphate-limited, and nutrient-replete conditions. Nitrogen limitation produced the highest lipid titres, reaching up to 9.2 g L^{-1}, whereas phosphate limitation reduced biomass formation but yielded the highest specific lipid production rate, up to 0.0037 g $gCDW^{-1}$ h^{-1} in *S. podzolica*, thereby identifying phosphate limitation as a process-relevant alternative for nitrogen-rich substrates. To improve substrate realism and economic relevance, untreated industrial crude glycerol was evaluated as sole carbon source for *C. oleaginosum*. Direct batch cultivation caused complete growth arrest, confirming severe early-phase inhibition by impurities. However, a simple stepwise feeding strategy reduced the inhibitor-to-biomass ratio during early growth and restored biomass formation, respiration, and lipid accumulation. At 2.5 L scale, apparent growth rates up to 0.51 h^{-1} and volumetric productivities up to 0.22 g L^{-1} h^{-1} were achieved, with lipid contents around 30% of cell dry weight and oleate-dominated fatty acid profiles. The process remained stable after transition to 19 L repeated-batch cultivation for more than 640 h, maintaining lipid contents of approximately 30–36% and oleate fractions of about 51–53% despite marked substrate-batch variability.

Finally, because representative AGF metabolite mixtures strongly impaired the growth of wild-type *C. oleaginosum*, especially in the presence of formate, a microfluidic adaptive laboratory evolution strategy was implemented to improve downstream compatibility without genetic engineering. The best evolved isolates exhibited improved growth and significantly enhanced uptake of ethanol, lactate, and formate, demonstrating that physiological adaptation can substantially increase robustness toward complex, inhibitor-rich fungal metabolite mixtures. In a final step, the practical feasibility of directly linking both biological platforms was assessed in a consecutive cultivation concept. These preliminary coupling experiments showed that the integration of anaerobic fungal fermentation broths with oleaginous yeast cultivation is more challenging than initially anticipated. Although the fungal metabolites constitute a promising carbon platform in principle, direct downstream utilization was hindered by an unexpected inhibitory effect, indicating the presence of a toxic factor in the fungal broth. Based on the current observations, this inhibition is consistent with a compound that is likely formed intracellularly and subsequently released, thereby impairing downstream growth unless the broth is diluted. These findings highlight that successful coupling will not depend solely on matching carbon sources and product spectra, but also on controlling inhibitory broth components and establishing suitable conditioning or dilution strategies. Thus, the final outcome of this work is not only the demonstration of the biological potential of a “straw-to-oil” concept, but also the identification of a critical compatibility barrier that must be overcome for future implementation of an integrated process.

Zusammenfassung

Die Erschließung hemi- und lignocellulosehaltiger Reststoffe ist ein zentraler Schritt auf dem Weg zu einer zirkulären Bioökonomie. Ihre biotechnologische Nutzung wird bislang jedoch durch die hohe strukturelle Stabilität der Biomasse, den Aufwand konventioneller Vorbehandlungen und die begrenzte Wirtschaftlichkeit vieler nachgeschalteter Prozesse erschwert. Vor diesem Hintergrund verfolgt die vorliegende Arbeit ein zweistufiges Upcycling-Konzept: Im ersten Schritt werden pflanzliche Reststoffe mithilfe anaerober Darmpilze (AGF) in Wasserstoff und lösliche Fermentationsprodukte überführt; im zweiten Schritt dienen diese Produkte als Ausgangsbasis für die Lipidbildung in oleogenen Hefen.

Als Grundlage der ersten Prozessstufe wurden sechs AGF-Stämme – *Aestipascuomyces dupliciliberans*, *Caecomyces churrovis*, *Khoyollomyces ramosus*, *Orpinomyces joyonii*, *Pecoramyces ruminantium* und *Neocallimastix cameroonii* – systematisch hinsichtlich Kultivierbarkeit, Substratnutzung und Metabolitbildung untersucht. Die höchste metabolische Gesamtaktivität wurde bei den meisten Stämmen bei etwa 39 °C beobachtet, während die Temperaturoptima der Wasserstoffbildung stammspezifisch waren und bis 41 °C reichten. Gröbere Weizenstrohfraktionen förderten die Wasserstoffproduktion teilweise, und insbesondere Glukose sowie Cellobiose wurden effizient umgesetzt. Xylose führte dagegen bei mehreren Stämmen zu einem stressassoziierten Stoffwechsel mit geringer Wasserstoffbildung. Mit steigender Zuckerkonzentration verschob sich der Stoffwechsel reproduzierbar in Richtung Overflow-Metabolismus, was sich in erhöhten Lactat- und Formiatmengen zeigte. Eine Fed-Batch-Führung verbesserte die Gesamtleistung nicht, was darauf hindeutet, dass die Grenzen des Systems eher in der Physiologie der Pilze als in der bloßen Substratversorgung liegen. Darüber hinaus erwiesen sich verschiedene niedrigpreisige Reststoffe, insbesondere Gurken-, Karotten- und Kartoffelschalen, als gut verwertbare Substrate. Zusätzlich wurde bei *O. joyonii* während längerer Kultivierung auf löslichen Kohlenstoffquellen eine bislang nicht beschriebene, offenbar stressinduzierte Wachstumsform beobachtet.

Um die grundlegenden Anforderungen an die Kultivierung anaerober Darmpilze besser zu verstehen, wurde das klassische CO_2/HCO_3^--System der Serumflaschenkultivierung gezielt entkoppelt. Dabei wurden Gasatmosphäre, Puffersystem, Bicarbonatversorgung, pH-Wert und Stickstoffangebot unabhängig voneinander untersucht. Der Ersatz von CO_2 durch N_2 steigerte die Wasserstoffbildung, während Medien ohne Bicarbonat trotz stabilem externem pH-Wert kein dauerhaftes Wachstum ermöglichten. Bicarbonat übernimmt damit für AGF offenbar mehr als eine reine Pufferfunktion. Erst die erneute Zugabe von $NaHCO_3$ stellte das Wachstum wieder her, und zwar bereits bei niedrigen, jedoch stammabhängigen Schwellenkonzentrationen; alternative Carbonsäuren konnten diese Funktion nicht ersetzen. Unter definierten Bedingungen lag die höchste metabolische Aktivität bei pH 6,4. Ergänzend wurde eine OD_{750}-basierte Methode zur Biomassebestimmung etabliert, die auch für filamentöse Kulturen eine übertragbare Quantifizierung ermöglicht. Bioelektrochemische Untersuchungen zeigten zudem, dass die in früheren AGF-Fermentationen beobachteten Elektronenlücken nicht allein durch redoxaktive Medienkomponenten erklärbar sind. Ferricyanid erzeugte reproduzierbare, pilzabhängige Stromsignale und lieferte damit den ersten experimentellen Hinweis auf eine vermittelte extrazelluläre Elektronenübertragung bei einem anaeroben Darmpilz. Insgesamt definiert die Arbeit damit den physiologischen und prozesstechnischen Rahmen, in dem AGF als primäre Biokatalysatoren für die Lignocelluloseverwertung eingesetzt werden können.

Für die zweite Prozessstufe wurden vier oleogene Hefen, *Cutaneotrichosporon oleaginosum*, *Saitozyma podzolica*, *Scheffersomyces segobiensis* und *Apiotrichum porosum* im 2,5-L-Rührkesselbioreaktor unter Stickstofflimitierung, Phosphatlimitierung und nährstoffreichen Bedingungen verglichen. Die höchsten absoluten Lipidtiter wurden unter Stickstofflimitierung erreicht und lagen bei bis zu 9,2 g L^{-1}. Die Phosphatlimitierung führte zwar zu geringerer Biomassebildung, ermöglichte jedoch mit bis zu 0,0037 g $gCDW^{-1}$ h^{-1} bei *S. podzolica* die höchste spezifische Lipidbildungsrate und stellt damit eine interessante Alternative für stickstoffreiche Einsatzsubstrate dar. Um die wirtschaftliche Relevanz der Hefeplattform zu erhöhen, wurde außerdem unbehandeltes industrielles Rohglycerin als alleinige Kohlenstoffquelle für *C. oleaginosum* untersucht. Eine direkte Batch-Kultivierung führte zu vollständigem Wachstumsstillstand und bestätigte damit die starke Inhibition in der frühen Prozessphase. Durch eine schrittweise Fütterungsstrategie konnte die inhibitorische Belastung pro vorhandener Biomasse jedoch gezielt reduziert werden, sodass Wachstum, respirative Aktivität und Lipidakkumulation unter diesen Bedingungen möglich waren. Im 2,5-L-Maßstab wurden scheinbare Wachstumsraten von bis zu 0,51 h^{-1} und Volumenproduktivitäten von bis zu 0,22 g L^{-1} h^{-1} erreicht; die Lipidgehalte lagen bei rund 30 % der Zelltrockenmasse, und die Fettsäureprofile waren durch hohe Ölsäureanteile geprägt. Auch im 19-L-Repeated-Batch-Betrieb über mehr als 640 Stunden blieb das Verfahren trotz deutlicher Chargenschwankungen des Substrats stabil; Lipidgehalte von etwa 30–36 % bei der getrockneten Biomasse und Ölsäureanteile von rund 51–53 % des Ölgehaltes blieben erhalten.

Da repräsentative AGF-Metabolitmischungen das Wachstum des Wildtyps von *C. oleaginosum*, insbesondere aufgrund von Formiat, deutlich einschränkten, wurde zur Verbesserung der Systemkompatibilität eine mikrofluidische adaptive Laborevolution ohne gentechnische Eingriffe durchgeführt. Die erfolgreichsten adaptierten Isolate zeigten nicht nur ein verbessertes Wachstum, sondern auch eine signifikant gesteigerte Aufnahme von Ethanol, Lactat und Formiat. Damit konnte gezeigt werden, dass sich die Robustheit des nachgeschalteten Organismus gegenüber komplexen und inhibitorischen Pilzmetabolitmischungen gezielt erhöhen lässt. Abschließend wurde die direkte Verknüpfung beider biologischer Plattformen in einer konsekutiven Kultivierung untersucht. Dabei zeigte sich, dass die praktische Kopplung deutlich anspruchsvoller ist als zunächst erwartet: Zwar stellen die von anaeroben Pilzen gebildeten Metabolite grundsätzlich eine vielversprechende Kohlenstoffplattform dar, ihre unmittelbare Nutzung wurde jedoch durch einen unerwarteten inhibitorischen Effekt erschwert. Die bisherigen Befunde sprechen dafür, dass ein toxischer Faktor intrazellulär gebildet und anschließend freigesetzt wird, sodass derzeit eine Verdünnung der Fermentationsbrühe erforderlich ist, um nachgeschaltetes Wachstum zu ermöglichen. Insgesamt zeigt die Arbeit damit nicht nur das Potenzial eines „straw-to-oil“-Ansatzes, sondern identifiziert zugleich eine zentrale Kompatibilitätsgrenze, die für die zukünftige Umsetzung eines integrierten Prozesses gezielt adressiert werden muss.

Table of contents

Preamble **1**
Acknowledgements **5**
Abstract **10**
Zusammenfassung **12**
Table of contents **14**
1. Theoretical background **16**
1.1 Climate pressure, finite resources, and the logic of a circular bioeconomy **16**
1.2 Lignocellulosic biomass as an abundant but recalcitrant substrate class **17**
1.3 Biofuels, hydrogen, and the importance of intermediary energy carriers **18**
1.4 Anaerobic gut fungi: ecology, taxonomy, and biological significance **19**
1.5 Life cycle, morphology, and cellulosome-based biomass attack **20**
1.6 Hydrogenosomes, mixed-acid fermentation, and the formation of a metabolite platform **21**
1.7 Cultivation challenges: strict anaerobiosis, buffering, atmosphere, and preservation **22**
1.8 Oleaginous yeasts and the industrial promise of single-cell oils **23**
1.9 Process determinants of single-cell oil production and downstream recovery **24**
1.10 Low-cost feedstocks, inhibitor-rich substrates, and the importance of adaptation **25**
1.11 From metabolite platforms to integrated upgrading: the logic of consecutive bioprocessing **26**
2. Research proposal **27**
2.1 Toward an integrated “straw-to-oil” upcycling process based on anaerobic gut fungi and oleaginous yeasts **27**
3. Experimental Investigations, Results and Discussion **29**
3.1 Preparing the upstream platform: understanding anaerobic gut fungi as biocatalysts **30**
3.1.1 Metabolic and physiological analysis of anaerobic gut fungi under diverse cultivation conditions **30**
3.1.2 Extracellular electron transfer in anaerobic gut fungi in a miniaturized bioelectrochemical system **53**
3.1.3 Decoupling headspace composition, buffering, and bicarbonate availability in anaerobic gut fungi cultivation **67**
3.2 Establishing the downstream platform: microbial lipid production as upgrading strategy **96**
3.2.1 Reactor-scale comparison of nutrient limitation strategies for microbial lipid production **96**
3.2.2 Robust lipid production on untreated crude glycerol through adapted feeding strategies **116**
3.3 Engineering the interface: improving compatibility between fungal broths and yeast lipid production **141**

3.3.1 Microfluidic adaptive laboratory evolution of an oleaginous yeast on fungal metabolite mixtures **141**

3.3.2 Feasibility of linking anaerobic fungal fermentations with oleaginous yeast lipid production **158**

4. Final Conclusions and Future Perspectives **176**

5. List of references **180**

6. List of publications **196**

7. List of figures **198**

8. List of tables **204**

9. List of abbreviations **205**

10. Supplementary Information **206**

11. Verification of the contribution from the co-authors **242**

12. Curriculum Vitae ..... Fehler! Textmarke nicht definiert.

1. Theoretical background

1.1 Climate pressure, finite resources, and the logic of a circular bioeconomy

The transition from a fossil-based economy to a circular and biologically grounded carbon economy has become a scientific, technological, and societal imperative. Anthropogenic climate change, the finite nature of economically accessible fossil reserves, and the steadily increasing demand for energy, fuels, materials, and platform chemicals together create a structural pressure that cannot be addressed by incremental efficiency gains alone. Climate change is no longer understood merely as an environmental externality of industrial production; it is increasingly recognized as a systemic consequence of linear carbon use, in which fossil resources are extracted, transformed, consumed, and emitted without regenerative feedback loops. At the same time, global development trajectories indicate a sustained rise in demand for food, mobility, energy, and industrial products, meaning that resource pressure and climate pressure will continue to reinforce one another unless carbon flows are fundamentally reorganized. Circular-economy-thinking therefore goes beyond recycling in a narrow sense. It implies the design of regenerative production systems in which renewable feedstocks, side streams, residues, and waste-derived substrates are valorized repeatedly and strategically, rather than being treated as terminal outputs of a linear economy [1-6].

In biotechnological terms, this reorganization requires two complementary developments. First, it requires new substrate strategies, especially those based on renewable, low-cost, and non-food-competing carbon sources. Second, it requires integrated bioprocesses capable of converting such substrates into products with sufficient technological and economic value. These two developments are inseparable. A circular economy without appropriate bioconversion routes remains aspirational; a highly efficient microbial process based on refined sugars may be scientifically elegant but industrially misaligned with the realities of resource scarcity and cost. What is needed instead is a form of process design that starts from the carbon source itself and asks how complex, heterogeneous, and structurally recalcitrant biomass can be transformed into a cascade of increasingly valuable intermediates and products. In this broader context, agricultural residues such as straw become more than waste or low-value biomass. They become central feedstocks for a future carbon economy precisely because they are abundant, inexpensive, renewable, and currently underexploited. The significance of this shift is particularly evident when one considers that the ultimate challenge is not simply to replace one fossil process with one biogenic process. The larger goal is to establish carbon-conserving process chains in which a single feedstock can pass through several stages of valorization, each one preserving and redirecting carbon and reducing power toward new products. Such a strategy is especially attractive for low-value but widely available residues, because it allows the economic value of the feedstock to be built up stepwise rather than forced into a single conversion endpoint [4,5,7,8].

1.2 Lignocellulosic biomass as an abundant but recalcitrant substrate class

Among renewable feedstocks, lignocellulosic biomass is particularly attractive because of its scale, ubiquity, and limited direct competition with food production. Agricultural residues, forestry side streams, crop-processing by-products, and other forms of lignocellulosic biomass are generated continuously and globally. Yet their vast availability stands in sharp contrast to the difficulty of their biotechnological utilization. Plant cell walls are not simple carbohydrate stores; they are highly evolved structural composites in which cellulose, hemicellulose, and lignin form an integrated, protective matrix. This matrix is exceptionally effective at resisting chemical, enzymatic, and microbial attack, which is why lignocellulose functions so well in planta and why it is so difficult to exploit industrially. The challenge is not the absence of carbon, but its embedding in a form that is structurally shielded, chemically complex, and energetically demanding to deconstruct [7,9-11].

Cellulose provides the main load-bearing scaffold of the wall through β-1,4-linked glucose polymers assembled into microfibrils stabilized by hydrogen bonding and van der Waals interactions. Hemicellulose surrounds and connects these fibrils but is itself chemically heterogeneous, consisting of different sugar backbones and substitution patterns, including xylans, mannans, xyloglucans, glucomannans, and mixed-linkage glucans. This heterogeneity is highly relevant for biotechnology because it means that lignocellulose is not only a difficult substrate but also a chemically diverse one. The hemicellulosic fraction, in particular, contains a broad spectrum of pentoses and hexoses that could in principle support multiple fermentation pathways if liberated efficiently. Lignin then adds a second layer of recalcitrance by embedding the carbohydrate matrix in a phenolic network of p-coumaryl, coniferyl, and sinapyl alcohol-derived structures, thereby restricting access even further. The resulting composite is therefore a paradoxical feedstock: abundant, cheap, renewable, and chemically rich, but only accessible through substantial physical, chemical, or biological effort [7,11,12].

This recalcitrance explains why conventional lignocellulose processing often relies on pretreatment, hydrolysis, and fermentation as separate operations. Pretreatment strategies such as acid treatment, alkaline treatment, steam explosion, or physicochemical disruption are designed to increase enzyme accessibility, but they are typically energy intensive and can generate by-products that inhibit downstream biocatalysts. Hydrolytic enzyme cocktails can improve sugar release but often represent a substantial process cost, especially at industrial scale. These constraints have long limited the economic feasibility of lignocellulose-based bioprocessing. Consequently, one of the central questions in modern biomass biotechnology is not whether lignocellulose is available, but whether it can be accessed biologically in a way that is both efficient and scalable. This question is where anaerobic gut fungi become particularly important. Their ecological specialization suggests that the deconstruction of lignocellulose need not always be decomposed into separate industrial steps; in nature, it is already carried out by specialized organisms that combine attachment, penetration, hydrolysis, and fermentation in a single biological system [7,10,11,13,14].

An important conceptual consequence follows from this. If lignocellulose is approached only as a difficult source of fermentable sugars, then much of its process potential remains hidden. If, however, it is approached as the starting point of a metabolically coupled valorization chain, then the objective changes. The challenge is no longer simply to release glucose and xylose, but to generate a set of soluble intermediates that can be fed directly into downstream upgrading steps. In such a framework, the most interesting output of biomass deconstruction may not be a purified sugar stream but a biologically generated metabolite platform. This is one of the key ideas behind integrating lignocellulose conversion with subsequent microbial product formation [5,13,14].

1.3 Biofuels, hydrogen, and the importance of intermediary energy carriers

Discussions of lignocellulosic valorization are often framed in terms of biofuels, but the term “biofuel” itself encompasses fundamentally different strategies. First-generation systems rely on starches, sugars, or plant oils and are often criticized for competing with food production and land use. Second-generation systems instead seek to exploit residues, side streams, and lignocellulosic materials, thereby aligning more closely with circular-economy objectives. Within this second-generation framework, it is important to distinguish between direct fuel molecules and intermediary energy carriers. Hydrogen belongs to the latter class. It is already indispensable in established industrial sectors such as refining, ammonia synthesis, methanol production, and steel processing, and it is increasingly discussed as a strategic energy vector in future low-carbon infrastructures. Yet most hydrogen is still produced through fossil-based routes, especially steam reforming or gasification, while truly low-carbon pathways remain relatively underdeveloped [1,15-18].

Biological hydrogen production is therefore attractive not because it is already a mature industrial substitute, but because it offers a conceptually important low-temperature, low-pressure alternative to conventional hydrogen generation. A wide range of biological strategies has been explored, including biophotolysis, photofermentation, dark fermentation, microbial electrolysis, and combined or hybrid systems. Among these, dark fermentation is especially relevant in a residue-based context because it can process organic feedstocks without dependence on light. Even so, dark fermentation has well-known limitations when implemented with canonical bacterial systems: yields are constrained, by-products compete for reducing power, and many systems still require comparatively accessible substrates or substantial pretreatment. For this reason, hydrogen must be viewed here not only as a target product, but as part of a broader residue-conversion logic. A biologically meaningful question is therefore not simply how hydrogen can be produced, but which organisms can produce hydrogen while simultaneously opening access to otherwise inaccessible feedstocks and generating co-products that remain useful for downstream conversion [15,16,19,20].

This perspective is particularly relevant for anaerobic gut fungi because hydrogen formation in these organisms is not an isolated pathway but part of a larger mixed-acid fermentative metabolism. In that setting, hydrogen production is intertwined with acetate, formate, ethanol, lactate, and succinate formation, and it reflects the allocation of reducing equivalents under anaerobic conditions. Hydrogen thus occupies a dual position in residue-based fungal fermentation. It is simultaneously a potential energy product and a readout of intracellular redox management. This makes it especially informative from a process perspective. Any factor that changes fungal hydrogen production is also likely to alter the composition of the metabolite broth available for subsequent bioconversion. As a consequence, the discussion of biological hydrogen production cannot be separated cleanly from the discussion of lignocellulose valorization or metabolite-platform design. It is embedded in both [14,20,21].

Hydrogen is also useful because it reveals a more general design principle: efficient biorefineries may not always convert biomass directly into a final end-product. Instead, they may pass through intermediary energy carriers and soluble redox-active metabolites before arriving at the final target. Such intermediates increase process flexibility, because they allow different metabolic modules to be connected in sequence. A primary converter can be optimized for deconstruction and fermentative energy carrier release, while a downstream converter can be optimized for synthesis and accumulation of more complex products. In this sense, hydrogen belongs to the same conceptual category as acetate, ethanol, or formate: it is part of a metabolite economy through which lignocellulosic carbon becomes accessible to later process steps [5,8,14].

1.4 Anaerobic gut fungi: ecology, taxonomy, and biological significance

Anaerobic gut fungi (AGF), currently classified within the phylum *Neocallimastigomycota*, are obligately anaerobic eukaryotes adapted to the digestive tracts of herbivorous animals. Their ecological importance within the rumen and related gut environments lies primarily in their role as early colonizers of plant biomass. Rather than waiting for prior degradation by bacteria or chemical processes, they attack lignocellulosic particles directly, penetrate tissues, and expose otherwise inaccessible carbohydrates to the wider gut microbiome. This role has major implications both biologically and technologically. Biologically, it means that these fungi support host nutrition and influence microbial community structure through the initial disruption of recalcitrant fibers. Technologically, it means that they represent a natural solution to one of the hardest problems in residue biotechnology: the opening of intact plant cell wall structures under anaerobic conditions [13,14,22].

Taxonomically, the group has expanded considerably in recent years. Earlier studies identified only a limited number of genera and species, but improved culturing and sequence-based approaches have broadened the recognized diversity substantially. Review work on AGF taxonomy has emphasized that isolation and maintenance difficulties have complicated comparative biology and slowed taxonomic resolution, while large-scale sequence surveys of herbivorous mycobiomes indicate that the true diversity of AGF is even greater than current cultured collections suggest. This matters because metabolic and morphological diversity in the group is not merely taxonomic detail; it is likely to translate into different capacities for substrate utilization, fermentation, and process robustness. In practical terms, this means that industrial and biotechnological discussion of AGF should not assume a single generic physiology. The group is diverse, early-branching, and still incompletely captured by cultivated representatives [22-24].

The biological importance of AGF also extends beyond biomass breakdown itself. Their presence is associated with improved fiber digestion in herbivorous systems, and their interactions with bacteria, methanogens, and protozoa are part of broader ruminal syntrophy and resource partitioning. Hydrogen transfer, in particular, has long been recognized as a key interaction axis, because hydrogen-consuming partners can relieve product inhibition and support continued fungal activity. This ecological embedding is significant for biotechnology because it reminds us that AGF metabolism evolved not in isolation, but within a network of interspecies interactions and physicochemical feedbacks. When these fungi are brought into pure or semi-defined cultivation, some of the natural balancing mechanisms of the gut environment disappear. This partially explains why their laboratory cultivation remains challenging and why process development must consider not only medium composition, but also gas phase, redox state, and the fate of reduced end-products [13,20,22,25].

1.5 Life cycle, morphology, and cellulosome-based biomass attack

A major part of the distinctive biology of AGF lies in their life cycle and morphology. These fungi alternate between a motile zoospore stage and a vegetative thallus stage. The zoospores are flagellated and chemotactically responsive, which enables them to locate freshly available or structurally favorable plant surfaces. After attachment, they lose motility, encyst, and initiate invasive development. Depending on the genus and growth form, the resulting vegetative structures can be highly rhizoidal and polycentric or more bulbous and monocentric, but in both cases the outcome is the same from a functional standpoint: intimate physical association with plant particles and progressive penetration into biomass. This invasive habit is central to AGF function. It means that substrate utilization is not limited to what soluble enzymes can access from the outside. Mechanical penetration and enzymatic attack proceed together, allowing the fungus to breach the structural defenses of lignified tissues more effectively than free enzymes alone [13,14,22,23].

The enzymatic dimension of this attack is mediated by unusually rich carbohydrate-active enzyme repertoires and by cellulosome-like structures. Comparative genomics and proteomic studies have shown that AGF possess large arrays of CAZymes and cellulosomal components, including dockerin-like and scaffold-related features, that support efficient attack on insoluble polysaccharides. These systems are not static. Their localization can vary across life stages, and their organization differs in important ways from classical bacterial cellulosomes even while preserving the general principle of synergistic enzyme clustering. From a technological perspective, this is crucial because it explains why AGF can deconstruct substrates that resist conventional hydrolysis and why they have attracted interest not only as whole-cell biocatalysts but also as sources of enzymatic tools for biofuel and biorefinery applications [13,26-28].

This morphological-enymatic integration is one of the clearest examples of why AGF matter for residue processing. In a conventional industrial setting, physical pretreatment and enzymatic hydrolysis are separate operations performed by different means. In AGF, both are embodied within one organism. Rhizoids and appressorium-like penetration structures open the substrate; cellulosomal and non-cellulosomal enzymes hydrolyze it; and the resulting soluble intermediates are immediately metabolized. This is more than ecological elegance. It is a blueprint for a compact bioconversion logic in which several unit operations are effectively collapsed into one biological step. Such a step does not eliminate the need for process engineering, but it changes its focus profoundly. Instead of investing primarily in external pretreatment severity, one can invest in optimizing the physiology and cultivation of the organism that performs the deconstruction internally [11,14,26,27].

1.6 Hydrogenosomes, mixed-acid fermentation, and the formation of a metabolite platform

The downstream value of AGF depends not only on their ability to access plant biomass, but on what they produce from it. Their fermentative metabolism is unusually well suited to the generation of a chemically versatile metabolite platform. Once lignocellulose-derived sugars enter central carbon metabolism, carbon flux is distributed through glycolysis and associated branch pathways into a mixed-acid fermentation regime. Unlike aerobic fungi, AGF do not rely on conventional mitochondria and oxidative phosphorylation. Instead, they use hydrogenosomes, organelles of mitochondrial origin that support ATP generation and hydrogen production under anaerobic conditions. The recognition that hydrogenosomes are derived from mitochondria resolved a long-standing evolutionary debate, but for biotechnology the more immediate consequence is that AGF naturally connect lignocellulose utilization to the formation of reduced metabolites and molecular hydrogen [21,22].

The products that emerge from this metabolism are especially relevant because they are not merely waste compounds. Acetate, formate, lactate, succinate, ethanol, carbon dioxide, and hydrogen all have potential value either as products or as substrates for further processing. Their exact proportions depend on organism, substrate, concentration, and cultivation environment. This variability is not a disadvantage; rather, it is one of the reasons AGF are attractive as primary converters. A fungal fermentation broth is not simply the residual liquid left after biomass degradation. It is a metabolite-rich intermediary phase whose composition can, in principle, be tuned or selected for downstream compatibility. In that sense, AGF generate not just one fermentation product but a flexible metabolite spectrum that can be viewed as a biochemical interface between recalcitrant biomass and later synthesis-oriented microorganisms [14,20,25].

The relevance of hydrogen in this context deserves special emphasis. Hydrogen generation reflects the handling of reduced ferredoxin and other redox carriers within the hydrogenosome and therefore acts as a sensitive marker of how efficiently reducing equivalents are being disposed of. This helps explain why hydrogen production is so responsive to environmental changes. Alterations in headspace composition, substrate level, or co-metabolic conditions can shift the balance between hydrogen, organic acids, and alcohols. In practical terms, a change in hydrogen yield often signals a broader reorganization of carbon and electron flow. Because the same fermentation broth may later feed a downstream production organism, this makes hydrogen an especially useful integrative variable in the design of linked bioprocesses. Hydrogen is thus both a potential value stream and a window into the redox economy of fungal biomass conversion [14,20].

1.7 Cultivation challenges: strict anaerobiosis, buffering, atmosphere, and preservation

Despite their promise, AGF remain difficult organisms to handle experimentally. Isolation, routine cultivation, preservation, and comparative experimentation are all more challenging than for most conventional industrial microbes. Existing review literature emphasizes that their strict anaerobiosis, complex life cycle, particle-associated growth, and sensitivity to cultivation conditions have all slowed progress in developing reproducible and scalable protocols. Even long-term storage remains a challenge, and while cryopreservation strategies have improved, cultivation and maintenance still impose a significant barrier to broader biotechnological deployment [13,23].

A particularly important issue is the classical use of bicarbonate-buffered, CO_2-containing serum-bottle systems. These systems are historically rooted in rumen microbiology and remain highly effective for routine maintenance, but they also intrinsically couple gas phase, buffering chemistry, and inorganic carbon availability. This coupling complicates mechanistic interpretation. When a cultivation uses a CO_2 headspace and bicarbonate buffer simultaneously, any shift in gas accumulation or removal influences pH stability, dissolved inorganic carbon levels, and potentially metabolic fluxes. As a result, it becomes difficult to determine whether an observed physiological effect is caused by gas phase composition, buffering capacity, or carbon supply itself. This problem is especially significant in AGF cultivation because hydrogen and CO_2 are central fermentation products, meaning that the atmosphere is not simply an external setting but part of the metabolic system under study. The broader literature on biological buffering, beginning with the original rationale for Good's buffers, shows why CO_2-independent systems can be valuable for disentangling such effects, even if they do not automatically replace physiological bicarbonate functions [13,29]. These cultivation challenges matter for more than method development. They directly shape the reliability of fungal fermentation as an upstream bioprocess. If gas phase, pH, and carbon speciation cannot be controlled or interpreted, then the resulting metabolite spectrum remains difficult to standardize. Likewise, if biomass quantification is confounded by filamentous or particle-associated growth, then differences in metabolic output cannot easily be traced back to differences in actual fungal growth. Such issues are not merely technical inconveniences. They determine whether AGF can move from promising ecological specialists to robust biotechnological platforms. A credible residue-upgrading strategy therefore requires not only admiration for fungal deconstruction capacity, but also a rigorous understanding of the cultivation systems through which that capacity is expressed [13,14,22,29].

1.8 Oleaginous yeasts and the industrial promise of single-cell oils

If AGF define a powerful entry point into lignocellulosic residues, oleaginous yeasts define one of the most attractive routes for upgrading soluble carbon into dense, easily recoverable, and application-relevant products. Oleaginous microorganisms are commonly defined by their ability to accumulate lipids above 20% of their dry cell mass, and yeasts are especially attractive among them because they combine high lipid accumulation with relatively fast growth, process robustness, and fatty acid compositions similar to those of many plant oils. This has made microbial single-cell oils a long-standing target in biotechnology, with relevance for biodiesel, lubricants, oleochemicals, food ingredients, and nutraceuticals. The underlying appeal is clear: unlike crop-based oil production, microbial lipid production does not depend directly on arable land, seasonal patterns, or conventional agricultural yield structures, and it can in principle be integrated with a much broader range of carbon sources [8,30-33].

Among oleaginous yeasts, *Cutaneotrichosporon oleaginosum* has emerged as a particularly compelling organism because of its broad substrate range, high lipid potential, and tolerance for low-cost feedstocks. More broadly, the field now recognizes several yeast species and lineages capable of substantial lipid accumulation, and current reviews emphasize both the progress achieved and the remaining challenges for commercialization. These challenges include substrate cost, oxygen demand, foaming, nutrient control, harvesting, cell disruption, extraction, and overall process economics. The central industrial opportunity lies in the fact that microbial lipids can be tailored or selected for different uses while remaining compatible with fermentation-based process control. The central industrial obstacle lies in the fact that high titers alone do not guarantee economic viability if the substrate is expensive or if downstream recovery is too energy intensive. This is why the most relevant developments in the field increasingly focus on waste-derived substrates, process intensification, and integrated biorefinery logic rather than on maximal lipid percentages alone [8,31,34-36].

At the biochemical level, lipid accumulation in oleaginous yeasts is tightly linked to nutrient limitation and central carbon metabolism. Nitrogen limitation is the classical trigger, redirecting carbon away from biomass growth and toward triacylglycerol synthesis. However, the physiology is more nuanced than a simple growth-versus-storage dichotomy. Carbon-to-nitrogen ratio, oxygen availability, phosphorus supply, pH, temperature, and feeding strategy all influence not only the amount of lipid produced but also biomass composition and fatty acid profile. This is why reactor-scale studies and process-oriented analyses are so important for the field. They reveal that microbial oil production is best understood as a controlled fermentation state rather than as an intrinsic strain trait expressed independently of cultivation context. That understanding is essential if lipid-producing yeasts are to function as realistic downstream modules within residue-based process chains [30,31,34,36,37].

1.9 Process determinants of single-cell oil production and downstream recovery

From a process-engineering perspective, microbial oil production is shaped by several interdependent determinants. Carbon source availability must be sufficient to support both growth and subsequent lipid accumulation, but excess substrate can also provoke overflow metabolism or undesirable by-product formation. Oxygen supply is essential because lipid biosynthesis in yeasts is tightly coupled to aerobic metabolism and reducing-power management. Nutrient limitation must be imposed neither too early nor too late if biomass and lipid productivity are to be balanced effectively. Phosphorus has become increasingly interesting in this context because it is both biologically indispensable and globally finite, making phosphate-limited lipid production strategically relevant in ways that go beyond classical fermentation optimization. Alternative limitation regimes may therefore offer both metabolic and resource-management advantages, particularly when unconventional or nitrogen-rich feedstocks are involved [30,31,37-40].

Another major determinant is downstream processing. Unlike soluble fermentation products, microbial lipids are intracellular and therefore require harvesting of biomass, some form of cell disruption or extraction enhancement, and a subsequent lipid recovery step. Reviews of single-cell oil production consistently emphasize that downstream processing is not a secondary consideration but one of the defining economic constraints of the entire platform. Biomass pretreatment, extraction solvent choice, wet versus dry processing, and the compatibility of recovery methods with the intended end use all affect the overall viability of the process. This is especially important when moving from high-value specialty lipids to bulk applications such as biodiesel or lubricants, where margins are tighter and process inefficiencies become decisive. Accordingly, a realistic “straw to oil” concept cannot stop at lipid biosynthesis. It must also remain mindful of how biomass composition, substrate impurities, and cultivation mode influence downstream recovery [8,31,34].

For this reason, one of the strongest arguments for oleaginous yeasts in integrated bioprocesses is not only that they produce lipids, but that they do so in a form that is relatively compatible with existing fermentation technology. Agitation, aeration, pH control, foam suppression, off-gas monitoring, and fed-batch or repeated-batch operation are all familiar from industrial microbial processing. This means that once a suitable substrate and limitation strategy are identified, scaling and control become tractable in principle. The unresolved difficulty lies less in the unit operations themselves than in the feedstock. Low-cost, heterogeneous, and inhibitor-rich carbon sources remain the main barrier to broad implementation. It is therefore unsurprising that so much current research focuses on coupling oleaginous yeasts to industrial side streams or waste-derived substrates [8,34,41].

1.10 Low-cost feedstocks, inhibitor-rich substrates, and the importance of adaptation

The economics of microbial oils are determined to a large extent by feedstock cost. Refined sugars remain useful model substrates, but they are difficult to justify for high-volume applications unless the process yields very high product value. This is why low-cost side streams such as crude glycerol, hydrolysates, volatile fatty acids, and other industrial residues are of such sustained interest. Crude glycerol is especially important because it is a major by-product of biodiesel production, is highly reduced, and can, in principle, support efficient lipid biosynthesis. Yet its composition is variable and often inhibitory due to methanol, salts, soaps, catalyst residues, and other contaminants. This combination of promise and difficulty makes it highly instructive in the broader context of residue-based yeast processing [41-44].

The same general problem appears, albeit in a different chemical form, when one considers the metabolite mixtures produced by AGF. These mixtures may contain carbon sources of clear value to a downstream yeast, such as acetate, ethanol, or lactate, but they can also contain compounds that are inhibitory or metabolically destabilizing, especially formate. In addition, they represent mixed-substrate environments rather than single-carbon-source media. This matters because substrate preference, catabolite repression, redox demands, and maintenance costs all influence how a yeast behaves in complex media. A downstream organism designed or selected only for simple sugar media may therefore perform poorly in fungal fermentation broths even if the latter contain substantial usable carbon. This is one of the strongest reasons why adaptive laboratory evolution has become relevant in the broader context of integrated microbial bioprocessing. Adaptation is not merely a tool for improving titer; it is a way of bringing microbial physiology closer to the real chemical complexity of low-cost feedstocks [45-49].

Adaptive laboratory evolution is particularly attractive when non-GMO routes are desired and when the selective environment can be designed to resemble the intended industrial substrate landscape. Recent work on ALE methodology and microfluidic adaptation platforms highlights how controlled gradients and prolonged selection under defined stress can accelerate the emergence of improved phenotypes. In a residue-upgrading context, this means that organisms need not be evaluated only in their wild-type form. They can be systematically trained toward tolerance of inhibitor-rich, mixed-substrate, and waste-derived environments. This point is conceptually very important for linking anaerobic fungal fermentation and oleaginous yeast lipid production. The compatibility of the two modules need not be a fixed property of the native organisms; it can itself become a target of process-oriented strain development [45,46,50,51].

1.11 From metabolite platforms to integrated upgrading: the logic of consecutive bioprocessing

The convergence of all these considerations leads naturally to the idea of consecutive or two-stage bioprocessing. If one organism is highly specialized for deconstructing lignocellulosic biomass and producing a mixture of soluble reduced metabolites, while another is highly specialized for turning soluble carbon into lipids, then a functional coupling between the two becomes an obvious process concept. Such a strategy avoids forcing fundamentally different physiological demands into the same vessel or environmental regime. Instead, each organism can be cultivated under conditions favorable to its own biology. The upstream organism performs deconstruction and primary fermentation; the downstream organism performs upgrading and storage-product accumulation. In a circular-economy context, this logic is especially appealing because it treats the output of the first process not as waste but as feedstock, and the overall residue stream as a cascade of value-generation opportunities [2,5,8,52].

The strength of such a modular design is that it aligns with the real heterogeneity of biological functions. AGF thrive under strict anaerobiosis, respond strongly to gas-phase composition, and naturally generate hydrogen and mixed-acid fermentation products. Oleaginous yeasts thrive in controlled aerobic fermentations and require carefully managed nutrient limitation to accumulate lipids efficiently. Rather than seeing these differences as incompatibilities, consecutive cultivation treats them as complementary divisions of labor. The challenge then becomes one of interface engineering: Which fungal metabolite profiles are most suitable as downstream substrates? Which compounds need to be tolerated, removed, or moderated? Which nutrient limitation strategy makes best use of the imported carbon in the yeast stage? How can side streams such as crude glycerol or other low-cost feeds be used to tune the balance between inhibition, growth, and lipid storage? These are not isolated questions. They are all facets of the same central problem: how to move carbon and reducing power from a structurally recalcitrant agricultural residue into a readily recoverable microbial oil. Seen from this perspective, “straw to oil” is best understood as a process principle rather than a slogan. It begins with the recognition that agricultural residues such as straw are abundant and strategically important but difficult to use directly. It continues with the identification of AGF as biological systems capable of opening these residues and converting them into an intermediary metabolite economy. It then turns to oleaginous yeasts as upgrading organisms that can condense soluble carbon into lipids of industrial relevance. Finally, it recognizes that the true challenge lies at the interface: in cultivation technology, redox management, substrate compatibility, nutrient limitation, and strain adaptation. A residue-based circular bioeconomy will depend on exactly such interfaces, because future industrial feedstocks are likely to be mixed, impure, and biologically demanding. The intellectual value of integrating AGF with oleaginous yeasts therefore extends beyond a single product concept. It offers a model for how complex biomass, microbial specialization, and process modularity can be combined in the service of a more circular carbon economy [2,8,13,14,34,42,52].

2. Research proposal

2.1 Toward an integrated “straw-to-oil” upcycling process based on anaerobic gut fungi and oleaginous yeasts

In response to climate change, fossil resource depletion, and the urgent need for a circular carbon economy, this dissertation proposes the development of a biologically integrated upcycling concept in which hemi- and lignocellulosic residues are converted into microbial lipids. Although lignocellulosic side streams such as straw are abundant, inexpensive, and non-food competing, their industrial use remains limited by structural recalcitrance and the cost of conventional pretreatment and hydrolysis. Anaerobic gut fungi of the phylum *Neocallimastigomycota* offer a promising biological entry point into this problem because they can directly attack complex plant biomass and convert it into hydrogen and soluble fermentation intermediates such as acetate, formate, lactate, ethanol, and succinate. In parallel, oleaginous yeasts represent highly attractive downstream production organisms because they can accumulate plant-oil-like lipids from a broad range of carbon sources under controlled fermentation conditions. Taken together, these two microbial platforms suggest the possibility of a consecutive “straw-to-oil” process. However, the physiological requirements of anaerobic gut fungi, the process limits of single-cell oil production, and the compatibility of both systems remain insufficiently understood for a rational biotechnological implementation.

This dissertation therefore aims to establish the scientific and process-engineering basis of an integrated upcycling platform that links lignocellulose degradation by anaerobic gut fungi with lipid production by oleaginous yeasts. The work is guided by four interconnected objectives.

First, the dissertation will systematically characterize anaerobic gut fungi as primary biocatalysts for lignocellulosic conversion. To this end, six fungal strains will be examined with respect to their metabolic and physiological responses to key cultivation variables, including temperature, carbon source, substrate particle size, and feeding strategy. Particular emphasis will be placed on identifying robust cultivation conditions and on understanding how these parameters affect hydrogen formation and the spectrum of soluble fermentation products. Beyond classical bottle cultivation, the work will also address fundamental cultivation bottlenecks by disentangling the roles of gas atmosphere, buffer chemistry, bicarbonate supply, pH, and nitrogen availability. In parallel, a transferable biomass quantification strategy will be established to improve reproducibility and comparability in filamentous, particle-associated cultures. Finally, the dissertation will investigate fungal redox balancing in greater depth by assessing whether missing electrons in fermentation datasets may be linked to extracellular electron transfer. Together, these studies will define the physiological operating window of anaerobic gut fungi and clarify their value as upstream converters of hemi- and lignocellulosic materials.

Second, the dissertation will establish a robust and scalable single-cell oil platform with oleaginous yeasts under production-relevant conditions. Four oleaginous yeast strains will be benchmarked in controlled stirred-tank reactors in order to compare biomass formation, lipid accumulation, specific lipid production rates, biomass composition, and fatty acid profiles under nitrogen-limited, phosphate-limited, and nutrient-replete conditions. This will identify physiologically and technologically suitable lipid-induction regimes beyond final lipid titre alone. In addition, the work will evaluate the use of low-cost industrial side streams, with particular focus on untreated crude glycerol, in order to improve the economic feasibility of microbial lipid production. Here, process-oriented feeding strategies will be developed to mitigate early inhibition, restore growth and lipid formation, and assess process robustness under transition-scale conditions. These studies will provide the downstream process framework required for future coupling with anaerobic fungal fermentations.

Third, the dissertation will address the compatibility gap between fungal fermentation broths and oleaginous yeasts. Because representative anaerobic fungal metabolite mixtures can severely inhibit the growth of yeast, especially in the presence of formate, adaptive improvement of the selected yeast platform will be pursued. A microfluidic adaptive laboratory evolution approach will be used to generate non-GMO yeast variants with improved robustness and substrate utilization on mixtures of ethanol, acetate, lactate, succinate, formate, and crude glycerol. Follow-up characterization will determine whether adaptation improves growth, carbon assimilation, and metabolic performance on inhibitor-rich and industrially relevant media. In this way, the dissertation will not only test process compatibility but actively engineer it at the physiological level.

Fourth, the dissertation will evaluate the feasibility of linking both microbial platforms into a consecutive bioprocess. The most promising fungal strains, metabolite spectra, and yeast phenotypes will be selected and assessed for process compatibility. The work will examine whether fungal fermentation products can serve as realistic substrates for microbial lipid formation and will identify the key constraints that must be controlled for future implementation. The ultimate objective is not merely to study two independent microbial systems, but to define the biological and engineering prerequisites of a coherent residue-based conversion chain in which straw-derived carbon is first mobilized by anaerobic gut fungi and subsequently upgraded to lipids by oleaginous yeasts.

Overall, this dissertation seeks to bridge a critical gap between lignocellulose deconstruction and lipid biomanufacturing. By combining anaerobic fungal physiology, redox analysis, reactor-based yeast process development, waste-stream valorization, and adaptive strain improvement, it aims to lay the foundation for a scalable and mechanistically informed “straw-to-oil” platform within a future circular bioeconomy.

3. Experimental Investigations, Results and Discussion

This dissertation is built as a cumulative body of work, yet its individual chapters are not intended to function as isolated contributions. Rather, they are arranged in a deliberate scientific sequence that reflects the development of a broader process concept. The overarching aim is the establishment of the biological and process-engineering basis of a **two-stage "straw-to-oil" upcycling strategy**, in which hemi- and lignocellulosic materials are first converted by anaerobic gut fungi into hydrogen and reduced soluble intermediates and are subsequently upgraded to microbial lipids by oleaginous yeasts. Such a concept cannot be developed by studying only one organism group, one substrate, or one conversion step. It requires a gradual construction of knowledge, beginning with the biological foundations of the upstream system, continuing through the definition of a robust downstream production platform, and culminating in the identification and analysis of the interface between both systems.

The logic of the dissertation therefore follows the logic of process development itself. Before anaerobic gut fungi can be used as primary biocatalysts in a residue-based process, their cultivation requirements, metabolic flexibility, and product spectra must be understood in sufficient detail. Before oleaginous yeasts can function as efficient downstream upgrading organisms, their lipid-production behavior must be characterized under controlled and industrially meaningful conditions. And before both systems can be coupled into a coherent process chain, the physiological and chemical mismatches between them must be made visible and, where possible, reduced. Each chapter in this dissertation addresses one of these requirements. Read together, they define a progression from **biological exploration**, through **mechanistic clarification**, to **process integration**.

For the reader, it is therefore important to understand that the dissertation does not begin with the final coupling problem. It begins with the question of how anaerobic gut fungi behave as individual organisms, because without a reproducible and mechanistically interpretable upstream platform, any downstream coupling would rest on an unstable foundation. Only after this upstream platform has been characterized does the focus shift toward lipid production with oleaginous yeasts. And only once both platforms have been independently established does the dissertation address compatibility, adaptation, and finally process linkage. In this sense, the dissertation moves from **understanding the individual modules** to **engineering the relationship between them**.

3.1 Preparing the upstream platform: understanding anaerobic gut fungi as biocatalysts

The first three chapters are united by one central concern: they establish anaerobic gut fungi as a usable and interpretable upstream biotechnological system. Although these organisms have long been recognized for their remarkable capacity to degrade untreated lignocellulosic material, they remain comparatively understudied in terms of cultivation physiology, metabolic regulation, and process behavior. For a future “straw-to-oil” process, however, it is not enough to know that they can grow on plant biomass. It must also be known under which conditions they grow robustly, which products they form, how flexible their metabolism is, and which cultivation variables exert the strongest effects on their performance.

The dissertation therefore opens with a broad physiological study that provides a first structured map of the fungal system. This is followed by a mechanistic expansion into fungal redox physiology and extracellular electron transfer, and finally by a cultivation-engineering study that disentangles the physicochemical variables hidden in the classical AGF bottle system. These three chapters together define the fungal platform not merely as a biological curiosity, but as a candidate primary conversion stage with increasingly clear operating rules.

3.1.1 Metabolic and physiological analysis of anaerobic gut fungi under diverse cultivation conditions

The first chapter marks the true biological starting point of the dissertation. Its role is to establish the basic physiological landscape of the anaerobic gut fungal platform. At the outset of this work, it was clear that anaerobic gut fungi possessed exceptional lignocellulose-degrading abilities, but it remained unclear how robust different strains would be under varying cultivation conditions, how flexible their metabolism was, and which parameters would most strongly affect their performance. This first study therefore asks the most fundamental question of the entire dissertation: **What can these organisms do under controlled conditions, and how stable is that behavior across different strains and substrates?**

The importance of this chapter extends well beyond descriptive strain screening. By comparing multiple anaerobic gut fungal isolates across temperature regimes, straw particle sizes, soluble and insoluble carbon sources, substrate concentrations, and feeding strategies, this study defines the first operational framework for the upstream system. It shows that fungal metabolism is not uniform across strains, that hydrogen production and metabolite formation depend strongly on cultivation conditions, and that substrate class and substrate load influence not only growth but also the internal distribution of reducing equivalents. In doing so, the chapter turns the fungal fermentation broth from an undefined outcome into a measurable metabolite platform.

This first chapter also performs a crucial conceptual shift for the whole dissertation. It demonstrates that anaerobic gut fungi should not be viewed merely as biomass degraders or enzyme suppliers. Rather, they are **primary converters** that transform recalcitrant plant-derived material into a spectrum of reduced products. That insight is the first essential step toward the later “straw-to-oil” logic: the output of the fungal stage is not simply degraded biomass, but a chemically meaningful and biotechnologically relevant pool of intermediates.

Chapter 1: Anaerobic gut fungi as biocatalysts: metabolic and physiological analysis of anaerobic gut fungi under diverse cultivation conditions

Kevin Edward Schulz[1*], Dominik Scholz[1], Anto Rafael Sikirić[1], Daniela Rambow[1], Anke Neumann[1*] and Katrin Ochsenreither[2]

[1]Institute of Process Engineering in Life Sciences 2: Electrobiotechnology, Karlsruhe Institute of Technology (KIT), Karlsruhe, Germany, [2]Kaiserslautern University of Applied Sciences, Campus Pirmasens, Pirmasens, Germany, * corresponding authors

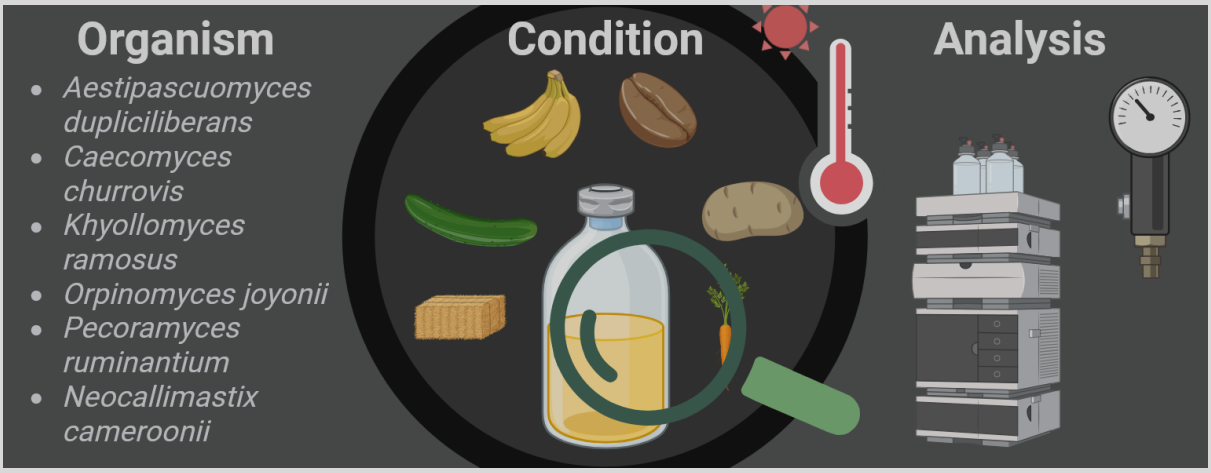

Publishing details:
Front. Microbiol.
Vol. 16
Published on 19 September 2025
doi: 10.3389/fmicb.2025.1662047

Author contributions: K.E.S.: Conceptualization, Formal analysis, Investigation, Methodology, Supervision, Validation, Visualization, Writing – original draft, Writing – review & editing. D.S.: Writing – review & editing, Investigation, Validation. A.S.: Investigation, Validation, Writing – review & editing. D.R.: Investigation, Writing – review & editing. A.N.: Writing – review & editing, Resources, Supervision. K.O.: Conceptualization, Supervision, Writing – review & editing.

Chapter 1: 1 Background

The steadily increasing global demand for platform chemicals, driven by globalization and population growth, necessitates the development of renewable and readily available resources [53-55]. Traditional fossil-based chemicals are not only finite but also contribute considerably to environmental pollution [56,57]. Consequently, a shift toward sustainable alternatives is essential. One promising approach is the utilization of lignocellulosic side streams derived from biowaste, such as residues from the paper and food industries, crop cultivation, and animal husbandry [3,12,58]. These lignocellulosic materials could serve as a future base material for the production of various platform chemicals, which are vital for numerous industrial processes [59].

Current methods for processing lignocellulosic biomass often rely on harsh chemical pre-treatments that are both energy- and cost-intensive. Biological approaches, while more environmentally friendly, are typically uneconomical due to the high cost associated with enzyme treatments [7]. A potential biotechnological solution lies in the use of evolutionarily adapted organisms. Anaerobic gut fungi, which inhabit the digestive track of herbivores, have demonstrated exceptional efficiency in degrading lignocellulosic materials [24]. Extracellular fungal cellulosomes—non-membrane-bound enzyme complexes composed of carbohydrate-binding domains and carbohydrate-active enzymes (CAZymes)—combined with mechanical penetration via appressorium-like structures, enable conversion rates of up to 48% for lignin-rich plant biomass [60-62]. The use of cellulosomes has been shown to be up to 12 times more effective than single-enzyme applications [63]. This underscores the potential of anaerobic fungi as biotechnological tools for efficient biomass conversion. However, effective application requires deeper understanding of their cultivation.

The phylum *Neocallimastigomycota* comprises strictly anaerobic fungi that play a key role in the digestion of plant material in herbivores [64]. Despite being discovered nearly 50 years ago, optimal cultivation conditions for these fungi remain poorly understood, resulting in suboptimal cultivation practices [65]. Recent findings suggest that unique metabolites are produced in depending on the hosts species, indicating species-specific microbial interactions and metabolic profiles that depend on a balancedrumen microbiome [66]. Therefore, analyzing ecological parameters, growth conditions and media composition is essential for biotechnological applications such as biowaste utilization.

Anaerobic fungi generate energy through mixed-acid fermentation, which is linked to an incomplete citric acid cycle [67,68]. The primary products—some of which are formed in hydrogenosomes, mitochondria-derived organelles—include acetate, formate, ethanol, lactate, hydrogen and succinate [21,25]. While genetic and transcriptomic data offer insight into possible metabolic pathways, physiological studies remain scarce and are mostly limited to representatives of *Neocallimastix* and *Piromyces* [69,70]. Building on the data and strains obtained and described by Stabel et al. (2021) [71], this study aims to expand the understanding about carbon source utilization and process engineering for anaerobic gut fungi.

Therefore, the experimental design of this study followed a structured and progressive approach, beginning with the evaluation of the external environmental factor temperature, which is known to influence fungal growth and metabolism. Building on this, the impact of substrate particle size using the standard carbon source wheat straw. Subsequently, the metabolic responses to soluble carbon sources, including glucose, fructose, cellobiose, and xylose, was studied with additional consideration given to feeding strategies such as batch and fed-batch cultivation. Furthermore, biowaste-derived substrates were evaluated with regard to substrate biodegradability and metabolic output. Finally, this study concludes with the observation of a previously uncharacterized morphological growth form under starvation conditions, representing a novel finding with potential implications for fungal stress response and life cycle dynamics. This stepwise progression—from well-established parameters to exploratory observations—was designed to build upon existing knowledge while uncovering new insights into anaerobic fungal physiology.

Chapter 1: 2 Methods

Chapter 1: 2.1 Strains of anaerobic gut fungi

The anaerobic fungal strains used in this study, namely *Aestipascuomyces dupliciliberans* A252, *Caecomyces churrovis* PP313, *Khyollomyces ramosus* X2152, *Orpinomyces joyonii* W212, *Pecoramyces ruminantium* SA222, and *Neocallimastix cameroonii* G341, were isolated and characterized by Stabel et al. (2021), from various animal dung samples [71]. The strains were cultivated in 7-day batch cycles.

Chapter 1: 2.2 Cultivation medium

The minimal medium used was based on the formulation by Stabel et al. (2021) with slight modifications [71]. The composition included per liter: 150 mL of salt solution 1 (3 g/L dipotassium hydrogen phosphate in demineralized water), 150 mL salt solution 2 (3 g/L potassium dihydrogen phosphate, 6 g/L ammonium sulfate, 6 g/L sodium chloride, 0.6 g/L magnesium sulfate heptahydrate, 0.6 g/L calcium chloride dihydrate in demineralized water), 2 mL of a zoospore inducer solution (0.5 g/L hemin chloride in 50% ethanol and 50% 0.05 M sodium hydroxide solution), 2 mL of a redox indicator solution (1 g/L resazurin sodium salt in demineralised water). Demineralised water was added to a weight of either 990 g when a solid carbon source was used, or to 890 g if a soluble carbon source was added, depending on the experimental setup. Solid carbon sources were added directly to the serum flasks before autoclaving, while soluble carbon sources were sterilized separately and added after autoclaving the salt medium. The medium was mixed in Fernbach flasks, anaerobized with 100% CO2. The pH was adjusted to 6.9. Subsequently, 6 g/L sodium hydrogen carbonate (buffer), 1 g/L L-cysteine hydrochloride monohydrate and 10 mL trace element solution (0.25 g/L manganese(II) chloride tetrahydrate, 0.25 g/L nickel(II) chloride hexahydrate, 0.25 g/L sodium molybdate dihydrate, 0.25 g/L boric acid, 0.2 g/L iron(II) sulfate heptahydrate, 0.05 g/L cobalt(II) chloride hexahydrate, 0.05 g/L sodium selenite pentahydrate, 0.05 g/L sodium metavanadate, 0.025 g/L zinc sulfate, and 0.0319 g/L copper(II) sulfate pentahydrate in 0.2 M hydrochloric acid) were added. Unless otherwise stated, 1 mm sized wheat straw particles (Waldhof Qualitätsstroh, Landwirtschaftlicher Betrieb Uwe Hoferichter) were added as a solid carbon source to a final concentration of 5 g/L. The pH was adjusted using a 4 M NaOH solution. After aliquoting the medium into 50 mL (solid carbon source) or 45 ml (soluble carbon source) portions in 100 mL serum bottles, serum bottles were sealed with a butyl stopper and crimp caps, then autoclaved. Prior to inoculation, the medium is supplemented with 5 mL of the respective soluble carbon source from a 50 g/L stock solution resulting in a final concentration of 5 g/L, 0.5 mL of sterile vitamin solution (0.01 mg/L thiamine hydrochloride, 0.652 g/L panthothenic acid hemicalium salt, 0.6 g/L nicotinic acid, 0.02 g/L cyanocobalamin, 0.2 g/L biotin, 0.012 g/L pyridoxine hydrochloride, 0.05 g/L folic acid, and 0.05 g/L P-aminobenzoic acid 0.2 g/L riboflavin in demineralised water) and 0.5 mL antibiotic solution (50 g/L ampicillin sodium salt, 50 g/L streptomycin sulfate, 50 g/L penicillin sodium salt in demineralised water). Strain maintenance was performed by weekly subculturing. Every 7 days, 5 mL of actively growing culture (inoculum) were transferred into a freshly prepared and fully supplemented serum bottle containing medium with 1 mm wheat straw as solid carbon source. This routine ensured continuous vitality and metabolic activity of all fungal strains under standardized conditions.

Chapter 1: 2.3 Experimental conditions

Under standard cultivation conditions, all fungal strains were maintained in serum bottles containing a minimal medium based on the formulation by Stabel et al. (2021), supplemented with wheat straw particles (1 mm, 5 g/L) as the solid carbon source [71]. The medium was anaerobized with CO2, adjusted to pH 6.9, and enriched with trace elements, vitamins, and antibiotics. Cultures were incubated at 39 °C, and subcultured weekly to ensure consistent vitality. To investigate the metabolic flexibility and environmental responsiveness of the strains, several key parameters were systematically varied. These included temperature, substrate particle size, carbon source type and concentration, feeding strategy, and the use of alternative biowaste materials. Each modification aimed to assess its impact on metabolite production, substrate utilization, and fungal morphology under controlled conditions

Chapter 1: 2.3.1 Temperature screening

The medium was prepared with a solid carbon source (wheat straw) and inoculated with 5 mL inoculum of the respective strain. Cultivation was carried out in biological and technical triplicates over a period of 7 days at various incubation temperatures. The temperature range tested was from 33 to 44 °C in 2 °C increments, with additional measurements at 34 and 42 °C, to further investigate the boundaries of fungal growth. During cultivation, the incubator temperature was recorded daily using the external temperature sensor Pt100 GMH 3700 Series (Greisinger). Endpoint concentrations were analyzed for growth and the formation of gaseous and liquid metabolites as described in the Analysis section.

Chapter 1: 2.3.2 Temperature shock

The medium was prepared with a solid carbon source (wheat straw). A preculture prepared for each strain was taken from the incubator and incubated at room temperature. Main cultures were inoculated with 5 mL of inoculum of the respective strain every 10 min over a period of 2 h, following the transfer of the pre-cultures to room temperature. Additionally, a final inoculation was performed after 24 h of incubation of the pre-culture at room temperature. Cultures were subsequently incubated at 39 °C for 7 days. This experiment was conducted as a single replicate. Analysis of the new generation was performed as described in the Analysis section.

Chapter 1: 2.3.3 Substrate particle size

Wheat straw (Waldhof Qualitätsstroh, Landwirtschaftlicher Betrieb Uwe Hoferichter) was chopped to 2 mm and sieved into the following size fractions using standardized sieves (Retsch): <0.5 mm, 0.6–0.8 mm, 1–1.18 mm, 2–3 mm. These fractions were used as sole solid carbon source in the medium. Additionally, wheat straw was cut to 5 cm and also applied. Inoculation was carried out in duplicate with 5 mL of the respective culture. Cultivation was carried out for 7 days at the standard temperature of 39 °C as reported in literature [71]. Endpoint parameters were analyzed for growth and the formation of gaseous and liquid metabolites as described in the Analytics section.

Chapter 1: 2.3.4 Usage of soluble carbon sources

To evaluate the influence of different initial soluble carbon source concentrations, salt media were supplemented after autoclaving to final concentrations of 1, 3, 5, 7, and 9 g/L of the soluble carbon sources glucose, fructose, xylose or cellobiose. Additionally, 5 g/L of 1 mm wheat straw particles were used as reference substrate. Inoculation was performed with 5 mL of the respective culture. The experiment was repeated three times. Cultivation was carried out for 7 days at 39 °C. Endpoint parameters were analyzed for growth and the formation of gaseous and liquid metabolites as described in the Analysis section.

Chapter 1: 2.3.5 Evaluation batch vs. fed batch cultivation

A single addition of 5 mL sterile 50 g/L glucose solution was compared with a daily addition of 0.714 mL. Inoculation was performed with 5 mL of the respective culture. Incubation was carried out for 7 days at 39 °C. The experiment was carried out in biological and technical triplicates. Analysis was performed as described in the Analysis section.

Chapter 1: 2.3.6 Biowaste valorization

To determine the potential of authentic biowaste streams with varying composition and degrees of lignification, reed, coffee grounds, organic cucumber peels, organic banana peels, organic carrot peels and organic potato peels were cut in small pieces and dried in the ED53 (WTCbinder) drying oven at 80 °C for 24 h. The cultivation medium was prepared differently than described above, using 5 g/L of each biowaste type as sole carbon source. Wheat straw was included as a reference substrate. Inoculation was performed with 5 mL of the respective culture and cultivation was carried out for 7 days at 39 °C. After cultivation the medium and residual carbon sources were transferred into pre-weighed 50 ml reaction tubes and dried in the ED53 (WTCbinder) at 80 °C until complete dry. The biomass was then weighed on the ADB 200-4 (Kern). The collected data was evaluated with the formular shown in Equation (1), where:

a: Percentage of biomass converted

b: Weight of the dried biomass + reaction tube

c: weight of the empty reaction tube

d: amount of biomass added to the bottle.

The experiment was conducted in technical triplicates. The weight of the fungal biomass was not accounted.

$$a = ((b - c)/(d)) \times 100 \quad (1)$$

Chapter 1: 2.3.7 Starvation experiment with *Orpinomyces joyonii*

In pre-conducted experiments, the growth of *O. joyonii* on glucose was considerably lower than on wheat straw. Therefore, starvation experiments were conducted on glucose. Cultivation was carried out in a two-step process. 5 mL of *Orpinomyces joyonii* pre-culture cultivated on wheat straw was used to inoculate medium with 5 g/L glucose as a carbon source. After incubation for 7 days at 39 °C, 5 mL of culture was transferred into a 2 L Schott bottle filled with 1 L medium containing 5 g/L glucose as a carbon source and again cultivated for 7 days at 39 °C. The resulting structures were photographed, sliced with a scalpel and examined under the microscope using the Eclipse E200 LED (Nikon Instruments Europe BV).

Chapter 1: 2.4 Analytics

All experiments were examined and analyzed using the techniques listed below, if not stated otherwise.

Chapter 1: 2.4.1 Pressure measurement as vitality measurement

The gases formed during cultivation increase the pressure inside the inoculated serum bottles (Ochs Glasgeräte). The pressure was measured at the fermentation endpoint using either the vacuum gauge G 1111-VAC (Greisinger) and/or with the barometer GDH 14 AN (Greisinger) via neoprene tubes (Watson Marlow) using a Minisart NML 0.22 µm sterile filter (Sartorius) and a cannula (BD MicrolanceTM) by piercing the butyl stopper. The serum bottles were kept at cultivation temperature during measurement to avoid errors caused by temperature changes.

Chapter 1: 2.4.2 Gas chromatography for metabolite analysis

The composition of the gas phase in the serum bottles was determined at the endpoint of the fermentation. Bottles were transferred to the water bath ONE 10 (Memmert GmbH + Co. KG) set to cultivation temperature. A gas sample of 3–5 mL was withdrawn and injected into the 3000 Micro GC System (INFICON Holding AG), which performed automatic sample intake at 10 mL/min using an internal vacuum pump. The sample inlet, the injection valve and the columns were operated at 80 °C. A two-channel analysis was used. For the quantification of hydrogen, nitrogen and oxygen, channel A was operated with a pre-column PLOTU column (Agilent Technologies), the main column Rt-Molsieve 5Å (Agilent Technologies) and helium as carrier and reference gas at 1.72 bar. The carbon dioxide concentration was analyzed via channel B with a Rt-Q-Bond column (Agilent Technologies) and 1.38 bar operating pressure. Detection was performed using a previously calibrated (using seven point calibrations) thermal conductivity detector (INFICON Holding AG).

Chapter 1: 2.4.3 High performance liquid chromatography for metabolite analysis

Liquid metabolites were analyzed at the endpoint. A 2 mL sample was withdrawn from each of the serum bottles using a cannula (BD MicrolanceTM), transferred to a 2 mL reaction tube (Eppendorf) and centrifuged for 10 min at 13,000 rpm using a Heraeus TM Pico 17 (Thermo Fischer Scientific). One milliliter of the supernatant was filtered through a 0.22 µm sterile filter made of cellulose acetate (Restek) and transferred to a vial (Brown Chromatography Supplies), which was sealed with a Teflon cap. Analysis was performed using the 1100 HPLC system (Agilent Technologies). The pre-column used was the Rezex ROA organic acid H+ (8%) guard column (50 mm × 7.8 mm) (Phenomenex Ltd.), the main column a Rezex ROA organic acid H+ (8%) (300 mm × 7.8 mm, 8 m) (Phenomenex Ltd.), the eluent 5 mM sulphuric acid and the detectors RID (Agilent Technologies) and VWD (Agilent Technologies). The method ran for 40-min at a flow rate of 0.5 mL/min, with column and RID temperatures set to 50 °C and a VWD wavelength of 220 nm. Calibration was performed with the standards 0.1, 0.25, 0.5, 1, 2.5, 5, and 10 g/L of the chemicals acetate, ethanol, succinate, formate, lactate, malate, xylose, glucose and cellobiose.

Chapter 1: 3 Results

The effects of temperature, various solid and soluble carbon sources, carbon source concentrations and solid particle sizes on anaerobic fungal metabolism of six different species were analyzed. To evaluate metabolic activity, the total amount of metabolites produced—i.e., the final amount of organic acids, ethanol and hydrogen—was used as an aggregate parameter. To minimize bias resulting from stochiometric differences among these compounds, carbon or electron balances have been proposed as a good practice. However, previous studies have shown that the total metabolite concentration serves as a reliable indicator of anaerobic fungal vitality, due to its strong correlation with overall metabolic enzyme activity [20]. Production of single metabolites over time depending on strain and carbon source, i.e., temporal changes in the metabolic profile, are evaluated in Section 6.4.

Chapter 1: 3.1 Temperature screening

As part of the basic characterization of the strains, their general growth temperature range and the optimal growth temperature were determined by cultivation over a wide temperature range using wheat straw as the carbon source. The total amounts of metabolites produced are presented in Figure 1, with a detailed breakdown shown in Figure S1 and an overview provided in Table S1.

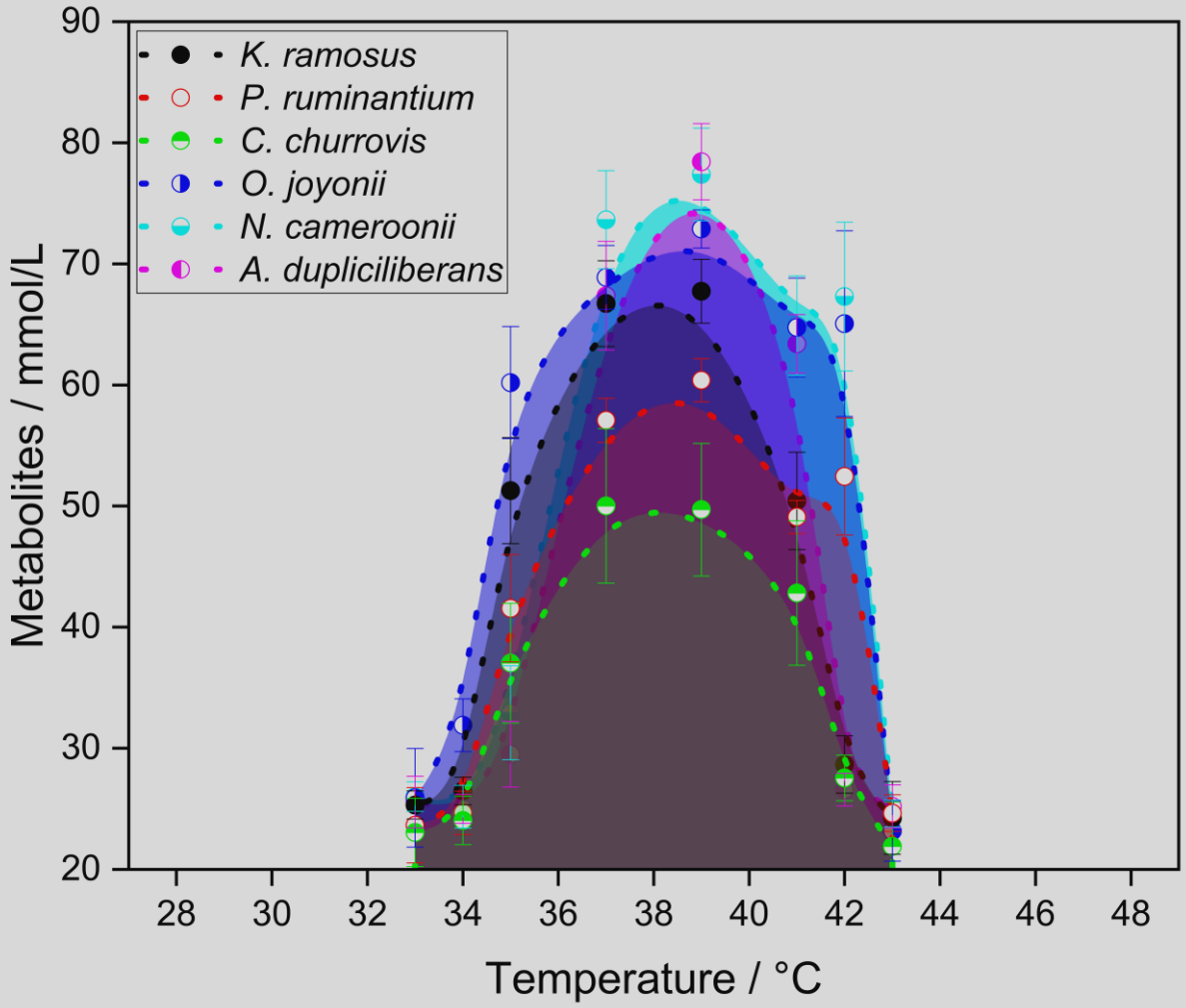

Figure 1: Total amount of metabolites produced after 7 days of cultivation of the tested strains in serum bottles with CO2 atmosphere and bicarbonate buffer on the carbon source wheat straw (n = 3).

All anaerobic gut fungi exhibited similar behavior across the tested temperature range. The general growth temperature range was defined by the minimum and maximum temperatures at which hydrogen production was still detectable. All strains grew at temperatures between 35 and 41 °C, with the exception of *A. dupliciliberans* A252 which showed a lower growth temperature limit of 37 °C. Two temperatures were considered as candidates for the optimal growth temperature: one corresponding to the highest total metabolite production, and the other to the highest hydrogen yield. While most strains reached their peak metabolite production at 39 °C, *C. churrovis* showed the highest yield at 37 °C. In terms of hydrogen production, the optimal temperature varied among strains: 37 °C for *K. ramosus*, 39 °C for *C. churrovis*, and *A. dupliciliberans* and 41 °C for *P. ruminatium*, *O. joyonii*, and *N. cameroonii*, respectively.

Chapter 1: 3.2 Temperature shock

Additionally, the resilience of anaerobic fungi to an induced room temperature shock was assessed by comparing the metabolic activity of the next generation of a non-shocked culture and shocked culture cultured on wheat straw as carbon source. Therefore, one culture of each strain was placed from 39 °C to room temperature and was used to inoculate subsequent cultures in 10-min intervals over 2 h and after 24 h. The inoculated cultures (next generation cultures) were cultivated at 39 °C. Figure 2 illustrates the relative metabolic activity of the next generation. A more detailed tracking of the first 2 h of the temperature exposure is provided in Figure S2.

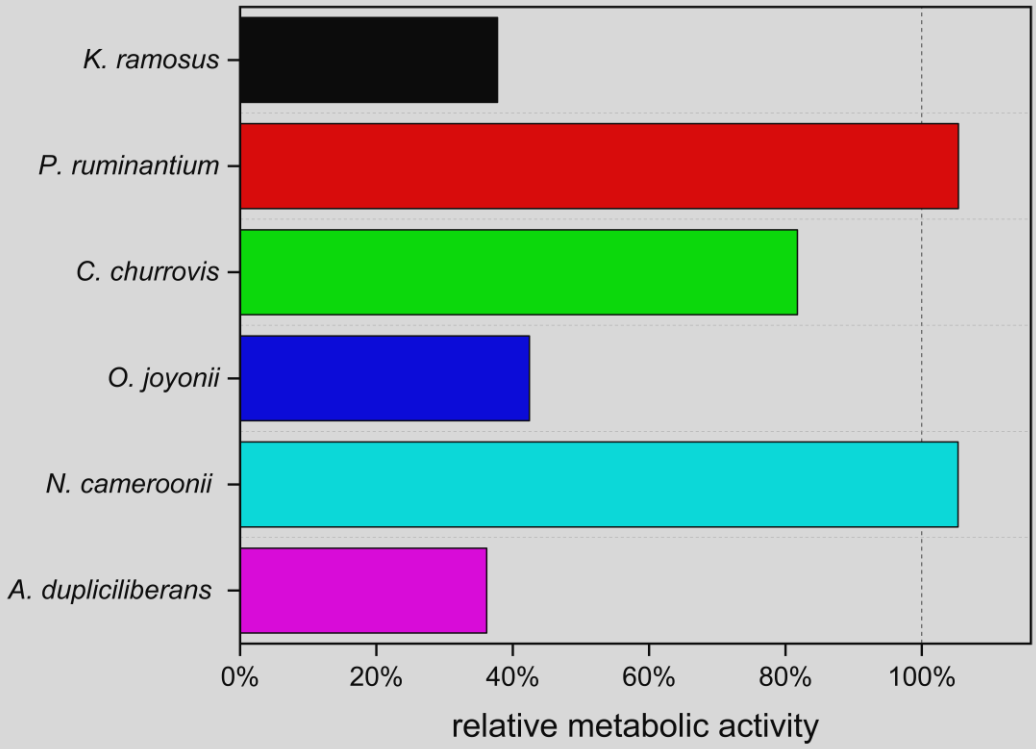

Figure 2: Effect of 24 h preculture room temperature shock to the metabolic activity of the next generation (n = 1).

The treatment revealed varying sensitivities to the temperature shock. While next generation cultures of *K. ramosus* X2152, *O. joyonii* W212, and *A. dupliciliberans* A252 showed a considerable decrease in metabolic activity, the remaining three strains were largely unaffected.

Chapter 1: 3.3 Substrate particle size

Following the investigation of temperature as a process parameter, attention was directed toward the properties of the solid carbon source. Standard cultivation protocols for anaerobic fungi typically utilize lignocellulosic biomass, such as wheat straw, which is cut into small particles. In previous experiments, a particle size of 1 mm was used [1]. The metabolites produced by all tested anaerobic fungal strains were normalized and subsequently analyzed statistically using the Tukey test, as shown in Figure 3. Further statistical analysis is provided in Table S2.

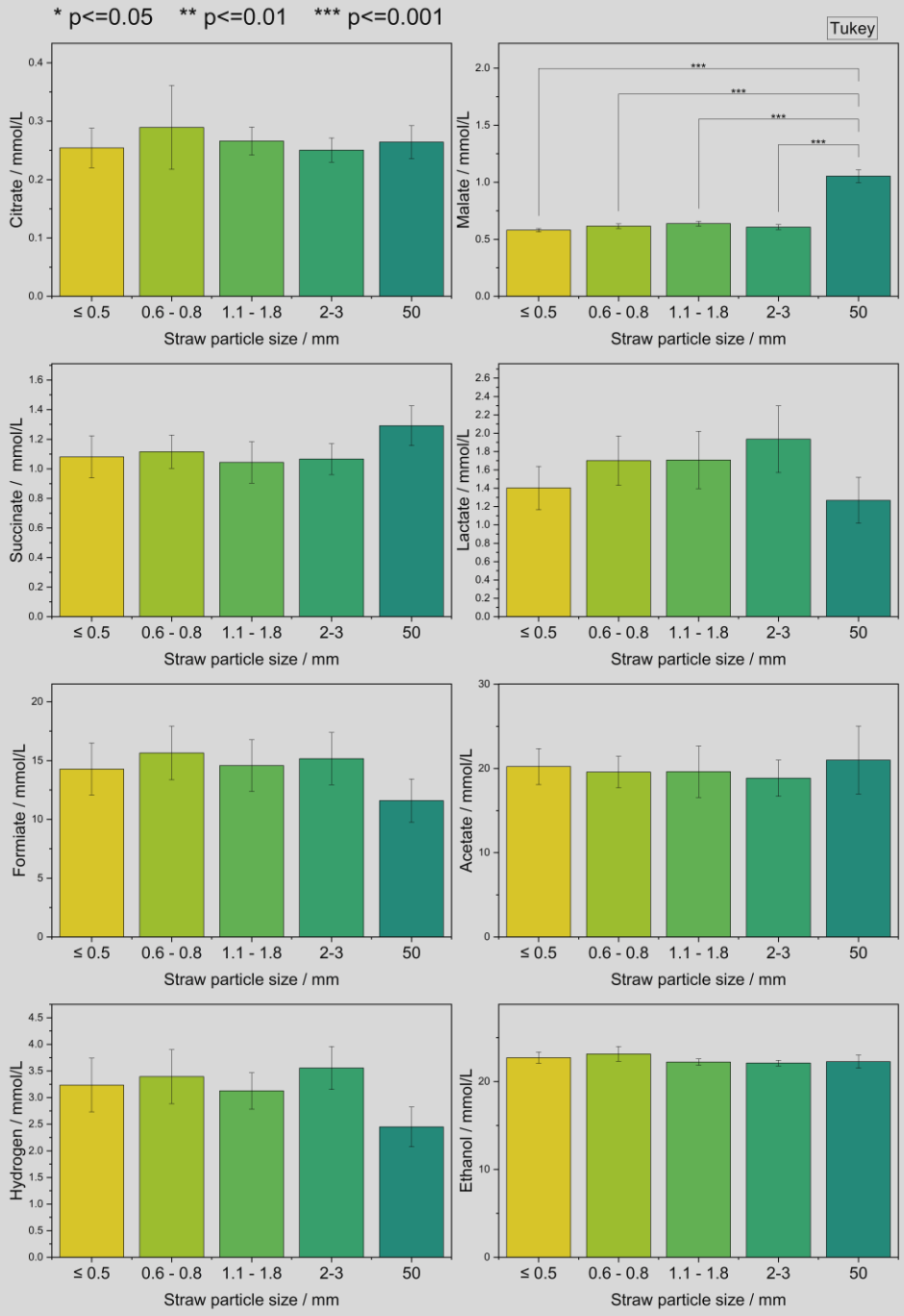

Figure 3: Statistical comparison for evaluation of significant differences in metabolite production based on particle size. All six tested strains are combined (n = 12).

The only statistically significant correlation with $p \leq 0.001$ observed was an increase in malate concentration associated with the largest particle size tested. No other significant differences in metabolite production were detected across the various substrate particle sizes. Absolute concentrations of the individual metabolites for each individual strain are presented in Figure S3.

Chapter 1: 3.4 Usage of soluble carbon sources

While most anaerobic gut fungi are known to grow particularly well on solid lignocellulosic carbon sources, i.e., a complex substrate source, cultivation on defined soluble carbon sources offers the potential for deeper insights into their metabolic activity. The four soluble carbon sources selected for this study—glucose, xylose, fructose and cellobiose—were chosen based on the publication by Stabel et al. (2021) and applied over a wide initial concentration range [71]. The quantities of metabolites produced by each tested strain, along with the residual concentrations of the carbon sources after 7 days of cultivation, are displayed in Figure 4.

With increasing initial carbon source concentration, a metabolic shift was detected—from hydrogen production toward elevated acetate and formate synthesis, eventually culminating in lactate production. Overall, this indicates a transition from hydrogenosomal to cytosolic metabolic pathways. Further analysis of hydrogen yields displayed in Figure 5, reveals a clear trend in the strains *N. cameroonii*, *C. churrovis*, and *K. ramosus*, with progressively higher hydrogen production observed at increasing carbon source concentrations.

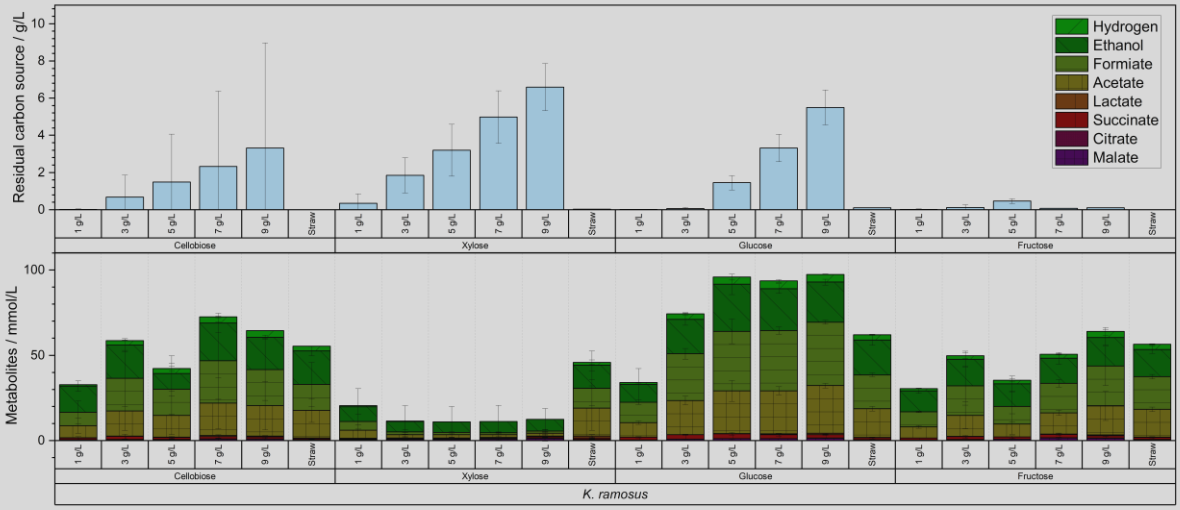
Residual carbon source / g/L
Hydrogen
Ethanol
Formiate
Acetate
Lactate
Succinate
Citrate
Malate
Metabolites / mmol/L
1 g/L
3 g/L
5 g/L
7 g/L
9 g/L
Straw
Cellobiose
Xylose
Glucose
Fructose
K. ramosus

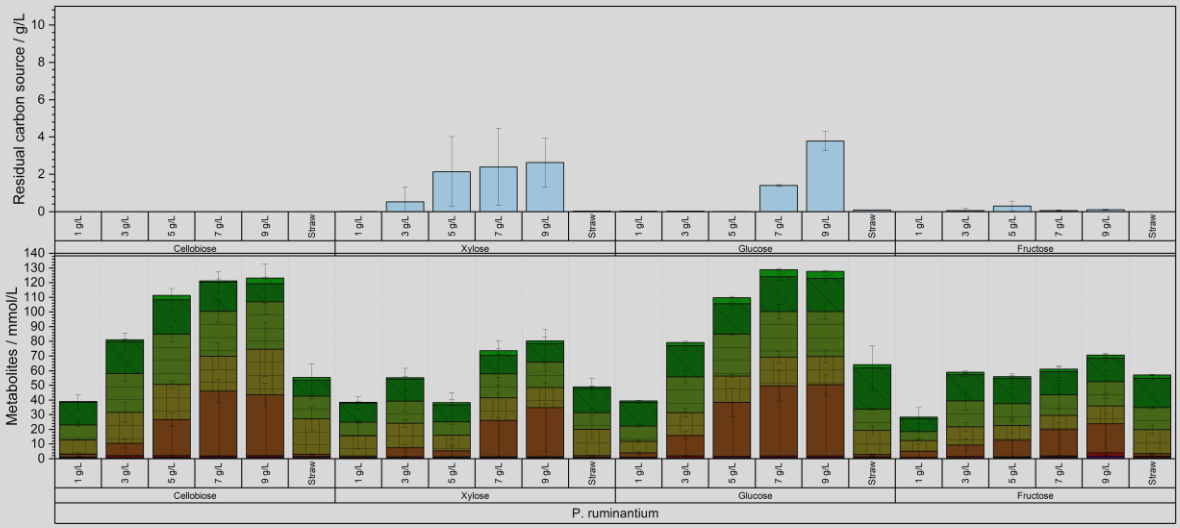
Residual carbon source / g/L
Metabolites / mmol/L
1 g/L
3 g/L
5 g/L
7 g/L
9 g/L
Straw
Cellobiose
Xylose
Glucose
Fructose
P. ruminantium

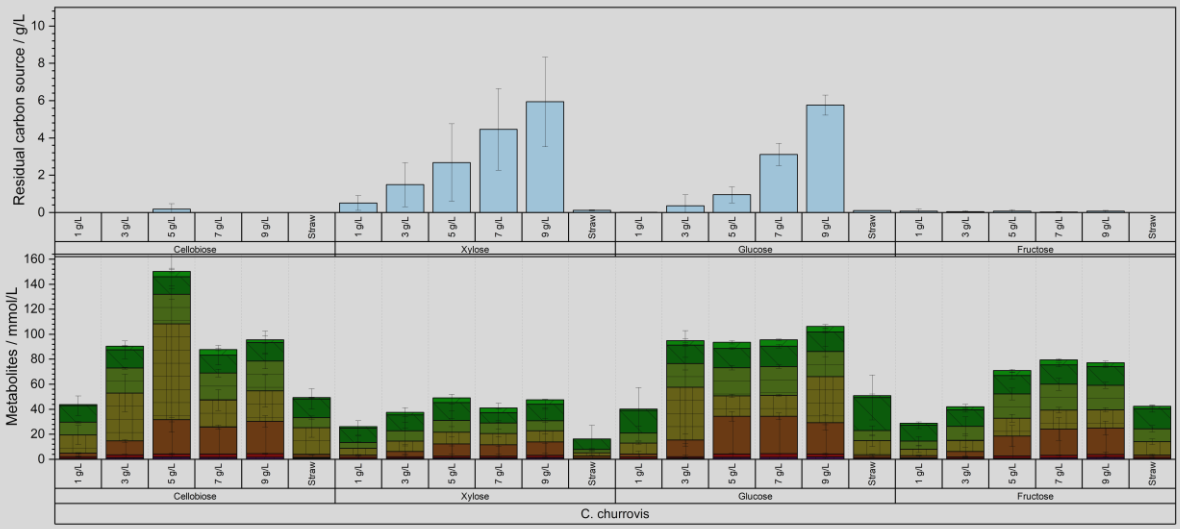
Residual carbon source / g/L
Metabolites / mmol/L
1 g/L
3 g/L
5 g/L
7 g/L
9 g/L
Straw
Cellobiose
Xylose
Glucose
Fructose
C. churrovis

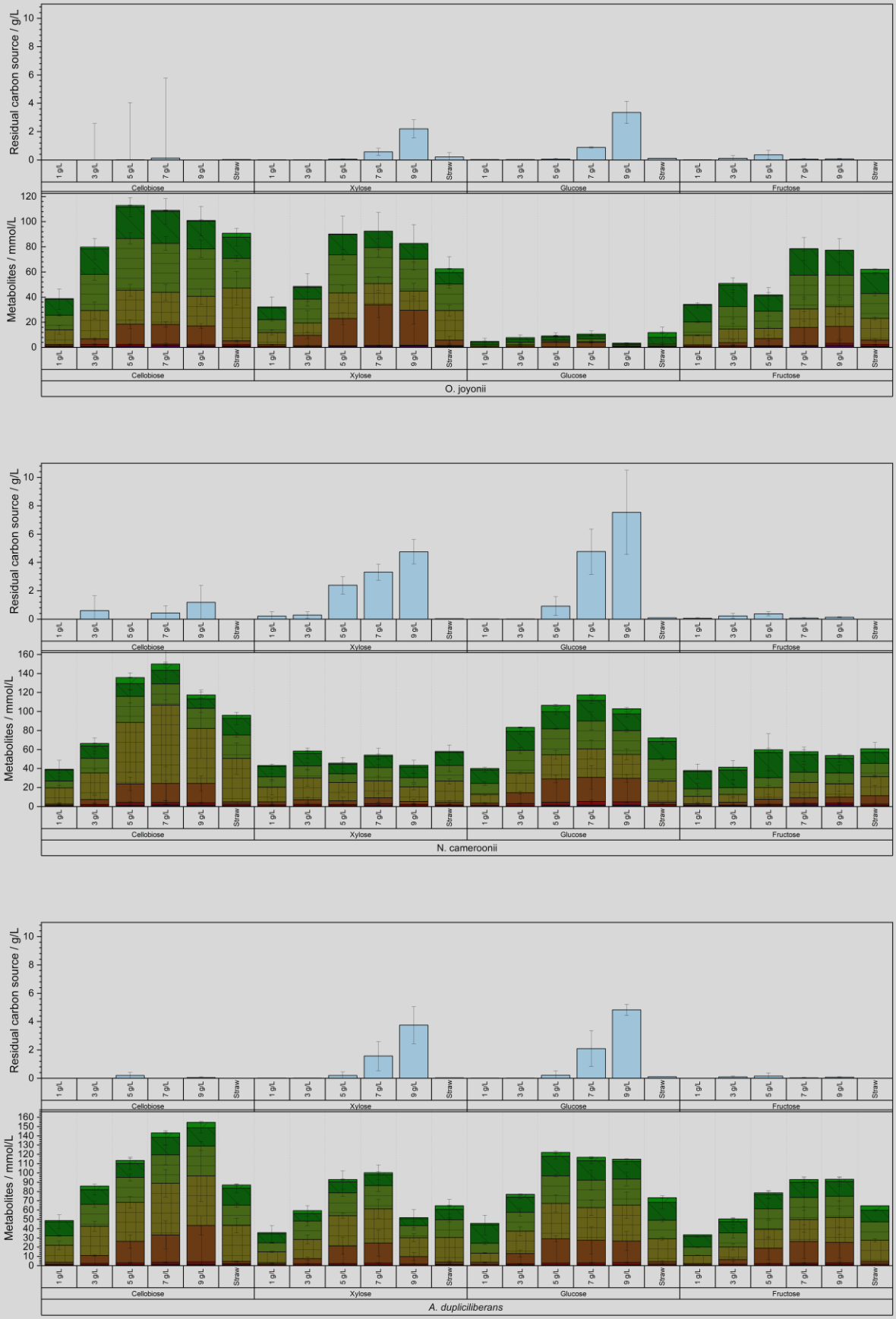

Figure 4: Produced metabolites with the different used soluble C-sources and residual concentration per experiment (n = 3).

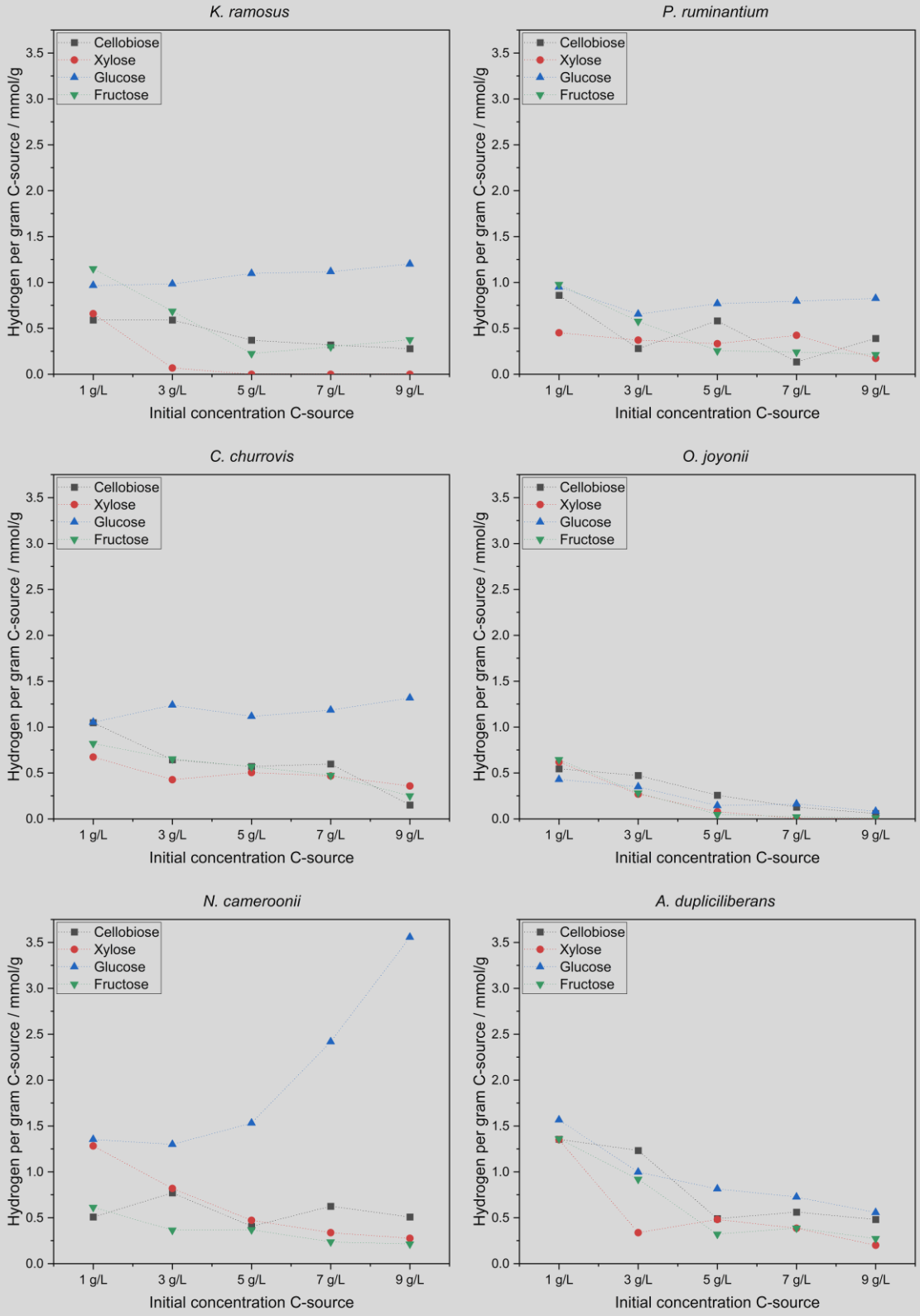

Figure 5: Hydrogen per gram carbon source produced.

Figure 6 gives an overview of the fungal metabolisms and summarizes the observed trends in the collected data.

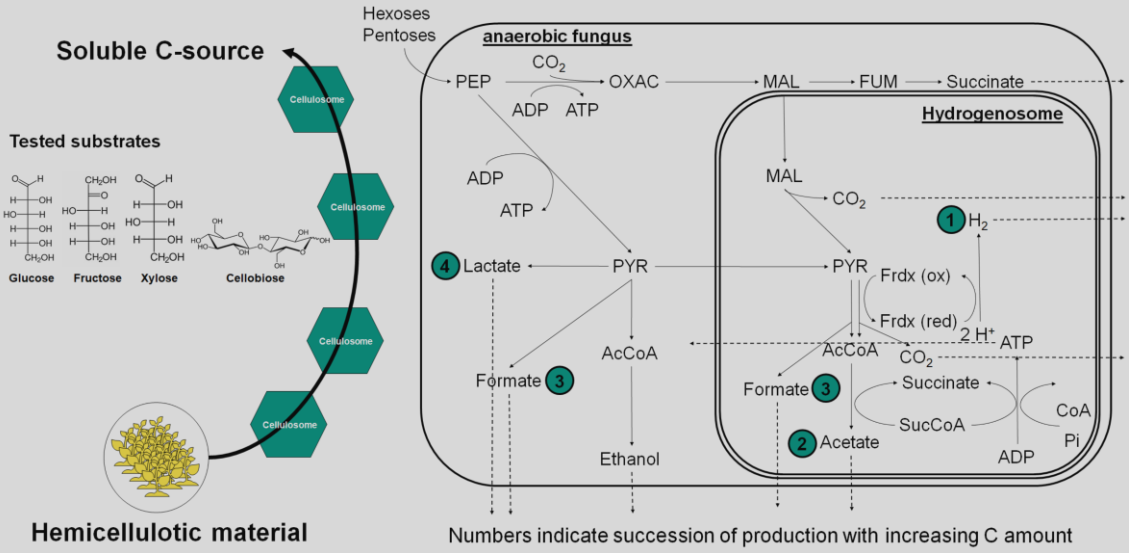

Figure 6: General overview of anaerobic gut fungi metabolic pathways and the succession in production of metabolites with increasing concentrations of soluble carbon source based on growth experiments with the six chosen fungal strains and data from Wilken et al, 2021 [69].

Chapter 1: 3.5 Evaluation batch vs. fed batch

Following the evaluation of different carbon sources and initial carbon source concentrations, two feeding strategies were compared. In both tested approaches, the same amount of liquid carbon source (glucose) was used. In the batch fermentation, the entire amount was added at the start of cultivation. In contrast, the fed-batch fermentation involved daily additions of 1/7 of the total amount over a period of 7 days. Statistical analysis of the differences between the two strategies was performed using the Tukey test as displayed in Figure 7. A detailed analysis of the produced metabolites per strain is displayed in Figure S4. Further statistical analysis is provided in Figure S3.

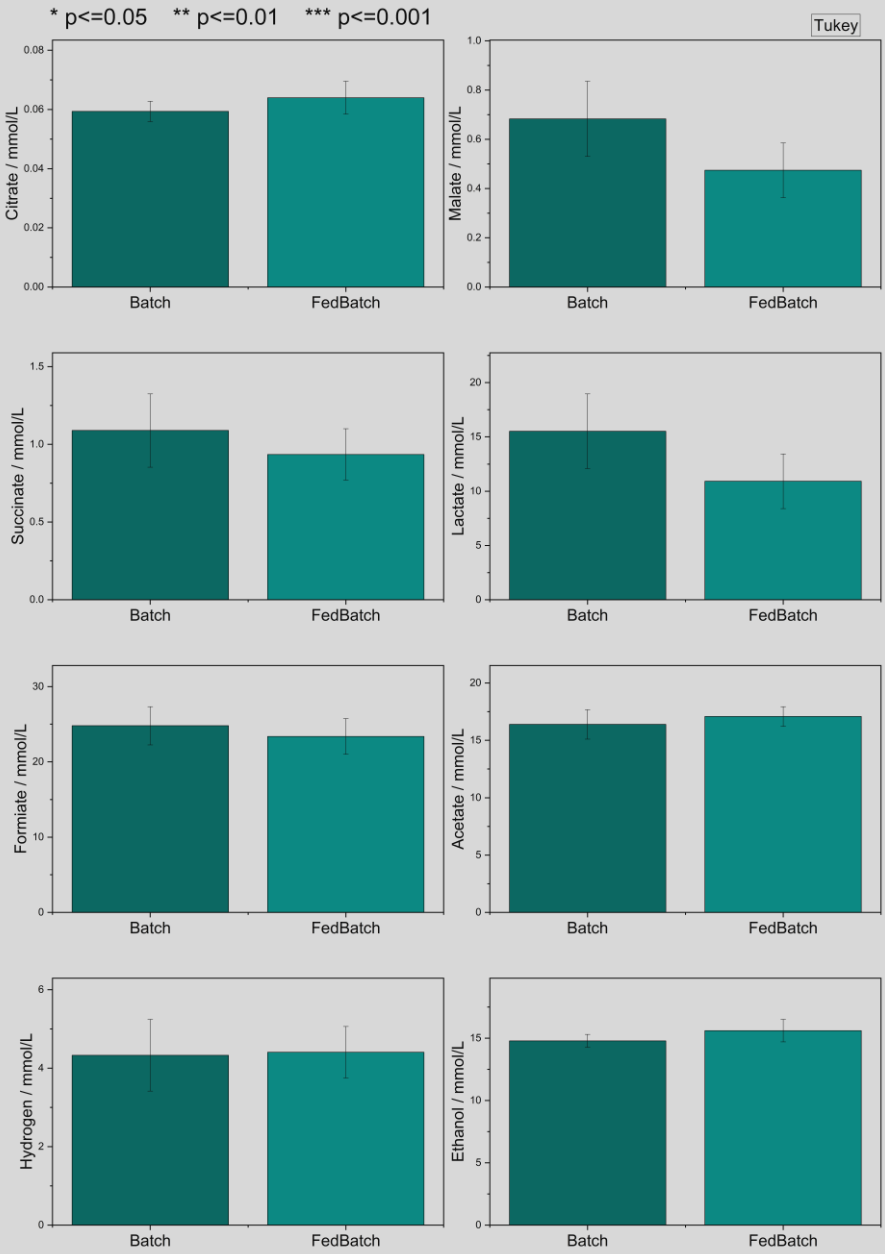

Figure 7: Statistical analysis of the produced metabolites after 7 days of incubation with the Tukey test for all conducted batch and fed batch fermentations in pairwise comparison (n = 18).

No statistically significant differences with $p \leq 0.05$ in the absolute metabolite production were observed between the two feeding strategies across all tested strains.

Chapter 1: 3.6 Biowaste valorization

Based on the results presented above, further questions arose regarding the biotechnological potential of anaerobic fungi, particularly in relation to their versatility in the valorization of various biowastes. To evaluate this potential, the mass of solid carbon source consumed during cultivation—using reed, coffee grounds, organic cucumber peels, organic banana peels, organic carrot peels and organic potato peels—was determined and compared to wheat straw as reference substrate. Relative consumption values, calculated from the total metabolite production in comparison to wheat straw cultivation, are illustrated in Figure 8.

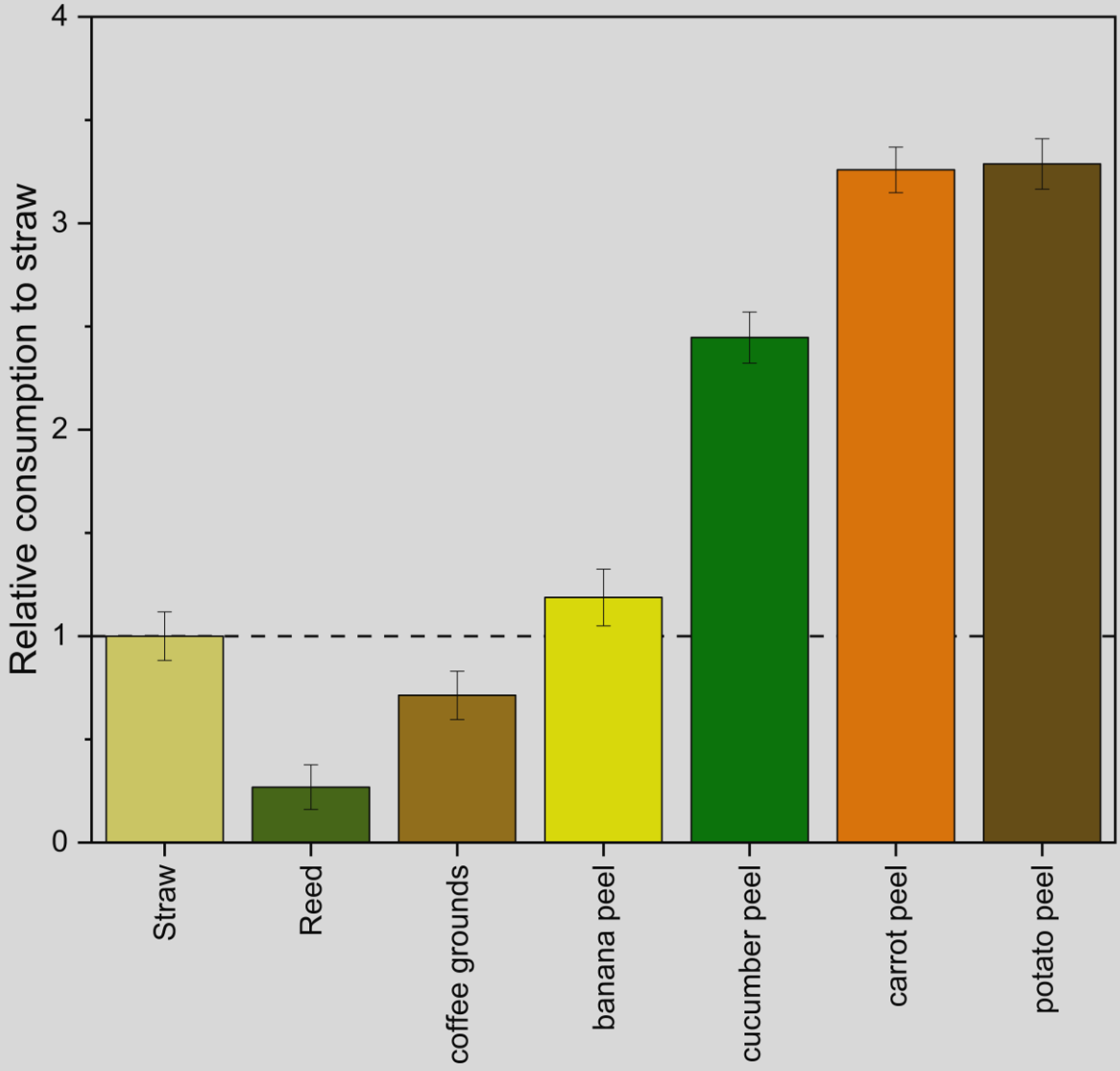

Figure 8: Relative consumption of solid carbon sources tested in comparison to wheat straw (n = 3).

Banana peels, cucumber peels, carrot peels, and potato peels were consumed to a greater extent than wheat straw, indicating higher biodegradability and a promising potential for biowaste valorization. In contrast, reed and coffee grounds exhibited lower consumption rates, suggesting limited suitability as substrates. These findings highlight the promising potential of selected kitchen and environmental waste materials as alternative substrates for anaerobic fungal cultivation.

Chapter 1: 3.7 Starvation experiment with *Orpinomyces joyonii*

Finally, the behavior of *O. joyonii* strain W212 under nutrient-limitation was investigated. This strain had previously shown the highest dependency on solid carbon sources in unpublished pre-experiments—a trend also reflected in the results presented in Figure 5. During prolonged cultivation on a soluble carbon source, a novel growth form emerged. This morphology was documented photographically and is shown in Figure 9. The observed form was consistently reproduced in independent cultivations (data not shown).

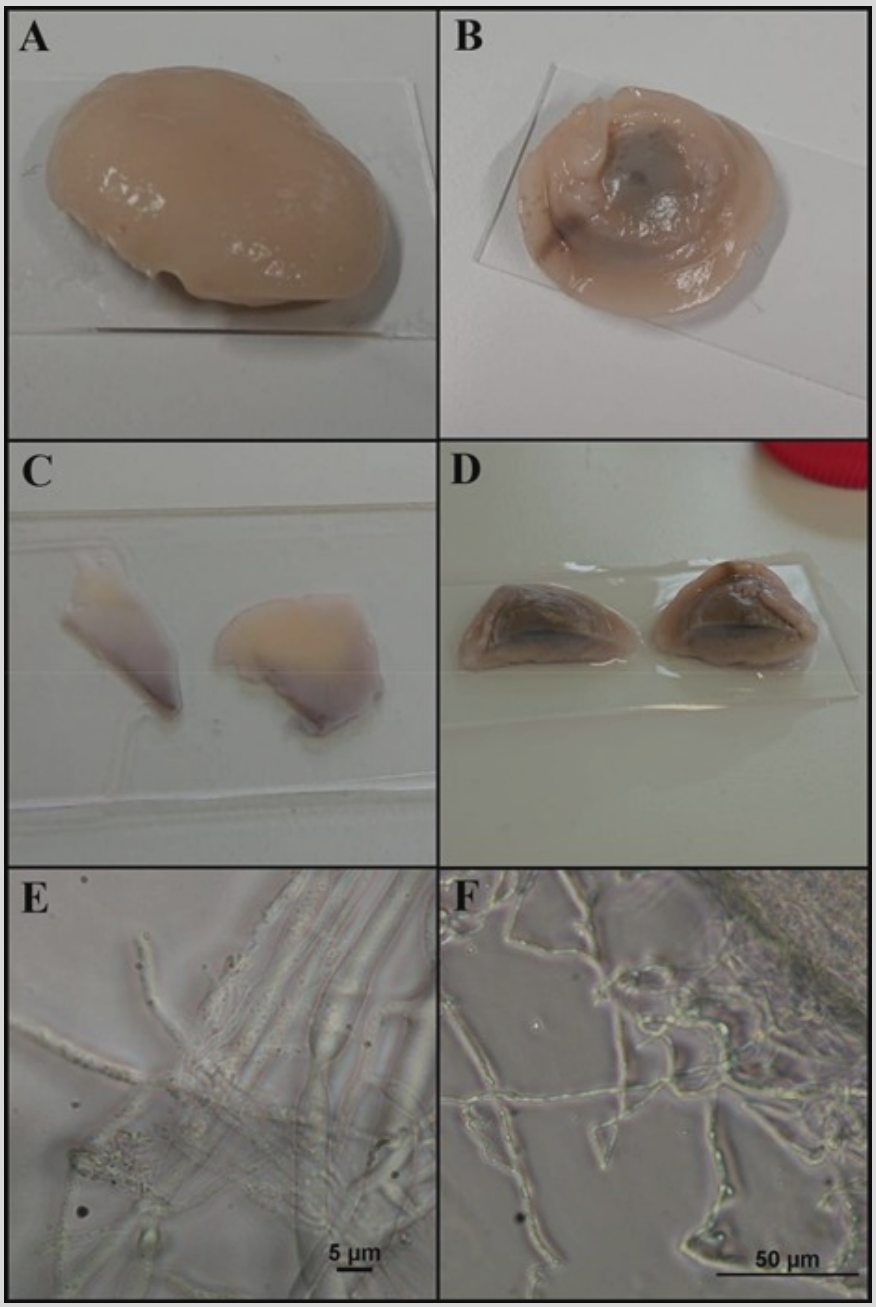

Figure 9: New growth form of O. joyonii emerged after prolonged cultivation on the soluble carbon source glucose. For comparison a standard slide with 26 mm x 76 mm was used. A: View from above, small holes/ channels are visible; B: View from the bottom; C: Slices of the biomass showing a shift in color with the bright sight showing the upper side and the purple side the lower side; D: Biomass cut in half; E and F: Microscopic pictures of the structure in bright field.

Chapter 1: 4 Discussion

To comprehensively assess the metabolic versatility of the investigated strains, a broad screening was conducted to evaluate their ability to utilize a variety of carbon sources. Effective assimilation of these substrates depends not only on the presence of the required genetic and enzymatic machinery, but also on the environmental conditions under which these pathways are activated. Among these, temperature plays a critical role, as enzymatic activity is inherently temperature-dependent [72]. To account for this, temperature screening experiments were performed across a range of conditions. Although all strains exhibited comparable tolerance ranges, distinct differences in their optimal growth temperatures were observed, indicating strain-specific thermal preferences. In addition to identifying optimal growth conditions, the robustness of the strains under suboptimal—particularly cold—conditions was evaluated. *A. dupliciliberans*, *C. churrovis*, and *N. cameroonii* exhibited enhanced thermotolerance and resilience to cold exposure, which is advantageous for industrial applications. This increased robustness facilitates easier handling, storage, and transportation, thereby reducing logistical constraints and associated costs [73].

Another critical factor in the biotechnological application of lignocellulosic biomass is the pretreatment of the selected carbon sources. Such processes are often energy-intensive and economically challenging [7]. To investigate whether substrate particle size influences fungal metabolism, substrates of varying sizes were tested. Interestingly, no significant changes in the overall metabolic profiles of the anaerobic fungi were observed, except for a notable increase in malate concentration when particles of 50 mm were used. Since malate is an intracellular metabolite, its release may indicate cell lysis or metabolic stress. In filamentous fungi such as *Mucor circinelloides*, malate transport is closely linked to metabolic reorganization under stress conditions [74]. It is therefore conceivable that exposure to large particle sizes—which may limit nutrient availability—leads to increased malate release, potentially as a result of prolonged stress or nutrient limitation [75]. This delayed substrate utilization suggests an extended adaptation or starvation phase prior to the onset of active metabolism. These findings imply that, under certain conditions, extensive pretreatment may not be necessary—particularly in large-scale fermentations. Reducing the degree of pretreatment could significantly lower operational costs without compromising metabolic efficiency [76].

Although solid carbon sources are traditionally used for the cultivation of anaerobic fungi, soluble carbon sources offer several notable advantages. These include improved dosing accuracy, enhanced bioavailability, and the potential use of inexpensive side streams like glucose syrup [77,78]. In addition, soluble substrates provide logistical benefits, including reduced transportation costs due to their higher packing density and easier handling in automated systems [79]. Based on the findings from Stabel et al. (2021) the soluble carbon sources glucose, fructose, cellobiose and xylose were investigated [71]. Anaerobic fungi of the phylum *Neocallimastigomycota* exhibit pronounced metabolic flexibility in response to both type and concentration of carbon sources, with significant implications for hydrogen production and metabolite profiles. In the strains *N. cameroonii*, *C. churrovis*, and *K. ramosus*, increasing concentrations of glucose led to elevated hydrogen yields per gram of substrate, despite a reduction in substrate uptake efficiency. Hydrogenosomal metabolism—typically associated with acetate and hydrogen production—was dominant at lower substrate concentrations but declined as cytosolic pathways became more active. The bifurcating hydrogenase proposed by Wilken et al. (2021) may explain the sustained hydrogen output even under high glucose conditions [69].

Overall, this decoupling of substrate uptake and product yield suggests a shift toward overflow metabolism, in which excess pyruvate is redirected from hydrogenosomal pathways to cytosolic mixed-acid fermentation. This results in increased production of lactate, formate, and succinate, mirroring metabolic phenomena such as the Crabtree and Warburg effects observed in other organisms [80]. Notably, *A. duplicilibera*ns and *N. cameroonii* showed increased lactate production at higher sugar concentrations, while *K. ramosus*, lacking lactate dehydrogenase activity, favored the accumulation of formate and succinate. The presence of malate and citrate in the extracellular medium—particularly under xylose-rich conditions—indicates cellular lysis and metabolic stress, especially in strains such as *K. ramosus* and *O. joyonii*. Cellobiose and glucose emerged as the most efficiently metabolized substrates across nearly all strains, likely due to the fungi's robust cellulolytic enzyme systems, including CAZymes and cellulosomes. In contrast, xylose was poorly utilized by most strains, as evidenced by high residual concentrations and low hydrogen yields. An exception was *O. joyonii*, which demonstrated efficient xylose uptake but limited conversion to hydrogen, further supporting a shift toward non-hydrogenogenic metabolic pathways. These findings highlight a dynamic reprogramming of central carbon metabolism in anaerobic fungi, driven by substrate availability and concentration. The transition from hydrogenosomal to cytosolic fermentation under substrate-rich conditions reflects a trade-off between energy efficiency and metabolic throughput. This metabolic shift has important implications for optimizing biotechnological processes such as biohydrogen production and lignocellulosic biomass conversion.

An additional critical parameter for optimizing the production of target metabolites in anaerobic fungal fermentations is the applied feeding strategy. To assess its impact, conventional batch and fed-batch cultivation modes were compared in terms of metabolic output. However, the transition from batch to fed-batch cultivation did not result in any statistically significant improvement in metabolite production. This outcome suggests two potential limiting factors: first, the likelihood of substrate overfeeding in the fed-batch setup, which may have led to metabolic saturation or stress responses; and second, the accumulation of inhibitory end-products, such as organic acids, ethanol or hydrogen—which can negatively affect cellular metabolism and growth. These findings indicate that simply increasing substrate availability through fed-batch operation does not necessarily lead to higher metabolite yields. Instead, they underscore the importance of carefully balancing substrate input with the metabolic capacity of the organism, as well as mitigating the accumulation of inhibitory by-products. Future optimization efforts should therefore consider dynamic feeding strategies—such as feedback-controlled feeding—in combination with in situ product removal or pH control. These approaches can help maintain favorable metabolic conditions and prevent pathway inhibition, thereby enhancing overall process efficiency.

In addition to soluble carbon sources, biowaste materials were considered for further improvement. Comparative analysis revealed that banana peels, cucumber peels, carrot peels, and potato peels exhibited higher consumption rates than wheat straw, indicating superior biodegradability and enhanced suitability as substrates for anaerobic fungal cultivation. These materials likely provide more accessible carbon sources and fewer structural barriers, making them promising candidates for biowaste valorization in fungal bioprocesses [81,82]. In contrast, reed and coffee grounds showed lower degradation levels, suggesting limited applicability due to their recalcitrant composition or potential inhibitory compounds [83,84]. Overall, these findings underscore the potential of selected kitchen waste streams as sustainable and efficient alternatives to conventional lignocellulosic feedstocks in anaerobic fungal biotechnology.

A previously uncharacterized growth form was observed in strain *O. joyonii*, representing a potentially impactful discovery in the life cycle or stress response of anaerobic fungi. Preliminary observations suggest that this morphological shift is induced under conditions of prolonged fiber limitation and sustained environmental stress. The applied cultivation method, which involved gradual starvation, appears to have triggered this transformation. A comparable phenomenon was reported by Stabel et al. (2022) who documented the formation of fungal pellets during fermentation, indicating that morphological plasticity may be a common response to adverse conditions [20]. The nature of this newly observed form remains to be elucidated, but its emergence under stress conditions raises the possibility that it may represent a survival structure or even a sexual reproductive stage. Intriguingly, the formation of such structures may also be influenced by mechanical stimuli, as suggested by the experimental setup from Stabel et al. (2022) [20]. If this hypothesis holds true, it could imply that mechanical forces encountered during gut passage—such as peristalsis or abrasive interactions with digesta—may play a role in triggering developmental transitions. This would have profound implications for understanding the ecology and transmission of anaerobic gut fungi within herbivorous hosts, potentially revealing a mechanism by which fungal propagules are activated or dispersed during host-to-host transfer. Further investigation, including microscopic characterization, transcriptomic profiling, and controlled mechanical stimulation experiments, will be essential to elucidate the biological function and regulatory mechanisms underlying this novel growth form.

Chapter 1: 5 Conclusion

This study provides several novel insights into the metabolic behavior and biotechnological potential of anaerobic gut fungi that go beyond the scope of previous research. While earlier studies such as Stabel et al. (2021) focused on the biochemical characterization of individual strains and their metabolite profiles under standard conditions, and Wilken et al. (2021) explored genomic adaptations like horizontal gene transfer, and Omondi et al. (2024) offered a comparative multi-omics perspective across host species, the present work delivers a systematic, multifactorial analysis of fungal metabolism under varying environmental and nutritional conditions using six distinct strains [66,69,71]. One of the most significant contributions is the discovery of a previously uncharacterized growth form in *O. joyonii* under starvation conditions, which may represent a survival or reproductive stage. This morphological shift, potentially triggered by mechanical stimuli, introduces a new dimension to the ecological understanding of anaerobic fungi and their transmission within herbivorous hosts. Furthermore, the study demonstrates a concentration-dependent metabolic reprogramming, where increasing substrate availability leads to a shift from hydrogenosomal to cytosolic fermentation pathways. This shift is characterized by increased production of lactate, formate, and succinate, and reflects overflow metabolism similar to the Crabtree and Warburg effects observed in other organisms. The sustained hydrogen production under high glucose conditions, potentially mediated by bifurcating hydrogenase activity as proposed by Wilken et al., highlights the metabolic flexibility of these fungi [69]. In addition, the work evaluates the biodegradability of various kitchen waste materials—such as banana, carrot, and potato peels—revealing them as superior substrates compared to wheat straw, which has direct implications for sustainable feedstock selection in industrial applications. Unlike previous studies that focused primarily on lignocellulosic substrates, this research expands the substrate spectrum and demonstrates the fungi's capacity to valorize diverse biowaste streams. Another important finding is that fed-batch cultivation does not improve metabolite yields, likely due to overfeeding and end-product inhibition, emphasizing the need for adaptive feeding strategies and in situ product removal. Moreover, the observation that substrate particle size has minimal impact on overall metabolite production suggests that costly pretreatment steps may be unnecessary, offering economic advantages for scale-up. Taken together, these findings significantly advance the current understanding of anaerobic fungal metabolism and provide actionable insights for optimizing biotechnological processes, from substrate selection to fermentation strategy and ecological interpretation. To further expand the understanding of anaerobic fungal metabolism and its biotechnological potential, we propose several additional experiments. First, pH-dependent cultivation trials should be designed to investigate how varying acidity levels influence metabolic fluxes and product distribution, particularly the balance between hydrogenosomal and cytosolic fermentation. Second, long-term cultivation experiments should be initiated to assess adaptive responses over multiple generations, potentially revealing strain-specific improvements in substrate utilization and stress tolerance, and also showing limitations in the current cultivation strategy. Additionally, co-feeding strategies combining soluble sugars with biowaste-derived substrates should be tested to evaluate synergistic effects on metabolic output and substrate degradation efficiency. To mitigate end-product inhibition, in situ product removal techniques—such as membrane filtration and adsorptive resins—should be explored, aiming to enhance metabolite yields by maintaining favorable fermentation conditions in serum bottles. Mechanical stimulation experiments should also be conducted to simulate peristaltic forces and assess their role in triggering morphological transitions, including pellet formation or stress-induced growth forms. Finally, mixed-strain cultures should be evaluated to determine whether interspecies interactions could promote complementary metabolic pathways and improve overall process performance.

The first chapter therefore establishes the fungal system biologically. However, once the basic product spectrum had been mapped, it became apparent that conventional metabolite analysis might not fully capture the redox behavior of these organisms. Historical and newly generated datasets suggested that under certain conditions a fraction of reducing equivalents could not be adequately accounted for by the standard panel of measured products. This raised a second, more mechanistic question: **does fungal fermentation involve electron sinks or transfer routes that are not visible in classical product analysis?** That question motivates the transition to the next chapter.

3.1.2 Extracellular electron transfer in anaerobic gut fungi in a miniaturized bioelectrochemical system

Whereas the first chapter defines the fungal platform through comparative physiology, the second chapter deepens that platform through a redox-centered perspective. Its role within the dissertation is to investigate whether anaerobic gut fungi possess an additional, previously unrecognized means of electron disposal. This issue emerged directly from the upstream studies, in which electron balances became increasingly difficult to close at higher substrate concentrations. The second chapter therefore takes a step away from classical cultivation physiology and asks a more fundamental metabolic question: **Are there redox processes in anaerobic gut fungi that extend beyond the standard view of mixed-acid fermentation?**

By employing a miniaturized electrochemical cultivation platform, this study introduces a new methodological dimension into the dissertation. It does not simply measure more fermentation products; it tests whether fungal metabolism can interact with external electron acceptors. The identification of ferricyanide-dependent current generation suggests that this is indeed the case. In the broader context of the dissertation, this finding is highly significant, because it implies that fungal metabolism may be governed by a more complex electron economy than previously assumed.

The contribution of this chapter lies in the way it expands the conceptual scope of the upstream platform. The first chapter showed what kinds of products anaerobic gut fungi form. The second chapter asks how these products relate to fungal electron disposal and redox balancing. In that sense, it adds mechanistic depth to the fungal side of the process and prepares the ground for a more rigorous reconsideration of fungal cultivation itself.

Chapter 2: Ferricyanide-dependent current production by *Neocallimastix cameroonii* G341 in a miniaturized anaerobic bioelectrochemical system

Kevin Edward Schulz[1+], Daniel Baron Diaz[1+], Dirk Holtmann[1*]

[1]Institute of Process Engineering in Life Sciences 2: Electrobiotechnology, Karlsruhe Institute of Technology (KIT), Karlsruhe, Germany, [+] contributed equally, * corresponding authors

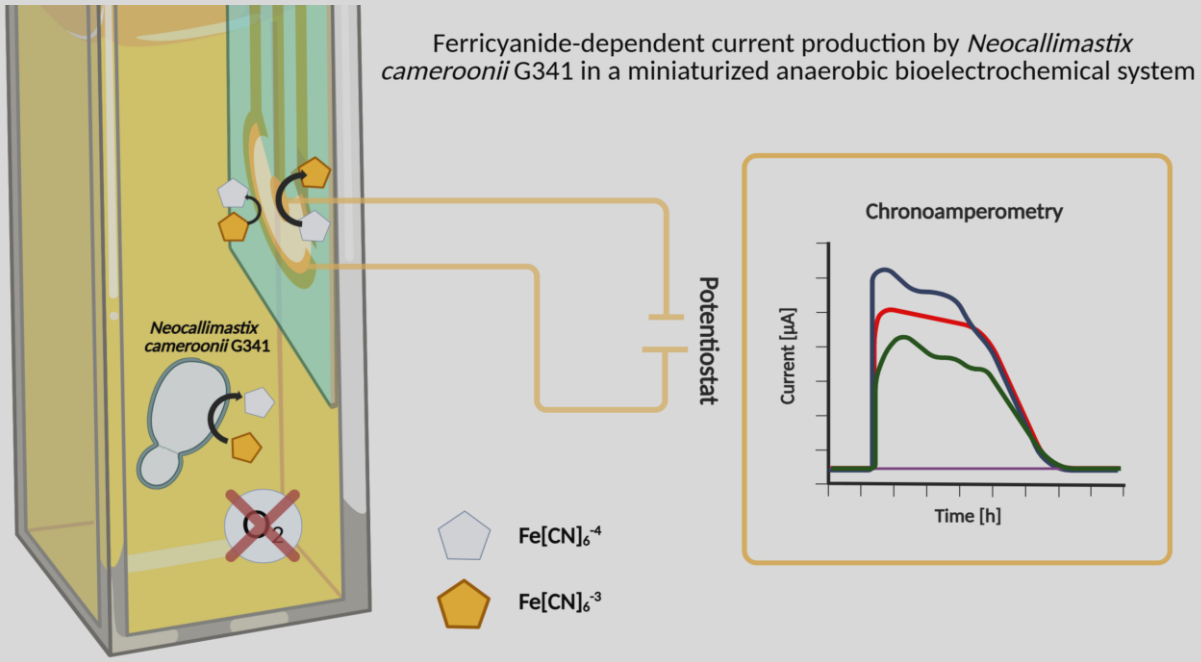

Publishing details:
FEMS Microbiology Letters.
Under Review, submitted 19 May 2026

Author contributions: K.E.S. and D.B.D. were responsible for the conceptualization of the study, carried out the experimental investigations, and developed the methodological framework. They also performed the validation and visualization of the data and jointly prepared the original manuscript draft. D.H. provided essential resources, secured funding for the project, and supervised the overall research activities, including project administration. D.H. also contributed to the writing through critical review and editing of the manuscript.

Chapter 2: 1 Introduction

Electron transfer underpins microbial energy conservation and redox homeostasis, supporting processes such as respiration, fermentation and intracellular redox balancing [85-87]. Research in electroactive bacteria has established several major modes of extracellular electron transfer: direct electron transfer (DET) via outer membrane, multiheme cytochromes or conductive appendages; mediated electron transfer (MET) through diffusible redox-active molecules such as flavins and quinones; and long-range electron conduction through conductive biofilms or protein-based nanowires that enable electron transport over micrometer distances [85-89]. In addition, recent work has shown that electron transfer in some extracellular pathways involves spin-selective multiheme cytochromes, highlighting further mechanistic diversity [90].

While these mechanisms have been extensively studied in prokaryotes, much less is known about how early branching eukaryotes manage electron transfer besides the intracellular electron flow. This knowledge gap is particularly relevant for anaerobic gut fungi (AGF), members of the phylum *Neocallimastigomycota*, which represent some of the most basal fungal lineages known today [22]. Their evolutionary position near the root of the fungal kingdom is reflected in ancient morphological and metabolic traits, including flagellated zoospores and the presence of hydrogenosomes instead of mitochondria, organelles specialized for anaerobic ATP generation and redox metabolism. Because hydrogenosomes rely heavily on electron transfer reactions and produce reduced equivalents such as H_2, they represent a plausible evolutionary precursor to more complex eukaryotic redox systems [28]. Ecologically, AGF are recognized as primary colonizers of lignocellulosic biomass in the digestive tracts of large herbivores. Their invasive rhizomycelia mechanically disrupt plant fibers, while their extensive repertoire of carbohydrate active enzymes initiates the deconstruction of cellulose and hemicellulose, making nutrients accessible for bacteria and archaea in the rumen ecosystem [22,28,91]. This early colonization role allows AGF to shape microbial succession and significantly influence carbon turnover within herbivore digestive systems [22].

Beyond their ecological relevance, AGF have gained attention for their biotechnological potential. Their ability to degrade untreated hemicellulose, positions them as powerful catalysts for sustainable bioprocessing. They can convert hemicellulosic material into reduced metabolites such as hydrogen, acetate, formate, ethanol, and lactate, offering a possible biological route for biohydrogen or electricity generation from plant biomass [92,93]. Given that microbial electrochemical systems rely on the controlled transfer of electrons from metabolic processes to external electrodes, determining whether AGF are capable of participating in such electron transfer is of fundamental interest [85]. Despite the central role of redox metabolism in AGF physiology, it remains unknown whether anaerobic gut fungi can transfer electrons to external acceptors, either directly or through soluble redox mediators. Their hydrogenosomal pathways, syntrophic relationships with methanogens, and extensive oxidative–reductive enzyme systems all suggest that electron transfer might be possible, yet no experimental evidence currently supports this hypothesis.

To address this gap, the present work employs electrochemical techniques with a special focus on eCuvette-based assays. The eCuvette system integrates electrode surfaces directly into a spectrophotometrically compatible cuvette format, enabling simultaneous electrochemical measurement, microbial cultivation, and real-time optical monitoring within eight individual, anaerobic systems [94,95]. This is especially advantageous for AGF, which require strict anaerobic conditions and exhibit slow, filamentous growth that is otherwise difficult to maintain on standard electrochemical platforms. The enclosed geometry of the eCuvette minimize oxygen intrusion, allow continuous monitoring of redox processes, and provide reproducible electrode–biomass interfaces without disturbing delicate fungal structures [95].

The objective of this study is to investigate whether anaerobic gut fungi can perform extracellular electron transfer. Using eCuvette-based electrochemical assays, this study aims to offer the first empirical insight into the redox activity of these basal fungi. Demonstrating such a capability would expand the known functional repertoire of *Neocallimastigomycota*, deepen the understanding of early fungal evolution, and open new opportunities for integrating AGF into bioelectrochemical and lignocellulose-driven bioconversion systems, such as microbial fuel cells [92,93].

Chapter 2: 2 Material and methods

All experimental procedures described in the following sections were conducted with the anaerobic gut fungal strain *Neocallimastix cameroonii* G341, as reported in Schulz et al. [14]. Unless otherwise stated, all chemicals were purchased from Carl Roth GmbH (Karlsruhe, Germany).

Chapter 2: 2.1 Historical electron-equivalent calculations

Electron-equivalent (e-mol) calculations were performed based on the medium composition and fermentation profiles reported in Schulz et al. [14]. Electron equivalents of substrates and metabolites were derived from their degree of reduction, defined as the number of transferable electrons per mole of compound. For each experiment, total e-mol input was calculated from the amount of soluble carbon source converted during fermentation using its established electron-equivalent factor.

Correspondingly, the e-mol contained in fermentation products, including acetate, citrate, formate, lactate, malate, ethanol, and hydrogen were determined from their stoichiometric electron content. The sum of all product-associated e-mol values represented the total recovered electron equivalents. Electron recovery was expressed relative to the initial e-mol supplied via the carbon source, enabling a quantitative assessment of redox balance and reducing-power distribution across strains, treatments, and cultivation conditions.

Chapter 2: 2.2 Anaerobic gut fungal medium and preculture preparation

Preculture preparation and medium formulation followed the procedure described by Schulz et al. [14]. Briefly, the medium was prepared by combining two phosphate-based salt solutions with a hemin-containing zoospore inducer and resazurin as a redox indicator. Sodium bicarbonate was added as a buffering component, L-cysteine hydrochloride served as a reducing agent, and a defined trace element solution supported fungal growth.
Due to the fact that a soluble carbon source was used, demineralized water was added to reach a final mass of 890 g. The medium was mixed in Fernbach flasks, sparged with 100% CO_2 to establish anaerobiosis, and adjusted to pH 6.9. It was then dispensed into serum bottles, sealed with butyl rubber stoppers and aluminum crimps, and autoclaved. After sterilization, each bottle was supplemented with 45 g/L sterile glucose, a vitamin solution, and an antibiotic mix immediately prior to inoculation.

Chapter 2: 2.3 e-Cuvette Screening I

Electron transfer activity was quantified using the e-Cuvette system, which enable parallel electrochemical and photometric measurements in standard 4-mL cuvettes equipped with screen-printed gold electrodes (C220 AT Deutsche Metrohm GmbH & Co. KG, Germany) as described by Gemünde et al. integrated into a Cary 60 UV-Vis spectrophotometer (Agilent, USA) and controlled using a multi-channel potentiostat (PalmSens BV, Netherlands) [95]. Special care was taken to seal the cuvettes once assembled. This was done by including rubber sealings and closing the space between cuvette and lid using a two-part polymer, since the medium did not permit to use pure N2 to keep anaerobic environment as in the original setup by Gemünde et al.. The cuvettes were sealed first and then sparged with N_2 for 15 min at 12 mL/min to displace oxygen. Afterwards, the cuvettes were filled with medium and the potential of the anode was poised. After equilibration, 0.2 mL of inoculum was transferred into each cuvette using a syringe.

Electrochemical potentials applied for the reoxidation of the mediators and measurement parameters were applied as outlined by Gemünde et al. Anaerobic gut fungal medium was supplemented with redox mediators following the procedure of Gemünde et al. (2024), who demonstrated substantial variation in turnover number, reduction kinetics, and physiological impact depending on the mediator used. Mediator species and concentrations were therefore prepared according to Table 1, as in the referenced study to ensure consistency across experiments [94]. Additionally, to ensure that the current response results from a biological signal, temperature control was switched off for 5 hours after 24 h of cultivation and switched on again to see if the current could be recovered by cultivating at the optimal growth temperature. Due to extremely low biomass concentrations no optical detection in the applied system was applied.

Table 1: Redox mediators evaluated in the electrochemical screening, including the applied working electrode potentials (mV vs. Ag/AgCl, 3 M KCl) and the corresponding final concentrations in the e-Cuvette.

Compound name	Applied potential (mV *vs.* Ag/AgCl 3M)	Final concentration in cuvette (µM)
Ferricyanide	500	1000
Methyl red	300	50
Methyl viologen	-400	625
Phenazine ethosulfate	300	50
Phenazine methosulfate	300	50
Resazurin	0	100
Riboflavin	300	100

Chapter 2: 2.4 e-Cuvette Screening II

Based on the results of Screening I, the two most promising mediators were selected for further validation experiments. Each mediator was tested in duplicate at the same concentration as used in Screening I in order to confirm the previous findings under identical conditions, except for the temperature switch. For each mediator, two corresponding control experiments were performed under identical conditions: one control lacking cells to determine abiotic background signals, and one control lacking the respective mediator to assess baseline electrochemical activity of the culture. All assays were conducted using the same e-Cuvette setup and measurement parameters as described above, ensuring consistent electrochemical and photometric monitoring.

Chapter 2: 2.5 Electrochemical characterization

Cyclic voltammetry (CV) was performed following the method described by Gemünde et al. (2024) using screen-printed gold working electrodes and an 60 mm Ag/AgCl (3 M KCl) reference electrode (Pine Research, Durham, USA) [94]. Five CV scans were recorded at a scan rate of 10 mV s^{-1} at 39 °C, with the potential window depending on the redox potential of the mediator used according to Gemünde et al. (2024) [94]. Chronoamperometry (CA) was applied to monitor the re-oxidation of the mediators on the anode surface during the experiment, recording one datapoint every 30 seconds. The applied potential depended on the mediator used according to table 1 and on the cuvette w/o mediator a potential of 500 mV vs. Ag/AgCl (3M KCl) was used. The data was recorded using the MultiTrace Software V 4.5 (PalmSens BV, Netherlands).

Chapter 2: 3 Results and discussion

To place the electrochemical assays in a metabolic context, we first re-analysed previously published fermentation datasets from anaerobic gut fungi, including *N. cameroonii* G341, cultivated on different carbon sources. This analysis was used to assess the apparent distribution of electron equivalents among the routinely quantified fermentation products shown in Figure 1. In parallel, we evaluated known redox-active components of the cultivation medium to estimate whether medium-derived compounds could contribute to background redox activity in subsequent eCuvette assays. These analyses provided context for interpreting the electrochemical experiments but were not used as direct evidence for extracellular electron transfer. Figure 10 shows an apparent decrease in electron recovery at higher initial carbon concentrations. This indicates that a smaller fraction of the supplied electron equivalents was recovered in the routinely quantified product panel under these conditions. The pattern is compatible with a broader distribution of reducing equivalents into products or pools not captured by the applied analytical workflow, but it does not identify a specific sink. Possible contributors include shifts in fermentative product formation, gas-phase H2, low-abundance or transient metabolites, biomass formation, extracellular material, or medium-associated redox reactions [14,96].

Untargeted metabolomics studies indicate that AGF can produce strain- and condition-dependent metabolites that are not necessarily captured in routine HPLC-based fermentation panels. Reported examples include 2,3-dihydroxyisovaleric acid in *Anaeromyces robustus*, sugars such as maltotriitol, maltotriose and melibiose in *Caecomyces churrovis*, putative terpenoids, and products associated with polyketide synthase or non-ribosomal peptide synthetase potential [97,98]. Such compounds could contribute to incomplete electron recovery if present under the tested conditions, although their contribution was not quantified in the present analysis. Medium components with intrinsic redox activity may also contribute to background redox chemistry. For example, resazurin/resorufin exhibits reversible and pH-dependent electrochemical behaviour and could therefore affect apparent redox balances if reduced or oxidized forms are not quantified [99,100]. In addition, diffusible mediators or redox-active cofactors such as vitamins, quinones or flavins may contribute to incomplete apparent recovery if their reduced pools are not captured analytically [88]. Finally, electron equivalents may be distributed into biomass precursors, extracellular material, maintenance demands or transient polymer pools that are not included in routine product analysis; material-balance frameworks therefore emphasize comprehensive accounting of products and off-gas fractions when evaluating carbon and electron recoveries [96,101]. Overall, the electron-balance analysis suggests that the routinely quantified fermentation products do not fully account for the supplied electron equivalents at higher substrate loadings. The observed gap is likely multifactorial and should be interpreted as motivation for further measurements rather than as direct evidence for extracellular electron transfer.

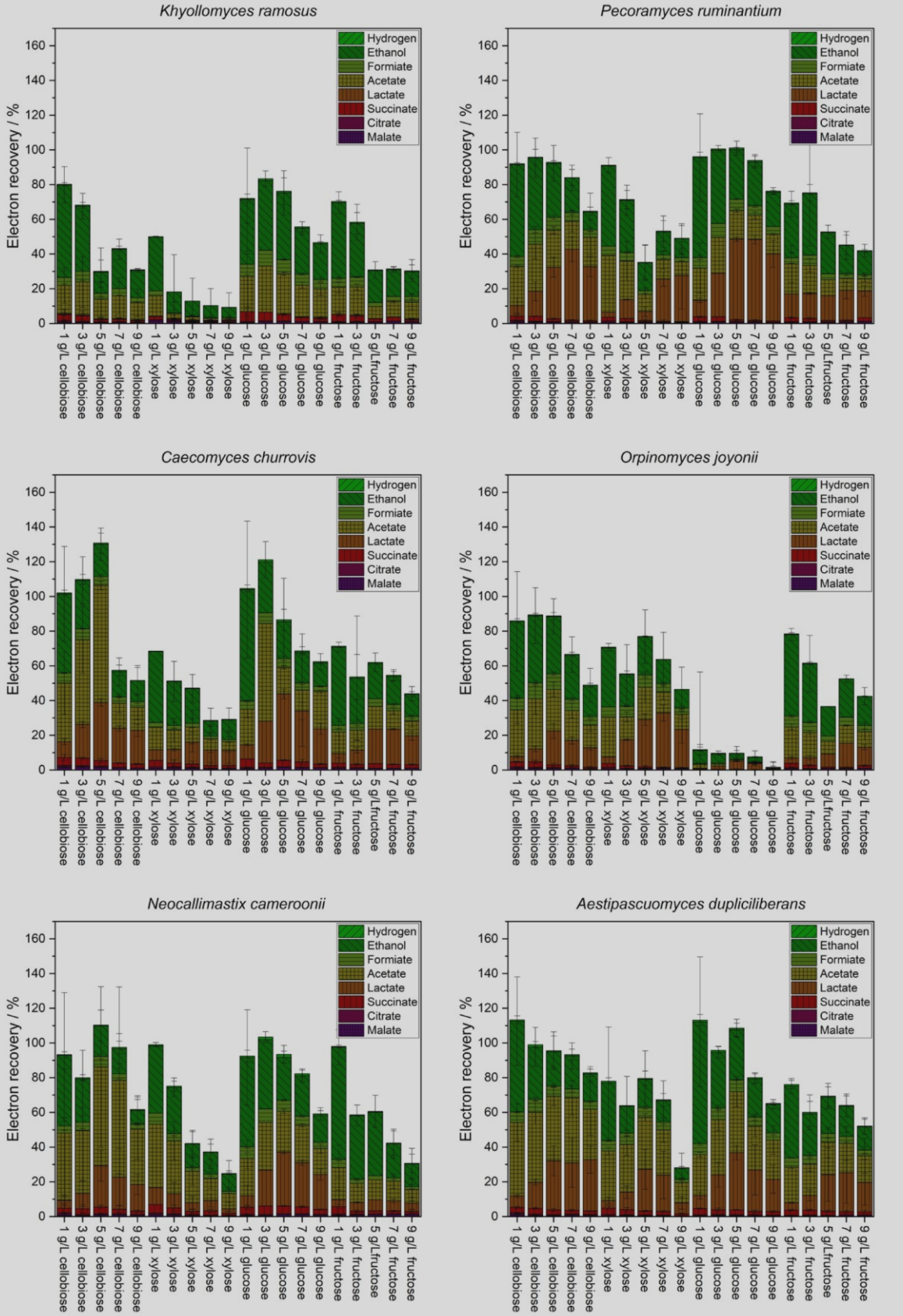

Figure 10: Electron recovery (%) of six anaerobic gut fungal species cultivated on different carbon sources and substrate concentrations, based on published data from Schulz et al. (n = 3) [14]. Stacked bars represent the relative contributions of individual fermentation products (hydrogen, ethanol, formate, acetate, lactate, succinate, citrate, and malate) to total electron recovery. Error bars indicate standard deviation of biological triplicates.

Given the apparent mismatch between supplied and recovered electron equivalents in Figure 10, we next asked whether known redox-active medium components could contribute to background electron-equivalent pools. To address this question, we estimated the theoretical electron-equivalent contribution of selected medium constituents present in the cultivation medium used here and in Schulz et al. (2025) [14]. Table 2 summarizes these calculations and indicates which components could, in principle, participate in redox chemistry under the cultivation conditions.

Several medium constituents, most notably hemin, resazurin, cysteine-HCl and vitamin-derived cofactors, may contribute to redox chemistry. However, the values in Table 2 should be interpreted as theoretical capacities rather than experimentally demonstrated electron sinks during cultivation. Hemin, resazurin and vitamin-derived cofactors are present at comparatively low estimated electron-equivalent concentrations. Cysteine-HCl has a higher theoretical electron-equivalent content, but it is included primarily as a reducing agent to maintain anaerobic conditions and cannot be assumed to function as a terminal electron sink for fungal metabolism. Thus, the medium composition may contribute to background redox chemistry, but the present calculation does not by itself resolve the electron-recovery gap. Instead, it indicates that subsequent electrochemical measurements require abiotic and mediator-free controls to distinguish cell-associated current responses from medium-derived background signals.

Table 2: Composition of the anaerobic gut fungus medium (based on in Schulz et al.) and assessment of intrinsic redox-active components. Listed are the individual medium constituents, their redox activity, and their final electron acceptor capacities in Emmol L^{-1} where applicable [14].

Medium component	Contains redox active species?	Emmol/L
Salt Solution 1	No	-
Salt Solution 2	No	-
Hemin	Yes	0.0031
Resazurin	Yes	0.0175
MilliQ Water	No	-
NaHCO3	No	-
Cystein HCL	Yes	6.3444
Trace Element Solution	Yes, but only in traces	-
Carbon Source	No	-
PAS	No	-
Vitamin Solution	Yes, Vitamin B2 and B12	Vitamin B2: 0.0097 Vitamin B12: 0.0003

The electron-balance and medium-composition analyses indicated that electrochemical experiments were needed to test whether *N. cameroonii* G341 can interact with externally supplied redox mediators under anaerobic conditions. We therefore performed an exploratory screening with seven chemically distinct mediators spanning a range of redox potentials and chemistries in the eCuvette platform. The aim of this screen was not to identify the physiological origin of the unrecovered electron equivalents in Figure 10, but to determine which mediators generated measurable current responses under the applied assay conditions.

Because the first screen was performed as single experiments, the data were used only to select mediators for follow-up validation rather than for inferential conclusions. Figure 11 shows mediator-specific current profiles under the applied conditions. Ferricyanide (FEC) and methyl viologen (MV) produced the largest normalized responses in this exploratory assay and were therefore selected for validation in duplicate cultures with abiotic and mediator-free controls.

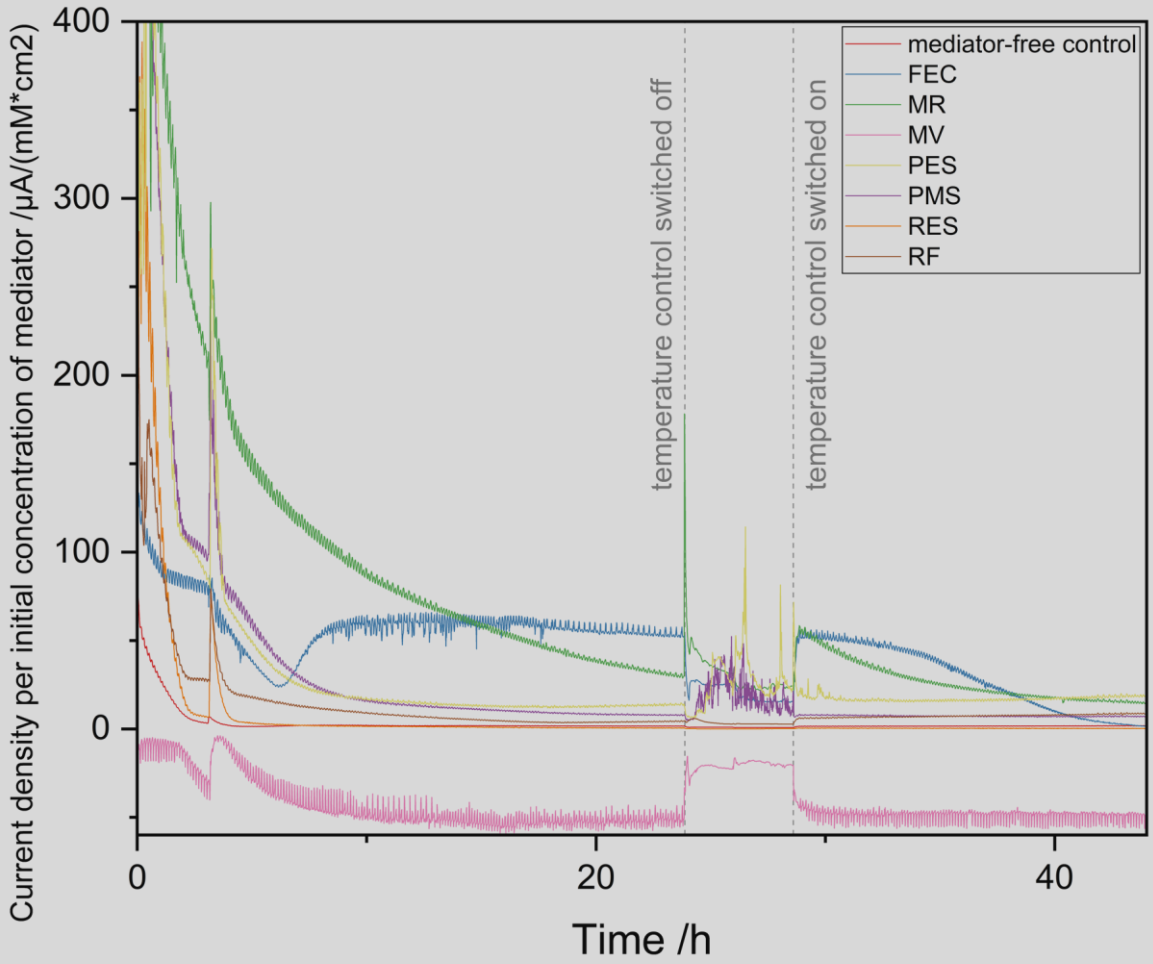

Figure 11: Screening of redox mediators for extracellular electron transfer in the eCuvette platform. Current density normalized to the initial mediator concentration (µA mM⁻¹ cm⁻²) is shown over time for cultures supplied with ferricyanide (FEC), methyl red (MR), methyl viologen (MV), phenazine ethosulfate (PES), phenazine methosulfate (PMS), resazurin (RES) and riboflavin (RF), alongside a mediator-free control. All experiments were conducted under anaerobic conditions at 39 °C. A temporary temperature switch off (indicated by dashed lines) after (24 h) was introduced to assess the biological contribution to current generation and the capacity for recovery upon reinstating cultivation temperature (29 h). Data represent single experiments (n = 1).

The exploratory screen revealed substantial differences in current response among the tested mediators. FEC and MV generated the highest normalized current densities, whereas the mediator-free culture showed a low background current under the applied conditions. FEC displayed a transient response that declined after approximately 35 h and approached baseline after approximately 45 h. The control without mediator yielded current densities around 2 µA cm-1, which were stable over time, suggesting either a direct interaction with the anode or through one or several of the dissolved redox molecules in the medium (see Table 2 and Figure S5). To ensure that signals indeed reflected fungus-mediated electron transfer and were not artifacts of mediator chemistry or electrode interactions, we performed a targeted replication experiment. In this follow-up assay, both FEC and MV were tested in biological duplicates alongside two separate control sets: (1) abiotic controls without cells, capturing mediator-only electrochemistry, and (2) biological controls without mediator, capturing endogenous electrode-culture interactions. The resulting dataset, presented in Figure 12, clearly separates biological and abiotic contributions and demonstrates that only FEC produces reproducible, fungus-dependent current responses that rise well above abiotic backgrounds. In contrast, MV which initially appeared promising in the broad screening of Figure 11—was revealed in the replicated experiment to generate predominantly abiotic current signals, with no consistent enhancement attributable to biological activity.

This validation step was essential to confirm that the electrochemical features previously interpreted as potentially biological in Figure 11 were not artifacts arising from mediator-specific redox chemistry. By isolating the mediator-only reaction, the culture-only background, and the mediator-with-cells condition, Figure 12 provides evidence that biologically mediated extracellular electron transfer in this system is detectable only with ferricyanide, while MV does not support biological electron harvesting under the tested conditions.

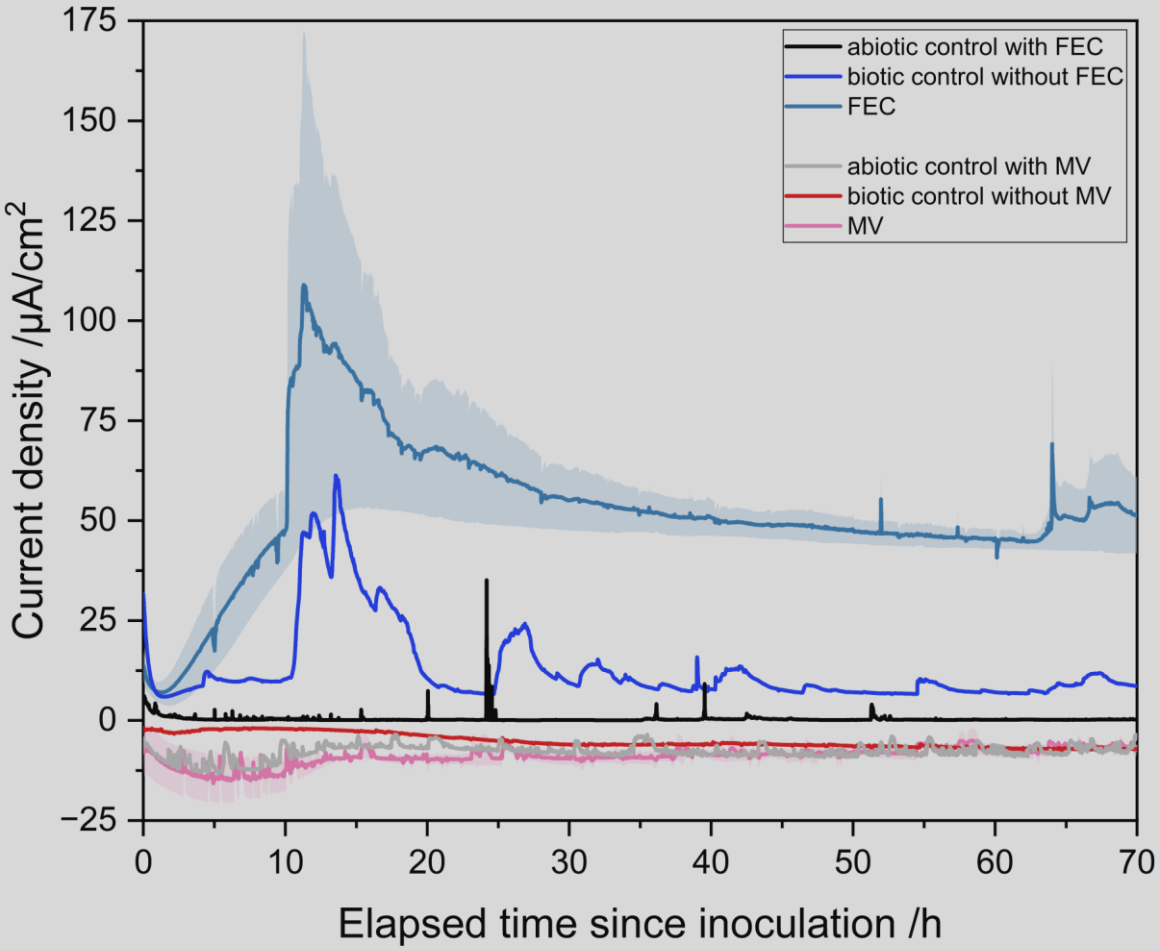

Figure 12: Chronoamperometric current density profiles of anaerobic gut fungal cultures cultivated in the eCuvette platform with methyl viologen (MV) or ferricyanide (FEC) as redox mediators. Shown are biological replicates for cultures with mediator (Cells + MV, Cells + FEC), corresponding biotic controls lacking mediator (Cells w/o MV, Cells w/o FEC), and abiotic controls containing mediator but no cells (MV abiotic control, FEC abiotic control). Current density (µA cm⁻²) is plotted against elapsed time since inoculation. A pronounced and reproducible current response is observed in the presence of ferricyanide and cells, whereas methyl viologen and all control conditions show no sustained positive current generation, confirming mediator-specific and fungus-dependent electron transfer.

Because mediator chemistry can contribute to current responses independently of cells, we next examined whether ferricyanide and methyl viologen retained characteristic electrochemical features after incubation in the cultivation medium. This control was important for assessing whether major changes in mediator electroactivity could have influenced the interpretation of the chronoamperometric data. Mediator-free cultures produced a low but detectable background current at 500 mV vs. Ag/AgCl (3 M KCl). Because this signal was noisy and was not resolved mechanistically, it was not interpreted as evidence for direct electron transfer. Possible contributors include endogenous redox-active medium components, electrode-associated background reactions or cell-associated redox processes that require further controls. Samples containing ferricyanide or methyl viologen from the validation experiment were therefore analysed by cyclic voltammetry (CV). CV provides electrochemical fingerprints of redox-active compounds and can reveal major changes in peak position, peak shape or reversibility. However, it does not exclude all possible chemical side reactions, complexation events or minor transformations in the medium. As shown in Figure 13, both mediators retained characteristic redox features in the cultivation medium. Ferricyanide showed the expected Fe(III)/Fe(II)-associated response in the positive potential range, whereas methyl viologen showed redox features consistent with its known stepwise reduction behaviour in the negative potential range. Additional peaks in the methyl viologen region likely reflected overlap with resazurin/resorufin species present in the cultivation medium. Overall, the CV data argue against a gross loss of mediator electroactivity during the assay, but they do not by themselves prove complete chemical stability.

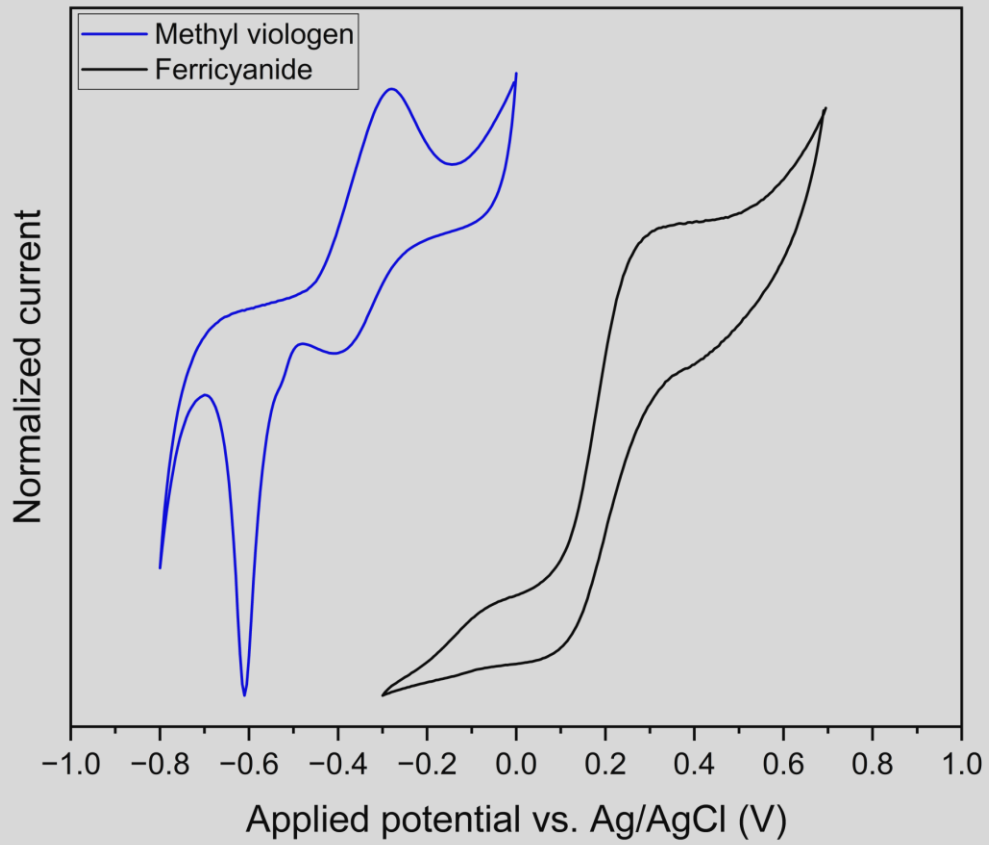

Figure 13: Cyclic voltammograms of the two mediators used in the second eCuvette experiments, methyl viologen (blue) and ferricyanide (black), recorded under anaerobic conditions. Current is normalized for better comparison, and potentials are reported versus Ag/AgCl (3 M KCl). The voltammograms confirm the characteristic redox behavior of both mediators within the applied potential window and indicate their electrochemical integrity in the experimental medium.

This study set out to probe whether AGF can engage in extracellular electron transfer (EET) under anaerobic, small-volume conditions using an integrated eCuvette platform. Across historical data and controlled fermentations, we first confirmed a consistent electron-recovery gap at increasing substrate load, which could not be reconciled by the limited pool of medium-intrinsic electron sinks (Table 1). This narrowed the plausible explanations to biological sinks (overflow metabolism, gas-phase H_2, episodic/low-abundance metabolites) and/or electron flow to external acceptors. That logic motivated a mediator screen (Figure 11), a targeted replication with controls (Figure 12), and mediator integrity checks by cyclic voltammetry (Figure 13). Together, these experiments indicate that ferricyanide (FEC) supports a reproducible, fungus-dependent current response in our system, while both mediators remained chemically intact in the medium.

Two lines of reasoning support a biological interpretation of the FEC signal. First, time-resolved current profiles exhibited characteristics of living systems (rapid onset, sustained plateaus, thermal responsiveness), and these features disappeared in abiotic controls. Second, cyclic voltammetry verified the expected redox signatures of ferricyanide/ferrocyanide without loss of reversibility or peak position, ruling out medium-induced degradation as a confounder. Hence, current arises from fungal redox activity capable of reducing FEC. Conceptually, such mediated electron transfer sits comfortably within the broader EET canon, in which soluble shuttles bridge intracellular redox metabolism and extracellular acceptors (e.g., flavins/quinones in bacteria) [88]. Notably, the observed stable current densities of approximately 50 µA cm^{-2} were achieved at very low biomass concentrations. Under the given cultivation conditions, AGF typically reach ~0.24 g L^{-1} biomass, corresponding to roughly 8 × 10^{-}4 g biomass in the cuvette volume. When normalized to biomass, this indicates a strong interaction between AGF and FEC (62500 µA cm-2 $gCDW^{-1}$). For comparison, current densities of ~150 µA cm^{-2} have been reported for *Cupriavidus necator*, a non-electroactive microorganism, cultivated in a bioelectrochemical system, representing a specific current density of 900 µA cm-2 $gCDW^{-1}$, highlighting the comparatively high biomass-specific electrochemical activity of AGF [94,102,103].

This brings up the question of how AGF could maintain such high specific current densities despite lacking bacterial outer-membrane cytochromes. There are several possibilities based on AGF physiology:

- Hydrogenosome-proximal electron disposal: AGF hydrogenosomes generate reduced products (e.g., H_2) that reflect strong intracellular electron pressure, and elevated reductant supply can broaden metabolic repertoires. Any exogenous shuttle with favorable potential could intercept electrons that would otherwise leave as reduced metabolites or H_2 [28,93].
- Secreted or surface-associated redox enzymes: While classical multiheme cytochromes are a bacterial hallmark, MET can be catalyzed by soluble or peripherally associated enzymes that reduce external mediators without requiring conductive appendages [87].
- Low-abundance or episodic metabolites as endogenous shuttles: Untargeted metabolomics increasingly reveals strain- and condition-specific minor metabolites (e.g., 2,3-dihydroxyisovaleric acid; sugars like maltotriitol/maltotriose/melibiose; putative terpenoids), and bioinformatic searches show PKS/NRPS potential in AGF; such compounds could transiently participate in redox cycling but escape routine analytics [97,98].

Using eCuvette-based electrochemistry under strict anaerobic conditions, we provide first experimental evidence that an anaerobic gut fungus can engage in mediated extracellular electron transfer with ferricyanide as the external acceptor. Establishing AGF as electroactive eukaryotes broadens the known functional repertoire of *Neocallimastigomycota* and opens routes to bioelectrochemical systems. The next steps are to generalize across strains and growth stages, map redox windows and enzymes, and couple electrochemical readouts to metabolite and gas balances, thereby resolving how EET integrates with hydrogenosomal metabolism and overflow pathways [1,3,23].

In summary, *N. cameroonii* G341's ability to directly utilize hemicellulose and achieve high biomass-specific current densities makes it a promising biocatalyst for microbial fuel cell applications. Its capacity to degrade complex, untreated lignocellulosic substrates enables the direct conversion of renewable biomass into electrical current, eliminating the necessity of expensive, energy-intensive pre-treatment procedures. The comparatively high biomass-specific electrochemical activity observed in this study suggests efficient coupling between metabolic turnover and extracellular electron transfer, even at low cell densities. These features establish anaerobic gut fungi as promising candidates for sustainable bioelectrochemical systems that have been previously underexplored.

After the second chapter, the dissertation has established anaerobic gut fungi as both metabolically versatile and redox-mechanistically intriguing organisms. Yet the question still remains under which cultivation framework these capacities can be expressed reproducibly and interpreted clearly. This becomes especially important because standard AGF cultivation intrinsically couples gas phase, bicarbonate buffering, and pH effects. To turn the fungal system into a true process module, these factors must be disentangled. This leads directly into the third chapter.

3.1.3 Decoupling headspace composition, buffering, and bicarbonate availability in anaerobic gut fungi cultivation

The third chapter constitutes the cultivation-engineering cornerstone of the fungal part of the dissertation. If chapter 1 defines what the fungi can produce, and chapter 2 suggests that their redox physiology is more complex than anticipated, then chapter 3 asks under what physicochemical conditions this biology can actually be stabilized, interpreted, and ultimately controlled. Its central role is to move AGF cultivation from an empirical tradition toward a more mechanistically defined framework.

Classical anaerobic gut fungal cultivation is built around a CO_2 atmosphere and bicarbonate-buffered media. Although practical, this setup makes it difficult to distinguish whether metabolic changes arise from gas atmosphere, buffering chemistry, dissolved inorganic carbon, or pH behavior. The third chapter therefore systematically separates these factors by independently varying headspace composition, non-carbonate buffers, bicarbonate supplementation, pH, and nitrogen supply. The resulting findings fundamentally revise the understanding of AGF cultivation: hydrogen production responds directly to headspace composition, bicarbonate cannot be replaced by external pH stabilization alone, and low but defined bicarbonate concentrations are necessary to restore sustainable activity under decoupled conditions.

Within the dissertation, this chapter performs a vital stabilizing function. It transforms the fungal stage from a promising but convention-bound system into one whose governing cultivation variables can be identified explicitly. This is important not only for fungal physiology itself, but also for any future process coupling, because a downstream interface can only be engineered meaningfully if the upstream process is based on defined and interpretable conditions.

Chapter 3: Beyond Carbon Dioxide: Decoupling Headspace and Buffering Reveals a Bicarbonate Requirement for Anaerobic Gut Fungi Growth

Kevin Edward Schulz[1*], Alisa Pfau[1], Tuba Tarhan[1], Charlotte van Almsick[1], Dominik Scholz[1], Anto Rafael Sikirić[1], Anke Neumann[1*], Katrin Ochsenreither[2]

[1]Institute of Process Engineering in Life Sciences 2: Electrobiotechnology, Karlsruhe Institute of Technology (KIT), Karlsruhe, Germany, [2]Kaiserslautern University of Applied Sciences, Campus Pirmasens, Pirmasens, Germany, * corresponding authors

Publishing details:
Springer Nature – Fungal Biology and Biotechnology
Under Review, submitted 07.05.2026

Author contributions: K.E.S. contributed to conceptualization, formal analysis, investigation, methodology development, validation, supervision, visualization, and writing of the original draft, as well as review and editing of the manuscript. A.P., T.T., C.v.A., D.S. and A.R.S. contributed to investigation and experimental work. A.N. and K.O. contributed to supervision as well as critical review and editing of the manuscript. All authors read and approved the final manuscript.

Chapter 3: 1 Background

Anaerobic gut fungi (AGF), classified within the phylum *Neocallimastigomycota*, are obligate anaerobic eukaryotes inhabiting the gastrointestinal tracts of herbivorous vertebrates, including mammals and reptiles [22,104]. Within the rumen ecosystem, AGF function as primary colonizers of lignocellulosic plant material. Through invasive rhizoidal growth and the formation of appressorium-like structures, AGF penetrate intact plant tissues, physically disrupt recalcitrant cell wall architecture, and thereby enhance enzymatic accessibility [22,105]. In parallel, AGF secrete a broad spectrum of carbohydrate-active enzymes (CAZymes), frequently organized into fungal cellulosome-like multi-enzyme complexes that mediate efficient polysaccharide depolymerization [26,27]. Through combined mechanical and enzymatic strategies, AGF substantially contribute to fiber degradation and carbon turnover in anaerobic digestive systems.

Beyond their ecological relevance, AGF have attracted increasing attention for biotechnological exploitation, particularly in the context of lignocellulose valorization and biological hydrogen production [13,93]. Hydrogen formation in AGF occurs within hydrogenosomes, mitochondria-derived organelles that couple pyruvate oxidation to molecular hydrogen production via reduced ferredoxin-dependent hydrogenases [21]. Because hydrogen represents a direct fermentation end product and a key determinant of redox balance, cultivation conditions that influence hydrogen partial pressure and intracellular carbon flux are expected to strongly affect metabolic performance.

Despite this potential, reproducible *axenic* cultivation of AGF remains technically challenging. Current cultivation strategies are largely derived from the classical Hungate serum bottle technique [106] and typically rely on CO_2-containing headspaces combined with bicarbonate-based buffering systems [13]. While this setup approximates ruminal conditions, it introduces an intrinsic physicochemical coupling between atmospheric composition, carbonate equilibria, dissolved gas concentrations, and medium pH. During batch cultivation in closed systems, metabolic production of H_2 and CO_2 increases headspace pressure, thereby altering gas solubility and shifting fermentation equilibria. In anaerobic fermentative systems, hydrogen partial pressure directly influences metabolic flux partitioning and end-product distribution [107]. Simultaneously, the CO_2/HCO_3^- equilibrium determines extracellular buffering capacity and pH stability. Consequently, atmospheric composition, the buffer system, and metabolic activity become interdependent variables, complicating mechanistic interpretation and reducing reproducibility.

Although earlier studies demonstrated that modified gas compositions can alter fermentation patterns in rumen fungi [107], these investigations did not systematically decouple headspace composition from carbonate-based buffers. Notably, even studies that include N_2 in the headspace often retain substantial CO_2 fractions (typically 30 - 35%) and/or maintain bicarbonate in the medium, such that carbonate equilibria remain functionally coupled to gas-phase composition [107-110]. Thus, the independent contribution of atmospheric composition versus soluble carbon buffers has not been resolved experimentally. Because bicarbonate fulfills a dual role, acting both as a pH buffer and as a participant in inorganic carbon equilibria, alterations in gas phase composition inherently modify medium chemistry. Nitrogen, in contrast, does not participate in carbonate equilibria under cultivation conditions and therefore enables experimental isolation of headspace-dependent effects. From a practical perspective, N_2-based cultivation may also simplify gas handling, because nitrogen can be generated on site using commercially established pressure-swing adsorption or membrane systems, thereby reducing dependence on premixed compressed-gas cylinders and potentially lowering gas-supply costs [111-113]. Establishing N_2-based headspace conditions therefore provides a defined experimental framework to isolate atmospheric redox effects independently of CO_2-driven buffering interactions.

However, atmospheric decoupling alone is insufficient if buffering chemistry remains intrinsically linked to carbonate equilibria. To isolate physicochemical from physiological effects, bicarbonate must be replaced by chemically defined, CO_2-independent buffer systems. Zwitterionic Good's buffers, designed to minimize biological reactivity and metal interactions [29], offer a suitable alternative for stable pH control independent of carbonate dynamics. This strategy enables independent manipulation of headspace composition and medium pH.
Yet, substitution of bicarbonate raises a fundamental physiological question. In many anaerobic systems, dissolved inorganic carbon is not merely a buffering component but functions as a substrate for anaplerotic carboxylation reactions, replenishing oxaloacetate and maintaining carbon flux through central metabolism [114,115]. In anaerobic gut fungi, cultivation has historically required CO_2-containing atmospheres and bicarbonate supplementation [13,116], suggesting that inorganic carbon availability may support metabolic functions beyond extracellular pH stabilization. Whether this reflects a direct metabolic requirement of hydrogenosomal or central carbon metabolism, or merely a physicochemical dependency of conventional cultivation systems, remains unresolved. Consequently, it is unclear whether bicarbonate acts solely as a buffering agent or as a physiologically enabling factor for sustained fungal growth. Whether alternative organic carboxylates can functionally replace this role remains unresolved.

Within such a framework, interpretation of metabolic shifts also requires at least an approximate distinction between altered flux distribution and altered biomass formation. Because anaerobic gut fungi form extensive rhizomycelial networks and strongly associate with particulate substrates, biomass determination remains challenging in structurally heterogeneous cultures [13,108]. This complicates the interpretation of metabolite data, particularly when changes in product formation may reflect either altered flux distribution or differences in biomass accumulation. Because no universally robust method is currently available for all AGF morphologies and cultivation formats, an OD_{750}-based calibration approach was additionally explored as a pragmatic proxy for biomass estimation under defined cultivation conditions. This becomes particularly relevant when nutrient effects are considered. In standard AGF media, ammonium sulfate serves as the primary nitrogen source [13]. The carbon-to-nitrogen (C:N) ratio influences anabolic capacity, biomass formation, and potentially hydrogen productivity. Distinguishing between inorganic carbon limitation and nitrogen limitation is thus critical for rational medium optimization. An initial nitrogen-variation experiment was therefore included to test whether moderate changes in ammonium availability measurably affect biomass formation or hydrogen output under otherwise constant cultivation conditions.

This study first compares CO_2- and N_2-based headspaces while keeping bicarbonate constant, then tests whether non-carbonate buffers can sustain growth in the absence of bicarbonate, determines minimal bicarbonate thresholds under N_2, and examines whether structurally diverse carboxylates can substitute bicarbonate. pH stabilization is then decoupled from bicarbonate supply to identify pH optima under defined inorganic carbon conditions. Finally, an OD_{750}-based biomass proxy is established and applied in an initial nitrogen-variation experiment. The working hypothesis is that inorganic carbon availability and headspace composition dominate metabolic performance, whereas moderate variation in nitrogen supply exerts a smaller effect within the tested range. By experimentally decoupling gas phase, buffering system, and nutrient balance, and by evaluating a practical biomass estimation approach, this study aims to establish a mechanistically interpretable and reproducible cultivation framework for anaerobic gut fungi.

Chapter 3: 2 Methods

The experimental procedures were adapted from previously established anaerobic gut fungi cultivation and analytical workflows [14]. All methods are described in full below to ensure independent reproducibility. Any deviations from the referenced protocol are explicitly indicated in the corresponding sections.

Chapter 3: 2.1 Fungal strains

The anaerobic gut fungal strains used in this study were *Aestipascuomyces dupliciliberans* A252*, Caecomyces churrovis* PP313, *Khoyollomyces ramosus* X2152, *Orpinomyces joyonii* W212, *Pecoramyces ruminantium* SA222, and *Neocallimastix cameroonii* G341. All strains belong to the phylum *Neocallimastigomycota* and were originally isolated from herbivore dung samples and taxonomically characterized as described by Stabel et al. [71]. Strains were maintained under standardized batch cultivation conditions with a seven-day transfer cycle at 39 °C. Unless otherwise stated, inoculation was performed by transferring 5 mL of a 7-day preculture into 50 mL of fresh medium. Prior to transfer, cultures were gently homogenized by manual agitation to disrupt rhizoidal aggregates and ensure comparable biomass distribution within the inoculum. For mechanistic analyses focusing on atmospheric effects, bicarbonate dependency, and metabolic flux distribution, experiments were primarily conducted using filamentous (polycentric) anaerobic gut fungi (*A. dupliciliberans, O. joyonii, P. ruminantium, N. cameroonii).* Polycentric strains form extensive rhizoidal networks and exhibit robust hydrogenosomal activity, providing greater experimental stability under perturbation conditions. Monocentric (bulbous) taxa such as *C. churrovis* and *K. ramosus* were included in the initial atmospheric screening and in biomass quantification experiments to account for strain variability. Preliminary experiments indicated reduced growth stability of monocentric strains under strictly carbonate-independent conditions; therefore, subsequent mechanistic experiments were restricted to polycentric taxa.

Chapter 3: 2.2 Cultivation medium

The minimal cultivation medium used in this study was based on the formulation established by Schulz et al. (2025) [14], with modifications as indicated in the respective experimental sections. The complete composition is provided here to ensure reproducibility. Per liter of medium, 150 mL of salt solution I (3 g L^{-1} dipotassium hydrogen phosphate in demineralized water) and 150 mL of salt solution II (3 g L^{-1} potassium dihydrogen phosphate, 6 g L^{-1} ammonium sulfate, 6 g L^{-1} sodium chloride, 0.6 g L^{-1} magnesium sulfate heptahydrate, and 0.6 g L^{-1} calcium chloride dihydrate in demineralized water) were combined. To support zoospore formation and anaerobic redox control, 2 mL of a hemin solution (0.5 g L^{-1} hemin chloride dissolved in a 1:1 mixture of ethanol and 0.05 M NaOH) and 2 mL of a resazurin solution (1 g L^{-1} resazurin sodium salt in demineralized water) were added. Depending on the experimental setup, demineralized water was added to reach a final mass of 990 g for non-soluble carbon source cultivation or 890 g when soluble carbon sources were used. Unless otherwise specified, sodium hydrogen carbonate (6 g L^{-1}) was included as buffering agent, L-cysteine hydrochloride monohydrate (1 g L^{-1}) was added as reducing agent, and 10 mL L^{-1} of a trace element solution was supplemented. The trace element solution contained (per liter of 0.2 M HCl): 0.25 g manganese(II) chloride tetrahydrate, 0.25 g nickel(II) chloride hexahydrate, 0.25 g sodium molybdate dihydrate, 0.25 g boric acid, 0.2 g iron(II) sulfate heptahydrate, 0.05 g cobalt(II) chloride hexahydrate, 0.05 g sodium selenite pentahydrate, 0.05 g sodium metavanadate, 0.025 g zinc sulfate, and 0.0319 g copper(II) sulfate pentahydrate. Unless stated otherwise, milled wheat straw (particle size 1 mm; Waldhof Qualitätsstroh, Landwirtschaftlicher Betrieb Uwe Hoferichter, Germany) was used as solid carbon source at a final concentration of 5 g L^{-1} and was placed directly into serum bottles prior to sterilization. Soluble carbon sources were sterilized separately and added after autoclaving. After adjustment to pH 6.9 with 4 M NaOH or 4 M phosphoric acid, the medium was dispensed as 50 mL aliquots into 100 mL serum bottles. The bottles were sealed with butyl rubber stoppers and aluminum crimp caps and sterilized by autoclaving. Unless otherwise specified, media were prepared in Fernbach flasks and flushed with 100 % CO_2 prior to distribution to ensure anaerobic conditions. When CO_2 flushing was applied, the medium was sparged until the resazurin indicator turned colorless and was subsequently pH-adjusted under continued CO_2 flow to stabilize the target pH. When N_2-based cultivation was performed, anaerobiosis was established by 20 sequential evacuation and nitrogen overpressure cycles using a custom-built anaerobization station (Figure S6). Each cycle consisted of vacuum application followed by nitrogen pressurization to ensure complete removal of residual oxygen prior to incubation. Immediately before inoculation, each bottle was supplemented with 0.5 mL vitamin solution (not anaerobized, containing 0.01 mg/L thiamine hydrochloride, 0.652 g/L panthothenic acid hemicalium salt, 0.6 g/L nicotinic acid, 0.02 g/L cyanocobalamin, 0.2 g/L biotin, 0.012 g/L pyridoxine hydrochloride, 0.05 g/L folic acid, and 0.05 g/L P-aminobenzoic acid 0.2 g/L riboflavin) and 0.5 mL antibiotic solution (ampicillin sodium salt, streptomycin sulfate, and penicillin sodium salt at 50 g L^{-1} each). Vitamin and antibiotic stock solutions were prepared and sterile-filtered according to Schulz et al. (2025); when not stated otherwise, supplementation volumes were kept constant across all experiments to avoid dilution effects. Unless explicitly stated otherwise, no additional reductants (e.g., sulfide) were used beyond L-cysteine hydrochloride monohydrate.

Chapter 3: 2.3 Experimental setups

Chapter 3: 2.3.1 Gas Atmosphere: CO_2 vs. N_2

To systematically evaluate the influence of atmospheric composition on anaerobic gut fungi cultivation, parallel serum bottle cultures were established under either a CO_2- or N_2-based headspace while maintaining identical medium composition and buffering conditions. The bicarbonate buffer system (6 g L^{-1} $NaHCO_3$) was retained in both treatments to isolate headspace effects from buffer substitution. For the N_2 condition, sealed serum bottles were rendered anaerobic using a custom-built anaerobization unit applying 20 sequential evacuation and 100% nitrogen overpressure cycles (approximately 2 min per cycle). This procedure resulted in removal of dissolved CO_2 from the bicarbonate equilibrium system and caused a reproducible alkaline pH shift. Immediately after completion of the N_2 cycles, pH was determined by aseptically withdrawing a 3 mL sample under minimal atmospheric exposure. The measured pH value (typically 7.5 at room temperature) was used as the reference for both treatments. For the CO_2 condition, bottles were anaerobized using 100% CO_2 and subsequently adjusted with 5 M NaOH to match the pH measured in the N_2-treated bottles. Thus, both treatments were initiated at identical pH values (pH 7.5), reflecting the equilibrium state of the bicarbonate system after CO_2 removal in the N_2 condition. This approach ensured that headspace composition differed exclusively in gas phase chemistry while medium pH was matched between treatments. All conditions were performed in biological triplicates across three independent weekly batches (n = 9 per strain and condition). Cultures were incubated at 39 °C for seven days.

Chapter 3: 2.3.2 Buffer System Evaluation

Following the isolated assessment of atmospheric effects, a second experimental series investigated the impact of buffer substitution under a 100% N_2 headspace. To eliminate the intrinsic coupling between CO_2 and bicarbonate chemistry, all buffer screening experiments were conducted under nitrogen while systematically replacing the bicarbonate buffer system. The minimal medium described in section 2.2 was prepared without sodium hydrogen carbonate for all buffer substitution experiments unless explicitly stated otherwise. $NaHCO_3$ was completely omitted prior to anaerobization to prevent carbonate-based buffering effects. All bottles were rendered anaerobic using 100% N_2 via repeated evacuation and overpressure cycles before autoclaving (121 °C, 20 min). Chemically defined non-carbonate buffering systems were evaluated at discrete concentration levels (0.5–10 g L^{-1}): MOPS, MOPSO, BES, PIPES, ACES, Bis-Tris, Bis-Tris-Propan, phosphate buffer, and citrate–phosphate buffer. Buffering capacity ranges of the tested systems are summarized in Figure S7. For each condition, medium pH was adjusted to 6.9 at room temperature prior to anaerobization using 5 M NaOH or 4 M H_3PO_4. After sterilization and cooling to room temperature, pH was re-measured. Only buffer–concentration combinations maintaining a post-sterilization pH of 6.9 ± 0.1 were considered sufficiently stable and selected for biological evaluation. Because inoculation was performed using precultures maintained under standard $NaHCO_3/CO_2$ conditions, transfer-associated carryover of dissolved inorganic carbon could not be fully excluded during the first cultivation cycle. To minimize potential carryover effects, strains were propagated in a consecutive transfer cycle under the respective N_2-buffer condition before growth stability was evaluated. Conclusions regarding buffer compatibility were based on sustained hydrogen production and metabolite formation observed after serial transfer rather than on the initial adaptation cycle. Buffer stability screening and initial biological evaluation were performed using the model organism strain *N. cameroonii*, selected due to its robust growth and consistent hydrogen production under standard conditions. All conditions were conducted in biological triplicate. Cultures were incubated at 39 °C for seven days under otherwise identical conditions. Growth performance was assessed by headspace pressure development, hydrogen formation via µGC, liquid metabolite profiling via HPLC, and microscopic verification of rhizomycelial network formation.

Chapter 3: 2.3.3 Determination of Minimal Bicarbonate Levels

Based on the results of section 2.3.2, which demonstrated loss of sustained growth under strictly bicarbonate-free conditions, a follow-up experiment was conducted to determine the minimal bicarbonate concentration required to restore reproducible metabolic activity under CO_2-independent conditions. The objective was to assess whether bicarbonate fulfills a physiological role beyond extracellular pH stabilization and to quantify the concentration threshold necessary for stable growth. All experiments were performed under a 100% N_2 headspace to exclude reintroduction of CO_2-dependent carbonate equilibria. The minimal medium described in section 2.2 was prepared without $NaHCO_3$ and subsequently supplemented with defined concentrations of sodium hydrogen carbonate (0, 0.125, 0.25, 0.375, 0.5, 1.0, 2.0, and 3.0 g L^{-1}). The selected concentration increments were chosen to bracket the transition range observed in preliminary adaptation experiments that showed successful growth with 3 g/L sodium hydrogen carbonate (data not shown). The pH was adjusted to 6.9 at room temperature prior to anaerobization using 5 M NaOH or 4 M H_3PO_4. After sterilization (121 °C, 20 min), pH was re-measured to confirm stability before inoculation. To discriminate between bicarbonate-specific effects and potential sodium-associated influences, control conditions were established in which NaCl was added at concentrations equivalent to the molar Na^+ contribution of the respective $NaHCO_3$ treatments. Serum bottles were inoculated with actively growing pre-cultures and incubated at 39 °C for seven days under otherwise identical conditions. Restoration of sustained growth was assessed by headspace pressure development, hydrogen production quantified by µGC, liquid metabolite formation measured by HPLC, and microscopic verification of rhizomycelial network formation. To minimize confounding effects from bicarbonate carry-over via the inoculum, cultures were propagated for at least two consecutive transfer cycles under the respective bicarbonate concentrations. Only growth and metabolic activity observed from the second transfer onward were considered indicative of stable bicarbonate-supported growth. All polycentric anaerobic fungi strains (*A. duplicilibera*ns, *O. joyonii, P. ruminantium,* and *N. cameroonii*) were examined in biological triplicate.

Chapter 3: 2.3.4 Screening of Alternative Carboxylic Acids

To determine whether bicarbonate can be functionally replaced by structurally distinct carboxylic acids, screening experiments were performed under a defined 100% N_2 atmosphere. For the substitution experiment, a concentration of 4 g L^{-1} sodium hydrogen carbonate was selected to ensure non-limiting conditions relative to bicarbonate-supported growth and to minimize the risk of false-negative growth responses due to marginal bicarbonate availability. Accordingly, all candidate carboxylic acids were evaluated at a final concentration of 4 g L^{-1} to allow direct comparison with a growth-permissive bicarbonate condition. The screening was conducted exclusively with *A. duplicilibera*ns A252 in biological triplicate. This strain was selected based on preliminary experiments demonstrating high hydrogen production and total metabolite formation under standard cultivation conditions, thereby providing a sensitive model for detecting growth-supporting or inhibitory effects of alternative carboxylates. Each candidate acid was added to the bicarbonate-free base medium described in section 2.2 at a final concentration of 4 g L^{-1}. Following addition, the medium pH was readjusted to 6.9 at room temperature prior to anaerobization to ensure comparability between treatments. A $NaHCO_3$-containing medium (4 g L^{-1}, added after autoclaving) cultivated under identical N_2 conditions served as positive control. All bottles were anaerobized with 100% N_2 using repeated evacuation and overpressure cycles, sterilized (121 °C, 20 min), supplemented with vitamin and antibiotic solutions, and inoculated with actively growing pre-cultures. Cultures were incubated at 39 °C for seven days. Following cultivation, growth performance was assessed by headspace pressure development, gas composition analysis (H_2, CO_2, N_2) via µGC, and liquid-phase metabolite quantification by HPLC.

Chapter 3: 2.3.5 Metabolic screening using a Dual Buffer System

To systematically evaluate pH-dependent growth effects while minimizing carbonate-driven artefacts, a defined pH gradient experiment was performed under a 100% N_2 atmosphere using a dual-buffer strategy. All cultures were established under nitrogen headspace conditions to eliminate CO_2-dependent carbonate dynamics. The primary buffering system consisted of Bis-Tris (6 g L^{-1}), providing CO_2-independent pH stabilization. Based on the bicarbonate titration experiment (section 2.3.3), $NaHCO_3$ was supplemented at a fixed concentration of 0.5 g L^{-1}, representing the lowest concentration previously shown to support reproducible growth. This concentration was selected to provide minimal inorganic carbon supplementation while limiting perturbation of the predefined pH gradient. Prior to anaerobization, the medium was adjusted at room temperature to defined initial pH values of 5.8, 6.1, 6.4, 6.7, or 7.0. Following nitrogen-based anaerobization, serum bottles were sterilized (121 °C, 20 min). After cooling, $NaHCO_3$, vitamin solution, and antibiotic solution were added aseptically. Cultures were inoculated with actively growing pre-cultures and incubated at 39 °C for seven days under otherwise identical conditions. All polycentric anaerobic fungi strains (*A. dupliciliberans* A252*, O. joyonii* W212*, P. ruminantium* SA222*, and N. cameroonii* G341) were tested in biological triplicate. At the end of incubation, metabolic activity was assessed by headspace pressure development, gas composition analysis (H_2, CO_2, N_2) via µGC, and liquid-phase metabolite quantification by HPLC.

Chapter 3: 2.3.6 Establishment of Biomass detection Using OD_{750} and activated carbon

To establish a reproducible and transferable OD-based biomass quantification method for anaerobic gut fungi, a two-step calibration strategy was implemented. The approach was designed to address both the morphological complexity of AGF cultures and the need for inter-device comparability while minimizing repeated fungal biomass production for calibration purposes. Fungal biomass was generated in 2 L batch cultivations using glucose as sole carbon source (5 g L^{-1}) to ensure homogeneous growth without interference from particulate substrates. Cultures of all six strains were incubated under standard anaerobic conditions at 39 °C until sufficient biomass accumulation was achieved. The biomass was harvested by centrifugation, washed repeatedly with sterile 0.9 g L^{-1} saline solution to remove soluble metabolites, and subsequently freeze-dried to constant weight to obtain defined dry mass samples. Defined dry masses of fungal biomass were weighed and resuspended in saline solution. From these, twelve defined concentration levels were prepared (0.005–0.5 g L^{-1}). Optical density measurements were performed at 750 nm using two independent photometric systems (SPECTRONIC 200 and GENESYS™ 30, Thermo Scientific, USA). Each concentration was measured in ten technical replicates per device and mean values with standard deviations were calculated to assess intra-device variability and inter-device comparability. The wavelength of 750 nm was selected to ensure that measurements predominantly reflected light scattering (turbidity) rather than wavelength-dependent optical absorption. In parallel, activated carbon was processed identically and used as an inert optical reference material at the same mass intervals and concentration levels. The activated carbon standard was measured on both photometric systems under identical conditions. This reference material served two primary purposes: (i) determination of the linear detection range of each photometric system independent of fungal morphology, and (ii) establishment of a transferable calibration reference enabling cross-device standardization by applying instrument-specific correction factors derived from activated carbon response curves. By generating OD_{750} response curves for both fungal biomass and activated carbon on both instruments, instrument-dependent differences in optical response were quantified and normalized, allowing comparability of OD measurements across photometric systems. This strategy provides a non-invasive, turbidity-based biomass detection framework that accounts for AGF morphological complexity while ensuring reproducibility, inter-device comparability, and methodological transferability.

Chapter 3: 2.3.7 Impact of nitrogen source availability

To evaluate the influence of nitrogen source availability on fungal growth and metabolic performance, the nitrogen concentration of the cultivation medium was systematically varied while maintaining a constant carbon supply. The experiment was performed using *Caecomyces churrovis* PP313. This monocentric strain was selected due to its compact thallus morphology and reduced aggregation compared to extensively rhizoidal polycentric taxa, resulting in more homogeneous suspended biomass and improved suitability for turbidity-based quantification. Glucose was used as a defined and soluble carbon source at a fixed final concentration of 5 g L^{-1} in all experiments. Nitrogen availability was modulated by varying the concentration of ammonium sulfate ($(NH_4)_2SO_4$), the primary nitrogen source in the minimal medium. The following concentrations were tested: 0.3, 0.5, 1, 2, and 4 g L^{-1}. At constant glucose concentration (5 g L^{-1}), ammonium sulfate supplementation corresponded to nominal molar C/N ratios of 36.7, 22.0, 11.0, 5.5, and 2.75. These values refer to the variable ammonium sulfate fraction only. All cultures were established in 100 mL serum bottles containing 50 mL medium under standard CO_2 atmosphere with 6 g L^{-1} $NaHCO_3$ buffering at an initial pH of 6.9, consistent with the conventional cultivation setup described in section 2.2. After anaerobization and sterilization (121 °C, 20 min), bottles were inoculated with 5 mL actively growing pre-cultures and incubated at 39 °C for seven days. All conditions were performed in biological triplicate. At the end of the cultivation period, metabolic activity was assessed by headspace pressure measurement and gas composition analysis (µGC), while liquid-phase metabolites were quantified by HPLC. Biomass formation was determined using the OD_{750}-based calibration framework described in section 2.3.6.

Chapter 3: 2.4 Analytics

Chapter 3: 2.4.1 Pressure Measurement as Indicator of Metabolic Activity

Gas formation during cultivation leads to an increase in internal pressure within the sealed serum bottles. Headspace pressure was therefore used as an indicator of metabolic activity. At the end of the cultivation period, bottle pressure was measured while maintaining the bottles at cultivation temperature (39 °C) to avoid temperature-dependent pressure fluctuations. A sterile BD Microlance™ cannula was inserted through the butyl rubber stopper and connected via neoprene tubing (Watson Marlow) and a 0.22 µm sterile filter (Minisart NML, Sartorius) to either a vacuum gauge (G 1111-VAC, Greisinger) or a digital barometer (GDH 14 AN, Greisinger). Pressure values are reported as overpressure relative to ambient atmospheric pressure (Δp, bar). Measurements were performed immediately prior to gas sampling to ensure consistency between pressure and gas composition analysis.

Chapter 3: 2.4.2 Gas Chromatography for Gas Phase Analysis

Headspace gas composition was determined at the end of each cultivation period using a 3000 Micro GC System (INFICON Holding AG) equipped with a thermal conductivity detector (TCD). Prior to sampling, serum bottles were equilibrated at cultivation temperature (39 °C) in a thermostated water bath (ONE 10, Memmert GmbH + Co. KG) to minimize temperature-dependent variability in gas solubility and pressure. A gas sample of 3–5 mL was withdrawn through the butyl rubber stopper using a sterile syringe and introduced into the µGC system, which automatically aspirated the sample at a rate of 10 mL min^{-1} using its internal vacuum pump. Gas separation was performed using a two-channel configuration. Channel A consisted of a PLOTU pre-column coupled to an Rt-Molsieve 5Å main column (Agilent) for quantification of hydrogen (H_2), nitrogen (N_2), and oxygen (O_2), using helium as carrier and reference gas at an operating pressure of 1.72 bar. Channel B employed an Rt-Q-Bond column (Agilent) for carbon dioxide (CO_2) analysis at an operating pressure of 1.38 bar. The injection system, valves, and columns were maintained at 80 °C throughout analysis. Quantification was performed based on peak area integration. Instrument calibration was conducted using a seven-point standard gas mixture covering the expected concentration ranges of hydrogen and carbon dioxide. This analytical setup enabled reproducible and simultaneous determination of headspace hydrogen, carbon dioxide, and nitrogen concentrations under all experimental conditions.

Chapter 3: 2.4.3 High-Performance Liquid Chromatography for Liquid Metabolite Analysis

Liquid-phase metabolites were quantified at the end of each cultivation period using high-performance liquid chromatography (HPLC). From each serum bottle, 2 mL of culture supernatant were withdrawn through the butyl rubber stopper using a sterile BD Microlance™ cannula and transferred into 2 mL microcentrifuge tubes. Samples were centrifuged for 10 minutes at 13,000 rpm using a Heraeus™ Pico 17 centrifuge (Thermo Fisher Scientific) to remove suspended particles and residual fungal biomass. Subsequently, 1 mL of the clarified supernatant was filtered through a 0.22 µm cellulose acetate syringe filter (Restek) and transferred into chromatography vials (Brown Chromatography Supplies) sealed with Teflon-lined caps. Metabolite analysis was performed on an Agilent 1100 HPLC system equipped with a Rezex ROA Organic Acid H^+ (8%) guard column (50 mm × 7.8 mm) and a corresponding analytical column (300 mm × 7.8 mm, 8 µm particle size; Phenomenex Ltd.). The mobile phase consisted of 5 mM sulfuric acid (H_2SO_4) delivered at a flow rate of 0.5 mL min^{-1}. The total run time was 40 minutes. The column compartment and refractive index detector (RID) were maintained at 50 °C to ensure stable baseline conditions. In addition to RID detection, a variable wavelength detector (VWD) set to 220 nm was used for compound-specific absorbance monitoring. Quantification was performed using external calibration curves generated from analytical standards of acetate, ethanol, citrate, succinate, formate, lactate, malate and glucose in the concentration range of 0.1–10 g L^{-1}. Peak areas were integrated using instrument-specific software, and metabolite concentrations were calculated based on linear regression of the respective calibration curves. All calibration curves exhibited coefficients of determination (R^2) ≥ 0.995. This analytical procedure enabled reproducible quantification of major fermentation products and residual carbon sources across all experimental conditions.

Chapter 3: 2.4.4 Statistical analysis

Unless otherwise stated, cultivation experiments were performed in biological triplicate. For the comparison of CO_2- and N_2-based headspaces, biological triplicates were conducted across three independent weekly batches, resulting in n = 9 per strain and condition. OD_{750} calibration measurements were performed in ten technical replicates per concentration and photometric device. Quantitative data were summarized as arithmetic means ± standard deviation (SD), and error bars represent SD. Technical replicates were used to assess measurement variability and were not treated as independent biological replicates. Data were evaluated descriptively on the basis of headspace pressure, gas composition, liquid metabolite concentrations, OD_{750} values, and derived biomass estimates. For inter-device normalization of OD_{750} measurements, polynomial regression of the activated carbon calibration curves was used to derive instrument-specific correction functions.

Chapter 3: 3 Results and discussion

Chapter 3: 3.1 Experimental overview

To guide interpretation of the results, the study was designed as a stepwise dissection of cultivation variables that are coupled in conventional AGF serum-bottle systems. CO_2- and N_2-based headspaces were first compared while retaining bicarbonate to isolate atmospheric effects, and non-carbonate buffers were then screened under N_2 to test whether stable external pH can sustain growth in the absence of bicarbonate. Bicarbonate was subsequently reintroduced in defined concentrations and substituted by structurally diverse carboxylic acids to distinguish a quantitative inorganic carbon requirement from a more general carboxylate effect. Based on these findings, pH optima were determined using a dual-buffer strategy, after which an OD_{750}-based biomass proxy was established and applied in an initial nitrogen-variation experiment (Figure 14).

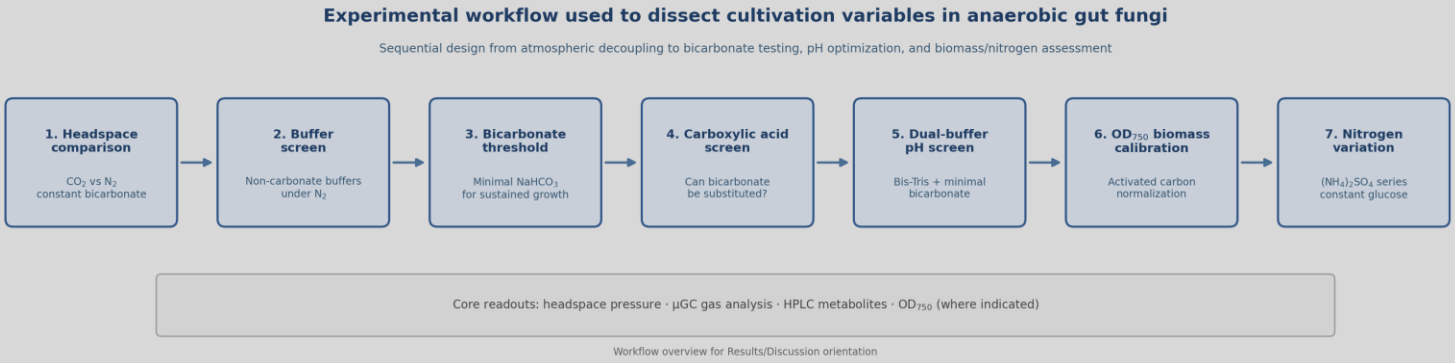

Figure 14: Experimental workflow used to systematically disentangle cultivation variables in anaerobic gut fungi (AGF). Starting from conventional CO_2/HCO_3^--based cultivation, the study sequentially evaluated (i) headspace composition (CO_2 vs. N_2), (ii) non-carbonate buffer systems, (iii) minimal bicarbonate requirements, (iv) substitution by structurally diverse carboxylic acids, (v) pH optima using a dual-buffer strategy, and (vi) an OD_{750}-based biomass proxy, which was subsequently applied in an initial (vii) nitrogen-variation experiment. Core readouts included headspace pressure, µGC gas analysis, HPLC metabolite profiling, and OD_{750} where indicated.

In the following analyses, total metabolite formation refers to the sum in mmol/L of quantified fermentation products measured in the liquid phase by HPLC (acetate, formate, lactate, succinate, malate, and citrate) and in the gas phase by µGC (hydrogen). The combined accumulation of these products is used as an integrative indicator of metabolic activity, as cumulative fermentation product formation correlates with active growth in anaerobic gut fungi [14].

Chapter 3: 3.2 Headspace gas composition shifts hydrogen production

To systematically dissect the physicochemical constraints governing anaerobic gut fungi cultivation, the influence of atmospheric composition was first evaluated while keeping the culture medium composition and pH constant. Because CO_2, bicarbonate buffering, and dissolved-gas equilibria are tightly coupled in conventional cultivation systems, headspace composition is expected to affect redox balance, gas solubility, and metabolic flux distribution. To determine headspace effects independently from buffering chemistry, cultures were established under either CO_2- or N_2-based atmospheres while retaining identical medium composition and bicarbonate concentration. By adjusting both systems to the same initial pH, differences in growth performance and metabolite formation could be attributed specifically to atmospheric conditions rather than to pH variation or buffer substitution. Therefore, hydrogen production was quantified under CO_2- and N_2-based headspace conditions while maintaining identical bicarbonate-buffered medium and matched initial pH (Figure 15).

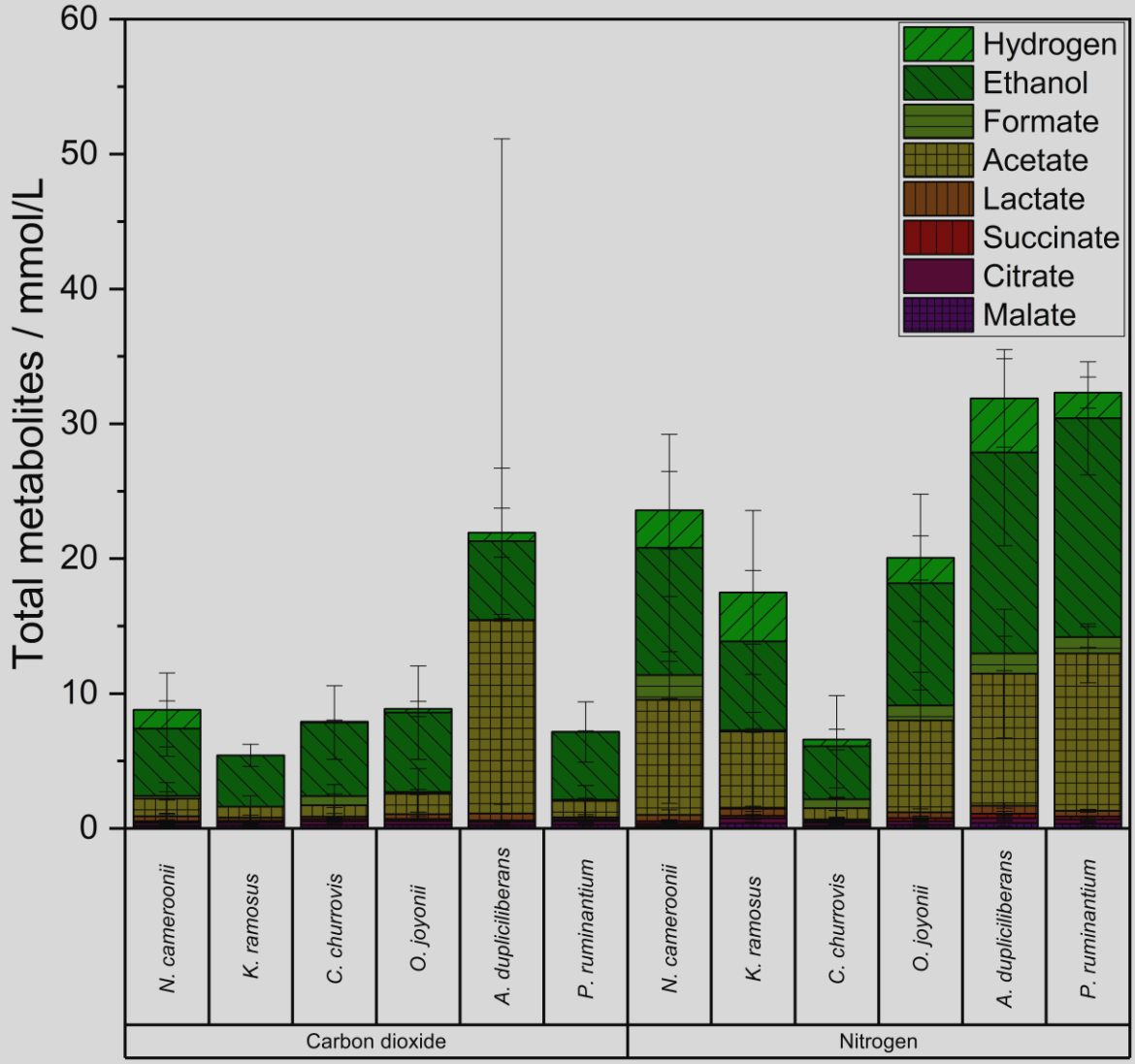

Figure 15: Atmospheric screening: influence of headspace gas composition (CO_2 vs. N_2) on metabolite production of six anaerobic gut fungal strains after 7 days of cultivation. All cultures were grown in identical bicarbonate-buffered medium and initiated at the same pH (7.5) to control for pH shifts associated with CO_2 removal under N_2. Cultivations were performed in biological triplicates across three independent weekly batches (n = 9). Error bars represent standard deviation. Hydrogen production was consistently higher under N_2 headspace across all strains.

Across all six strains, hydrogen formation was consistently elevated under an N_2 atmosphere compared to CO_2. In addition, total metabolite output was also higher under N_2 in all strains except *C. churrovis*. This effect was particularly pronounced in strain *A. duplicilibera*ns, which showed the highest hydrogen yield under N_2 atmosphere. Hydrogen production in anaerobic gut fungi is associated with hydrogenosomal metabolism, where pyruvate is oxidized and electrons are transferred via reduced ferredoxin to hydrogenases, resulting in molecular hydrogen formation [21]. Because hydrogen is a fermentation end product, its accumulation or removal from the system influences the thermodynamic feasibility of upstream redox reactions. Elevated hydrogen partial pressures are known to constrain fermentation by shifting reaction equilibria toward reduced intermediates, thereby limiting further substrate oxidation [20,117]. The reduced hydrogen formation observed under CO_2 atmosphere suggests that CO_2-rich headspace conditions may indirectly influence hydrogenosomal activity, potentially through altered gas solubility dynamics or shifts in intracellular redox balance. This effect may be particularly pronounced in axenic batch culture, where no hydrogen-consuming partner is present to relieve reducing pressure. In mixed or co-culture systems, methanogens can lower hydrogen partial pressure, stimulate cellulolytic enzyme activity, and increase hydrogenosomal metabolism, suggesting that the atmospheric response observed here reflects the unbuffered redox constraints of monoculture rather than the full *in vivo* rumen situation [118-120]. It is known that carbonic anhydrases link environmental CO_2 availability to intracellular HCO_3^- formation and downstream signaling/metabolism in (aerobic) fungi. Although this has not yet been demonstrated directly in AGF, it provides a plausible mechanism by which headspace composition could affect physiology even when bulk medium composition is unchanged [121-124]. Sensitivity of ruminal fungi to headspace composition has previously been reported, where altered gas atmospheres affected end-product patterns and fermentation intensity [107].

Recent work on *N. cameroonii* has demonstrated that hydrogen yield can be modulated by cultivation conditions, reflecting flexible metabolic flux distribution [20]. The present results extend these findings by showing that atmospheric composition alone, even in the presence of identical bicarbonate concentrations, consistently alters hydrogen output across multiple phylogenetically distinct strains. Because bicarbonate was retained in both atmospheric treatments, the observed headspace effect could not yet be separated from carbonate chemistry. This motivated the subsequent experiments, in which bicarbonate was replaced by non-carbonate buffer systems under N_2 atmosphere.

Chapter 3: 3.3 Non-carbonate buffers stabilize pH but do not sustain bicarbonate-free growth

The six strains investigated represent both polycentric and monocentric AGF morphotypes. In the initial atmosphere screening (Figure 15), polycentric strains showed higher and more reproducible hydrogen production than monocentric strains. They were therefore prioritized for subsequent mechanistic experiments that required serial transfer and sustained growth under carbonate-independent conditions. The next step was to examine whether fungal growth can be sustained under strictly CO_2-independent conditions when bicarbonate is completely removed from the medium. For this purpose, the bicarbonate buffer system was systematically replaced by chemically defined non-carbonate buffers and all cultivations were conducted under N_2 atmosphere. This design enabled evaluation of buffering capacity independent of carbonate equilibria and assessment of whether alternative buffer systems can support growth in the absence of bicarbonate.

However, because autoclaving and anaerobization can induce substantial pH shifts, a preliminary stability screening was performed prior to biological evaluation. In this initial experiment, the pH of all candidate buffer systems was measured after anaerobization and autoclaving to determine whether the target pH (6.9 ± 0.1) could be maintained under cultivation conditions. The results of this physicochemical stability assessment are presented in Figure 16. Only buffer systems that exhibited stable post-sterilization pH values were subsequently selected for fungal cultivation experiments. Figure 16 summarizes the post-sterilization pH measured for each buffer across the tested concentration series (0.5–10 g L^{-1}). The two red lines indicate the acceptance window used in this study (pH 6.9 ± 0.1). Across most Good's-type zwitterionic buffers (e.g., MOPS, MOPSO, BES, PIPES, ACES, Bis-Tris) and the citrate–phosphate and phosphate systems, the post-sterilization pH remained close to the target range over large parts of the concentration series, indicating that these buffers maintain target pH values under the applied anaerobic and sterilization conditions. This behavior is consistent with the design goals of Good's buffers, which were developed to provide buffering with minimal chemical reactivity [29].

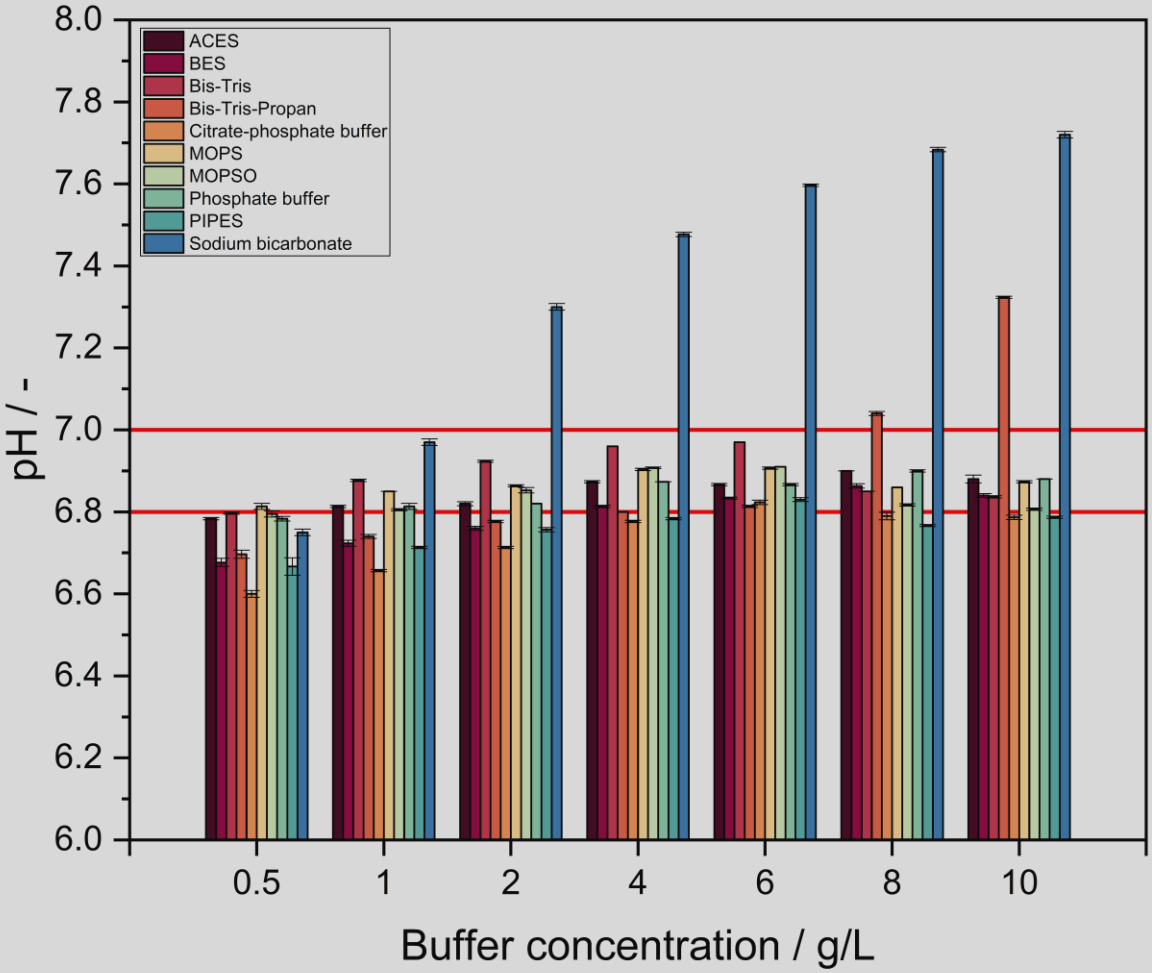

Figure 16: Post-sterilization pH values of the indicated buffer systems after anaerobization under 100% N_2 and autoclaving (121 °C, 20 min) across the tested concentration range (0.5–10 g L^{-1}; n = 3). Red lines denote the predefined acceptance window for pH stability (6.9 ± 0.1). Sodium hydrogen carbonate exhibits a concentration-dependent alkaline shift following N_2 treatment, whereas several non-carbonate buffer systems maintain pH values within the target range.

In contrast, sodium hydrogen carbonate showed a pronounced concentration-dependent alkaline shift after N_2 anaerobization/autoclaving, with pH increasing progressively at higher $NaHCO_3$ levels. This is expected for a volatile CO_2/HCO_3^- system: removal of CO_2 from the gas phase (here by N_2 exchange) perturbs the carbonate equilibrium and changes the effective buffer speciation, causing pH drift rather than stable control [125,126]. Similar sensitivity of CO_2/HCO_3^- systems, and the risk of introducing pH artefacts when pH is not continuously regulated, has been emphasized in broader guidance on buffering regimes [127]. Notably, Bis-Tris-Propan buffer also displayed an alkaline shift at high concentrations, indicating that pH stability must be empirically validated for each buffer under the exact anaerobic/sterilization workflow rather than assumed *a priori*. For the subsequent biological evaluation of pH-stable buffer conditions, *N. cameroonii* G341 was used as model strain due to its robust growth and consistent hydrogen production in the initial atmosphere screening (Figure 15), enabling sensitive detection of growth loss under carbonate-free conditions.

Subsequently, only those buffer–concentration combinations that maintained the target pH (6.9 ± 0.1) after anaerobization and autoclaving were selected for biological evaluation under N_2 atmosphere (Table S4). Because inoculation was performed from standard $NaHCO_3/CO_2$ precultures, residual dissolved inorganic carbon could not be fully excluded during the first transfer cycle. Figure 17 therefore summarizes the first-transfer growth performance of the model organism *N. cameroonii* in these pH-stable, bicarbonate-free buffer systems. While limited metabolic activity was still detectable in the initial transfer culture, no measurable growth, hydrogen production, or sustained metabolite formation was observed after subsequent transfers, when inoculum-associated carbonate carryover was no longer expected to contribute appreciably. These results indicate that stable external pH alone is insufficient to sustain growth in the absence of bicarbonate. One plausible explanation is that, once inoculum-associated carryover is depleted, intracellular bicarbonate supply becomes limiting for carbonic-anhydrase-mediated CO_2 hydration and downstream bicarbonate-dependent metabolic or signaling processes. In fungi, carbonic anhydrases are broadly implicated in maintaining bicarbonate homeostasis and coupling environmental CO_2 availability to cellular physiology [121,122].The failure to re-establish growth after transfer argues against a purely transient adaptation effect and supports the interpretation of a physiological requirement for carbonate not explained by extracellular pH control alone. Because AGF energy metabolism depends on hydrogenosomal pyruvate oxidation and associated redox balancing [21], removal of bicarbonate may disturb central metabolic fluxes rather than merely extracellular pH. This interpretation is consistent with bicarbonate-dependent carboxylation reactions described in other anaerobic systems [115].

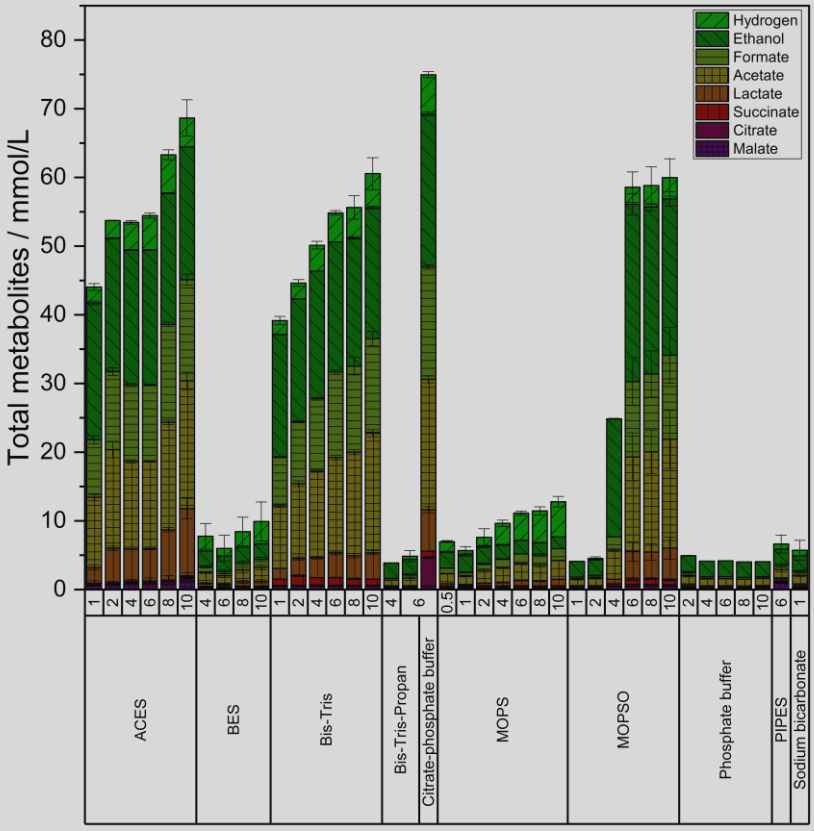

Figure 17: Total metabolite production (mmol per bottle) of N. cameroonii cultivated with chemically stable, bicarbonate-free buffer systems after N_2 anaerobization and autoclaving. Only buffer–concentration combinations maintaining post-sterilization pH 6.9 ± 0.1 were evaluated. Limited metabolic activity was observed during the first cultivation cycle (shown above); however, no sustained hydrogen production or metabolite formation was detected after transfer into fresh medium in the subsequent week. Data represent biological triplicates (n = 3); error bars indicate standard deviation. For ACES-containing samples, apparent succinate signals reflect chromatographic co-elution; a representative fixed background value (0.2 mmol L^{-1}) is shown. The numbers on the X-Axis indicate the concentration of the buffer in mM.

Chapter 3: 3.4 Low bicarbonate thresholds restore activity under N_2

To further examine the physiological function of bicarbonate, sodium hydrogen carbonate was systematically reintroduced into carbonate-free medium under nitrogen atmosphere across a defined concentration gradient (0, 0.125, 0.25, 0.375, 0.5, 1, 2, and 3 g L^{-1}). Figure 18 summarizes the strain-specific response of the polycentric anaerobic gut fungi *A. dupliciliberans*, *N. cameroonii*, *O. joyonii*, and *P. ruminantium* to increasing bicarbonate availability. In the absence of bicarbonate (0 g L^{-1}), hydrogen production and total metabolite formation were negligible across all tested strains, consistent with the absence of sustained growth under carbonate-free conditions. Upon gradual supplementation of sodium hydrogen carbonate, hydrogen formation reappeared in a concentration-dependent manner. For *N. cameroonii* and *O. joyonii*, reproducible metabolic activity was restored at low bicarbonate concentrations (≥0.25 g L^{-1}), whereas *A. dupliciliberans* required slightly higher levels (≥0.5 $g\ L^{-1}$) to re-establish stable hydrogen production. *P. ruminantium* exhibited a similar recovery pattern but with reduced overall hydrogen output compared to *N. cameroonii*. Notably, hydrogen production did not increase proportionally with bicarbonate concentration beyond the minimal threshold; instead, a plateau-like behavior was observed once sufficient bicarbonate was available. For better visualization hydrogen production of *N. cameroonii* is shown exclusively in Figure S9. This pattern is consistent with a threshold-dependent requirement rather than a simple concentration-dependent stimulation effect. The concentration-dependent recovery of hydrogen formation suggests that bicarbonate availability affects hydrogenosomal metabolism. The threshold-like character of this response is compatible with a system in which a minimum external bicarbonate level is required before intracellular HCO_3^- pools become sufficient to support bicarbonate-dependent carboxylation and related metabolic functions, rather than with a simple linear stimulation by increasing buffer concentration [114,115,121]. The strain-specific bicarbonate thresholds observed may be explained with the broader physiological diversity reported across AGF taxa and may reflect differences in intracellular inorganic carbon handling, hydrogenosomal flux partitioning, or carboxylation capacity rather than a single universal bicarbonate requirement [22,128]. Early physiological studies on *Neocallimastix* demonstrated that carbon dioxide availability affects fungal growth and metabolism [116]. Furthermore, genomic analyses of anaerobic gut fungi have identified carboxylation-associated enzymes that may require CO_2-derived intermediates in central metabolism [128]. To exclude sodium-associated effects as the primary driver of growth recovery, control experiments were performed in which NaCl was added at molar concentrations equivalent to the Na^+ contribution of the respective $NaHCO_3$ treatments. As shown in Figure S8, NaCl supplementation did not restore hydrogen production or sustained metabolite formation, indicating that the observed recovery was specific to bicarbonate rather than to sodium ions.

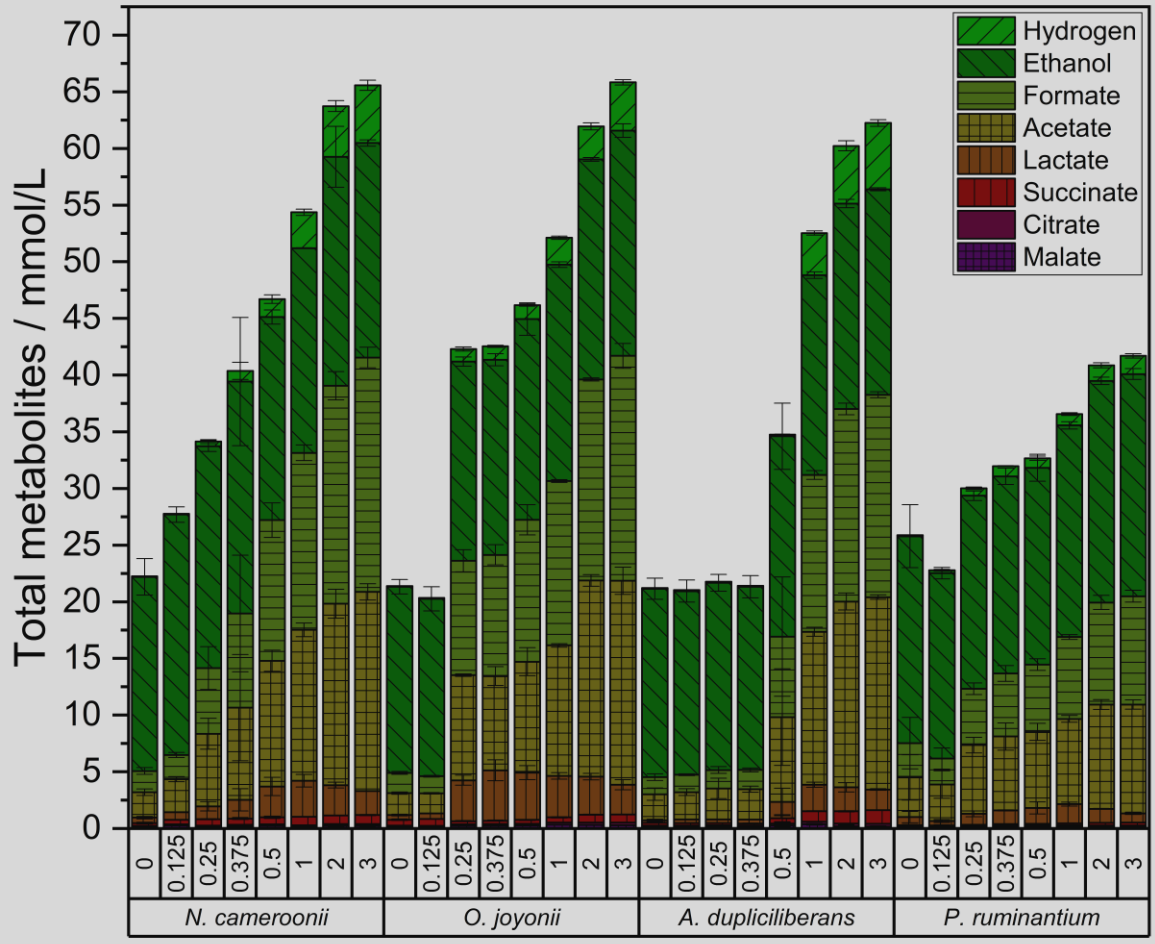

Figure 18: Strain-specific restoration of metabolic activity by sodium hydrogen carbonate under a 100% N_2 atmosphere. Total metabolite production (mmol L^{-1}) of polycentric anaerobic gut fungal strains (A. dupliciliberans, N. cameroonii, O. joyonii, and P. ruminantium) is shown for the second cultivation cycle across increasing sodium hydrogen carbonate concentrations (0–3 g L^{-1}). Carbonate-free conditions (0 g L^{-1} $NaHCO_3$) resulted in negligible hydrogen formation, whereas sodium hydrogen carbonate supplementation restored hydrogen production in a strain-specific, concentration-dependent manner. Data represent biological triplicates (n = 3); error bars indicate standard deviation. The numbers on the X-Axis indicate the concentration of NaHCO3 in g L-1.

Chapter 3: 3.5 Alternative carboxylates do not substitute bicarbonate

The concentration-dependent restoration of metabolic activity by sodium hydrogen carbonate (Figure 18) is consistent with a bicarbonate requirement for sustained growth under nitrogen atmosphere. However, this finding does not resolve whether the observed dependency is specific to bicarbonate itself or whether other structurally related carboxylate-containing compounds could functionally substitute its role. To address this question, alternative carboxylic acids were systematically screened under N_2 atmosphere. This screening was conducted exclusively with *A. duplicilibera*ns, selected based on its high hydrogen production and total metabolite formation in preceding experiments. The use of a metabolically robust strain increases sensitivity for detecting both growth-supporting and inhibitory effects of alternative carboxylates. The results of this screening are summarized in Figure 19. Across all tested carboxylic acids, total metabolite formation remained substantially lower than in the $NaHCO_3$ control, and hydrogen production did not recover to bicarbonate-supported levels. This pattern indicates that none of the screened organic carboxylates was able to functionally substitute bicarbonate in restoring the characteristic hydrogenosomal fermentation phenotype. Instead, end-product profiles were dominated by metabolites typically associated with cytosolic redox balancing, including lactate, succinate, and malate, whereas hydrogen formation remained comparatively low. In anaerobic metabolism more broadly, dissolved inorganic carbon participates in anaplerotic C_3-carboxylation reactions that replenish oxaloacetate pools and sustain central carbon flux. Limitation of intracellular CO_2/HCO_3^- availability can constrain anaplerosis and growth, whereas supplementation can restore metabolic flux distribution [114,115]. Consistent with fungal CO_2/HCO_3^- signaling models, carbonic anhydrase activity might generate bicarbonate that can be sensed directly or indirectly by cAMP-associated pathways. Under such a framework, externally supplied organic carboxylates would not be expected to substitute for bicarbonate if the critical requirement is intracellular HCO_3^- generation rather than provision of a generic organic acid [121,123,124]. Together, these observations are consistent with the interpretation that bicarbonate contributes to central metabolic flux beyond extracellular pH control. An additional consideration is that several tested organic acids may impose weak-acid stress rather than simply acting as alternative carbon-bearing species. In fungi, membrane-permeant weak acids can cause cytosolic acidification, anion accumulation, and ATP-consuming pH homeostasis responses, which may suppress growth even when extracellular pH is readjusted before inoculation [129-131]. However, maleic acid represented a notable exception. Maleate supplementation resulted in elevated apparent total metabolite formation compared to other tested acids, yet this increase was not accompanied by proportional hydrogen production. Detected metabolites indicate a redistribution of carbon flux toward cytosolic end products rather than restoration of balanced hydrogenosomal metabolism. One possible explanation relates to the chemical properties of unsaturated dicarboxylates such as maleate and fumarate. In various anaerobic systems, fumarate can function as an electron acceptor and support cytosolic redox balancing through reduction to succinate [132,133]. Provision of structurally related compounds may therefore influence intracellular redox distribution without replacing bicarbonate-dependent anaplerotic flux. In addition, maleate has been reported to interact with enzymes of central carbon metabolism, including fumarase and pyruvate kinase [134,135], potentially contributing to altered carbon partitioning. These mechanisms remain speculative in the context of anaerobic gut fungi but may explain the observed decoupling between soluble metabolite formation and hydrogen production.

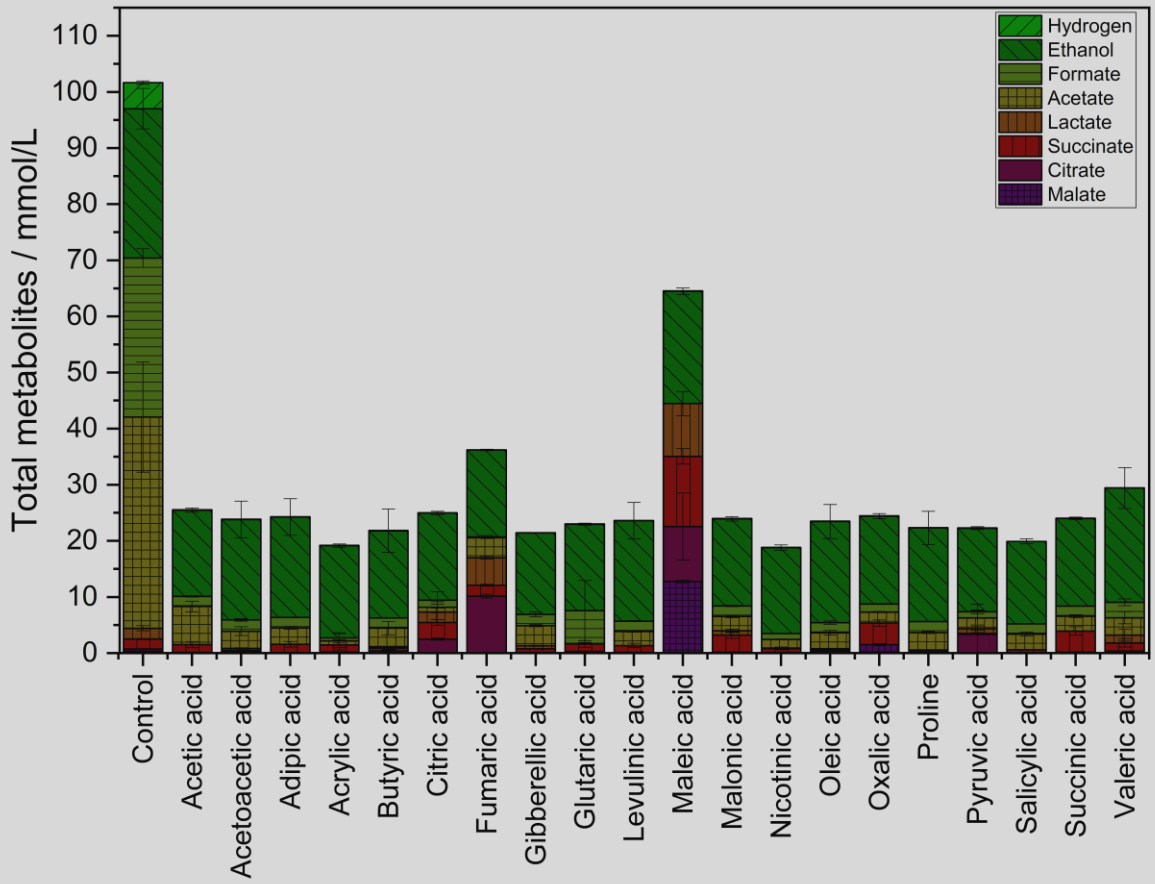

Figure 19: Metabolite production by A. dupliciliberans under a 100% N_2 atmosphere in media with structurally diverse carboxylic acids. Stacked bars show the individual and total concentrations of quantified metabolites (hydrogen, ethanol, formate, acetate, lactate, succinate, citrate, and malate) after seven days of cultivation in bicarbonate-free medium supplemented with 4 g L^{-1} of the indicated carboxylic acid; the control contained 4 g L^{-1} sodium hydrogen carbonate. Values were corrected for compound-specific background and co-elution artefacts identified by independent standard measurements. None of the tested carboxylic acids restored the bicarbonate-supported hydrogen production observed in the control. Maleic acid yielded the highest metabolite accumulation among the tested carboxylic acids; however, acetate is not shown for this condition because maleic acid can isomerize and generate an interfering HPLC signal, preventing reliable acetate quantification. Data represent biological triplicates (n = 3); error bars indicate standard deviation.

Taken together, the data indicate that bicarbonate provides an enabling function that is not substituted by the tested organic carboxylates. While certain unsaturated dicarboxylates may partially sustain cytosolic metabolite formation, none restored the balanced hydrogenosomal phenotype observed under bicarbonate supplementation. This supports the hypothesis that dissolved inorganic carbon availability, rather than generic carboxylate chemistry, underlies the observed growth dependency. Future experiments should further distinguish between buffering effects and inorganic carbon supply, for example by combining non-carbonate pH buffers with defined CO_2 dosing or supplementation with specific C_4 intermediates to probe potential anaplerotic limitations.

Chapter 3: 3.6 Dual-buffer cultivation identifies a pH optimum at 6.4

To determine pH optima under nitrogen atmosphere, a dual-buffer strategy was implemented in which pH stabilization was provided by Bis-Tris Buffer while a minimal concentration of sodium hydrogen carbonate (0.5 g L^{-1}) was supplied as a defined inorganic carbon supplement. This experimental design allowed independent control of external pH while maintaining a constant, low bicarbonate background. Only polycentric anaerobic gut fungal strains were evaluated in this mechanistic assay (Figure 20).

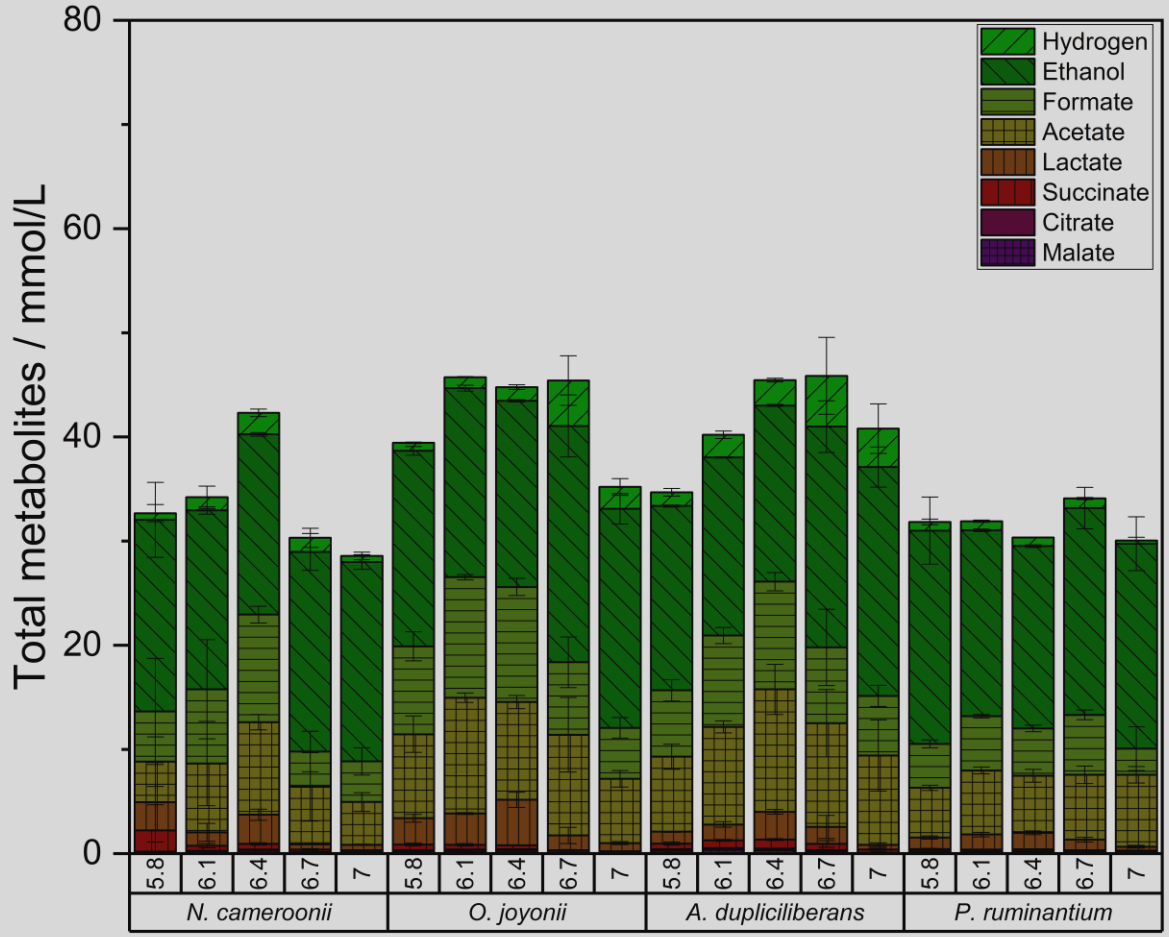

Figure 20: Total metabolite production by four polycentric anaerobic gut fungal strains under a 100 % N2 atmosphere at initial pH between 5.8 and 7. Cultures were grown with Bis-Tris (6 g L^{-1}) as the primary buffer and 0.5 g L^{-1} $NaHCO_3$ as a minimal inorganic carbon supplement. Data represent biological triplicates (n = 3); error bars indicate standard deviation.

Across the tested pH range (5.8–7.0), hydrogen production and total metabolite formation displayed a distinct optimum at pH 6.4. At more acidic conditions (pH 5.8–6.1), metabolic output declined, whereas at neutral conditions approaching pH 7.0, hydrogen production was reduced relative to the optimum. The observation that pH 6.4 yields maximal activity is biologically consistent with the natural ruminal environment. *In vivo* measurements of rumen fermentation typically report a physiological pH range between approximately 6.0 and 6.8, depending on diet and fermentation intensity [136]. Anaerobic gut fungi are adapted to this mildly acidic niche and are known to exhibit optimal growth and fermentation activity within this window [116]. Deviations toward higher pH may reduce proton availability for redox reactions and alter membrane potential dynamics, whereas excessive acidity can impair enzyme activity and intracellular homeostasis. Importantly, because Bis-Tris buffer maintained stable external pH independent of CO_2/HCO_3^- equilibria, the observed optimum is consistent with a physiological pH preference rather than an artefact of carbonate buffering. This distinction may be particularly relevant for bicarbonate handling, because carbonic-anhydrase-catalyzed interconversion of CO_2 and HCO_3^- links inorganic carbon availability to proton balance and thereby integrates pH and carbon supply at the cellular level in fungi [121,122]. Hydrogen production in anaerobic gut fungi is associated with hydrogenosomal pyruvate oxidation [21], and hydrogenosomal enzymes are sensitive to intracellular pH conditions. The alignment of maximal hydrogen production at pH 6.4 therefore supports the interpretation that hydrogenosomal metabolism is tuned to rumen-like acidity. Notably, even at the optimal pH, hydrogen production did not exceed levels observed under full bicarbonate supplementation in earlier experiments. This also suggests that the identified pH optimum is conditional on the low-bicarbonate background used in the dual-buffer setup and may shift under conditions of higher inorganic carbon supply or continuous product removal. Continuous-culture studies have shown that AGF metabolic fluxes can be tuned by cultivation regime, indicating that pH optima should be interpreted in the context of both carbon availability and product accumulation [137]. This finding suggests that bicarbonate contributes metabolic functions beyond external pH stabilization, potentially through inorganic carbon availability required for balanced carbon flux and energy metabolism.

Chapter 3: 3.7 OD_{750} calibration provides a practical biomass proxy

While the preceding experiments used metabolic output as a proxy for growth, interpretation of fermentation patterns alone does not allow discrimination between altered metabolic flux distribution and genuine differences in biomass formation. Because anaerobic gut fungi exhibit complex morphologies and substrate-associated growth, reliable biomass quantification represents a methodological challenge. To address this limitation, an OD_{750}-based biomass detection approach calibrated against defined dry weight standards and an inert activated carbon reference was established and validated. In contrast to previous mechanistic assays focusing primarily on polycentric model strains, the calibration procedure included all six fungal strains to assess inter-strain variability in light scattering behavior and to evaluate transferability across morphotypes. Inter-device normalization based on activated carbon calibration is shown in Figure 21. Activated carbon exhibited reproducible and concentration-dependent optical responses on both photometric systems. Polynomial regression of activated carbon extinction values was used to derive instrument-specific calibration functions, which were subsequently applied to generate calculated transfer curves for Photometer 2 (GENESYS™ 30, Thermo Scientific, USA). These predicted values were compared with experimentally measured OD_{750} values of fungal biomass suspensions measured on photometer 2. Across all tested strains, measured extinction values closely followed the predicted curves derived from activated carbon normalization within the defined working range. Although deviations were observed at very low and very high biomass concentrations, absolute differences remained limited within the operational range relevant for cultivation experiments (0.05–0.5 g L^{-1}). These results indicate that activated carbon provides a suitable optical reference for normalizing OD measurements between photometric systems as approximation of biomass formation. At the same time, this calibration should be interpreted as a comparative proxy rather than an absolute biomass assay, because differences in aggregation state, pellet architecture, and branching density can alter light scattering independently of dry mass. This likely explains the larger deviations observed at the extremes of the calibration range and underscores that strain-specific optical behavior remains relevant in morphologically heterogeneous AGF cultures [108].

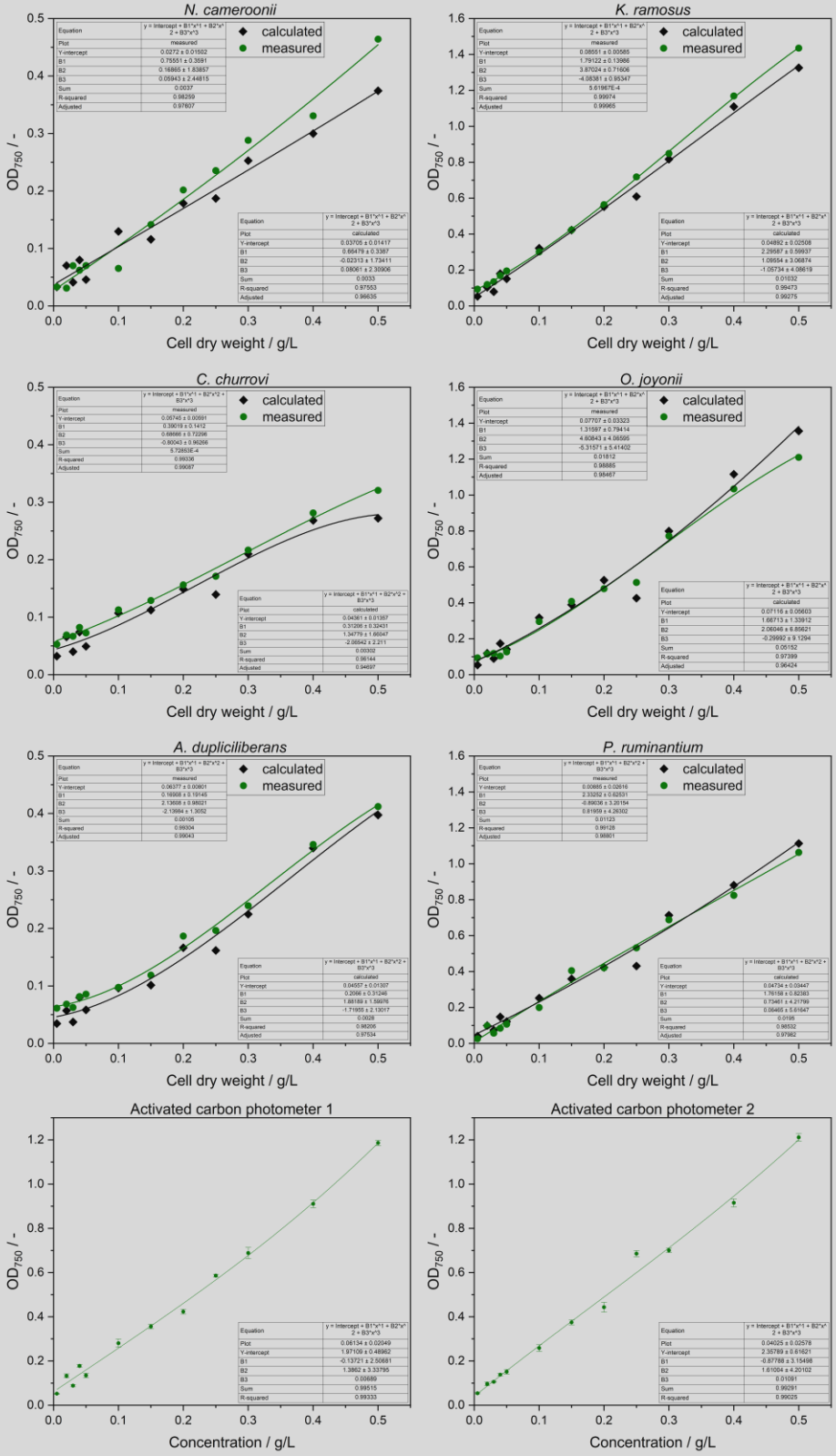

Figure 21: Comparison of measured and calculated OD_{750} values for fungal biomass after activated carbon-based inter-device normalization. In the six upper panels, green circles show the OD_{750} values experimentally measured for fungal biomass suspensions of known dry weight concentration (0.005–0.5 g L^{-1}) on Photometer 2 (GENESYS™ 30), whereas black diamonds show the OD_{750} values calculated for the same biomass concentrations from the activated carbon-based normalization function. The two lower panels show the activated carbon calibration curves measured on Photometer 1 and Photometer 2, which were used to derive the normalization function. Measured data represent mean values of ten technical replicates; error bars indicate standard deviation.

Chapter 3: 3.8 Nitrogen variation has limited effects within the tested range

While Figure 21 establishes a transferable OD_{750}-based biomass detection framework, its practical applicability must be evaluated under defined physiological perturbations. To assess both the sensitivity of the method and the influence of nutrient balance on fungal growth, the impact of nitrogen availability on biomass formation and metabolic performance was investigated. *C. churrovis* was selected for this experiment due to its monocentric growth morphology characterized by compact thalli and reduced rhizoidal aggregation compared to polycentric taxa. This morphology results in more homogeneous suspension behavior in liquid culture and reduced clumping, thereby improving the reliability of turbidity-based biomass measurements. Because OD-based quantification relies on light scattering of suspended particles, a strain with minimal aggregation artifacts provides a suitable system for evaluating changes in optical density under variable nutrient conditions. The results are presented in Figure 22.

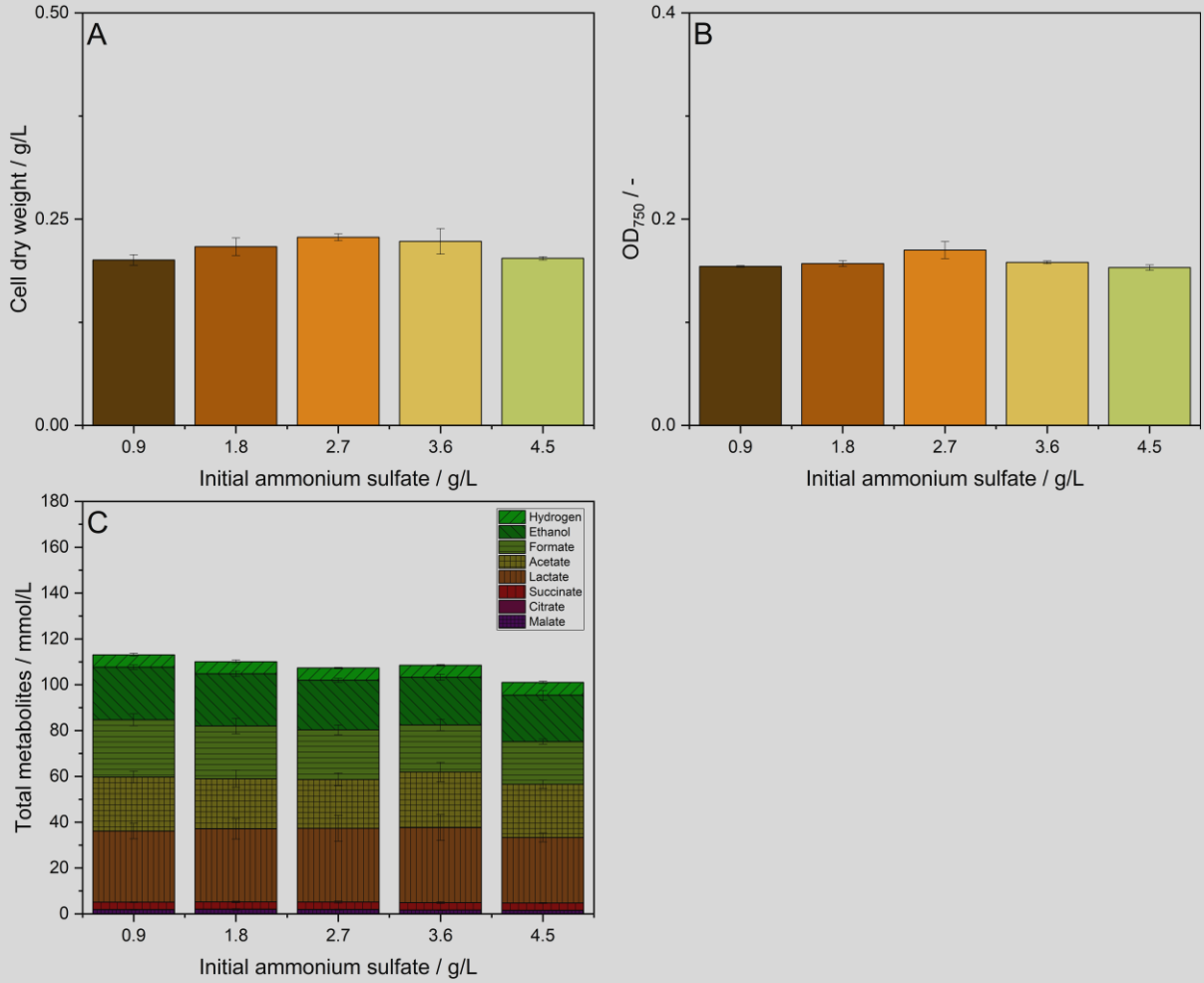

Figure 22: Impact of ammonium sulfate concentration on biomass formation and metabolic output. A: Biomass (OD_{750}-derived dry mass); B: OD_{750} values; C: Total metabolites (mmol L-1) of Caecomyces churrovis PP313 with varying ammonium sulfate concentrations. No major differences in biomass accumulation or hydrogen production were observed across the tested nitrogen range, indicating non-limiting nitrogen conditions. Data represent biological triplicates; error bars indicate standard deviation.

Across the tested ammonium sulfate concentrations, no consistent trend in biomass accumulation was observed. OD_{750} values and calculated biomass concentrations remained within a narrow range across all nitrogen levels and did not display a clear dose–response relationship. Similarly, total metabolite formation and hydrogen production remained comparable across the tested concentration range. These observations indicate that, within the applied concentration window, nitrogen availability did not impose a detectable growth limitation under the experimental conditions. At the same time, this conclusion applies specifically to the defined glucose-based, bicarbonate-buffered medium used here, which also contained constant background nitrogen from additional supplements. The absence of a response therefore likely indicates that the tested ammonium sulfate window remained above the threshold of true nitrogen limitation rather than that nitrogen is generally unimportant for AGF physiology. Comparable findings have been reported in other fungal systems, where growth reduction becomes apparent only when nitrogen availability drops below a threshold required to sustain anabolic processes [138]. The stability of hydrogen production across nitrogen concentrations further suggests that hydrogenosomal metabolism was not constrained by nitrogen supply within the tested range. Taken together, these results indicate that, under the present cultivation conditions, atmospheric composition and inorganic carbon availability exert stronger effects on metabolic output than moderate variations in nitrogen concentration. Future experiments extending into clearly nitrogen-limited regimes, combined with direct quantification of residual ammonium and cellular protein content, would be required to resolve potential C:N-dependent regulatory effects in anaerobic gut fungi.

Chapter 3: 4 Conclusions

This study systematically disentangles atmospheric composition, buffer chemistry, bicarbonate availability, pH control, and ammonium concentration as interacting variables in anaerobic gut fungal growth and metabolism. The results show that conventional CO_2-based cultivation intrinsically couples gas-phase composition with carbonate buffering, complicating mechanistic interpretation. By implementing nitrogen headspace conditions and non-carbonate buffer systems, atmospheric and buffering effects could be experimentally separated. The results are consistent with a physiological role of bicarbonate beyond extracellular pH stabilization. Complete removal of bicarbonate abolished sustained growth even under stable pH conditions, whereas reintroduction at low concentrations restored hydrogen production in a strain-specific manner. Alternative organic carboxylic acids did not substitute this function. Although maleic acid induced elevated cytosolic metabolite accumulation, this response was not accompanied by proportional hydrogen formation and did not restore the balanced hydrogenosomal fermentation phenotype observed under bicarbonate supplementation. The dual-buffer pH experiment identified maximal hydrogen production at pH 6.4 under nitrogen atmosphere, consistent with reported ruminal pH conditions. However, pH optimization alone did not compensate for bicarbonate limitation. Furthermore, variation of ammonium sulfate within the tested range did not impose a detectable growth limitation, indicating that nitrogen availability was not the dominant regulatory factor under the applied conditions. The establishment of a transferable strain specific OD_{750}-based biomass calibration framework enables reliable, non-invasive quantification of fungal growth across experimental perturbations and supports discrimination between altered metabolic flux and biomass effects. Collectively, these findings indicate that atmospheric composition and inorganic carbon availability are key determinants of metabolic performance in anaerobic gut fungi. Several targeted follow-up experiments are required to further resolve the precise physiological role of bicarbonate. Future studies should more rigorously decouple inorganic carbon supply from buffering effects, for example by combining non-carbonate pH buffers with controlled CO_2 dosing under N_2 atmospheres. Direct quantification of dissolved inorganic carbon, alongside supplementation with defined C_4 intermediates (e.g., malate, succinate, fumarate, or aspartate), would help clarify whether bicarbonate primarily supports anaplerotic carbon flux, intracellular redox balance, or both. Additional time-resolved and multi-strain analyses will be required to determine the generality of bicarbonate thresholds and pH optima across *Neocallimastigomycota*. Such mechanistic resolution is essential for developing reproducible and scalable cultivation strategies for the biotechnological exploitation of anaerobic gut fungi.

At this point, the first major block of the dissertation is complete. The fungal platform has been established biologically, explored mechanistically, and clarified in terms of its core cultivation requirements. Only with this upstream foundation in place does the dissertation turn to the second major module of the future process: microbial lipid production with oleaginous yeasts. The next two chapters therefore shift the focus from biomass deconstruction and metabolite generation toward product formation, reactor operation, and substrate realism on the downstream side.

3.2 Establishing the downstream platform: microbial lipid production as upgrading strategy

The downstream half of the dissertation is centered on the question of how soluble carbon streams can be converted efficiently into an industrially relevant storage product. Oleaginous yeasts are particularly attractive in this respect because they can accumulate plant-oil-like lipids while remaining fully compatible with conventional fermentation technology. Yet, as with the fungal platform, their usefulness in a future integrated process cannot be assumed from literature precedent alone. It must be tested under relevant conditions.

The first downstream study therefore benchmarks several yeasts under controlled nutrient-limitation regimes in stirred-tank reactors. The second downstream study introduces industrial realism by replacing clean model substrates with untreated crude glycerol. Together, these chapters define the operational basis of the yeast platform and establish the process principles that later become important for fungal metabolite utilization as well.

3.2.1 Reactor-scale comparison of nutrient limitation strategies for microbial lipid production

The fourth chapter marks the beginning of the downstream process narrative. Its role is to establish how different oleaginous yeasts behave under controlled reactor conditions and how nutrient limitation determines lipid formation, biomass accumulation, and product quality. This is the first point in the dissertation at which the final target product of the larger concept, microbial lipids, moves into the center of attention.

The significance of this study lies in its systematic and comparative design. By benchmarking four oleaginous yeasts under nitrogen-limited, phosphate-limited, and nutrient-replete conditions in stirred-tank reactors, it moves the discussion of single-cell oil production away from isolated shake-flask observations and toward process-relevant performance metrics. It shows that the downstream platform is not a single generic lipid-production process, but a tunable system in which the choice of nutrient limitation regime has far-reaching effects on growth, lipid accumulation, and fatty acid composition.

In the broader dissertation context, this chapter serves two purposes. First, it defines the second biological module in a way that mirrors the role of chapter 1 for the fungi: it establishes the platform on its own terms. Second, it lays the process-engineering groundwork for future coupling by showing how lipid production can be directed under well-defined reactor conditions.

Chapter 4: Phosphate Versus Nitrogen Limitation: A Reactor-Scale Process Comparison for Single-Cell Oil Production in Oleaginous Yeasts

Kevin Edward Schulz[1*], Paula Hegmann[1], Bastian Dreher[1], Lena Regenauer[1], Carlota Delso Muniesa[2], Wolfgang Frey[2], Katrin Ochsenreither[3] and Anke Neumann[1*]

[1]Institute of Process Engineering in Life Sciences 2: Electrobiotechnology, Karlsruhe Institute of Technology (KIT), Karlsruhe, Germany, [2]Institute for Pulsed Power and Microwave Technology, Karlsruhe Institute of Technology, Eggenstein-Leopoldshafen, Germany, [3]Kaiserslautern University of Applied Sciences, Campus Pirmasens, Pirmasens, Germany, * corresponding authors

Publishing details:
MDPI Fermentation
Vol. 12 Issue 4
Published on 24 March 2026
doi: 10.3390/fermentation12040172

Author contributions: Conceptualization, K.E.S.; methodology, K.E.S.; validation, K.E.S., B.D., P.H. and L.R.; formal analysis, K.E.S.; investigation, K.E.S., B.D., P.H. and L.R.; resources, A.N.; data curation, K.E.S.; writing—original draft preparation, K.E.S.; writing—review and editing, K.E.S., A.N., C.D.M., W.F. and K.O.; visualization, K.E.S.; supervision, K.E.S., A.N. and K.O.; project administration, A.N. and W.F.; funding acquisition, A.N., W.F. and K.O. All authors have read and agreed to the published version of the manuscript.

Chapter 4: 1 Introduction

Single-cell oils (SCOs), also referred to as microbial oils, are intracellular storage lipids mainly composed of triacylglycerols that are produced by oleaginous microorganisms. A microorganism is generally classified as oleaginous when it is capable of accumulating more than 20% lipid on a cell dry weight basis, with some species reaching lipid contents of up to 70–80% depending on cultivation conditions such as nutrient limitation and excess carbon availability [8,139]. Oleaginous microorganisms occur across several phylogenetic groups, including microalgae, fungi (filamentous fungi and yeasts), and bacteria. Microalgae such as *Chlorella*, *Nannochloropsis*, or *Botryococcus braunii* are widely studied for lipid production and typically accumulate between approximately 20 and 75% lipids of their cell dry weight depending on species and cultivation conditions [140]. Filamentous fungi and oleaginous yeasts, including *Mortierella*, *Yarrowia*, *Rhodosporidium*, and *Cutaneotrichosporon* species, can reach lipid contents of about 70–75% of cell dry weight under optimized cultivation conditions [30,31]. In addition, several bacterial species such as *Rhodococcus opacus* and *Acinetobacter calcoaceticus* are known to accumulate storage lipids, with reported lipid contents typically ranging from approximately 20 to 50% of cell dry weight [141]. Due to their high lipid accumulation capacity and metabolic versatility, these microorganisms represent promising platforms for sustainable lipid production using renewable carbon sources.

SCOs have attracted increasing interest as a sustainable alternative to plant- and fossil-derived oils, as their production is independent of climate, arable land availability and seasonal fluctuations [1,32,142-145]. In contrast to conventional plant oils such as soybean, palm or sunflower oil, microbial lipid production does not compete directly with food or feed supply chains and can achieve higher water-use efficiency [32,146]. Consequently, SCOs are considered promising feedstocks for a broad range of applications, including oleochemicals, cosmetics, nutraceuticals, pharmaceuticals and renewable fuels [147-151]. Among oleaginous microorganisms, yeasts are particularly attractive due to their high lipid contents, reported up to 75% of cell dry weight, fast growth, simple cultivation requirements and fatty acid profiles comparable to plant oils [139,152].

In yeasts, lipids fulfil multiple cellular functions, ranging from membrane formation to energy storage and signal transduction [153]. De novo lipid accumulation is typically induced as a secondary metabolic response to nutrient limitation, most commonly nitrogen limitation [30,34,154]. Industrially, this is often implemented as a two-stage process, where biomass formation occurs during an initial growth phase followed by lipid accumulation once nitrogen is depleted and carbon is supplied in excess [30,34,155]. At the metabolic level, nitrogen limitation leads to a decrease in intracellular adenosine monophosphate (AMP) concentrations due to the activity of AMP deaminase, which converts AMP to inosine monophosphate. The resulting reduction in AMP levels decreases the activity of the AMP-dependent isocitrate dehydrogenase in the tricarboxylic acid cycle, leading to citrate accumulation in the mitochondria. Citrate is subsequently transported to the cytosol, where it is cleaved to acetyl-CoA, providing the precursor for fatty acid and triacylglycerol synthesis in oleaginous yeasts [30]. Lipid accumulation can be further enhanced by increasing the carbon-to-nitrogen ratio in the cultivation medium [139].

Despite its effectiveness, nitrogen-limited SCO production poses limitations with respect to economic feasibility and feedstock flexibility. Industrial side streams such as molasses or other agro-industrial residues often contain high nitrogen concentrations, rendering strict nitrogen limitation difficult or impractical [156,157]. In this context, alternative nutrient limitation strategies have been proposed, including phosphate or sulfur limitation, yet these approaches remain comparatively understudied, particularly under process-relevant cultivation conditions [34]. Phosphorus is a key cellular element, being an integral component of nucleic acids, ATP and phospholipids, and its limitation strongly affects microbial metabolism and growth [38,158]. Moreover, phosphorus is a finite and increasingly critical resource, which may become a limiting factor for future large-scale bioprocesses [39,159].

Several studies have demonstrated that phosphate limitation can promote lipid accumulation in oleaginous microorganisms. For example, *Rhodosporidium toruloides* reached a cellular lipid content of 62.2% and a lipid yield of 0.205 g g^{-1} glucose under phosphate-limited conditions, even in the presence of excess nitrogen. In that study, lipid accumulation was observed at a C/N ratio of 6.1 and a C/P ratio of 9552, highlighting that phosphate limitation alone can trigger substantial lipid storage [160]. In *Yarrowia lipolytica*, phosphate limitation likewise enhanced lipid accumulation. In synthetic medium, reducing phosphate from 10.1 g L^{-1} to 0 g L^{-1} increased lipid content from 23.1 ± 0.5% to 44.4 ± 0.9% of cell dry weight and lipid yield from 0.14 ± 0.01 to 0.30 ± 0.01 g g^{-1}. In real digestate, lowering phosphate from 5.1 g L^{-1} to 1 g L^{-1} increased lipid content from 18.7 ± 1.1% to 37.7 ± 0.7% [37]. Similar effects have also been reported in microalgae, although the response is strongly species- and condition-dependent. For example, in *Isochrysis sp.* IOAC724S, cultivation without phosphorus for two days increased total lipid content from 21.0% to 55.6% of dry weight. In this context, phosphorus stress in microalgae is commonly described as moderate at 0.019–0.01 g L^{-1} P, strong at <0.01 g L^{-1} P, and complete phosphorus starvation at 0 g L^{-1} P [161]. However, existing work predominantly focuses on individual strains, strain-specific process optimization or small-scale cultivation systems, and typically emphasizes lipid content or final titres as primary performance metrics. Systematic, reactor-scale comparisons of phosphate- and nitrogen-limited SCO production across multiple oleaginous yeast species under identical process conditions, particularly including rate-based performance indicators, remain largely lacking. As a result, the process-level implications of phosphate limitation relative to conventional nitrogen-limited strategies are still insufficiently understood.

In the present study, we address this gap by conducting a reactor-scale, cross-strain benchmark of phosphate-limited, nitrogen-limited and nutrient-replete cultivations using four oleaginous yeasts, *Cutaneotrichosporon oleaginosum* ATCC 20509, *Saitozyma podzolica* DSM 27192, *Scheffersomyces segobiensis* DSM 27193 and *Apiotrichum porosum* DSM 27194, in 2.5 L stirred-tank reactors. Using standardized media and cultivation conditions based on established protocols [162], we systematically compare biomass formation, lipid accumulation, specific lipid production rates, biomass composition and fatty acid profiles. By combining controlled reactor-scale cultivation with comprehensive analytical characterization, this study evaluates phosphate limitation as an alternative lipid induction strategy and provides process-relevant insights for feedstock-flexible and scalable SCO production.

Chapter 4: 2 Materials and Methods

Chapter 4: 2.1 Chemicals

Unless stated otherwise, all chemicals were obtained from Carl Roth GmbH & Co. KG (Karlsruhe, Germany).

Chapter 4: 2.2 Yeast Strains

The oleaginous yeast strains used in this study were *C. oleaginosum* ATCC 20509, *S. podzolica* DSM 27192, *A. porosum* DSM 27194 and *S. segobiensis* DSM 27193. *C. oleaginosum* ATCC 20509 has previously been described under the synonyms *Trichosporon oleaginosum*, *Candida curvata*, *Apiotrichum curvatum*, *Cryptococcus curvatus* and *Trichosporon cutaneum* [163-167]. *S. podzolica* DSM 27192 was formerly classified as *Cryptococcus podzolicus*, *A. porosum* as *Trichosporon porosum* and *S. segobiensis* as *Pichia segobiensis* [168].

Chapter 4: 2.3 Media Compositions for Bioreactor Cultivations

Bioreactor cultivations were conducted under nitrogen-limited, phosphate-limited and nutrient-replete (“unlimited”) conditions, with unlimited conditions defined as those in which neither nitrogen nor phosphate became growth-limiting during the cultivation, as confirmed by residual nutrient measurements throughout the cultivation (Section 3.1). All cultivation and preculture media were based on a previously described nitrogen-limited medium [162] and prepared from four separately sterilized solutions: (i) a mineral salt solution, (ii) a trace element solution, (iii) a salt solution and (iv) a glucose solution. The composition of the mineral salt solutions differed primarily in nitrogen and phosphorus content (Table S5). Based on the initial glucose concentration of 90 g L^{-1}, corresponding to approximately 3000 mmol C L^{-1}, the resulting elemental ratios differed substantially between the applied nutrient regimes. The nitrogen-limited medium exhibited an initial C/N ratio of approximately 396 and a C/P ratio of approximately 197, reflecting strong nitrogen limitation conditions. In contrast, the phosphate-limited medium showed an initial C/N ratio of approximately 18.7 and a C/P ratio of approximately 1724, indicating a pronounced excess of nitrogen while phosphate availability was strongly restricted. The nutrient-replete medium resulted in initial ratios of C/N ≈ 18.7 and C/P ≈ 197, ensuring that neither nitrogen nor phosphate became growth-limiting. These ratios were calculated based on the elemental nitrogen and phosphorus concentrations of the mineral salt solutions and are summarized in Table S5. The medium formulation was adopted from the nitrogen-limited cultivation medium described by Gorte et al. [162]. The elemental ratios were therefore not individually optimized for the investigated strains but were chosen to maintain comparability with previously reported cultivation conditions while ensuring clearly defined nutrient limitation regimes.

The nitrogen-limited mineral salt solution contained 8.99 g L^{-1} potassium dihydrogen phosphate, 0.12 g L^{-1} disodium hydrogen phosphate, 0.1 g L^{-1} sodium citrate dihydrate, 0.1 g L^{-1} yeast extract, 0.2 g L^{-1} magnesium sulfate heptahydrate and 4.72 g L^{-1} ammonium sulfate. For phosphate-limited cultivations, the mineral salt solution contained 4.922 g L^{-1} potassium chloride, 0.0788 g L^{-1} sodium chloride, 0.1 g L^{-1} sodium citrate dihydrate, 0.1 g L^{-1} yeast extract, 0.2 g L^{-1} magnesium sulfate heptahydrate, 288 µL L^{-1} of 86% phosphoric acid to provide defined phosphate limitation while minimizing buffering capacity and 100 g L^{-1} ammonium sulfate to ensure non-limiting nitrogen availability throughout the cultivation and did not result in any observable growth inhibition under the applied conditions. Preliminary cultivations performed prior to the reactor experiments indicated that sulfur limitation could occur during the fermentation when no additional ammonium sulfate was supplied. No direct sulfate quantification was performed in the preliminary cultivations. Instead, ammonium concentrations were monitored using the ammonium assay described in Section 2.7. With reduced ammonium sulfate concentrations, growth cessation was observed although ammonium remained in excess in the culture supernatant, indicating that nitrogen was not depleted under these conditions. Because ammonium sulfate represented the dominant sulfur-containing macronutrient source in the medium, this pattern was interpreted as indirect evidence that sulfur availability, rather than nitrogen availability, had become limiting. The elevated ammonium sulfate concentration was therefore selected to provide both nitrogen and sulfate in excess and thereby ensure that phosphate remained the sole limiting macronutrient during cultivation. Ammonium sulfate was intentionally used as the nitrogen source rather than increasing the yeast extract concentration. Yeast extract represents a complex and chemically undefined nutrient source that contains not only nitrogen but also additional phosphorus, trace elements and organic growth factors. Increasing its concentration would therefore introduce uncontrolled phosphorus into the medium and potentially interfere with the intended phosphate limitation. The use of ammonium sulfate as a defined nitrogen source allowed precise control of the nutrient limitation regime while avoiding unintended phosphate supplementation. The applied phosphate concentration was based on preliminary shake-flask experiments in which the phosphate consumption of the investigated yeast strains was determined using photometric phosphate measurements. The selected concentration ensured that phosphate became limiting during the cultivation while still allowing sufficient initial biomass formation across all strains. The nutrient-replete mineral salt solution consisted of 8.99 g L^{-1} potassium dihydrogen phosphate, 0.12 g L^{-1} disodium hydrogen phosphate, 0.1 g L^{-1} sodium citrate dihydrate, 0.1 g L^{-1} yeast extract, 0.2 g L^{-1} magnesium sulfate heptahydrate and 100 g L^{-1} ammonium sulfate. A trace element solution was added at 2% (v/v) after sterile filtration and contained 4 g L^{-1} calcium chloride dihydrate, 0.55 g L^{-1} iron(II) sulfate dihydrate, 0.475 g L^{-1} citric acid, 0.1 g L^{-1} zinc sulfate heptahydrate and 0.075 g L^{-1} manganese(II) sulfate monohydrate, supplemented with 100 µL L^{-1} concentrated sulfuric acid (96%). A salt solution, added at 2% (v/v) after autoclaving, consisted of 10 g L^{-1} yeast extract and 20 g L^{-1} magnesium sulfate heptahydrate. Glucose was supplied as a separately autoclaved solution at a concentration of 90 g L^{-1}.

Chapter 4: 2.4 Reactivation of Cryostocks and Precultures

Yeast strains were stored as cryostocks containing 150 µL glycerol and 850 µL yeast suspension at a biomass concentration of 20 g L^{-1} and kept at −80 °C until use. For reactivation, cryostocks were streaked onto YM agar plates composed of 10 g L^{-1} glucose, 3 g L^{-1} yeast extract, 3 g L^{-1} malt extract, 5 g L^{-1} peptone and 15 g L^{-1} agar, adjusted to pH 7.0, and incubated at 20 °C for 7 days. Single colonies were transferred aseptically into preculture flasks containing liquid cultivation medium corresponding to the nitrogen-limited bioreactor medium. This medium consisted of autoclaved nitrogen-limited mineral salt solution supplemented with 7.7% (v/v) sterile-filtered trace element solution, 7.7% (v/v) autoclaved salt solution and 7.7% (v/v) autoclaved glucose solution. Precultures were incubated for 4 days at 20 °C and 130 rpm. Nitrogen-limited conditions were chosen to ensure a uniform physiological state across all experiments and to reflect the standard cultivation conditions applied in this study. Although nitrogen limitation may induce physiological adaptations such as the onset of lipid accumulation, changes in nitrogen metabolism, and a redistribution of carbon flux, all experimental setups, including phosphate-limited and non-limited cultivations, were inoculated with cells originating from the same nitrogen-limited cultivation condition. Thus, any effects associated with nitrogen limitation were common to all conditions and did not bias the comparison between the different nutrient regimes. Subsequently, 1 mL of each preculture was transferred into fresh medium of identical composition and incubated for an additional 4 days under the same conditions to ensure physiological stabilization prior to bioreactor inoculation.

Chapter 4: 2.5 Bioreactor Cultivation

Main cultivations were performed in 2.5 L stirred-tank bioreactors (Minifors, Infors HT (Bottmingen, Switzerland)) with a working volume of 1.2 L and a total cultivation time of 144 h. Cultivation parameters were selected based on previously optimized conditions for *S. podzolica* DSM 27192 and applied uniformly to all strains to prioritize cross-strain comparability over strain-specific optimization [162]. Temperature was maintained at 22.5 °C, agitation at 600 rpm, and aeration at 1 vvm. The pH was controlled at 4.0 using automated addition of 4 M sodium hydroxide in combination with either 4 M phosphoric acid for nitrogen-limited and nutrient-replete cultivations or 4 M sulfuric acid for phosphate-limited cultivations to avoid phosphate supplementation. pH was monitored using an EasyFerm Plus PHI K8 225 probe (Hamilton Company, Bonaduz, Switzerland), while dissolved oxygen tension (pO_2) was measured using a VisiFerm DO Arc 225 H0 probe (Hamilton Company, Bonaduz, Switzerland). Off-gas analysis was conducted with BlueVary analyzers (BlueSens (Herten, Germany)), and all process data were recorded using BlueVis software (version 4.64.96). Bioreactors were inoculated to an initial optical density at 600 nm (OD_{600}) of 1.0, as determined spectrophotometrically. Foaming was controlled by daily addition of Contraspum A 4050 (Zschimmer & Schwarz, Lahnstein, Germany) during the first 72 h of cultivation, with 100 µL added for *C. oleaginosum*, *S. podzolica* and *S. segobiensis*, and 1 mL added for *A. porosum*. The potential influence of antifoam addition on oxygen transfer and analytical readouts was systematically evaluated as described in Section 2.16. Different antifoam volumes were required to achieve comparable foam control due to strain-specific foaming behavior.

During the first 72 h of cultivation, 24 mL d^{-1} of trace element solution and 24 mL d^{-1} of salt solution were supplied to prevent micronutrient limitation. Glucose feeding was adjusted to maintain a concentration of 90 g L^{-1}, as determined by an enzymatic D-glucose assay. To prevent sulfate limitation without affecting nitrogen limitation kinetics, ammonium sulfate was added to a final concentration of 50 g L^{-1} after 72 h in phosphate-limited and nutrient-replete cultivations. Samples were taken every 24 h, comprising 5 mL for optical density and cell dry weight determination and 20 mL for biomass and supernatant analyses. Biomass pellets were recovered by centrifugation, freeze-dried, and stored at −20 °C until further analysis. All cultivations were performed in biological duplicates, and nitrogen-limited and nutrient-replete cultivations additionally included technical duplicates.

Chapter 4: 2.6 Determination of Cell Dry Weight

Cell dry weight (CDW) was determined gravimetrically in triplicate for each sampling point. For this purpose, 1 mL of cultivation broth was transferred into pre-dried and pre-weighed 1.5 mL reaction tubes and centrifuged at 13,000 rpm for 10 min. The supernatant was removed and retained for subsequent analyses. The biomass pellet was washed once with deionized water and centrifuged again under identical conditions. After removal of the wash solution, the pellets were dried at 60 °C for 24 h and weighed using a precision balance (ADB220, Kern (Balingen, Germany)). Cell dry weight was calculated from the mass difference before and after drying.

Chapter 4: 2.7 Ammonium Quantification

Ammonium concentrations in the culture supernatant were quantified using the NH_4-N Spectroquant® assay (Merck KGaA (Darmstadt, Germany)), adapted to microplate format. Calibration standards ranging from 0 to 4 mg L^{-1} NH_4-N were prepared from ammonium sulfate dissolved in deionized water. For analysis, 250 µL of each sample or standard were transferred into 1.5 mL reaction tubes. Reagent 2 from the assay kit was dissolved in 600 µL of Reagent 1 to prepare the working reagent (Reagent 1 + 2), of which 30 µL were added to each tube. After thorough mixing and incubation for 5 min, 5 µL of Reagent 3 were added, followed by an additional 5 min incubation. Subsequently, 200 µL of each reaction mixture were transferred to a 96-well microplate, and absorbance was measured at 690 nm using a Tecan Infinite® 200 PRO plate reader (Tecan Trading AG (Männedorf, Switzerland)). Ammonium concentrations were calculated based on the calibration curve.

Chapter 4: 2.8 Phosphate Quantification

Orthophosphate concentrations in the supernatant were determined using the o-Phosphate Spectroquant® assay (Merck KGaA). Calibration standards ranging from 0 to 14.5 mg L^{-1} phosphate were prepared from phosphoric acid (85%) diluted in deionized water. For each measurement, 2 mL of sample or standard were transferred into 2 mL Safe-Lock reaction tubes. Two drops of Reagent 1 were added, followed by a small spatula of Reagent 2, approximately half the size of the provided micro-scoop. After thorough mixing and incubation for 5 min, 200 µL of each sample were transferred to a 96-well plate. Absorbance was measured at 710 nm at room temperature using a Tecan Infinite® 200 PRO (Tecan Trading AG), and phosphate concentrations were calculated using the corresponding calibration curve.

Chapter 4: 2.9 Fatty Acid Methyl Ester Analysis

Lipid-derived fatty acids were analyzed via direct transesterification of freeze-dried biomass to fatty acid methyl esters (FAMEs). For each sample, 30 mg of biomass were combined with 1.5 mL n-hexane, 0.5 mL of heptadecanoic acid solution (2 mg mL^{-1} in hexane) as an internal standard, and 2 mL of methanolic sulfuric acid (15%, v/v) in glass reaction tubes. Samples were incubated at 100 °C and 1000 rpm for 2 h in a thermoshaker, with additional vortexing every 30 min to ensure homogeneous mixing. The reaction was terminated by cooling on ice, followed by the addition of 1 mL deionized water to promote phase separation. The upper hexane phase containing the FAMEs was collected and transferred into chromatography vials. FAMEs were analyzed using a gas chromatograph (Agilent 6890N, Agilent, Santa Clara, CA, USA) equipped with a flame ionization detector and a DB-Wax capillary column (30 m × 0.25 mm). A volume of 2 µL was injected, and separation was achieved using a temperature program starting at 160 °C and increasing to 240 °C at a rate of 2 °C min^{-1}, followed by a final hold of 15 min. Fatty acids were identified and quantified using a marine oil FAME mix standard (Restek, Bellefonte, PA, USA), covering all fatty acids detected in yeast lipid samples.

Chapter 4: 2.10 Total Lipid Determination by Soxhlet Extraction

Total lipid content was determined gravimetrically by Soxhlet extraction according to Gorte et al. [169]. Briefly, 0.5 g of washed and freeze-dried biomass were bead-milled for 5 min at 30 Hz using 12 mm stainless-steel beads. The disrupted biomass was transferred into extraction thimbles and extracted with 50 mL n-hexane under reflux conditions for 3–4 h. After extraction, the solvent was removed, and lipid content was determined gravimetrically.

Chapter 4: 2.11 Protein Quantification

Protein content was determined using the DC™ Protein Assay (Bio-Rad, Hercules, CA, USA), based on the Lowry method, with bovine γ-globulin as calibration standard. Biomass samples (10 mg) were hydrolyzed in 1 mL of 1 M sodium hydroxide at 95 °C for 1 h. Aliquots of 5 µL were transferred into 96-well plates, followed by addition of Reagent A′ and Reagent B according to the manufacturer's instructions. Absorbance was measured at 750 nm after 15 min incubation, and protein concentrations were calculated from the standard curve.

Chapter 4: 2.12 Carbohydrate Quantification

Total carbohydrate content was quantified using the anthrone–sulfuric acid assay. Freeze-dried biomass (20 mg) was suspended in deionized water, diluted appropriately, and reacted with freshly prepared anthrone reagent (0.75 (w/v) anthrone in 88% (v/v) sulphuric acid). Samples were incubated at 95 °C for 10 min, cooled on ice, and absorbance was measured at 510 nm. Carbohydrate concentrations were calculated using glucose calibration standards.

Chapter 4: 2.13 Gluconic Acid Determination

Gluconic acid concentrations were quantified by HPLC using an Agilent 1100 system equipped with a Synergi™ Fusion-RP column (Phenomenex, Torrance, CA, USA) operated at 30 °C. Separation was achieved using 20 mM KH_2PO_4 (pH 2.5) as mobile phase, and detection was performed by UV absorbance at 220 nm. Quantification was based on external calibration with D-gluconic acid standards.

Chapter 4: 2.14 Ethanol Determination

Ethanol concentrations were determined by HPLC using an Agilent 1100 system equipped with a Rezex ROA organic acid H^+ column (Phenomenex, Torrance, CA, USA). Samples were separated at 50 °C using 5 mM sulfuric acid as mobile phase at a flow rate of 0.5 mL min^{-1} and detected with a refractive index detector. Ethanol concentrations were calculated from external calibration standards.

Chapter 4: 2.15 Fatty Acid Profile-Derived Parameters

Average unsaturation (AU), cetane number (CN), iodine value (IV), kinematic viscosity (KV), specific gravity (SG) and heating value (HV) were calculated from fatty acid profiles according to established equations reported by Qian et al. [170].
Mathematical equations after Qian et al.:

$$AU = \Sigma M \times Yi \quad (1)$$

M: number of double bonds, Yi: ratio of fatty acids

$$CN = -6.6684AU + 62.876 \quad (2)$$

$$IV = 74.373AU + 12.71 \quad (3)$$

$$KV = -0.6316AU + 5.2065 \quad (4)$$

$$SG = -0.0055AU + 0.8726 \quad (5)$$

$$HV = 1.7601AU + 38.534 \quad (6)$$

Chapter 4: 2.16 Influence of Antifoam on Analytical Measurements

The influence of the antifoam agent Contraspum A 4050 on oxygen transfer, optical density measurements and FAME analysis was systematically evaluated. Detailed experimental procedures and results are provided in the Supplementary Materials. The experiments described in this section were performed to assess the potential influence of antifoam addition on analytical measurements. The obtained data were not used to correct or adjust the lipid titres, fatty acid profiles or other reported values presented in this study. Instead, these results were used solely to evaluate the potential magnitude of antifoam-related analytical artifacts and to support the interpretation of the results in the discussion.

Chapter 4: 2.17. Statistical Analysis

Statistical comparisons between cultivation conditions were performed for the datasets presented in Figure 24 and Figure 26. Differences between groups were evaluated using Tukey test for multiple comparisons. The analysis was applied to compare the mean values obtained for the different nutrient regimes within each strain. All results are presented as mean values ± standard deviation based on biological replicates unless stated otherwise. Statistical significance was evaluated at $p < 0.05$. Statistical analyses were performed using OriginPro (VER. 10.0.0.154, OriginLab Corporation, Northampton, MA, USA).

Chapter 4: 3. Results

Economically viable SCO processes require not only high lipid contents but also sufficient biomass formation, favorable production rates, and process robustness, which were systematically evaluated in the following sections.
The four oleaginous yeasts investigated in this study exhibit distinct physiological traits that may affect their response to different nutrient limitation strategies. These differences motivated a systematic, reactor-scale comparison of phosphate-limited, nitrogen-limited and nutrient-replete (unlimited) cultivations across multiple strains under identical process conditions. For clarity, mean values across all four strains are presented in the main figures, while strain-specific results are provided in the Supplementary Materials.

Chapter 4: 3.1. Verification of Nutrient Limitation

While nitrogen limitation represents the established strategy for lipid induction in oleaginous yeasts, phosphate limitation remains comparatively understudied, particularly at bioreactor scale. Ensuring well-defined and reproducible nutrient limitation was therefore a prerequisite for this study. Figure 23 shows the temporal evolution of ammonium and phosphate concentrations averaged across all strains under the three cultivation regimes. Averaged profiles are shown to illustrate the general limitation patterns, while strain-specific nutrient dynamics are provided in the Supplementary Materials (Figure S10-Figure S13).

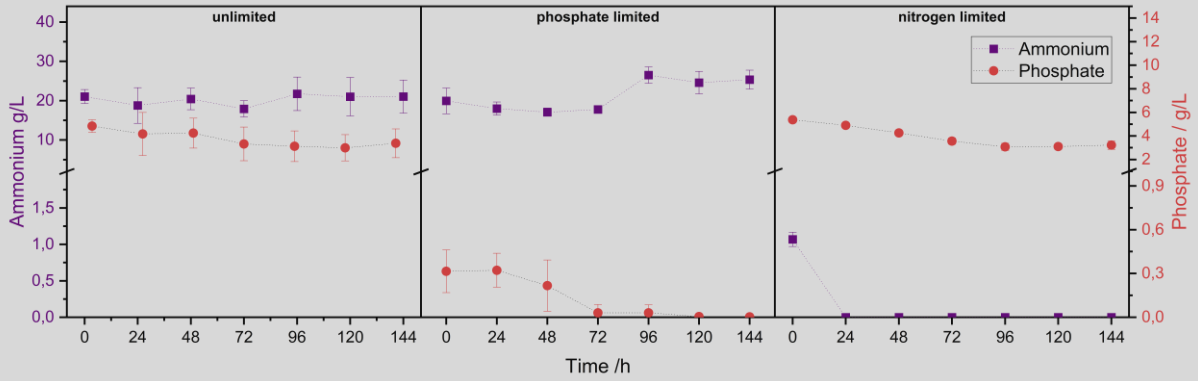

Figure 23: Temporal profiles of ammonium and phosphate concentrations during nitrogen-limited, phosphate-limited and nutrient-replete ("unlimited") bioreactor cultivations, shown as mean values across all duplicates of the four strains (n = 8). Dotted lines indicate trends for visual guidance only.

Under nutrient-replete conditions, neither ammonium nor phosphate concentrations decreased below 5 g L^{-1} throughout the cultivation, confirming the absence of macronutrient limitation. In phosphate-limited cultivations, phosphate concentrations decreased to undetectable levels (below the assay detection limit of 0.5 mg/L ortho-phosphate) after approximately 72 h, while ammonium concentrations remained above 15 g L^{-1}, confirming selective phosphate limitation. In contrast, nitrogen-limited cultivations reached undetectable ammonium concentrations (below the assay detection limit of 0.1 mg/L ammonium) after approximately 24 h, whereas phosphate concentrations remained above 2 g L^{-1}. The prolonged pH control phase observed in Figure S14 during nitrogen-limited cultivations until approximately 56 h coincided with the depletion of extracellular ammonium, whereas no comparable pH response was observed under phosphate-limited conditions. This difference reflects the distinct depletion kinetics of nitrogen and phosphate under the applied cultivation regimes and should be considered when interpreting lipid accumulation kinetics, particularly in short-term fermentations.

Chapter 4: 3.2. Biomass Formation Under Different Nutrient Regimes

Final cell dry weight (CDW) concentrations after 144 h are shown in Figure 24. The cultivation time of 144 h was selected to capture both the biomass formation phase and the subsequent production phase typically observed in oleaginous yeast cultivations. This duration corresponds to cultivation times commonly reported in the literature for oleaginous yeasts [162] and ensures that both growth and product formation beyond the exponential phase are adequately represented. Across all strains, phosphate-limited cultivations resulted in the lowest biomass concentrations, highlighting the pronounced influence of phosphate availability on growth. *A. porosum* achieved the highest CDW under nitrogen-limited conditions (35.74 ± 2.02 g L−1), exceeding biomass concentrations obtained under nutrient-replete conditions (32.45 ± 3.63 g L−1), while exhibiting the lowest CDW under phosphate-limited conditions (11.04 ± 3.22 g L−1). For this strain, CDW under nitrogen-limited conditions was significantly higher than under phosphate-limited conditions ($p \leq 0.001$; Figure 24). Observed trends were consistent across biological replicates and are interpreted in the context of a controlled cross-strain benchmark rather than strain-specific optimization.

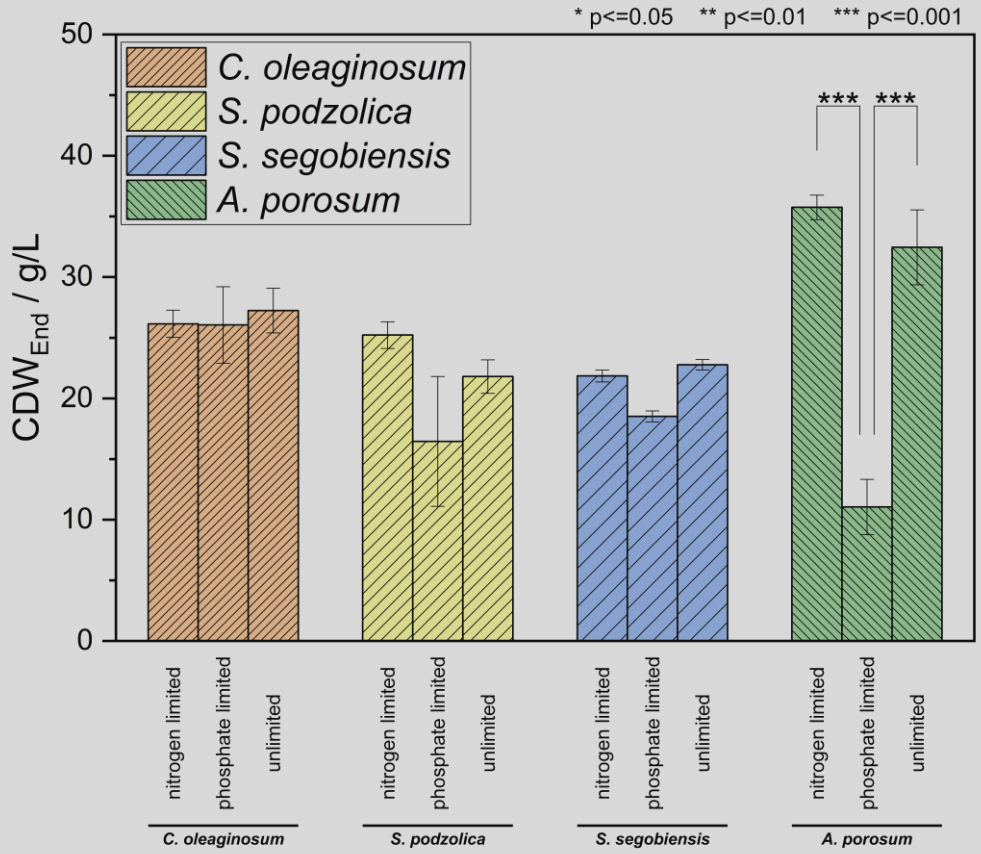

Figure 24: Final cell dry weight (CDW) concentrations after 144 h of bioreactor cultivation under nitrogen-limited, phosphate-limited and nutrient-replete ("unlimited") conditions for C. oleaginosum, S. podzolica, S. segobiensis and A. porosum. Bars represent mean values ± standard deviation of biological duplicates (n = 2). Statistical differences between nutrient regimes within each strain were evaluated using Tukey test. Statistical significance was tested at three predefined levels ($p \leq 0.05$, ** $p \leq 0.01$, and *** $p \leq 0.001$). However, only one comparison reached statistical significance and is therefore indicated in the graph as ***. The absence of additional * or ** annotations is intentional and indicates that all remaining comparisons did not meet any of the tested significance thresholds ($p > 0.05$).*

In contrast, for *C. oleaginosum* only minor differences in final CDW between nutrient regimes were observed, suggesting a limited impact of phosphate availability on biomass formation under the applied conditions. Slightly higher CDW values observed under nitrogen-limited compared to nutrient-replete conditions may reflect changes in biomass composition rather than differences in growth. Previous genomic and transcriptomic studies have highlighted pronounced strain-specific physiological diversity and regulatory adaptations in oleaginous yeasts, including *C. oleaginosum* and *S. podzolica* [171,172]. For *S. segobiensis*, lower biomass concentrations compared to previously reported values were achieved [173], which is consistent with the intentionally unified cultivation conditions (22.5 °C, pH 4.0) applied here to ensure cross-strain comparability rather than strain-specific optimization.

Chapter 4: 3.3. Biomass Composition and Lipid Titres

Because biomass concentration alone does not reflect lipid productivity, biomass composition and absolute lipid titres were analyzed in detail. Protein, carbohydrate and lipid fractions were quantified using complementary analytical methods and combined to assess relative biomass composition (Figure 25).

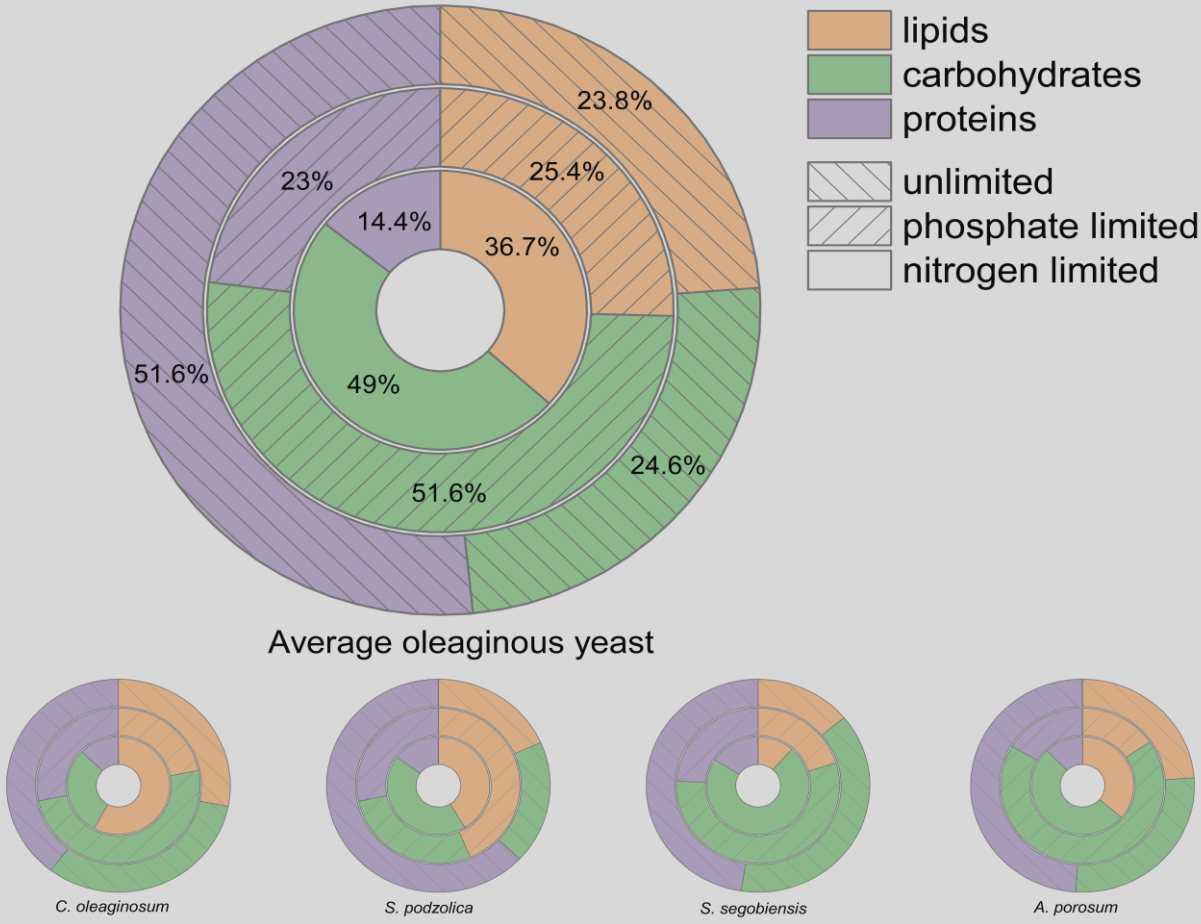

Figure 25: Average relative biomass composition of all oleaginous yeasts at the end of cultivation (144 h) under nutrient-replete ("unlimited"), phosphate-limited, and nitrogen-limited conditions measured in duplicate (n = 8). Strain-specific endpoint compositions are shown below (n = 2).

Clear trends emerged across nutrient regimes. On average, nitrogen limitation resulted in the highest relative lipid content (36.7%), whereas phosphate-limited biomass was characterized by the highest carbohydrate fractions (51.6%), and nutrient-replete biomass consisted predominantly of protein (51.6%). These differences highlight distinct carbon partitioning patterns under the applied nutrient regimes. Elevated carbohydrate fractions under phosphate- and nitrogen-limited conditions indicate sustained carbon incorporation into non-lipid biomass components under nutrient stress. The particularly high carbohydrate fractions observed under phosphate limitation suggest that carbon was preferentially redirected toward carbohydrate storage rather than lipid biosynthesis. In contrast to nitrogen limitation, phosphate limitation does not trigger the classical metabolic cascade associated with lipid accumulation in oleaginous yeasts, in which excess carbon is redirected toward acetyl-CoA and fatty acid synthesis following inhibition of isocitrate dehydrogenase [30]. Instead, phosphate scarcity primarily restricts growth-related processes while carbon assimilation continues, which may promote the accumulation of carbohydrate storage compounds. In addition, phosphate limitation occurred considerably later during the cultivation (~72 h) compared to nitrogen limitation (~24 h), thereby shortening the effective lipid accumulation phase. Consequently, cells had substantially less time to convert excess carbon into storage lipids, which likely contributed to the higher carbohydrate fractions observed under phosphate-limited conditions. This metabolic and temporal difference may explain why phosphate limitation resulted in higher carbohydrate fractions, whereas nitrogen limitation more strongly promoted lipid biosynthesis in the investigated strains.

Strain-specific analysis revealed that while *C. oleaginosum* and *A. porosum* achieved their highest relative lipid contents under nitrogen-limited conditions, *S. podzolica* and *S. segobiensis* accumulated relatively higher lipid fractions under phosphate limitation. Absolute lipid titres (Figure 26) followed a similar trend: nitrogen limitation generally yielded the highest lipid titres, except for *S. segobiensis*, which reached its highest lipid titre under phosphate-limited conditions despite overall low lipid accumulation. For *C. oleaginosum*, nitrogen-limited cultivations resulted in significantly higher lipid titres compared to nutrient-replete conditions ($p \leq 0.01$). Similarly, *S. podzolica* showed significantly higher lipid titres under nitrogen limitation compared to phosphate-limited ($p \leq 0.05$) and nutrient-replete conditions ($p \leq 0.01$). Although *S. segobiensis* showed its highest lipid titre under phosphate-limited conditions, this difference was not statistically significant. This observation nevertheless suggests that lipid accumulation in *S. segobiensis* may respond differently to nutrient limitation compared to the other strains investigated. Similar strain-specific responses have been reported previously and may reflect regulatory differences in carbon partitioning and fatty acid biosynthesis pathways in this organism [173]. In contrast, *A. porosum* did not accumulate substantial lipid amounts under phosphate-limited conditions, underscoring the strain-specific nature of lipid induction under phosphate limitation within the tested organism set. For this strain, nitrogen-limited cultivations resulted in significantly higher lipid titres than both phosphate-limited ($p \leq 0.001$) and nutrient-replete conditions ($p \leq 0.01$). This strain also exhibited markedly reduced biomass formation under phosphate limitation compared to nitrogen-limited and nutrient-replete conditions, suggesting a stronger growth dependency on phosphate availability. One possible explanation is that phosphate scarcity directly constrains cellular processes such as nucleic acid synthesis, ATP metabolism, and phospholipid biosynthesis, which are essential for cell proliferation [174]. Organisms with a stronger coupling between growth and membrane lipid turnover may therefore be more sensitive to phosphate limitation. In contrast, previous studies have shown that *C. oleaginosum* can exhibit considerable metabolic flexibility under nutrient stress, allowing continued lipid accumulation despite growth limitations. These differences highlight the strain-specific physiological responses to phosphate availability and further emphasize that phosphate-induced lipid accumulation is not universally conserved across oleaginous yeasts [30].

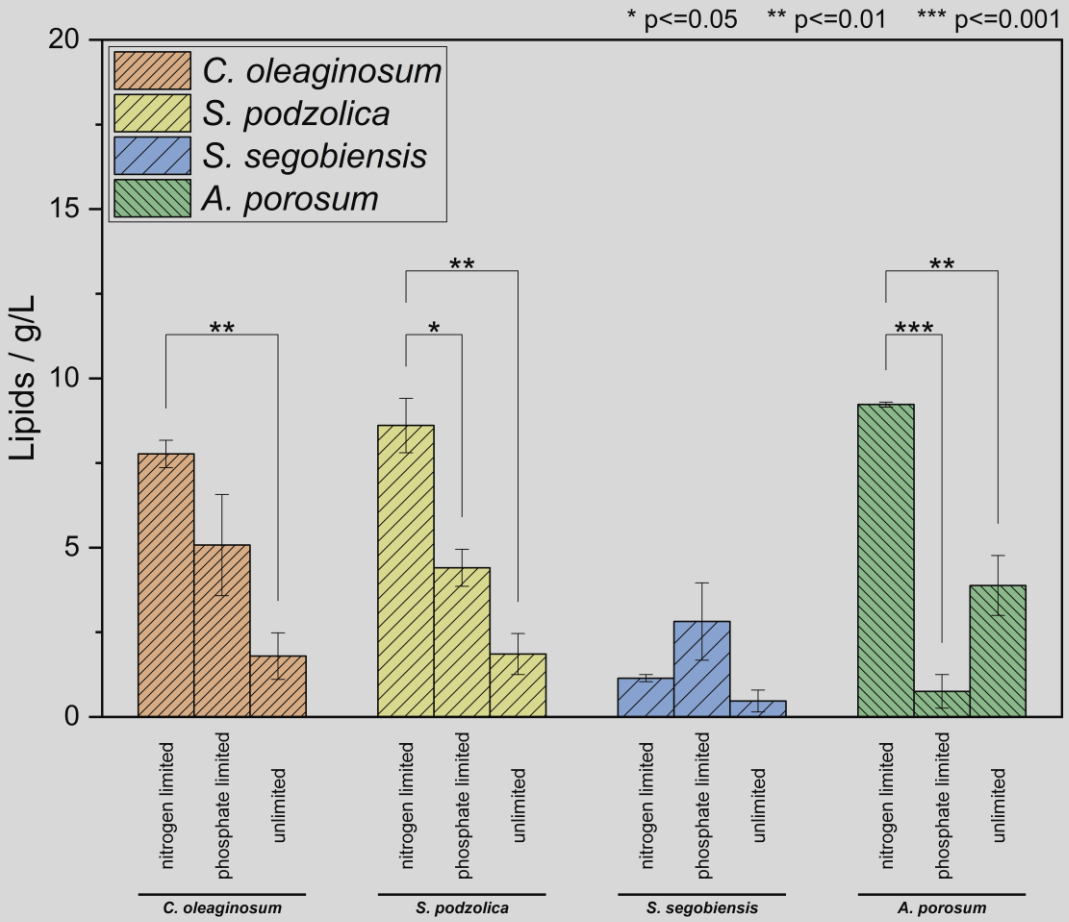

*Figure 26: Final lipid titres (g L−1) obtained after 144 h of bioreactor cultivation under nitrogen-limited, phosphate-limited and nutrient-replete ("unlimited") conditions for all tested oleaginous yeast strains. Bars represent mean values ± standard deviation of biological duplicates (n = 2). Statistical differences between nutrient regimes within each strain were evaluated using Tukey test. Significance levels are indicated as * p ≤ 0.05, ** p ≤ 0.01, and *** p ≤ 0.001.*

Chapter 4: 3.4. Oxygen Consumption, Carbon Utilization and By-Product Formation

Lipid biosynthesis is energetically demanding and requires substantial reducing power, which is predominantly generated under aerobic conditions through respiratory metabolism. Accordingly, nitrogen-limited cultivations exhibited higher oxygen consumption than phosphate-limited cultivations, while under both limitation regimes oxygen uptake exceeded that observed under nutrient-replete conditions (Figure S16-Figure S25). This trend reflects the increased metabolic activity associated with lipid accumulation under nutrient limitation.
Carbon source utilization differed markedly between nutrient regimes. Nitrogen-limited cultivations (with exception of *S. segobiensis*) consumed more glucose than phosphate-limited and nutrient-replete cultivations (Figure S26), resulting in higher lipid yields on glucose (Table S6). In contrast, nutrient-replete cultivations generally resulted in the lowest lipid yields, indicating preferential carbon allocation toward biomass formation rather than storage lipid synthesis. An exception was observed for *A. porosum*, which exhibited its lowest lipid yield under phosphate-limited conditions.

The formation of metabolic by-products such as gluconic acid and ethanol had further influence on process efficiency (Table S7). Under nitrogen limitation, highest gluconic acid yields were observed using *S. podzolica*, while highest ethanol yields were achieved by *S. segobiensis*. *C. oleaginosum* produced increased amounts of gluconic acid under phosphate limitation. Overall, by-product formation did not follow a consistent pattern across nutrient regimes and appeared to be predominantly strain dependent, suggesting that carbon flux to by-product formation is governed by organism-specific metabolic traits rather than by the applied limitation strategy.

Chapter 4: 3.5. Lipid Production Rates and Process Implications

To enable comparison independent of cultivation time and organism, volumetric and specific lipid production rates were evaluated and benchmarked against literature data (Table 3 and Table S8). When considering overall volumetric lipid production rates, nitrogen limitation generally resulted in higher values than phosphate limitation due to enhanced biomass formation, except for *S. segobiensis*. Production rates obtained for *C. oleaginosum*, *S. podzolica* and *A. porosum* were within the range of previously reported values under comparable reactor-scale conditions [162,170,175], while lower rates observed for *S. segobiensis* under nitrogen limitation are consistent with earlier reports [173].

Table 3: Volumetric lipid production rates (g L−1 h−1) and specific lipid production rates (g gCDW−1 h−1) calculated during the nutrient-limitation phase (N or P below detection limit in media until 144 h) for all tested oleaginous yeast strains under nitrogen- and phosphate-limited conditions (n = 3).

Condition	Organism	Lipid production rate [g L^{-1} h^{-1}]	Specific Lipid production rate [g $gCDW^{-1}$ h^{-1}]
Nitrogen limitation	*C. oleaginosum*	0.065 ± 0.005	0.0025 ± 0.0002
Phosphate limitation	*C. oleaginosum*	0.071 ± 0.029	0.0027 ± 0.0011
Nitrogen limitation	*S. podzolica*	0.072 ± 0.001	0.0028 ± 0.0004
Phosphate limitation	*S. podzolica*	0.061 ± 0.011	**0.0037 ± 0.0005**
Nitrogen limitation	*S. segobiensis*	0.010 ± 0.001	0.0004 ± 0.0006
Phosphate limitation	*S. segobiensis*	0.039 ± 0.022	0.0021 ± 0.0007
Nitrogen limitation	*A. porosum*	**0.077 ± 0.001**	0.0022 ± 0.0000
Phosphate limitation	*A. porosum*	0.021 ± 0.025	0.0006 ± 0.0011

Importantly, when evaluating lipid production rates specifically during the nutrient-limitation phase, differences between nitrogen- and phosphate-limited cultivations were substantially reduced. A particularly notable observation was obtained for *S. podzolica*, which exhibited a higher specific lipid production rate under phosphate limitation (0.0037 ± 0.0005 g $gCDW^{-1}$ h^{-1}) than under nitrogen limitation (0.0028 ± 0.0004 g $gCDW^{-1}$ h^{-1}). This finding directly supports the concept that phosphate limitation can enhance lipid productivity at the cellular level independently of biomass formation. Similar trends were also observed for *C. oleaginosum*, where specific lipid production rates under phosphate limitation were comparable or slightly higher than under nitrogen limitation despite lower biomass concentrations. These observations indicate that under phosphate-limited conditions biomass formation, rather than lipid synthesis capacity, represents the primary bottleneck. From a process perspective, these findings suggest that phosphate limitation is particularly suited for long-term or two-stage processes with controlled biomass formation, as well as for the utilization of nitrogen-rich side streams such as molasses, grass juice, wastewater-derived substrates, hydrolysates or protein-rich residues [176-182]. In contrast, nitrogen limitation remains advantageous for short-term fermentations targeting rapid biomass accumulation and high final lipid titres.

Chapter 4: 3.6. Fatty Acid Profiles and Derived Properties

While lipid titres and production rates represent the primary performance indicators for SCO processes, fatty acid composition may influence the suitability of the produced lipids for specific applications. Changes in fatty acid composition under nutrient limitation are primarily driven by alterations in central carbon metabolism and lipid biosynthetic regulation. Under nitrogen-limited conditions, excess carbon that cannot be utilized for biomass formation is redirected toward de novo lipid synthesis. This metabolic shift increases the availability of cytosolic acetyl-CoA and NADPH, thereby promoting fatty acid elongation and desaturation reactions that typically lead to higher proportions of C18 fatty acids such as oleic acid [30,153]. In contrast, phosphate limitation affects lipid metabolism mainly through changes in membrane lipid homeostasis. As phosphate is an essential component of phospholipids, phosphate scarcity can trigger adaptive remodeling of cellular lipid composition, including adjustments in fatty acid chain length and degree of unsaturation to maintain membrane functionality and cellular homeostasis under nutrient stress [38,39,174].
Fatty acid profiles determined after 144 h of cultivation are shown in Figure 27. In general, prolonged oleogenic phases were associated with increased proportions of longer-chain and more unsaturated fatty acids, with nitrogen limitation exhibiting the most pronounced effect, followed by phosphate limitation. Nitrogen-limited cultivations resulted in the highest relative oleic acid contents, whereas phosphate-limited and nutrient-replete conditions led to increased proportions of shorter-chain fatty acids such as myristic acid. The lipid profile of *S. segobiensis* displayed elevated palmitoleic acid fractions under nutrient-replete conditions.

Within the applied cultivation timeframe, phosphate limitation was associated with an increased overall degree of unsaturation. While a higher degree of unsaturation is advantageous for nutritional and medical applications, it can negatively affect combustion-related fuel properties [170,183]. Fuel-relevant parameters calculated from fatty acid profiles (Table S9) fell within ranges characteristic of biodiesel-like fuels, indicating that nutrient limitation influences lipid quality, although further optimization would be required for fuel-oriented applications.

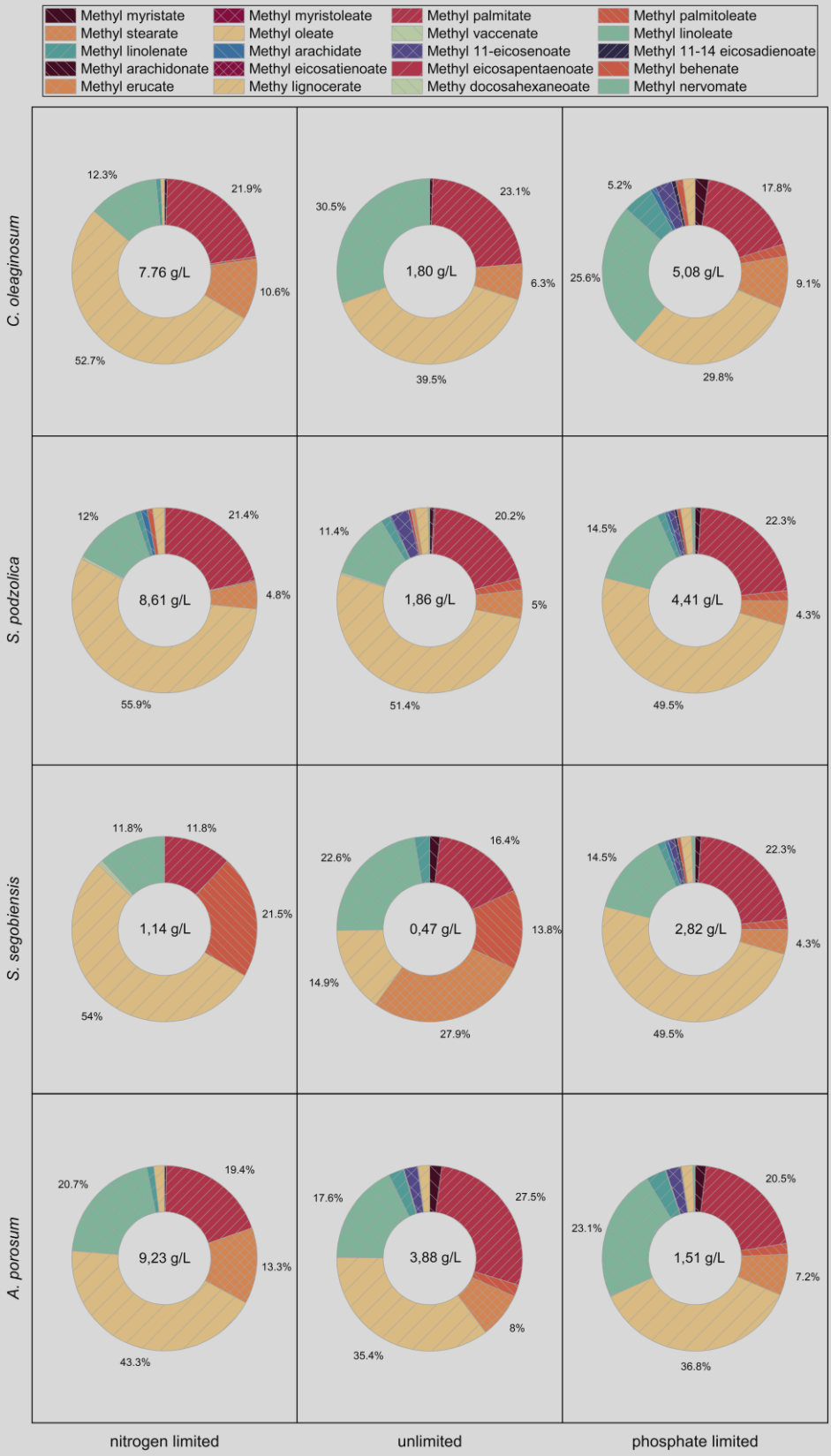

Figure 27: Fatty acid profiles after 144 h of cultivation under nitrogen-limited, phosphate-limited and nutrient-replete (unlimited) conditions. Fatty acids were quantified as fatty acid methyl esters by gas chromatography. The total lipid titre (g L−1) is indicated in the center of each diagram (n = 3).

Chapter 4: 3.7. Influence of Antifoam on Analytical Readouts

Finally, the influence of the antifoam agent Contraspum A 4050 on optical density measurements, oxygen transfer rates and FAME analysis was evaluated (Figure S28-Figure S30). Minor but measurable effects were observed across all analytical methods, highlighting the importance of considering antifoam-induced artifacts in quantitative bioprocess analyses. Increased antifoam addition was required for *A. porosum* cultivations due to pronounced foaming behavior observed under the applied cultivation conditions. Although higher antifoam concentrations were therefore applied for this strain, the performed control experiments demonstrated that the resulting analytical deviations remained small and within the overall experimental variability. Consequently, the increased antifoam usage was considered necessary for stable process operation but did not affect the comparability of the obtained results between strains.

Chapter 4: 4. Conclusions

This study provides a systematic, reactor-scale benchmark of phosphate- and nitrogen-limited SCO production across four oleaginous yeasts, with a specific focus on rate-based performance metrics. While nitrogen limitation yielded the highest lipid titres due to enhanced biomass formation, phosphate limitation resulted in comparable or higher specific lipid production rates in selected strains. These findings indicate that phosphate limitation can decouple cellular lipid productivity from biomass formation. However, the overall lipid titres remained lower under phosphate limitation due to reduced biomass formation, highlighting biomass generation as the primary limiting factor under these conditions.

From a process perspective, phosphate limitation may therefore be particularly advantageous in process configurations where biomass formation is controlled separately from the lipid production phase, such as two-stage fermentations or long-term processes using nitrogen-rich side streams. In contrast, nitrogen limitation remains advantageous for short-term fermentations targeting rapid biomass accumulation and high final lipid titres. By explicitly distinguishing between biomass-driven and rate-driven process regimes, this study provides a framework for selecting nutrient limitation strategies based on process objectives rather than final lipid titres alone. As a practical guideline, phosphate limitation becomes particularly attractive when nitrogen-rich substrates exhibit low initial C/N ratios (<20–30). Under such conditions, achieving the high C/N ratios typically required for nitrogen-limited lipid induction (commonly C/N ≈ 60–120) would require substantial carbon supplementation or nitrogen removal. In these cases, phosphate limitation allows lipid accumulation to be induced without extensive adjustment of the feedstock composition, making it a more practical strategy for nitrogen-rich side streams [30,139].

Future work may also explore whether targeted metabolic engineering strategies, guided by transcriptomic insights into nutrient-limitation responses, could mitigate the biomass bottleneck observed under phosphate-limited conditions. However, overcoming phosphate limitation through genetic engineering remains inherently challenging, as phosphorus is an essential component of central cellular processes including ATP synthesis, nucleic acid metabolism and membrane phospholipid formation [38,39]. Consequently, cellular growth under phosphate scarcity is fundamentally constrained by biochemical requirements. Future strain engineering approaches may therefore focus on improving phosphorus use efficiency or regulatory adaptation to phosphate stress rather than eliminating phosphorus dependency altogether [34,174].

Having established a robust yeast platform under model conditions, the next question naturally arises: can this platform remain productive on inexpensive and chemically challenging side streams? That question is essential for the economic relevance of the whole “straw-to-oil” concept, because a downstream process that depends on refined sugars would contradict the broader residue-based logic of the dissertation. This transition leads to the fifth chapter.

3.2.2 Robust lipid production on untreated crude glycerol through adapted feeding strategies

The fifth chapter introduces a decisive shift from physiological benchmarking to substrate realism. Its role within the dissertation is to test whether the downstream lipid-production platform remains viable when confronted with an industrial side stream that is inexpensive, abundant, but chemically difficult: untreated crude glycerol. This chapter is therefore not only about crude glycerol as a substrate, but about the broader principle of whether oleaginous yeasts can be operated robustly on impurity-rich, inhibitor-containing carbon sources.

The key contribution of this chapter is the demonstration that process design can outweigh substrate purity. Rather than detoxifying or refining the glycerol, the work shows that early inhibition can be mitigated by a simple but effective feeding strategy that lowers the inhibitor-to-biomass ratio during the initial growth phase. The result is a stable and scalable single-cell oil process that remains functional even under substantial substrate variability. In the context of the dissertation, this has great conceptual importance: it establishes that robust lipid production on chemically challenging feedstocks is possible if the process window is engineered appropriately.

This insight becomes especially relevant later, because fungal fermentation broths are similarly complex and inhibitory environments. Chapter 5 therefore provides more than a crude glycerol case study; it defines a general process principle that low-cost, variable, and physiologically difficult feedstocks can still be used productively if the process is adapted to them rather than forcing them into a rigid cultivation regime.

Chapter 5: Adapted Feeding Strategies Enable Efficient Growth and Lipid Accumulation Using Untreated Crude Glycerol in Transition Scale with *Cutaneotrichosporon oleaginosum* ATCC 20509

Kevin Edward Schulz[1*], Paula Hegmann[1], Bastian Dreher[1], Marina Schreidl[1], Katrin Ochsenreither[2] and Anke Neumann[1*]

[1]Institute of Process Engineering in Life Sciences 2: Electrobiotechnology, Karlsruhe Institute of Technology (KIT), Karlsruhe, Germany, [2]Kaiserslautern University of Applied Sciences, Campus Pirmasens, Pirmasens, Germany, * corresponding authors

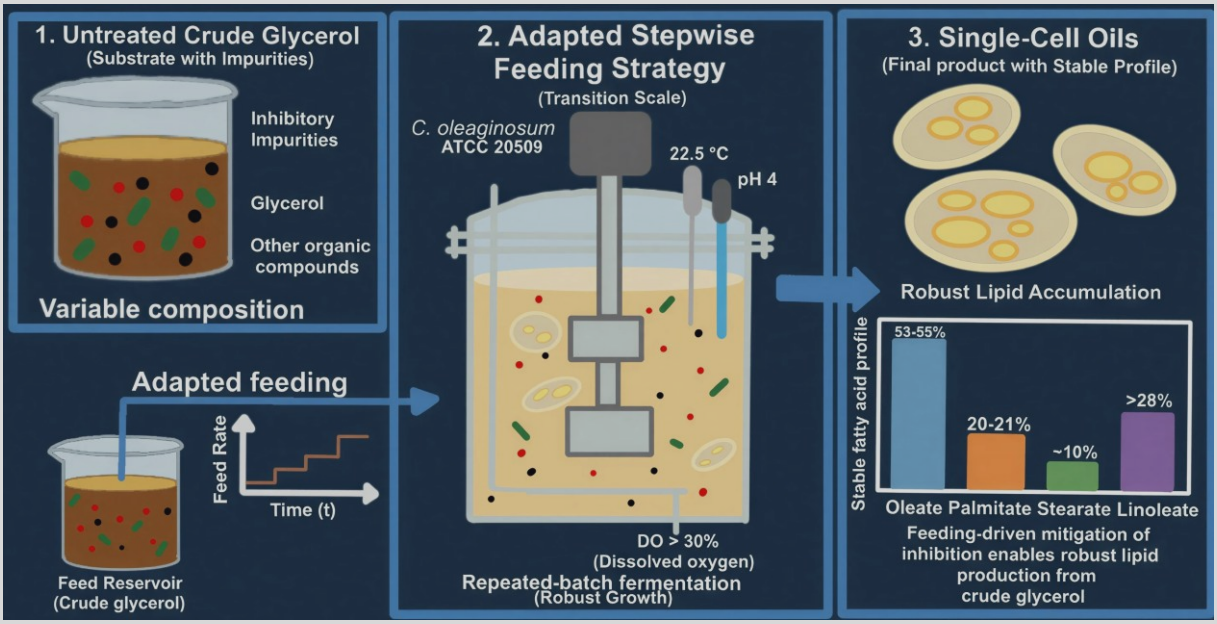

Publishing details:
MDPI Fermentation
Vol. 12 Issue 3
Published on 15 March 2026
doi: 10.3390/fermentation12030154

Author contributions: K.E.S., K.O. and A.N. conceived and designed the research. K.E.S. conducted experiments and wrote the manuscript. P.H., B.D. and M.S. conducted experiments. K.E.S. and A.N. supervised the experiments. K.E.S. analyzed data. K.E.S., K.O. and A.N. revised the manuscript. All authors have read and agreed to the published version of the manuscript.

Chapter 5: 1 Introduction

The progressive depletion of economically viable fossil fuel reserves, together with the steadily increasing global demand for fuels and platform chemicals, underscores the urgent need for sustainable alternatives to safeguard future living standards. Crude oil, the traditional feedstock for fuels and oleochemicals, is a finite resource, and its continued exploitation substantially contributes to greenhouse gas emissions, thereby revealing the inherent limitations of a linear economy. Consequently, innovative solutions that decouple industrial production from fossil resources while simultaneously minimizing environmental impacts are required.

Oleaginous microorganisms, including the unconventional yeast *Cutaneotrichosporon oleaginosum*, represent a promising alternative to fossil oil resources due to their ability to produce single-cell oils (SCOs) [139,184]. These microbial lipids can account for 20–85% of the cell dry mass and exhibit fatty acid compositions comparable to palm oil, rendering them suitable for applications in biofuels, lubricants, and oleochemicals [185-188]. In contrast to conventional oil crops, microbial lipid production is independent of climate and seasonality, does not require arable land, and allows for the utilization of a wide variety of carbon sources. This versatility positions SCOs as a key pillar of future bio-based industries [189,190]. Beyond energy applications, SCOs are gaining increasing relevance in nutraceutical, cosmetic, and environmentally acceptable lubricant markets, further expanding their commercial potential [191,192].

Despite these advantages, microbial lipid production remains economically constrained, largely due to the high costs associated with conventional carbon sources such as glucose. Crude glycerol (CG), the primary byproduct of biodiesel manufacturing, represents a promising low-cost alternative. During transesterification, it accounts for approximately 10% of biodiesel output and is characterized by low price and high energy density. However, CG typically contains inhibitory compounds, including methanol, soaps, and residual catalysts, which can adversely affect microbial growth and lipid biosynthesis [193]. Consequently, avoiding costly purification or detoxification steps is crucial to ensure overall economic viability. Typical CG purification approaches include methanol removal by evaporation or distillation, acidification to split soaps into free fatty acids and salts, ion-exchange or adsorption for catalyst and salt removal, and membrane- or solvent-based separation techniques; however, these steps substantially increase process complexity, capital expenditure, and operating costs, limiting their applicability for low-value bulk bioprocesses [194,195].

Global biodiesel output reached ~52 million tonnes in 2022, with the EU (~13.7 Mt), USA (~10.2 Mt, primarily soybean oil), and Indonesia (~9.7 Mt, palm oil) representing the largest contributors. As a consequence, soybean-, palm-, and animal-fat-derived biodiesel streams represent the major industrial origins of CG worldwide [196-198]. The rapid expansion of biodiesel manufacturing has created a structural surplus of CG as a major by-product of transesterification processes. The continued growth of the biodiesel industry has therefore resulted in large quantities of CG entering the global market. This persistent oversupply has substantially reduced its market value and stimulated increasing interest in alternative valorization routes, including microbial conversion processes. Economically, CG is considerably cheaper than conventional carbon sources such as glucose or sucrose. Historically, CG has been reported to trade at around 100 USD t^{-1} (≈\$0.05 lb^{-1}), making it an attractive substrate for large-scale bioprocesses [199,200]. Beyond economics, glycerol's biochemical properties make it an excellent substrate for lipid-accumulating yeasts. Glycerol is highly reduced; its catabolism generates more NADH per carbon than glucose, providing enhanced reducing power for lipid biosynthesis and offering a thermodynamic advantage for anabolic processes such as fatty acid and triacylglycerol synthesis [201]. Although the efficiency of glycerol assimilation varies markedly among yeast species, the underlying metabolic framework is broadly shared. According to Klein et al. (2017) [43], most current knowledge on glycerol uptake and catabolism stems from studies with laboratory strains of *Saccharomyces cerevisiae*, in which glycerol is funneled into central carbon metabolism through well-established enzymatic routes. These studies demonstrate that glycerol is converted through pathways that ultimately produce dihydroxyacetone phosphate, thereby linking glycerol assimilation directly to glycolysis and energy metabolism. While substantial diversity exists in the ability of different yeasts to grow on glycerol, the fundamental organization of these pathways is conserved across fungi, and the review highlights that the gene products required for glycerol utilization are well documented in *S. cerevisiae*. However, the authors also emphasize that knowledge regarding glycerol uptake and metabolism in non-*Saccharomyces* yeasts remains fragmentary, underscoring the need for further research on species that display superior growth on glycerol compared to conventional laboratory strains [43].

While several studies have demonstrated the feasibility of valorizing CG for microbial lipid production, important conceptual and methodological differences distinguish the present work from previous approaches. For example, a recent study utilizing *Rhodotorula glutinis* R4 investigated the combined valorization of sugarcane vinasse and CG within an integrated biorefinery framework, primarily aiming to couple biodiesel and bioethanol side streams to improve overall system sustainability [52]. That work focused on substrate co-utilization, nutrient supplementation via vinasse, and proof-of-concept lipid production under laboratory-scale batch conditions, with an emphasis on waste stream integration rather than on fermentation robustness or scalability.

Similarly, the study by Ram et al. on *Yarrowia lipolytica* SKY7 evaluated the effects of CG matrix composition and municipal wastewater sludge concentration on SCO production, highlighting the influence of substrate heterogeneity and co-substrate interactions on lipid accumulation [202]. This approach primarily addressed substrate quality effects and environmental biotechnological aspects at a small scale, rather than sustained process performance under industrially relevant fermentation conditions. In contrast, the present study focuses on CG as the sole carbon source, without co-substrate supplementation or detoxification, to reflect realistic industrial feedstock quality. By conducting transition-scale repeated-batch fermentations, the work emphasizes process scalability and stability, lipid accumulation dynamics, and biomass composition over multiple production cycles under representative hydrodynamic and feeding conditions. This process- and scale-oriented perspective provides novel insights into the robustness, scalability, and economic relevance of CG-based SCO production, thereby directly addressing the gap between laboratory-scale waste valorization studies and industrial bioprocess implementation. Prior reports have shown that feeding can offset crude-glycerol-related lag phases in various oleaginous yeasts, and two-stage or rate-controlled schemes can enhance oil titers [44,203,204]. However, most studies operated at a small scale, with pretreated substrates, or with different organisms. In contrast, our work employs untreated and non-sterilized industrial CG as the sole carbon source at transition scale (19 L) across more than 640 h of repeated-batch operation. A deliberately simple staged-feeding design was chosen to limit the inhibitor-to-biomass ratio during early growth, thereby restoring metabolism and lipid formation without substrate detoxification. We further show that lipid content and fatty acid composition remain robust despite substrate-batch variability, a requirement for biodiesel and oleochemical use.

Chapter 5: 2 Materials and Methods

If not stated otherwise, all chemicals were obtained from Carl Roth GmbH & Co. KG (Karlsruhe, Germany). Two different batches of CG, referred to as crude glycerol 1 (CG 1) and crude glycerol 2 (CG 2), were used in this study and were received as “untreated” crude glycerol from BRAIN Biotech AG (CG 1, Zwingenberg, Germany) and Hydroxy Energy GmbH (CG 2, Ochsenfurt, Germany). No further specification was received. CG batches were stored at room temperature in the dark and homogenized by thorough mixing prior to use. CG was used without further purification or sterilization and was added directly to the cultivation medium.
Due to the limited availability of industrial CG batches, all bioreactor fermentations were performed as single biological runs per condition. This constraint is explicitly acknowledged, and the study therefore focuses on robustness of operational trends, consistency across scales, and reproducibility of physiological patterns rather than statistical hypothesis testing.
Unless stated otherwise, all solutions and media were prepared using deionized water (conductivity < 1 µS cm^{-1}) produced using an in-house purification system. Inlet air was supplied via sterile filters prior to entering the bioreactors.
For 2.5 L scale fermentations, liquid media and heat-stable solutions were sterilized by autoclaving at 121 °C for 20 min. Heat-labile components, including trace element solutions, were sterilized by filtration through 0.2 µm pore-size membrane filters prior to use. The 19 L fermentation system was sterilized in situ by steam sterilization at 121 °C for 20 min.

Chapter 5: 2.1 Characterization of Crude Glycerol

Preliminary characterization of the CG batches was performed, including determination of ammonium, protein, carbohydrate, lipid, total carbon, and total nitrogen content, as described in Section 2.5 Analytics. Additionally, optical density at 600 nm was measured (see Section 2.6.9). Glycerol concentration was analyzed using HPLC (see Section 2.6.6).

Chapter 5: 2.2 Heuristic Simulation of Inhibitory Effects

For conceptual illustration and qualitative assessment of inhibitory effects during CG fermentation, a highly simplified heuristic simulation was implemented. The model was not intended to represent a quantitative kinetic description but to illustrate relative trends in inhibitor accumulation in relation to biomass development.
All variables were treated as relative, dimensionless quantities. Time represents discrete cultivation stages rather than continuous time. Inhibitory compounds in CG fermentation are defined as substances originating from biodiesel production or introduced during processing that negatively affect microbial growth and lipid synthesis. These include methanol, soaps (fatty acid salts), catalyst residues such as sodium or potassium hydroxide, and other trace impurities [195]. For the simulation, all inhibitory compounds were treated as a single aggregated factor rather than modeled individually. It was assumed that their effect on growth is proportional to their concentration in the fermentation broth and that these compounds are non-degradable under the applied process conditions. Each addition of CG was considered to introduce a fixed amount of inhibitors, which accumulate linearly over time with feeding events. No chemical or biological detoxification was assumed. The relative inhibition factor was defined as the ratio of inhibitor concentration to the biomass-related variable. Experimental validation was not performed through direct quantification of individual inhibitors; instead, the simulation was qualitatively compared to observed growth trends in bioreactor experiments. Growth delays and reduced biomass formation at higher CG concentrations were interpreted as indirect indicators of inhibitory effects. The simulation was implemented as a discrete step model, with inhibitor input occurring only at defined substrate feeding events.
Assumed exponential biomass increase:

$$B(t) = B_0 e^{(\mu t)} \quad (1)$$

where

- B(t): Relative biomass-related variable at time t
- B_0: Initial value of the biomass-related variable
- μ: Specific growth rate parameter

Abstract dilution term with compound addition:

$$V(t) = V_0 + T(t) \quad (2)$$

where

- V(t): Abstract dilution term.
- V_0: Initial reference value.
- T(t): Cumulative inhibitor-related input.

In this context, T(t) represents a cumulative relative input associated with CG addition rather than a physical quantity, and V(t) is treated as an abstract dilution term without physical units.
Inhibitor accumulation:

$$T(t) = \Sigma\, a(t) \quad (3)$$

where

- a(t): Relative inhibitor input associated with a feeding step.

Inhibitor-related concentration:

$$C(t) = T(t)/V(t) \quad (4)$$

Relative inhibition index:

$$R(t) = C(t)/B(t) \quad (5)$$

This simulation is intended solely as a qualitative conceptual illustration and not as a calibrated or predictive kinetic model.

Chapter 5: 2.3 Microorganism, Reactivation of Stored Cultures and Precultures

The strain used was *Cutaneotrichosporon oleaginosum* ATCC 20509. Previously prepared cryostocks consisting of 150 µL pure glycerol and 850 µL of a 20 g/L yeast culture were stored at −80 °C. For reactivation, cryostocks were streaked onto YM agar plates (10 g/L glucose, 3 g/L yeast extract, 3 g/L malt extract, 5 g/L peptone, 15 g/L agar; pH 7) and incubated for seven days. A single colony from the reactivated plate was transferred to a preculture flask containing liquid cultivation medium using a sterile inoculation loop. Precultures were performed in 250 mL baffled Erlenmeyer flasks with a working volume of 50 mL. The preculture medium corresponded to the nitrogen-limited bioreactor formulation and consisted of autoclaved nitrogen-limited mineral salt solution (8.99 g/L potassium dihydrogen phosphate, 0.12 g/L disodium hydrogen phosphate, 0.1 g/L sodium citrate dihydrate, 0.1 g/L yeast extract, 0.2 g/L magnesium sulfate heptahydrate, and 4.72 g/L ammonium sulfate) supplemented with 7.7% (v/v) sterile-filtered trace element solution (4 g/L calcium chloride dihydrate, 0.55 g/L iron(II) sulfate dihydrate, 0.475 g/L citric acid, 0.1 g/L zinc sulfate heptahydrate, 0.075 g/L manganese(II) sulfate monohydrate, and 100 µL/L sulfuric acid, 96%), 7.7% (v/v) autoclaved salt solution (10 g/L yeast extract and 20 g/L magnesium sulfate heptahydrate), and 7.7% (v/v) autoclaved glucose solution. Precultures were incubated for four days at 20 °C and 130 rpm. Subsequently, 1 mL of the first preculture was transferred to a second flask containing fresh medium, followed by an additional four-day incubation under identical conditions.

Chapter 5: 2.4 Stirred Tank Fermentations

Fermentations were carried out under nitrogen-limited conditions using the mineral salt medium described in 2.3, based on the formulation described by Gorte et al. [162]. The medium adjusted to pH 4 with 4 M phosphoric acid and 4 M sodium hydroxide consisted of four components: (i) a mineral salt solution; (ii) 2% (v/v) sterile-filtered trace element solution; (iii) 2% (v/v) autoclaved salt solution; and (iv) a carbon source adapted to the respective experimental setup further described below.

If not stated otherwise, fermentations were conducted for 144 h in 2.5 L Minifors bioreactor systems (INFORS HT, Bottmingen, Switzerland) with two Rushton turbines (INFORS HT, Bottmingen, Switzerland) controlled by Iris NT software (version 5.34.807.0997) with a working volume of 1.2 L. Cultivation parameters were selected based on the optimized conditions for *Saitozyma podzolica* DSM 27192 reported by Gorte et al. (2020) [162]: 22.5 °C, pH 4.0, agitation at 600 rpm, and aeration at 1 vvm. pH was monitored using an EasyFerm Plus PHI K8 225 probe (Hamilton Company, Reno, Nevada, USA), and dissolved oxygen tension (pO_2) was measured with a VisiFerm DO Arc 225 H0 probe (Hamilton Company, Reno, NA, USA). Exhaust gas composition was analyzed using freshly calibrated BlueVary sensors (BlueSens gas sensor GmbH, Herten, Germany), with data acquisition via BlueVis software (version 4.64.96). Automated pH control was achieved by addition of 4 M phosphoric acid and 4 M sodium hydroxide.

Inoculation volumes were calculated to achieve an initial optical density at 600 nm (OD_{600}) of 1.0, measured with a GENESYS 30 spectrophotometer (Thermo Fisher Scientific, Waltham, MA, USA). Foaming was controlled by daily addition of 100 µL Contraspum A 4050 (Zschimmer & Schwarz, Lahnstein, Germany) during the first 72 h, with dosage adjusted according to strain-specific requirements. Additionally, 24 mL of trace element solution and 24 mL of salt solution were fed daily during the first 72 h. Sampling was performed every 24 h, consisting of 5 mL for OD_{600} measurement and 20 mL for biomass and supernatant analysis. The 20 mL sample was centrifuged at 4700 rpm for 15 min; the supernatant was transferred to a 50 mL tube and stored at −20 °C, while the pellet was freeze-dried using a DW-10N freeze-dryer (Drawell Scientific Instrument Co., Ltd., Chongqing, China) for at least 72 h at −50 °C and 0.35 mbar before storage at −20 °C. All samples were preserved at −20 °C for subsequent analysis.

Three experimental setups were investigated. In the reference setup, pure glycerol was used as the sole carbon source at a concentration of 7.5% (v/v). In the second setup, pure glycerol was replaced by CG at the same concentration to assess the effects of impurities and compositional variability associated with industrial side streams. In the third setup, CG was supplied using an adapted feeding strategy while maintaining the same total substrate load of 7.5% (v/v). In this setup, untreated CG was added cumulatively, amounting to 9 mL after 24 h, 18 mL after 48 h, 27 mL after 72 h, and 36 mL after 96 h, with no further substrate addition thereafter.

Chapter 5: 2.5 Transition-Scale Fermentation

The scale-up from 2.5 L to 19 L was based on maintaining comparable oxygen-transfer conditions rather than specific power input or volumetric mass transfer coefficients due to different geometric properties of the used stir tank reactors. To ensure engineering equivalence, identical impeller design (Rushton turbines), and DOT-controlled aeration (>30% DOT at all times) were applied as primary scale-up criteria. Agitation and aeration rates were dynamically adjusted to maintain these conditions. Transition-scale fermentations were conducted in a 19 L stainless-steel stirred-tank bioreactor (Bioengineering AG, Wald, Zurich, Switzerland) equipped with two Rushton turbines and sensors for pH, temperature, and dissolved oxygen tension (DOT) using a nitrogen-limited mineral salts medium combined with an adapted glycerol feeding strategy similar to 2.4 with adapted volumes of 112.5 mL, 225 mL, 337.5 mL and 450 mL, respectively. Transition-scale experiments were performed with an initial working volume of 15 L. Repeated-batch operations were performed by partial harvest and medium replenishment at defined time points, while maintaining the same mineral medium composition if not stated otherwise and feeding strategy as described for lab-scale fermentations. One initial batch fermentation and three repeated-batch fermentations were conducted, each with a duration of 160 h. While the initial batch fermentation was conducted using CG 1 and was inoculated with 1% (v/v) inoculum, repeated batch 1 used an inoculum size of 5% (v/v). Repeated batch 2 was initiated with CG 2 with 5% (v/v) inoculum. Repeated batch 3 employed the same CG batch as repeated batch 2 but utilized 60% inoculum, reducing the mineral salt content in half due to volume constraints. Throughout all fermentations, pH was controlled at 4.0 by automated addition of 4 M phosphoric acid and 4 M sodium hydroxide. The temperature was maintained at 22.5 °C, sterile air was supplied for aeration, and both agitation speed and airflow rate were dynamically adjusted to meet oxygen demand >30% DOT, starting from the initial settings of 200 rpm and 1 vvm.

Chapter 5: 2.6 Analytics

Chapter 5: 2.6.1 Cell Dry Weight

Cell dry weight (CDW) was determined gravimetrically in triplicate for each sample. Pre-dried and pre-weighed 1.5 mL reaction tubes were filled with 1 mL of cultivation broth and centrifuged at 13,000 rpm for 10 min. The supernatant was retained for further analyses. The cell pellet was washed with deionized water and centrifuged again at 13,000 rpm for 10 min. After removing the remaining water, the pellet was dried at 60 °C for 24 h and weighed using a precision balance (ADB220, KERN & SOHN GmbH, Balingen, Germany).

Chapter 5: 2.6.2 Protein Analysis

Protein content was determined using the commercially available DC™ Protein Assay (Bio-Rad Laboratories, Inc., Laboratories, Inc., Hercules, CA, USA), based on the Lowry method [205]. Lyophilized bovine γ-globulin (Bio-Rad Laboratories, Inc., Laboratories, Inc., Hercules, CA, USA) served as the calibration standard. To prepare the working solution, 20 µL of Reagent S was added per mL of Reagent A, yielding Reagent A′. For the calibration curve, a dilution series of the γ-globulin standard was prepared in a 1:1 mixture of deionized water and 2 M sodium hydroxide, resulting in concentrations of 200 µg/mL, 400 µg/mL, 600 µg/mL, 800 µg/mL, 900 µg/mL, 1000 µg/mL, 1250 µg/mL, and 1500 µg/mL. Samples were prepared by hydrolyzing 10 mg of freeze-dried biomass in 1 mL of 1 M sodium hydroxide for 1 h at 95 °C using a Univortemp MT100/MT100-C Thermoshaker (Universal Labortechnik GmbH & Co. KG, Leipzig, Germany). For optical analysis, 5 µL of each standard or sample was pipetted into a 96-well microplate. Subsequently, 25 µL of Reagent A′ and 200 µL of Reagent B were added, and the plate was shaken for 5 s in a Tecan Infinite® 200 PRO (Tecan Trading AG, Männedorf, Switzerland). Absorbance was measured at 750 nm after 15 min of incubation at room temperature. Photometric measurements were performed with standards in duplicate and samples in triplicate on each plate. Protein concentrations were calculated based on the standard curve and applied dilutions.

Chapter 5: 2.6.3 Carbohydrate Analysis

Carbohydrate content was quantified using the Anthrone–sulfuric acid assay [206]. Glucose stock solutions of 10 g/L and 5 g/L were prepared. The 10 g/L solution was diluted to 1:100, 1:200, and 1:500, while the 5 g/L solution was diluted to 1:50, 1:100, 1:200, and 1:500. These dilutions served as standards and were processed in the same manner as the samples. The Anthrone reagent was freshly prepared by dissolving 0.75% (w/v) Anthrone in 95% sulfuric acid and deionized water to obtain a final concentration of 0.1% (w/v). For sample preparation, 20 mg of freeze-dried biomass were weighed into 2 mL Safe-Lock tubes (Eppendorf SE, Hamburg, Germany), followed by the addition of 2 mL deionized water and thorough mixing. Dilutions of 1:20, 1:100, and 1:200 were prepared from each sample. For measurement, 100 µL of each sample or standard was transferred into 2 mL Safe-Lock tubes, and 1 mL of ice-cooled Anthrone reagent was added. The mixture was homogenized by vortexing, kept on ice, and then incubated in a preheated Univortemp MT100/MT100-C Thermoshaker (Universal Labortechnik GmbH & Co. KG, Leipzig, Germany) at 800 rpm and 95 °C for 10 min. The reaction was stopped by placing the tubes on ice. Absorbance was measured in triplicate at 510 nm using a microplate reader, and carbohydrate concentrations were calculated based on the standard curve.

Chapter 5: 2.6.4 Fatty Acid Analysis

Lipid analysis of oleaginous yeast was performed via direct transesterification of biomass to fatty acid methyl esters (FAME) [207]. For transesterification, 30 mg of freeze-dried biomass were combined in glass test tubes with 1.5 mL n-hexane, 0.5 mL of heptadecanoic acid solution (2 mg/mL in hexane), and 2 mL of 15% sulfuric acid in methanol. The mixture was incubated in a Univortemp MT100/MT100-C Thermoshaker (Universal Labortechnik GmbH & Co. KG, Leipzig, Germany) at 100 °C and 1000 rpm for 2 h, with additional vortexing every 30 min to ensure thorough mixing. The reaction was stopped by cooling on ice. To improve phase separation, 1 mL of deionized water was added. Subsequently, 1 mL of the upper hexane phase containing FAME was transferred to an HPLC vial. Fatty acid profiles were analyzed qualitatively and quantitatively using gas chromatography (Agilent Technologies 6890 N Network GC System, Agilent Technologies, Santa Clara, CA, USA) equipped with a flame ionization detector (FID) operating at 1.9523 bar. Separation was achieved on an Agilent DB-Wax column (30 m × 0.25 mm). Two microliters of each sample were injected at an initial temperature of 160 °C. The oven temperature was increased from 160 °C to 240 °C at a rate of 2 °C/min and held at 240 °C for 15 min. A Marine Oil FAME Mix Standard (Restek Corporation, Bellefonte, PA, USA) was used for calibration and identification of FAME components.

Chapter 5: 2.6.5 Ammonium Analysis

To determine the ammonium concentration in the supernatant, the NH_4-N Spectroquant® test kit (Merck KGaA, Darmstadt, Germany) was employed in a downscaled format [208]. A calibration curve was prepared using ammonium sulfate dissolved in deionized water, with concentrations of 0 mg/L, 0.1 mg/L, 0.2 mg/L, 0.4 mg/L, 0.6 mg/L, 0.8 mg/L, 1.5 mg/L, 2 mg/L, 2.5 mg/L, 3 mg/L, 3.5 mg/L, and 4 mg/L. From each bioreactor sample and calibration standard, 250 µL were transferred into 1.5 mL reaction tubes. A micro-spoon of Reagent 2 from the kit was dissolved in 600 µL of Reagent 1 to prepare a combined reagent (Reagent 1 + 2). Subsequently, 30 µL of Reagent 1 + 2 were added to each tube, followed by thorough mixing. After a 5 min incubation, 5 µL of Reagent 3 were added to each tube. The samples were mixed again and incubated for an additional 5 min. Finally, 200 µL of each sample was transferred to a 96-well plate. Optical density at 690 nm was measured at room temperature using a Tecan Infinite® 200 PRO (Tecan Trading AG, Männedorf, Switzerland), and the ammonium concentration was calculated based on the calibration curve.

Chapter 5: 2.6.6 HPLC Analysis of Glycerin

Glycerol concentrations were determined using an Agilent 1100 Series high-performance liquid chromatography (HPLC) system equipped with an ion-exclusion Rezex ROA Organic Acid H^+ (8%) column (Phenomenex, Inc., Torrance, CA, USA). Separation was performed with a 10 µL injection volume at 50 °C, using a mobile phase of 5 mM sulfuric acid at a flow rate of 0.5 mL/min, and detection was achieved with a refractive index detector. Quantification was based on calibration curves prepared with glycerol concentrations ranging from 0.1 g/L to 10 g/L.

Chapter 5: 2.6.7 Total Carbon (TC) and Total Nitrogen (TN) Analysis

Total carbon (TC) content was measured using a TOC-VCPN analyzer (Shimadzu Corporation, Kyoto, Japan), and total nitrogen (TN) content was determined with a TNM-1 module (Shimadzu Corporation, Kyoto, Japan). The system operated with synthetic air containing 20.5% oxygen (Air Liquide, Paris, France) and an ASI SA24 autosampler (40 mL, Shimadzu). Air pressure was regulated to 200 kPa and 150 kPa via internal barometers. The combustion chamber temperature was set to 680 °C for TC analysis and 720 °C for TN analysis. Halogen gases generated during the process were removed using a halogen scrubber (model p/n 630-00992, Shimadzu Corporation, Kyoto, Japan). All analyses were managed through TOC-ControlV software, version 1.07.00 (Shimadzu Corporation, Kyoto, Japan). TC analysis was carried out with 2/3 injections, 2 washes, SD Max of 0.1000, CV Max of 2.00%, no acid addition with an injection volume of 50 µL, an expected concentration range of 767.5 and 4:50 min total integration time. TN analysis was carried out with 2/3 injections, 2 washes, SD Max of 0.1000, CV Max of 2.00%, no acid addition with an injection volume of 50 µL, an expected concentration range 250 and 4:50 min total integration time.

Chapter 5: 2.6.8 Gas Analytics

Calculations of gathered gas composition data were done similarly to Hartmann et al. [209]. The calculations for oxygen transfer rate (OTR), carbon transfer rate (CTR) and respiratory quotient (RQ) are shown in Equations (6)–(8).

$$OTR = \frac{p_{gas} F_{gas,in}}{R T_{gas}} \left(y_{O_2,in} - \frac{1 - y_{O_2,in} - y_{CO_2,in}}{1 - y_{O_2,off} - y_{CO_2,off}} y_{O_2,off} \right) \quad (6)$$

$$CTR = \frac{p_{gas} F_{gas,in}}{R T_{gas}} \left(y_{CO_2,off} \frac{1 - y_{O_2,in} - y_{CO_2,in}}{1 - y_{O_2,off} - y_{CO_2,off}} - y_{CO_2,in} \right) \quad (7)$$

$$RQ = \frac{CTR}{OTR} \quad (8)$$

Chapter 5: 2.6.9 Optical Density at 600 nm

Determination of optical density at 600 nm (OD_{600}) was conducted using a GENESYS 30 spectrophotometer (Thermo Fisher Scientific, Waltham, MA, USA). Optical density measurements were performed in 1 cm path-length transparent plastic cuvettes (BRAND GmbH + Co. KG, Wertheim, Germany).

Chapter 5: 2.6.10 Data Analysis

Data analysis and visualization were performed using Microsoft Excel and OriginPro Ver. 10.0.0.154. Excel was used for preliminary data processing, calculation of averages, and organization of experimental datasets. Graphical representation and advanced data evaluation were conducted in OriginPro Ver. 10.0.0.154. All analytical measurements (CDW, protein, carbohydrate, fatty acids, ammonium, glycerol) were performed in technical triplicate. Averages and standard deviations were calculated in Excel. Gas-analysis signals (OTR, CTR, RQ) were smoothed using LOWESS filtering in OriginPro Ver. 10.0.0.154 to reduce noise without imposing a kinetic model. Specific growth rates µ, volumetric productivities and substrate uptake rates were calculated from time-resolved concentration differences between sampling points. Gas-phase variables (OTR, CTR, RQ) were calculated according to Equations (6)–(8) in Section 2.6.8.

Chapter 5: 3 Results and Discussion

The following results are based on two untreated industrial CG batches. All fermentations were conducted as single biological runs (n = 1) due to the limited availability of industrial CG. This limitation is explicitly acknowledged, and results are interpreted as operational trends rather than statistically validated performance metrics, consistent with similar long-term CG studies relying on limited replication [199]. While CG 1 was used for the establishment of the feeding strategy in 2.5 L and as a reference in the 19 L scale fermentation, CG 2 was used to assess the general applicability of different CG batches and different inoculum sizes using the adapted feeding strategy.

Comprehensive compositional analysis of the two different CG batches revealed marked variability, most prominently in the carbon-to-nitrogen (C/N) ratio (Table 4). CG 1 exhibited an extremely high C/N (~2.0 × 104), whereas CG 2 showed a still very high but substantially lower value (~4.2 × 102). The observed compositional variability aligns with typical ranges reported for biodiesel-derived CG, which often exhibits strong fluctuations in glycerol purity, soap content, methanol residues, ash, and trace metals depending on the feedstock and catalyst system [196,199]. Such heterogeneity is characteristic of alkaline-catalyzed biodiesel processes and reflects upstream washing efficiency, methanol recovery, and catalyst selection, consistent with values reported for industrial CG streams in previous studies. Nitrogenous components were near or below detection, while protein and carbohydrate fractions were negligible, and the lipid fraction was <2% in CG 1 (Table 4). Given that nitrogenous components were at or below the detection limit, the calculated C/N ratios should be interpreted as indicative descriptors of substrate composition rather than biologically accessible C/N ratios. Such profiles are consistent with the well-documented heterogeneity of biodiesel-derived CG and reflect upstream differences in feedstock oil, alkaline catalysts (NaOH/KOH), methanol recovery, and subsequent neutralization and washing, which govern impurity carry-over (methanol, soaps/fatty acid salts, salts, ash, trace metals) and thereby the inhibitory burden during microbial conversion [195,196].

Table 4: General composition analysis of applied untreated non-sterilized crude glycerol (CG) batches received from industry. Protein content, carbohydrate content and lipid content were determined as percentual value while glycerol concentration is shown in g/L. The ammonium content of crude glycerol 2 (CG 2) was below the detection level of 0.01.

	Proteins/%	Carbohydrates/%	Lipids/%	Ammonium/g/L	C/N Ratio	OD_{600}	Glycerol Concentration/g/L
Crude glycerol 1	0.46	0.06	1.80	0.02 ± 0.02	20,357	0.235	620
Crude glycerol 2	0.02	0.35	n. d.	0.00 *	420	7.840	810

* Below the detection level of 0.01.

This variability matters bioprocess-wise: numerous studies show that CG impurities can slow down growth, shift metabolism (e.g., toward citric acid formation), or inhibit lipid accumulation, with ion content ($Na^+/K^+/SO_4^{2-}$) and residual soaps frequently implicated [195,210]. These observations are consistent with reports describing that methanol, fatty acid salts, and residual alkali exert their strongest inhibitory effects at low biomass concentrations, causing prolonged lag phases or complete growth arrest [199,211]. Untreated industrial CG contains methanol, soaps/fatty acid salts, residual alkaline catalysts (Na^+/K^+ hydroxides), ash, and other minor organics. These impurities can delay growth, trigger osmotic stress, alter pH, or shift carbon flux toward overflow products such as citric acid, with Na^+, K^+, and sulfate loads being particularly inhibitory to some yeasts.

Preliminary growth experiments indicated long lag phases on untreated CG, motivating a simple, qualitative inhibition model that relates an aggregated inhibitor input to biomass development (Section 2.2). While intentionally heuristic, the simulation shown in Figure 28 depicts a key operational insight confirmed across the lipid-fermentation literature: the magnitude of inhibition is highest when biomass concentration is low; consequently, large initial crude-glycerol doses can fully suppress growth, as observed in our batch controls. Staged feeding avoids this by lowering the effective inhibitor-to-biomass ratio in the early phase. This mechanistic rationale is consistent with previous studies reporting that pulsed or rate-controlled feeding circumvented inhibition and restored lipid formation in fermentations with toxic carbon sources. Consequently, high initial CG supplementation is risky, whereas pulsed or continuous addition mitigates inhibition, an approach echoed in fed-batch studies where adapted feeding avoided CG-induced inhibition and restored lipid productivity [44,203].

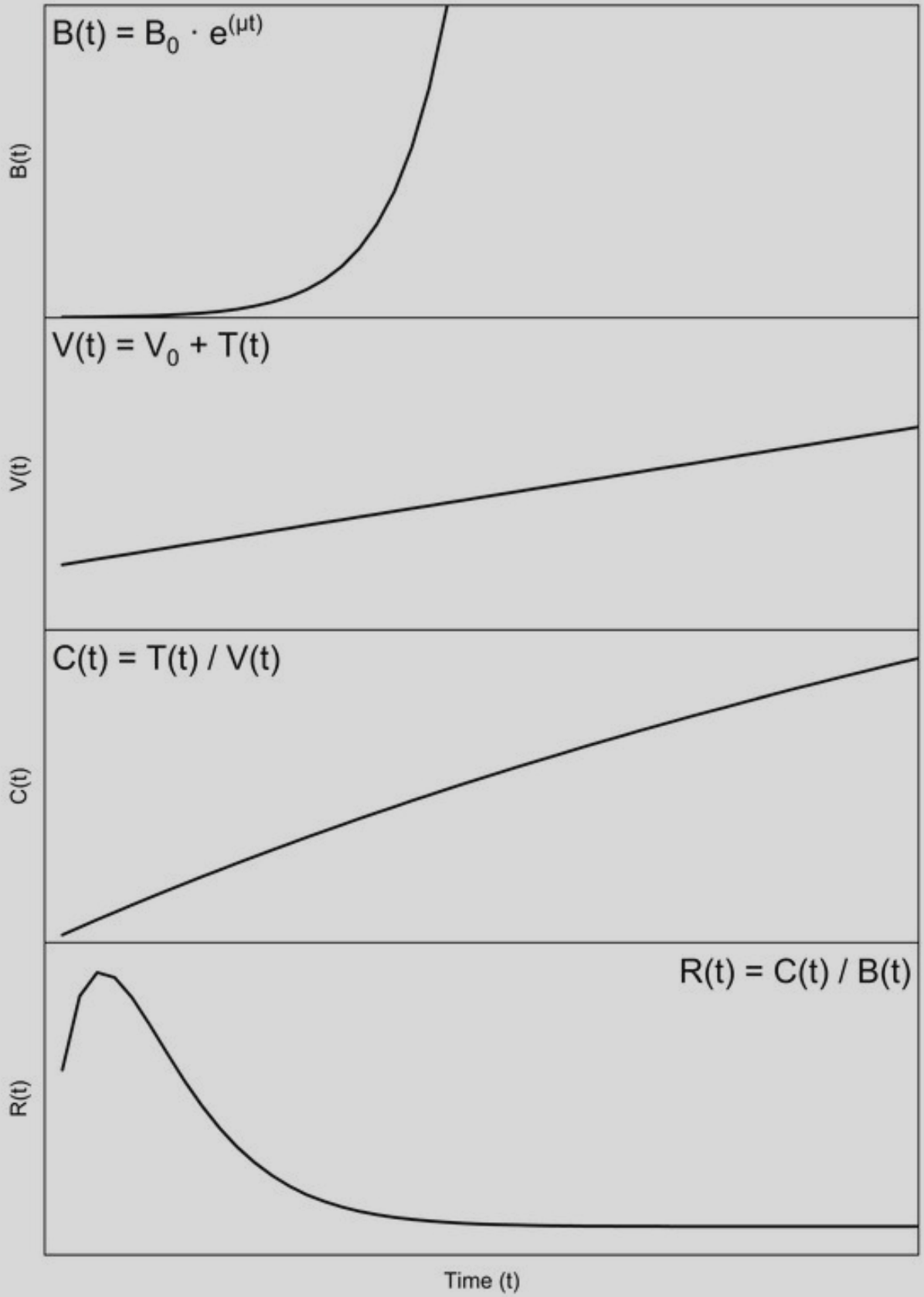

Figure 28: Simulated trends in time of relative biomass-related variable B(t); the change in the abstract dilution term V(t); the change in inhibitor-related concentration C(t); and the behavior of relative inhibition index R(t). All axes are displayed linearly. The conceptual illustration shown does not aim to predict kinetics but serves to visualize the qualitative dependency between initial biomass and effective inhibitor burden per cell. All used formulas are further explained in Section 2.

For *C. oleaginosum* specifically, modeling and experimental work in the literature support efficient lipid accumulation on glycerol at elevated C/N ratios and indicate different process levers to sustain lipid synthesis, reinforcing the rationale to keep inhibitory pressure low while carbon source supply remains abundant, suitable for our heuristic model [212].

As baseline three conditions in 2.5 L scale only using CG 1 to establish the adapted feeding strategy were studied: (i) CG 1 (7.5% (v/v) initial concentration), (ii) pure glycerol (7.5% (v/v) initial concentration) and (iii) CG 1 with adapted stepwise feeding (cumulative 9, 18, 27, 36 mL at 24 h intervals to 72 h), keeping total substrate concentration identical.

While the CG 1 batch fermentation (i) is a reference to evaluate growth without an adapted feeding strategy, the batch fermentation on pure glycerol (ii) was conducted to study growth on glycerol in general. In both fed-batch fermentations, a feeding strategy based on the simulation in Figure 28 was applied. The cumulative pulses (9, 18, 27, and 36 mL at 24 h intervals) were applied as fixed feeding steps. These predefined pulse volumes ensured that the total crude-glycerol input matched the batch control while distributing the inhibitory load over time to maintain a lower inhibitor-to-biomass ratio during early growth. CG was added without sterilization or detoxification. Each pulse was supplied after the scheduled 24 h sampling. In the CG 1 batch fermentation, without adapted feeding, measurable growth or respiratory activity (Figure 29A and Figure 30A) was not detected, consistent with inhibitors surpassing the tolerable per-biomass threshold. In contrast, adapted feeding resulted in growth (Figure 29C,D and Figure 30C,D), ammonium consumption, and off-gas profiles (rise in CTR and OTR) resembling the glycerol cultivation (Figure 29B and Figure 30B), indicating restored metabolic activity under CG despite impurities.

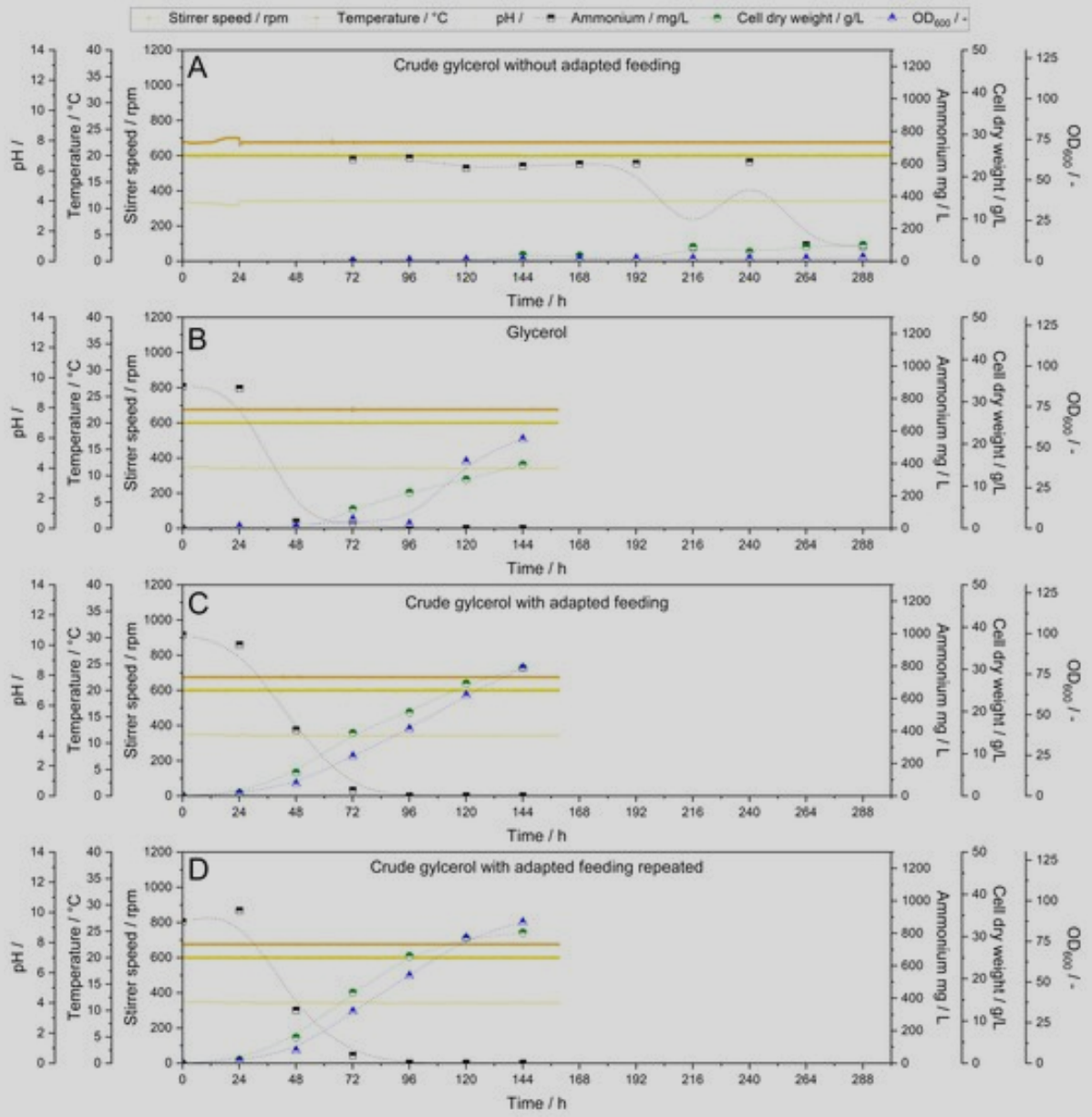

Figure 29: Cultivation parameters pH, temperature, stirrer speed, OD600, cell dry weight and ammonium concentration of 2.5 L stirred tank fermentations of references with (A) CG without adapted feeding, (B) pure glycerol, and of (C,D) with CG with adapted feeding of the strain C. oleaginosum. CG 1 was used. Dotted lines were added only for visual orientation (n = 1).

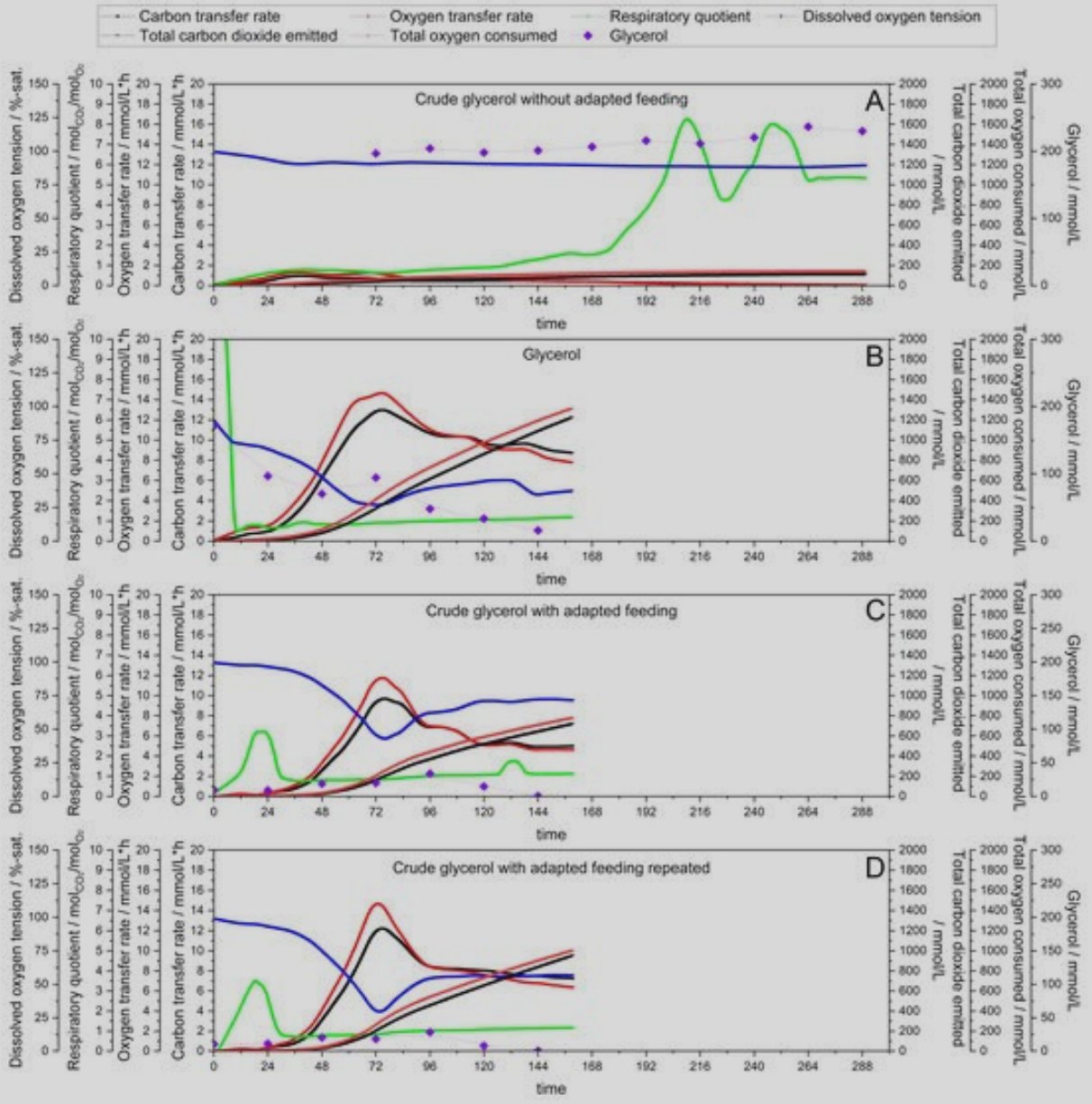

Figure 30: Gas analytics and glycerol concentration of 2.5 L stirred tank fermentations of references with (A) CG without adapted feeding, (B) pure glycerol, and of (C,D) with CG with adapted feeding of the strain C. oleaginosum. Crude glycerol 1 (CG 1) was used. The cumulative curves represent the total carbon dioxide emitted and the total oxygen consumed, which increase continuously over the course of the cultivation. In contrast, the carbon transfer rate and oxygen transfer rate are shown as peak-shaped profiles reflecting the instantaneous metabolic activity of the culture. Carbon dioxide–related parameters are shown in black, whereas oxygen-related parameters are shown in red. Dotted lines were added only for visual orientation (n = 1).

As shown in Table 5, adapted feeding substantially increased apparent growth and production performance, with μ_{Max} rising from 0.16 h^{-1} under batch cultivation on pure glycerol to approximately 0.5 h^{-1} under adapted feeding, and volumetric productivities (P_v) increasing from ~0.01 to ~0.21 g L^{-1} h^{-1}. While n = 1 precludes inference testing, the directional agreement across biomass, substrate, and gas analytics supports the operational value of incremental CG addition to overcome early-phase inhibition—in line with prior fed-batch reports where pulsed or low-rate feeds reduced lag and improved lipid titers on CG in other oleaginous yeasts [44,204].

Table 5: Key performance indicators μMax, YX/S and Pv of fermentations in a 2.5 L scale. Maximum growth rates represent apparent values calculated from biomass data obtained at 24 h sampling intervals, reflecting averaged kinetics rather than instantaneous specific growth rates.

Cultivation	μ_{Max}/h^{-1}	$Y_{X/S}$ $/g_{biomass}/g_{Substrate}$	$P_v/g \cdot L^{-1} \cdot h^{-1}$
Crude glycerol 1	no growth	no growth	0.013
Pure glycerol	0.157	0.116	0.123
Adapted feeding 1	0.514	0.763	0.211
Adapted feeding 2	0.499	0.560	0.215

For each fermentation, biomass was gathered at the endpoint of its respective cultivation and analyzed for biomass composition. The obtained composition data further support the beneficial effects of the adapted feeding strategy (Figure 31). Biomass from the CG 1 batch reference differed markedly in composition, showing reduced lipid content and carbohydrate fractions, and likely represents metabolically stressed cells derived from the inoculum. In contrast, in PG batch fermentation, biomass composition resembled a typical nitrogen-limited *C. oleaginosum* profile (proteins ~17%, carbohydrates ~25%, lipids ~31%). Adapted CG feeding resulted in a comparable lipid fraction (~30%), indicating that lipid accumulation can proceed on untreated CG when inhibition is managed by an appropriate feeding regime.

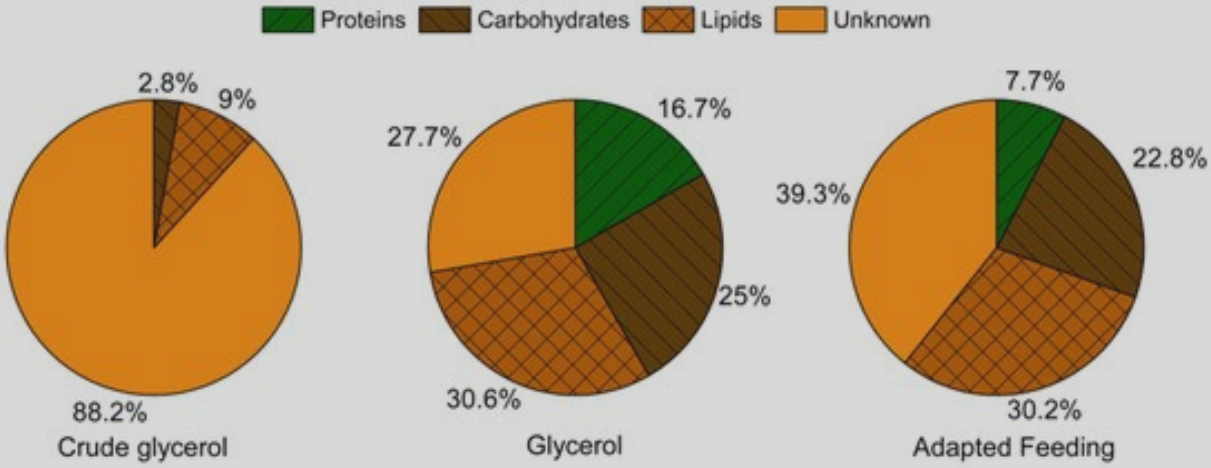

Figure 31: Relative endpoint biomass composition of 2.5 L stirred tank fermentations with C. oleaginosum after 144 h of fermentation time. For protein determination of the reference fermentation with CG not enough biomass was produced. The used CG batch was CG 1 (n = 1).

The reported lipid profile of oleaginous yeasts grown on glycerol is typically enriched in C18:1, C16:0, C18:2, and C18:0, which align with biodiesel and oleochemical specifications [213,214]. Differences in fatty acid profiles can be mechanistically explained by regulation of acetyl-CoA flux, NADPH availability, and desaturase activity. Nitrogen limitation typically favors oleate-rich profiles (C18:1), whereas metabolic stress or incomplete carbon assimilation increases polyunsaturated fractions such as linoleate (C18:2). These trends align with published FA shifts observed in glycerol-based fermentations [199,201]. The fatty acid (FA) profiles detailed in Figure 32 and Table S10 confirm a similar composition under adapted CG feeding in comparison to pure glycerol biomass (Figure 32): biomass from both PG and adapted-CG fermentations were dominated by oleate (~53–55%), with palmitate (~20–21%) and stearate (~10%) as major co-constituents—consistent with oleaginous yeast oils considered suitable for biodiesel due to cetane and oxidative stability contributions from monounsaturates [213,214]. By contrast, CG without adapted feeding (no growth) showed a stressed fatty acid profile with elevated linoleate fractions (>28%), consistent with starvation signatures rather than productive lipid biosynthesis. Further insights into the FA profile are provided in Figure 32; detailed numbers are available in the additional information in Table S10.

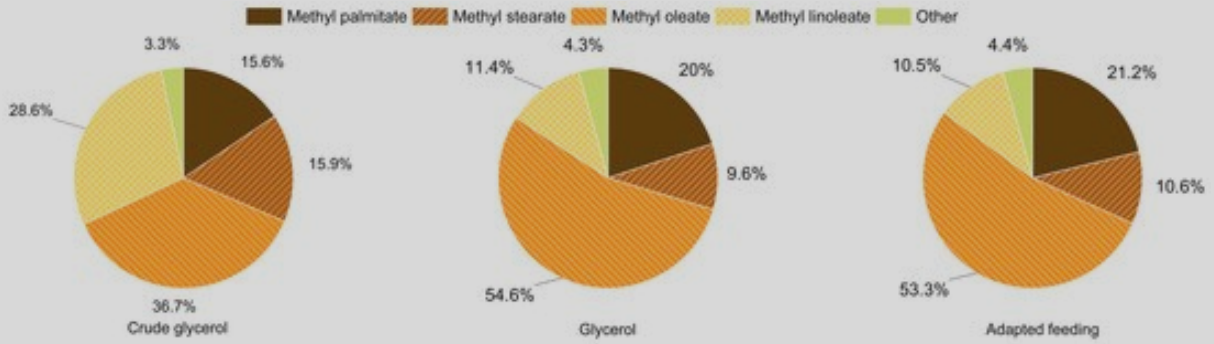

Figure 32: Fatty acid profile of endpoint biomass produced in 2.5 L stirred tank fermentations with C. oleaginosum using CG 1, pure glycerol and adapted feeding with CG 1 (n = 1).

Taken together, these results do not claim statistical equivalence (n = 1) but are consistent with findings from the related literature: for untreated CG, feed design is often sufficient to offset impurity-linked growth delays and to regain lipid titres and quality—especially when glycerol is the sole carbon source and the process remains oxygen-sufficient [44,195].

The fermentation process was scaled up from a 2.5 L laboratory scale to a 19 L transition scale to improve process representativeness and to reduce scale-up risk. At a 2.5 L scale, key engineering parameters such as mixing efficiency, oxygen transfer, and foaming behavior can differ significantly from larger-scale systems, potentially limiting the predictability of downstream scale-up. In addition, repeated-batch fermentations were tested to evaluate process robustness.

At the 19 L transition scale, a repeated-batch regime with DOT-guided adapted aeration and agitation was implemented to address dynamic oxygen demand. Across the initial batch fermentation and three repeated batches, key process variables remained within defined operational ranges (stable pH and temperature; DOT maintained above the set threshold of 30%), and growth trends in OD_{600} and CDW were consistent with expected repeated-batch cultivation patterns (Figure 33).

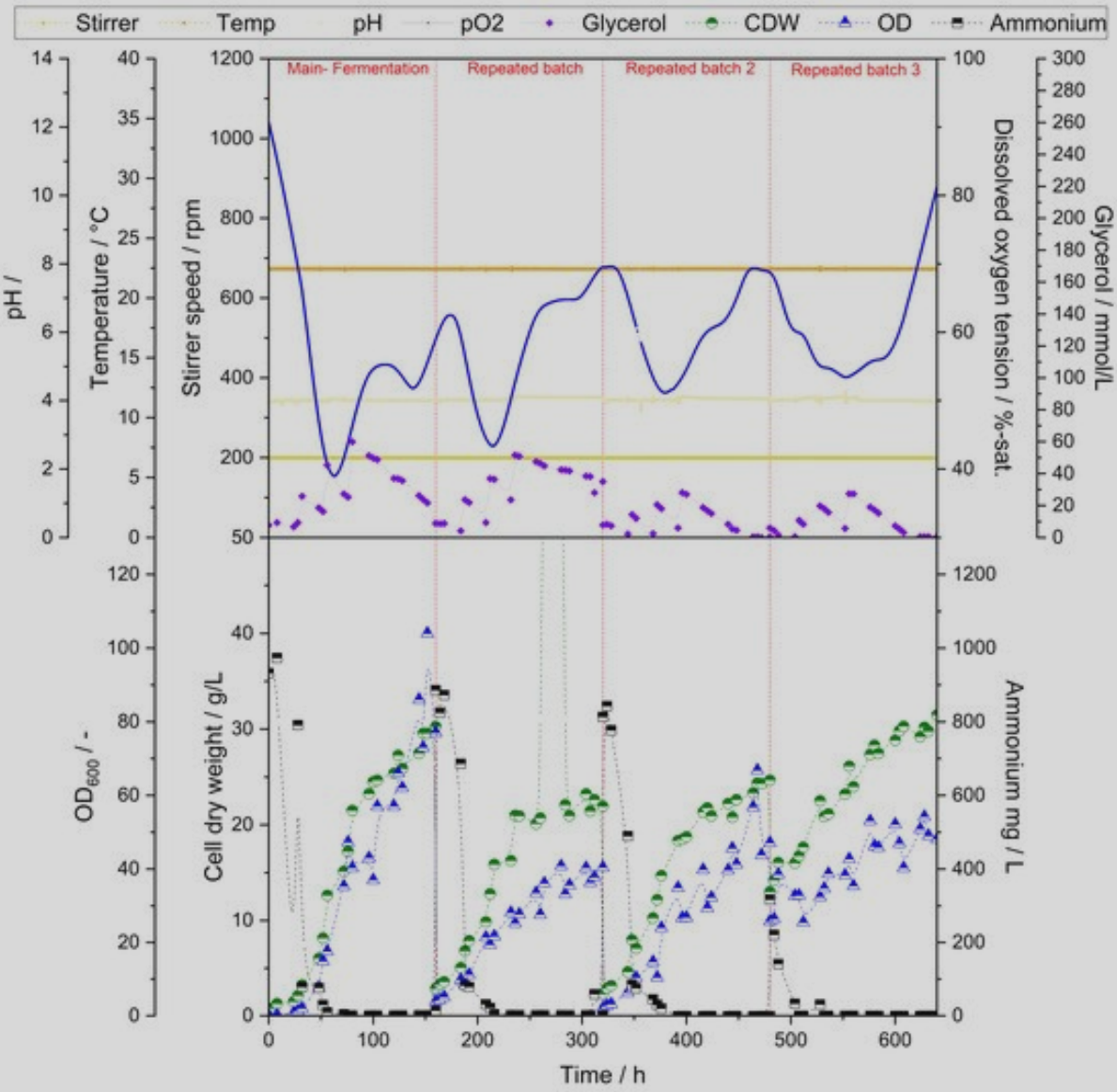

Figure 33: Cultivation parameters pH, temperature, stirrer speed, dissolved oxygen tension, glycerol concentration, cell dry weight, ammonium concentration and optical density at 600 nm of transition-scale fermentations with C. oleaginosum and separation in repeated batches. CG 1 was used for the initial batch and repeated batch 1 and CG 2 for repeated batch 2 and repeated batch 3. Dotted lines were added only for visual orientation (n = 1). Inoculum for initial fermentation was 1% (v/v), for repeated batch 1 and 2 it was 5% (v/v) and for repeated batch 3 it was 60% (v/v).

At the transition scale, the initial batch fermentation achieved an apparent maximum growth rate of μ_{Max} = 1.56 h^{-1} and a volumetric biomass productivity of P_v = 0.15 $g \cdot L^{-1} \cdot h^{-1}$ (Table 6).

Table 6: Key performance indicators of C. oleaginosum fermentations in a transition scale. The reported μ values should be interpreted as operational performance indicators rather than physiological maximum growth rates, as their calculation is constrained by sampling resolution. CG 1 was used for the initial batch and repeated batch 1 and CG 2 for repeated batch 2 and repeated batch 3.

Cultivation	μ_{Max}/h^{-1}	$Y_{X/S}$ $/g_{biomass}/g_{Substrate}$	$P_v/g \cdot L^{-1} \cdot h^{-1}$
Initial batch	1.559	0.580	0.146
Repeated batch 1	0.870	0.527	0.092
Repeated batch 2	1.378	0.352	0.104
Repeated batch 3	0.597	0.146	0.057

Scale-up from 2.5 L to 19 L was successful: transition-scale operation delivered substantially higher apparent growth rates (μ_{max} up to 1.56 h^{-1} at 19 L vs. ~0.50 h^{-1} with adapted feeding at 2.5 L; Table 5) while maintaining volumetric productivities in the same order of magnitude (0.10–0.15 $g \cdot L^{-1} \cdot h^{-1}$ at 19 L vs. ~0.21 $g \cdot L^{-1} \cdot h^{-1}$ at 2.5 L). The increased growth kinetics at 19 L are consistent with reports that improved oxygen transfer, reduced mixing gradients, and higher cell densities promote more stable lipid synthesis pathways during glycerol conversion [199]. The preservation of FA composition across repeated batches agrees with studies describing the high robustness of oleaginous yeast lipid profiles at elevated cell densities and oxygen-sufficient conditions. This indicates that scale-up primarily enhanced kinetic behavior (faster growth) without compromising overall biomass formation efficiency. Consistent with this, process variables remained within defined operational ranges (pH and temperature stable; DOT above the control threshold of 30%), across more than 640 h of transition-scale repeated-batch operations (Figure 33), and fatty acid composition was preserved, with oleate consistently representing ~51–53% of total fatty acids. This robustness is notable given the pronounced compositional variability between CG batches and the stronger nitrogen limitation enforced in later cycles. Product-composition stability under these conditions is essential for downstream biodiesel and oleochemical applications. Reports on semi-continuous or continuous systems with cell recycle demonstrate similarly high operational robustness for oleaginous yeasts, suggesting that strategies that maintain high cell density can further stabilize long-term production.

In subsequent repeated-batch fermentations, the effect of CG batch variability on process performance was evaluated at a constant inoculum size of 5% (v/v). As shown in Figure 33 and summarized in Table 6, the two untreated industrial glycerol batches exerted a pronounced influence on growth dynamics. Cultivation with CG 1 resulted in slower kinetics (μMax = 0.87 h−1) and a lower volumetric productivity (Pv = 0.09 g·L−1·h−1), whereas the use of CG 2 under otherwise identical conditions accelerated growth (μMax = 1.38 h−1) and increased productivity (Pv = 0.10–0.15 g·L−1·h−1). This indicates that at low inoculum levels, batch-specific differences in CG composition can substantially modulate growth kinetics, likely due to differences in the effective inhibitor burden per unit biomass.

For repeated batch 3, a high inoculum level of 60% (v/v) was deliberately combined with a partial replacement of mineral medium, resulting in an approximately halved initial mineral salt and nitrogen availability. This design choice reflects a typical repeated-batch operation, where medium replenishment is only partial and nutrient carry-over from previous cycles cannot be avoided. Maintaining a high inoculum ensured a low inhibitor-to-biomass ratio and minimized lag phase effects, while the reduced nitrogen supply imposed a stricter nitrogen-limited regime representative of prolonged repeated-batch cultivation. This combination allowed the decoupling of early phase inhibition effects from nutrient-driven metabolic responses, enabling assessment of process robustness under increasingly nitrogen-limited conditions. Such conditions are known to favor lipid accumulation over biomass formation in oleaginous yeasts, while simultaneously reducing maximum growth rates. The applied setup, therefore, reflects an industrially relevant trade-off between sustained process continuity and nutrient limitation rather than an experimentally imposed stress scenario [214,215]. Within this deliberately imposed process regime, cultivation in repeated batch 3 resulted in reduced growth kinetics. KPI of the repeated-batch fermentations are summarized in Table 6.

Overall, the key performance indicators signify that transitioning from batch to repeated-batch operation leads to a gradual reduction in biomass yield, reflecting the increasing influence of nutrient carry-over and partial medium replacement. While high inoculum levels and adapted feeding strategies effectively govern early-phase growth kinetics and volumetric productivity by mitigating inhibition, progressively reduced mineral salt and nitrogen availability shift process control toward a stricter nitrogen-limited regime. Under these conditions, growth rates decline as metabolic flux is redirected from biomass formation toward maintenance and lipid storage (30% to 36% increase). CG batch variability further modulates growth kinetics once nitrogen becomes limiting, whereas lipid content and fatty acid composition remain robust across repeated batches. This demonstrates that the applied repeated-batch strategy primarily affects kinetic and yield-related parameters, while lipid quality is preserved despite variations in inoculum regime, nutrient availability, and CG source.

Changes in inoculum size were reflected in biomass composition, as shown in Figure 34. Fermentations with small inoculum sizes displayed an increased protein fraction and a reduced lipid share, which is indicative of prolonged growth and a delayed transition into lipid storage metabolism. In contrast, repeated batch 3 initiated with a 60% inoculum approached lipid content of approximately 36% of dry biomass. This modulation of biomass composition as a function of inoculum history and physiological state is consistent with previous findings from Duman-Ozdamar et al., showing that key process parameters—including C/N ratio, temperature, and feeding strategy—systematically steer lipid accumulation in *C. oleaginosum* and related oleaginous yeasts [214].

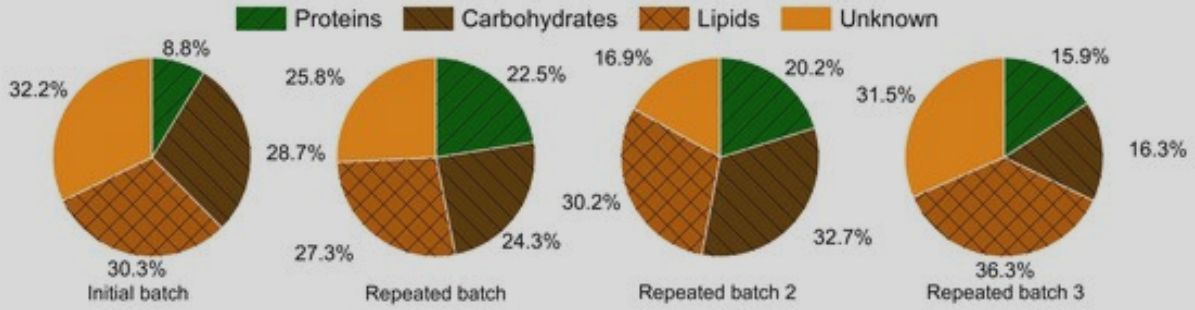

Figure 34: Endpoint biomass composition of the 19 L transition-scale fermentations with C. oleaginosum. CG 1 was used for the initial batch and repeated batch 1 and CG 2 was used for repeated batch 2 and repeated batch 3. Inoculum for initial fermentation was 1% (v/v), for repeated batch 1 and 2 it was 5% (v/v) and for repeated batch 3 it was 60% (v/v) (n = 1).

Despite these shifts in biomass composition, FA profiles remained stable across all repeated batches (Figure 35, Table S11). Detailed numbers are available in the additional information Table S11. Oleic acid consistently represented the dominant FA, accounting for approximately 51–53% of total FAs, irrespective of inoculum size or CG batch. This compositional stability indicates that repeated-batch operation and substrate variability did not lead to an adverse drift in lipid quality. Such robustness is characteristic of glycerol-based fermentations with oleaginous yeasts and is widely recognized as advantageous for biodiesel and oleochemical applications, where oleate-rich profiles are desirable due to their favorable physicochemical properties [213,214].

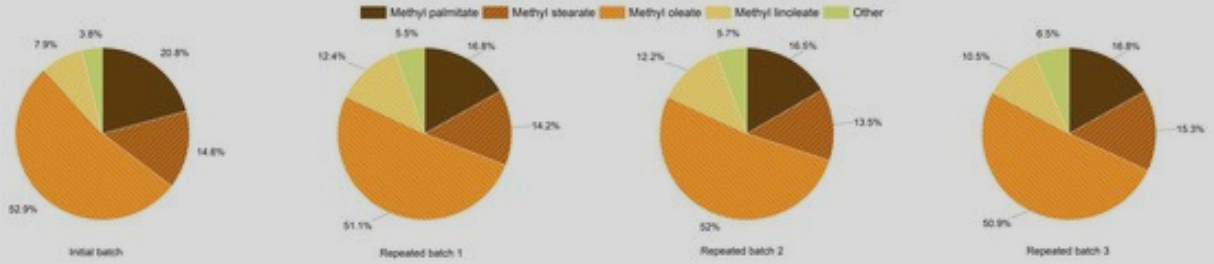

Figure 35: Fatty acid profile of the biomass of the endpoint of the 19 L transition-scale fermentations with C. oleaginosum. CG 1 was used for the initial batch and repeated batch 1, and CG 2 was used for repeated batch 2 and repeated batch 3. Inoculum for initial fermentation was 1% (v/v), for repeated batch 1 and 2 it was 5% (v/v) and for repeated batch 3 it was 60% (v/v) (n = 1).

In summary, the present results align well with and extend the existing literature in several important aspects. First, they reinforce the notion that untreated CG can be exploited as the sole carbon source for microbial lipid production by oleaginous yeasts, including *C. oleaginosum*, provided that appropriate feeding strategies are employed to mitigate inhibitory effects during early growth phases [44,212]. Second, they demonstrate that simple but effective process levers like staged feeding retain their effectiveness at the transition scale, which is fully consistent with previous reports on oxygen-managed, high-cell-density lipid fermentations [215,216]. Third, the maintenance of an oleate-dominated FA profile under CG feeding conditions highlights the robustness of lipid quality, an essential prerequisite for downstream biodiesel and oleochemical applications, and agrees with the generally reported FA patterns of yeast-derived SCO produced from glycerol [213].

Chapter 5: 4 Conclusions

This work closes an implementation gap between crude-glycerol (CG) feasibility studies and industrially relevant operation by demonstrating scalable, feeding-based inhibition control for *C. oleaginosum* on untreated, non-sterilized industrial CG. A single initial CG bolus caused complete growth arrest, underscoring that impurity-driven inhibition can dominate early cultivation phases. In contrast, distributing the same total crude-glycerol input via staged pulses restored respiratory activity, biomass formation, and lipid accumulation at 2.5 L and enabled robust transition-scale (19 L) repeated-batch fermentation for >640 h. Despite strong substrate-batch variability and increasing nitrogen limitation, the process maintained stable lipid levels (~30–36% CDW) and a consistent oleate-dominated fatty acid profile (~51-55% C18:1), indicating that lipid quality is resilient once inhibition is controlled. Collectively, the findings support a clear practical message: robust lipid production from CG does not require detoxification if feeding is designed to minimize the inhibitor-to-biomass ratio during early growth, enabling reliable valorization of industrial-grade side streams.

Chapter 5: 5 Outlook and Recommendations

Future work may leverage inline surrogate measurements (such as conductivity or alkalinity) to anticipate inhibitor loads and adapt feeding in real time, as suggested by reviews of crude-glycerol impurity profiles and upgrading routes. Low-rate, feedback-controlled feeding tied to respiratory indicators (OTR/CTR) may further smooth inhibitor exposure beyond the simple staged schedule used here. Semi-continuous or cell-recycle strategies, which have been shown to support very high cell densities in oleaginous yeast processes, could be combined with the present approach to enhance productivity while retaining quality. Finally, a systematic exploration of inoculum size, ionic impurity load, and C/N interactions would more precisely map the operational window for untreated CG and enable predictive control strategies for industrial implementation.

At this stage, both the upstream fungal platform and the downstream lipid-production platform have been established independently. The remaining challenge is no longer whether either system works in isolation, but whether they can be brought into productive contact. Preliminary experiments indicated that representative fungal metabolite mixtures strongly impaired wild-type yeast growth. The next chapter therefore takes the first direct step toward bridging this gap—not by changing the broth, but by improving the downstream organism itself.

3.3 Engineering the interface: improving compatibility between fungal broths and yeast lipid production

The final part of the dissertation shifts from platform establishment to interface engineering. This is the decisive transition from parallel biology to true process integration. Once it became clear that the two systems could not simply be connected without difficulty, the focus moved to compatibility itself as an independent research question. The sixth chapter addresses this by adapting the downstream yeast to the upstream metabolite environment, while the seventh chapter evaluates the direct practical feasibility of coupling both systems.

3.3.1 Microfluidic adaptive laboratory evolution of an oleaginous yeast on fungal metabolite mixtures

The sixth chapter occupies a pivotal position in the dissertation, because it is the first study that directly addresses the biological mismatch between the two process modules. Its purpose is to reduce the physiological distance between fungal fermentation products and oleaginous yeast growth requirements. Rather than assuming that the fungal broth must be perfectly adjusted to the yeast, this chapter asks whether the yeast itself can be evolved toward the metabolic environment created upstream.

This study therefore introduces an adaptive solution to the compatibility problem. By subjecting *Cutaneotrichosporon oleaginosum* to microfluidic adaptive laboratory evolution in the presence of representative fungal metabolite mixtures, it establishes that improved tolerance and improved substrate uptake can be achieved without genetic engineering. In the context of the dissertation, this is a major conceptual advance. It means that integration of both systems is not restricted to medium optimization and broth conditioning alone. The downstream organism becomes a process variable in its own right.

This chapter thus functions as the biological bridge of the dissertation. It does not yet solve the final coupling problem completely, but it makes the final step plausible by showing that compatibility is an evolvable and therefore engineerable property.

Chapter 6: Microfluidic adaptive laboratory evolution of the oleaginous yeast Cutaneotrichosporon oleaginosum

Kevin Edward Schulz[1+], Camilla Stolle[2+], Anne Rosa Maria Schwendemann[1], Dirk Holtmann[1], Kersten Stefan Rabe[2*]

[1]Institute of Process Engineering in Life Sciences 2: Electrobiotechnology, Karlsruhe Institute of Technology (KIT), Karlsruhe, Germany, [2]Institute for Biological Interfaces 1, Karlsruhe Institute of Technology (KIT), Karlsruhe, Germany, [+] contributed equally, * corresponding authors

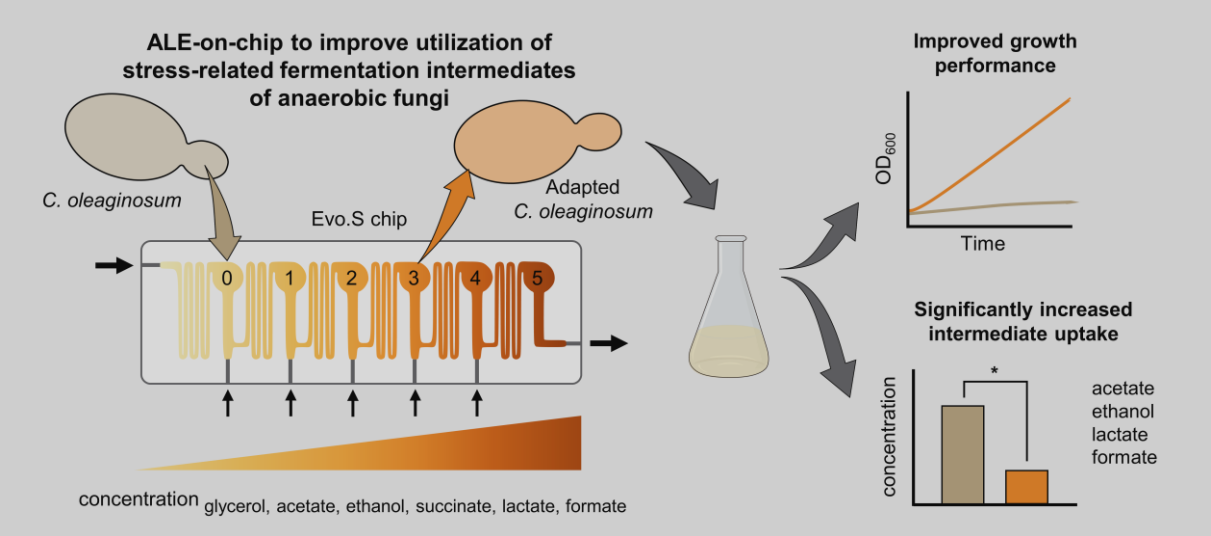

Publishing details:
Springer Nature - Applied Microbiology and Biotechnology
Under Review, submitted 21 April 2026

Author contributions: KES, CS, DH and KSR conceived and designed the research. KES, CS and ARMS conducted the experiments. KES and CS performed data analysis and visualization. ARMS contributed to experimental validation. DH and KSR provided resources and supervised the study. KES and CS jointly wrote the original draft of the manuscript. DH and KSR reviewed and edited the manuscript. KSR was responsible for project administration. All authors read and approved the final manuscript.

Chapter 6: 1 Introduction

The production of single-cell oils (SCOs) for high volume but low-value applications such as biofuels and biolubricants remains economically challenging, primarily due to the cost of conventional carbon sources and energy-intensive downstream processes. Although certain oleaginous yeasts can accumulate up to 85% of their cell dry weight as lipids, such processes are unlikely to compete with fossil- or plant-based alternatives unless significantly cheaper and more sustainable feedstocks are efficiently utilized [186,187,217-220]. In this context, hemicellulosic biomass represents an abundant and largely underutilized resource, comprising agricultural residues, food and kitchen waste, paper waste, and agro-industrial by-products, potentially available at costs as low as 45.72€ t^{-1} [3,12,58,221]. Its integration into microbial bioprocesses aligns with the principles of a circular bioeconomy and offers a viable pathway toward environmentally sustainable and economically feasible SCO production. Nevertheless, the inherent structural complexity and recalcitrance of lignocellulose typically necessitate energy- and cost-intensive pretreatment steps to release fermentable intermediates such as sugars and organic acids, posing a significant barrier to its widespread biotechnological utilization [7].

A promising strategy to overcome this bottleneck is consolidated bioprocessing using microorganisms capable of degrading hemicellulose and generating fermentable intermediates. Anaerobic gut fungi of the phylum *Neocallimastigomycota* are particularly efficient in this regard due to their highly active cellulosome-based enzyme systems. These fungi convert untreated hemicellulosic biomass into a mixture of low-molecular-weight metabolites, including acetate, formate, lactate, succinate, and ethanol [25,62,70]. While these compounds may serve as alternative carbon sources or platform chemicals, several of them, most notably formate, can inhibit the growth and productivity of secondary production organisms [41,217,222-226].

Building upon this concept, the oleaginous yeast *Cutaneotrichosporon oleaginosum* emerges as a highly promising candidate for the subsequent lipid production phase [227]. As an unconventional yeast, *C. oleaginosum* combines high lipid accumulation capacity with broad substrate versatility [189,190,228-231]. These traits are essential for efficient growth on waste-derived and chemically complex fermentation broths. Despite its advantages, this yeast remains underexplored in industrial biotechnology. Its integration into a multi-stage microbial conversion system, particularly in tandem with lignocellulose-degrading organisms such as *Neocallimastigomycota*, could significantly advance the development of economically viable SCO production platforms. Nevertheless, a key challenge persists: even with efficient lignocellulose breakdown, the total carbon yield may be insufficient to reach commercially relevant product titers [139]. One promising strategy to address this limitation involves the co-utilization of additional low-cost feedstocks, such as untreated crude glycerol which is a major byproduct of biodiesel production. Crude glycerol not only provides an economical carbon source but also helps achieve the high carbon-to-nitrogen (C:N) ratios required for lipid accumulation, avoiding reliance on costly substrates such as glucose. While economically attractive, crude glycerol introduces further complexity due to its variable composition and the presence of inhibitory compounds, which can negatively impact microbial growth and overall process performance [232].

To overcome these limitations, targeted strain optimization is essential. Adaptive Laboratory Evolution (ALE) offers a powerful, non-genetically modified (non-GMO) approach to enhancing microbial performance under industrially relevant stress conditions [45,46,233,234]. This method is particularly attractive within the regulatory framework of the European Union, where GMO-based processes often face public skepticism and legislative hurdles. ALE provides a widely accepted and scalable alternative by enabling the natural selection of improved strains through gradual exposure to challenging environments [50,235].

In the case of *Cutaneotrichosporon oleaginosum*, ALE can be employed to increase tolerance and metabolic efficiency by progressively adapting the yeast to mixed substrates such as fermentation-derived metabolites and crude glycerol. This evolutionary pressure promotes the emergence of strains with enhanced stress resistance, improved substrate utilization, and elevated lipid production capacity. Traditionally, ALE is conducted via serial batch cultivation under incrementally intensified stress conditions. While effective, this approach is inherently time-consuming, often requiring hundreds of generations to achieve meaningful phenotypic improvements. Recent advances in microfluidic technology have introduced novel platforms for accelerated evolution [193]. In bacterial systems, microfluidic chip-based ALE has demonstrated significantly reduced adaptation times and improved selection efficiency, thanks to precise environmental control and continuous selection pressure at the microscale [193,236]. The evo.S (evolution under stress) chip represents such a microfluidic platform designed to accelerate adaptation [236]. Its polydimethylsiloxane (PDMS) structure comprises six growth wells interconnected by channels, enabling the formation of adjustable and spatially stable concentration gradients. These gradients are generated by supplementing a main-flow with stepwise addition of increasing stressor concentrations through five co-flows, creating a continuous selection pressure. Cultivating bacterial cells within such gradients has resulted in rapidly adapted strains, demonstrating the effectiveness of this strategy in prokaryotic systems. However, its transferability to eukaryotic organisms remains largely unexplored. This gap represents a significant and largely untapped opportunity, as the successful implementation of such approaches in eukaryotic systems could unlock substantial advances in strain development and biotechnological applications.

In this study, we employed microfluidic ALE using the evo.S chip, which enables precise gradient-based selection, to accelerate adaptation of *Cutaneotrichosporon oleaginosum* to stress-related intermediates (ethanol, lactate, formate, acetate, succinate) from anaerobic fermentation of lignocellulosic biomass and supplemented with crude glycerol as a cost-effective co-carbon source. Our objective was to evaluate whether gradient-driven microfluidic ALE can generate non-GMO yeast strains with improved growth and substrate utilization under these complex conditions, thereby advancing cost-effective SCO production from lignocellulosic media supplemented with crude glycerol. This study evaluates the adaptive potential of unconventional yeasts in integrated, waste-based bioprocesses and contribute to establishing new frameworks for rapid, non-GMO strain development in eukaryotic systems.

Chapter 6: 2 Material and methods

If not stated otherwise, all chemicals were purchased from Carl Roth (Karlsruhe, Germany). The parental strain used in this study was *C. oleaginosum* ATCC 20509. The crude glycerol used in this study was kindly provided by Hydroxy Energy GmbH (Germany). All evolved strains generated in this work are available from the institutional strain collection of the Institute of Process Engineering in Life Sciences 2 upon reasonable request.
ALE is an inherently stochastic and path-dependent process in which genetic and phenotypic outcomes emerge from continuous selection under defined environmental constraints rather than from independent, repeatable experimental conditions. Consequently, biological replicates in the classical sense (for example parallel evolution experiments expected to yield identical outcomes) are not meaningful for ALE, as each evolutionary trajectory represents a unique solution to the applied selection pressure. In this study, each evo.S chip constituted an independent evolutionary experiment, and individual growth wells within each chip represented distinct selection environments along defined concentration gradients. Therefore, no biological triplicates were applied during the evolutionary phase itself. Instead, technical replication was employed exclusively for experimental steps that are repeatable by design, including microtiter-based growth screening and analytical quantification of metabolites.

Chapter 6: 2.1 Shake flask cultivation of *C. oleaginosum* ATCC 20509 in mineral salt medium with anaerobic fungi metabolites and with / without formate

To assess the baseline growth performance of *C. oleaginosum ATCC 20509* prior to any adaptive evolution steps, a growth experiment was conducted in 500 mL baffled Erlenmeyer flasks with a working volume of 130 mL. Each flask was prepared with minimal medium based on the published formular of Gorte et al. [162]. The medium contains 100 mL of yeast mineral salt medium (8.99 g/L potassium dihydrogen phosphate, 0.12 g/L di-sodium hydrogen phosphate, 0.1 g/L sodium citrate dihydrate, 0.1 g/L yeast extract, 0.2 g/L magnesium sulfate heptahydrate and 4.72 g/L ammonium sulfate), 10 mL of salt solution (10 g/L yeast extract and 20 g/L magnesium sulfate heptahydrate), and 10 mL of trace element solution (4 g/L calcium chloride dihydrate, 0.55 g/L iron(II) sulphate dihydrate, 0.475 g/L citric acid, 0.1 g/L zinc sulfate heptahydrate, 0.075 g/L manganese(II) sulfate monohydrate and 100 µL/L sulfuric acid 96 %). Additional 10 mL of one of three carbon source combinations (glucose, ethanol/acetate/lactate/succinate or ethanol/acetate/lactate/succinate/formate) was added. This resulted in the following conditions: growth control with 5 g/L glucose (medium Y-G), a complex mixture of potential carbon sources containing 10 mM ethanol, 10 mM acetate, 10 mM lactate and 1.2 mM succinate (medium Y-EALS), and the same mixture with 10 mM formate (medium Y-EALS+F). The selected concentrations represent a typical metabolite profile observed at the end point of anaerobic fungal fermentations and were chosen within the range that anaerobic fungi are physiologically capable of producing under typical cultivation conditions [14]. The cultures were inoculated with a freshly prepared pre-culture to an initial optical density at wavelength 600 nm (OD_{600}) of 0.5. Growth was monitored after 3 weeks by measuring cell dry weight (CDW). This experiment was conducted as an exploratory pre-experiment to qualitatively assess the general growth behavior of *C. oleaginosum* on anaerobic fungal fermentation intermediates. Therefore, this experiment was performed as a single biological replicate (n = 1) and was not intended for statistical comparison.

Chapter 6: 2.2 Production of the microfluidic evo.S chips used

Two chip components were fabricated using the previously established protocol described [236]. Each chip consisted of a structured base (76 × 26 mm, 2.5 mm thick) and a flat cover (76 × 26 mm, 0.75 mm thick). In brief, polydimethylsiloxane (PDMS; Sylgard 184, Dow Corning) was prepared by mixing the base polymer with the curing agent at a 10:1 (w/w) ratio and subsequently degassed in a vacuum chamber for 1 h. The degassed PDMS was then poured into the PMMA mold and cured at 70 °C for 1 hour. After curing, the components were assembled by plasma treatment (Plasma Technology GmbH, Germany) and sterilized by autoclaving at 121 °C for 20 minutes. The finished chips were stored under sterile conditions until further use (Figure S31).

Chapter 6: 2.3 Validation of microfluidic cultivation of *C. oleaginosum*

To establish the cultivation of *C. oleaginosum* within the microfluidic evo.S chip, the chip was first sterilized and subsequently transferred aseptically into a humidity chamber. The humidity chamber was prepared using a commercially available BPA-free polypropylene box (with tightly sealing lid). The bottom of the box was lined with sterile paper towels that were evenly moistened with sterile deionized water until fully saturated but without free-standing liquid. The evo.S chip was placed in the humidity chamber and was connected to the main-flow containing sterile mineral salt medium described in 2.1 using 10 g/L glucose as sole carbon source (medium Y-G2). Flow was regulated using a peristaltic pump (kdScientific, USA) set to a flow rate of 56.5 µL/min. For inoculation, the flow was stopped and 50 µL preculture of *C. oleaginosum* adjusted to OD_{600} = 0.1 was injected through the PDMS-cover into well 0 of the microfluidic chip using a 1 mL syringe with a sharp cannula (Ø 0.45 mm, B. Braun Melsungen AG, Germany) and the chip was secured in a polymethyl methacrylate (PMMA) holder. After allowing the cells to settle for 1 h without flow, the pump was restarted and operated continuously for one week with the lowest possible flow rate of 56.5 µL/min. The initial no-flow period was implemented to enable efficient cell attachment and stabilization within the cultivation chambers, thereby minimizing cell washout upon re-initiation of flow. The selected flow rate was chosen to ensure a continuous supply of nutrients while maintaining shear forces at a level that prevents detachment of adhered cells and supports stable long-term cultivation within the microfluidic environment.

Chapter 6: 2.4 Microfluidic ALE using gradients

Microfluidic ALE was conducted using a parallel screening approach using two independent evo.S chips under two distinct compound mixture concentration gradient profiles. In the first chip, cells were exposed to a gradually increasing concentration of substrate mixture referred to as the *smooth* gradient. In the second chip, cells were subjected to an immediate shift to the highest concentration investigated, termed the *steep* gradient (Figure S32).

The specific media compositions for the main-flow and co-flows for the smooth and steep condition are listed in Table 7 and Table 8, respectively. The used compositions of soluble carbon sources are displayed in Table 9. Both media are based on the anaerobic fungal minimal medium with exchanged buffer system (150 mL of salt solution 1 (3 g/L dipotassium hydrogen phosphate), 150 mL salt solution 2 (3 g/L potassium dihydrogen phosphate, 6 g/L ammonium sulphate, 6 g/L sodium chloride, 0.6 g/L magnesium sulphate heptahydrate, 0.6 g/L calcium chloride dihydrate), 2 mL of a zoospore inducer solution (0.5 g/L hemin chloride in 50% ethanol and 50 % 0.05 M sodium hydroxide solution), 2 mL of a redox indicator solution (1 g/L resazurin sodium salt), 6 g/L bis(2-hydroxyethyl)amino-tris(hydroxymethyl)methane, 1 g/L L-cysteine hydrochloride monohydrate, 10 mL trace element solution (0.25 g/L manganese(II) chloride tetrahydrate, 0.25 g/L nickel(II) chloride hexahydrate, 0.25 g/L sodium molybdate dihydrate, 0.25 g/L boric acid, 0.2 g/L iron(II) sulphate heptahydrate, 0.05 g/L cobalt(II) chloride hexahydrate, 0.05 g/L sodium selenite pentahydrate, 0.05 g/L sodium metavanadate, 0.025 g/L zinc sulphate and 0.0319 g/L copper(II) sulphate pentahydrate in 0.2 M hydrochloric acid), 5 g/L glucose, 0.5 mL vitamin solution (0.01 mg/L thiamine hydrochloride, 0.652 g/L panthothenic acid hemicalium salt, 0.6 g/L nicotinic acid, 0.02 g/L cyanocobalamin, 0.2 g/L biotin, 0.012 g/L pyridoxine hydrochloride, 0.05 g/L folic acid and 0.05 g/L P- aminobenzoic acid 0.2 g/L riboflavin) and 0.5 mL antibiotic solution (50 g/L ampicillin sodium salt, 50 g/L streptomycin sulphate, 50 g/L penicillin sodium salt) published in Schulz et al. [14]. The pH was adapted to pH 4 using 4 M phosphoric acid and 4 M sodium hydroxide. As previously reported by Zoheir et al., two main-flow syringes, each containing 100 mL of the main-flow medium, were installed in a syringe pump (AL-4000, World Precision Instruments) while ten syringes, each containing 20 mL of the appropriate co-flow medium, were installed in a second, independent syringe pump (Nexus 3000, Chemyx Inc., USA) [236]. Both main-flow and co-flow contained anaerobic fungal minimum medium with respective soluble carbon sources and a fixed crude glycerol content shown in Table 7, Table 8 and Table 9. The chip was connected to the corresponding inlets and filled with the appropriate medium. To start adaptation, 50 µL *C. oleaginosum* culture, grown in main-flow medium and concentrated on an OD_{600} = 1 was inoculated, to ensure a sufficiently high initial cell density, improving survival probability and adaptation efficiency under stress exposure, using a 1 mL syringe with a sharp cannula through the cover into well 0 of each chip. Afterwards, the chips were fixed in a PMMA holder and incubated for 1 h without flow to settle the cells. Flow rates were set to 10 µL/min for the main-flow and 2 µL/min for the co-flows. After two weeks of cultivation at room temperature (~23 °C), cells from individual growth wells were transferred with a 1 mL syringe with a sharp cannula (Ø 0.45 mm, B. Braun Melsungen AG, Germany) to 100 mL shake flasks containing 20 mL main-flow medium. After two weeks of incubation, the optical density at 600 nm (OD_{600}) was measured using a GENESYS 30 spectrophotometer (Thermo Fisher Scientific Inc., USA) to assess growth performance.

Table 7: Concentration of carbon sources used for the main-flow and co-flows for microfluidic adaptation in the smooth gradient chip. For soluble carbon source composition see Table 9.

Components	Main-flow	Co-flow 1	Co-flow 2	Co-flow 3	Co-flow 4	Co-flow 5
soluble carbon source	0.86 mL/L		1.73 mL/L	3.46 mL/L	6.92 mL/L	55.32 mL/L
crude glycerol	9 mL/L		9 mL/L	9 mL/L	9 mL/L	9 mL/L

Table 8: Concentration of carbon sources used for the main-flow and co-flows for the microfluidic adaptation in the steep gradient chip. For soluble carbon source composition see Table 9.

Components	Main-flow	Co-flow 1	Co-flow 2	Co-flow 3	Co-flow 4	Co-flow 5
soluble carbon source	0.86 mL/L		55.32 mL/L			
crude glycerol	9 mL/L		9 mL/L			

Table 9: Composition of soluble carbon sources supplied to the anaerobic fungi mineral salt medium in the main- and co-flow channels of the smooth and steep gradient microfluidic chips. Carbon source concentrations are given as absolute values (mmol/L) and represent defined fractions of the maximum concentration applied within the respective gradient setup. In the smooth gradient chip, co-flow channels were supplied with stepwise increasing concentrations (6.25–100% of the maximum concentration), whereas in the steep gradient chip, the maximum concentration was applied from co-flow channel 2 onward to generate an abrupt concentration increase. The main-flow channel contained the baseline concentration (6.25% of maximum) in both gradient configurations.

Condition			Fraction of maximum concentration [%]	Ethanol [mmol/L]	Acetate [mmol/L]	Lactate [mmol/L]	Succinate [mmol/L]	Formate [mmol/L]
Smooth	Main-flow		6.25	4.7	6.3	0.551	0.3	4.615
	Co-flow	1	6.25					
		2	12.5	9.4	12.6	1.1	0.6	9.2
		3	25	18.8	25.3	2.2	1.2	18.5
		4	50	37.7	50.6	4.4	2.4	36.9
		5	100	75.4	101.2	8.8	4.8	73.8
Steep	Main-flow		6.25	4.7	6.3	0.6	0.3	4.6
	Co-flow	1	6.25					
		2	100	75.4	101.2	8.8	4.8	73.8
		3	100	75.4	101.2	8.8	4.8	73.8
		4	100	75.4	101.2	8.8	4.8	73.8
		5	100	75.4	101.2	8.8	4.8	73.8

Potential contaminations were identified using an Eclipse E200 LED (Nikon Instruments Europe BV, Netherland) with the CFI Achromat DL 40X (Nikon Instruments Europe BV, Netherland) objective lens with the numeric aperture of 0.65. Pictures were taken using the DFK 23U274 light microscope camera (Imagingsource, Germany) and the NIS Elements D Software Version 5.21.00 (Nikon Instruments Europe BV, Netherland). The cultures from the microfluidic adaptation were transferred to YM-agar plates (3 g/L malt extract, 3 g/L yeast extract, 5 g/L peptone, 10 g/L sodium chloride, 10 g/L glucose, 15 g/L European agar) with main-flow medium and adjusted with 4 M sodium hydroxide to pH 4 for long term storage.

Chapter 6: 2.5 Microtiter-based screening of growth of adapted strains

From each agar plate representing each an individual culture from the microfluidic adaptation, a single colony was selected and transferred into a 100 mL Erlenmeyer flask containing 20 mL of main-flow medium. The cultures were incubated for one week at 30 °C with 130 rpm shaking conditions using the Multitron Incubator system (Infors HT, Switzerland). Following incubation, the OD_{600} was adjusted to 1 by centrifugation with 4700 rpm using the Heraeus Multifuge X3 (Thermo scientific, USA) of the culture and resuspension of the cell pellet in fresh main-flow medium. For microtiter cultivation, 96-well plates were prepared by adding 180 µL of the respective medium and 20 µL of the standardized inoculum to each well. Every clonal culture was cultivated in technical sextuplicate (n = 6). The plates were sealed with gas-permeable Breathe-Easy membranes (Diversified Biotech, USA) and incubated for one week at 30 °C on a Cerillo plate reader system (Cerillo, USA) placed on a ThermoMixer C plate shaker with a shaking frequency of 500 rpm (Eppendorf SE, Germany) within an TH30 incubation hood (Edmund Bühler GmbH, Germany).

Chapter 6: 2.6 Metabolic comparison

To compare the differences in metabolic activity among the strains that reached the highest OD_{600} values after 168 h in the screening experiments, shake flasks containing 100 mL of co-flow medium 3 of the smooth gradient, were inoculated with 100 µL of the respective strain or the non-adapted wild-type strain and incubated at 30 °C for 11 days in technical triplicates. (n = 3). Daily sampling was performed to measure OD_{600} and to analyze soluble metabolite consumption via high performance liquid chromatography (HPLC). Analysis was performed using the 1100 HPLC system (Agilent Technologies, USA). The pre-column used was the Rezex ROA organic acid H+ (8 %) guard column (50 mm x 7,8 mm) (Phenomenex Ltd., Germany), the main column a Rezex ROA organic acid H+ (8 %) (300 mm x 7,8 mm, 8 m) (Phenomenex Ltd., Germany), the eluent 5 mM sulphuric acid and the detectors RID (Agilent Technologies, USA) and VWD (Agilent Technologies, USA). The method ran for 40 min at a flow rate of 0.5 mL/min, with column and RID temperatures set to 50 °C and a VWD wavelength of 220 nm. Calibration was performed individually for ethanol, acetate, lactate, succinate, formate and glycerol at concentrations of 0.1 g/L, 0.25 g/L, 0.5 g/L, 1 g/L, 2.5 g/L, 5 g/L and if necessary up to 10 g/L. Characteristic results are shown in Figure S33 and calibrations are shown in Figure S34.

Chapter 6: 3 Results

To evaluate media resulting from anaerobic fermentation of hemicellulosic biomass as potential carbon sources for the cultivation of *C. oleaginosum*, the effect of typical anaerobic fungal metabolites (ethanol, acetate, lactate, succinate and formate) on growth was assessed in concentrations reported as feasible from dark fermentation [14,20]. For this purpose, *C. oleaginosum* was cultivated in a mineral salt medium with glucose (medium Y-G), which is the reference carbon source, alongside two additional cultivations in either mineral salt medium containing a mixture of the potential carbon sources ethanol, acetate, lactate and succinate (medium Y-EALS) or the same mixture with additional formate (medium Y-EALS+F) [237]. After three weeks of cultivation in shake flasks at 30 °C with 130 rpm shaking, the cell dry weight was determined representing the growth of the cells in the respective medium Figure 36.

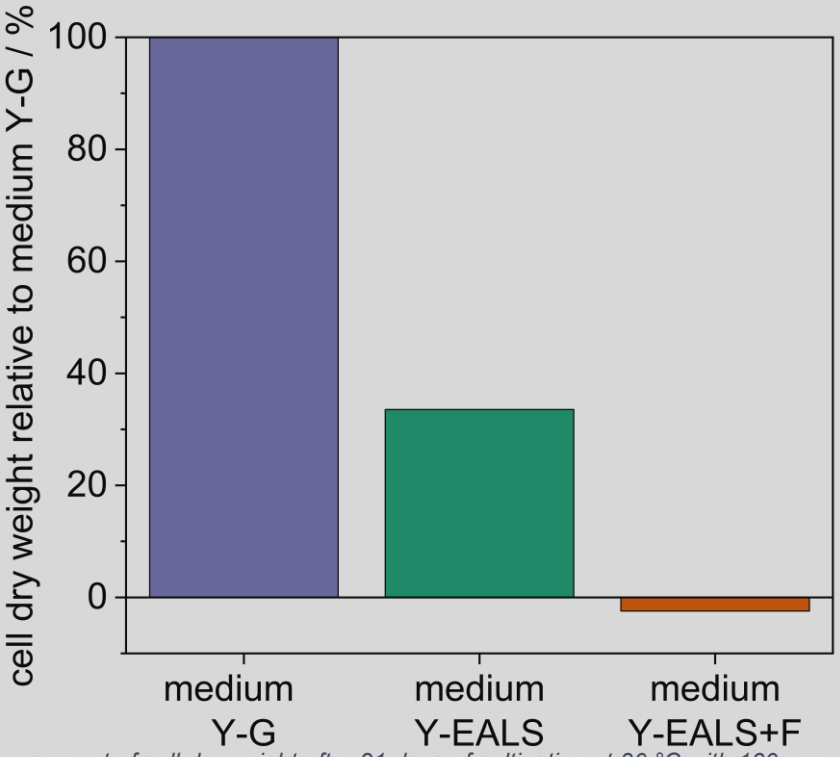

Figure 36: Relative amount of cell dry weight after 21 days of cultivation at 30 °C with 130 rpm of C. oleaginosum ATCC 20509 in designated media compositions (n = 1).

The cultivation under standard conditions (medium Y-G) resulted in 3.28 g CDW L^{-1}, which was defined as 100%. Cultivation in medium Y-EALS resulted in 34% relative CDW. In medium Y-EALS+F, no measurable CDW was detected. Table 10 summarizes the concentrations of the individual compounds in the applied media and reported toxicity thresholds for *Saccharomyces cerevisiae*.

Table 10: Comparison of concentrations of individual compounds in medium Y-EALS and Y-EALS+F and respective literature values for toxicity for the conventional yeast Saccharomyces cerevisiae.

Compound	Concentration media used in this study [mmol/L]	Concentration with first toxic effects reported in literature [mmol/L]	Source
ethanol	10	82	[225]
acetate	10	10	[223]
lactate	10	59	[217]
succinate	1.2	150	[224]
formate	10	40	[226]

In preliminary experiments (Figure S35), no growth was observed when formate was supplied as the sole carbon source, whereas all other tested compounds supported measurable growth. To investigate microfluidic cultivation, *C. oleaginosum* was inoculated into the evo.S chip Figure 37A, Figure S36) and cultivated for one week using mineral salt medium with glucose (medium Y-G2). Growth was monitored by a time-dependent turbidity increase (Figure 37B).

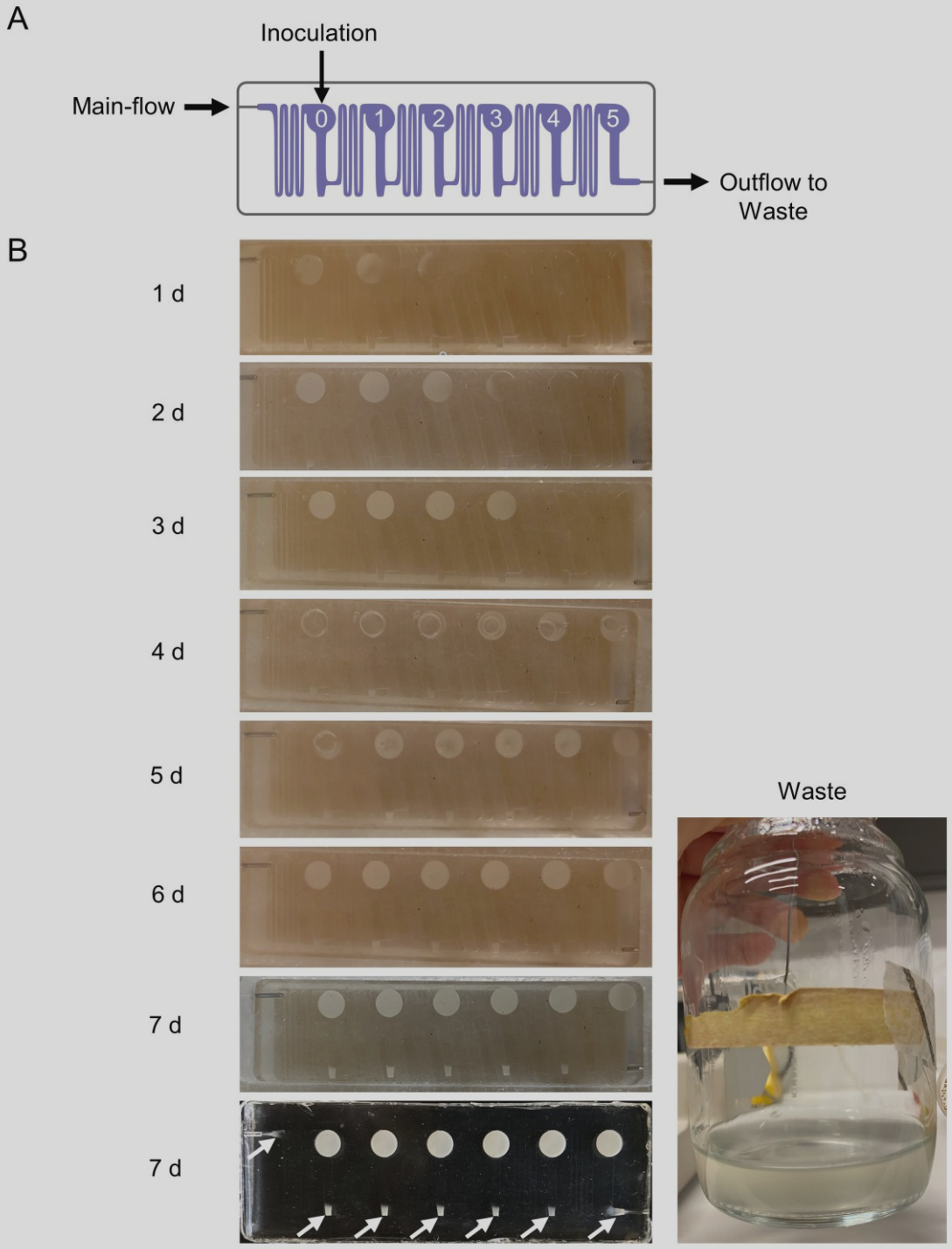

Figure 37: Cultivation of C. oleaginosum in the microfluidic evo.S chip. A) mineral salt medium with glucose (medium Y-G2) was supplied only via the main-flow inlet and C. oleaginosum cells were inoculated into well 0. B) The chip (n=1) was photographed daily during the one-week cultivation to document the growth of the cells via the increase in turbidity. Arrows indicate turbidity in areas of the inlets with lower flow velocities. In addition, the waste bottle was documented photographically at the end of the microfluidic cultivation after 7 days. Please note that after 7 days the chip was removed from the chamber and photographed on a black background to improve the contrast.

Temporary air bubble formation was detected on day 4 but did not prevent further growth. After 7 days, growth was observed in the wells and at inlet regions, while connecting channels remained free of visible biomass. Subsequently, *C. oleaginosum* was cultivated in the evo.S chip under increasing concentrations of stress-related intermediates using smooth and steep gradient profiles (Figure 38A, B). After 7 days, only weak turbidity increases were observed (Figure 38C). After 14 days, turbidity was detectable in both gradient systems.

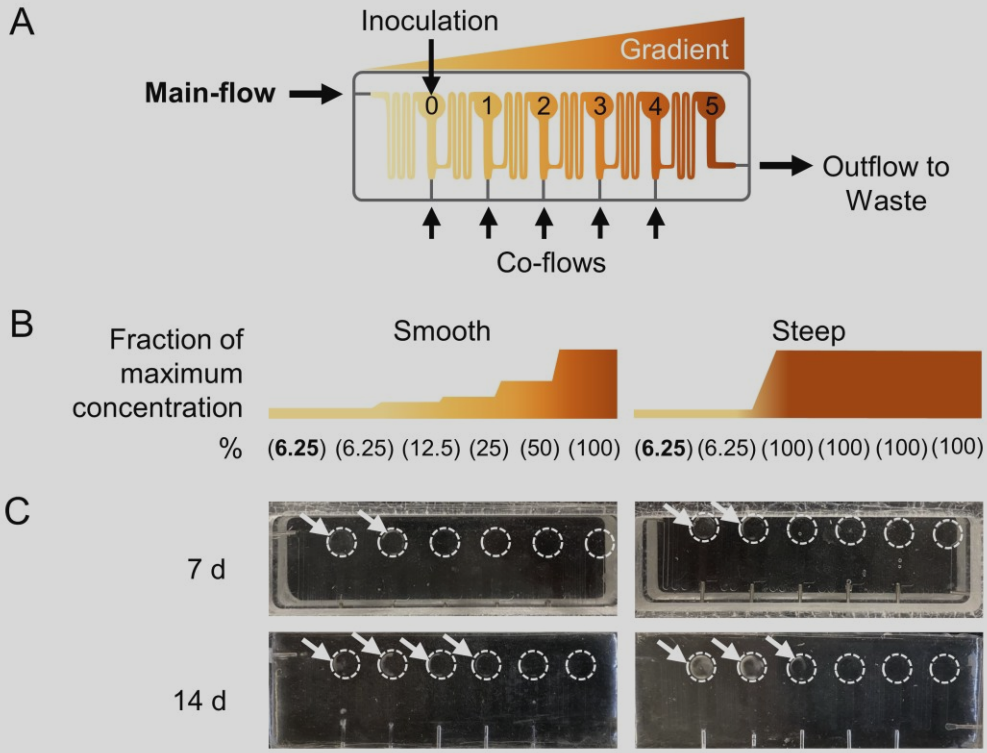

Figure 38: Adaptation of C. oleaginosum to stress-relative intermediates using the microfluidic evo.S chip. A) Increasing concentrations of the stress-relative intermediates continuously supplied to the main-flow through co-flows resulted in a concentration gradient across the interconnected growth wells 0-5 (n = 1). B) A smooth and steep gradient profile were implemented on separate chips, both ranging from 6.25% to 100% fraction of maximum intermediate concentration in anaerobic fungi mineral salt medium. C) Photographs of the chips after 7 days and 14 days adaptation. Dotted outline around the growth wells was added for visual purposes. Arrows show turbidity indicating growth.

Growth was mainly observed in wells 0 to 3, while wells 4 and 5 showed only weak or no detectable turbidity. In the steep gradient, turbidity decreased from wells 0 to 5, whereas the smooth gradient showed overall lower turbidity. Biomass from all wells was sampled and transferred to shake flask cultures. After contamination screening (Figure S37, Figure S38), one culture (smooth gradient, well 5) was excluded and the remaining cultures were successfully re-cultivated (Figure S39). To quantify growth, adapted strains were cultivated in 96-well plates and optical density (OD_{600}) was monitored over 7 days (Figure 39).

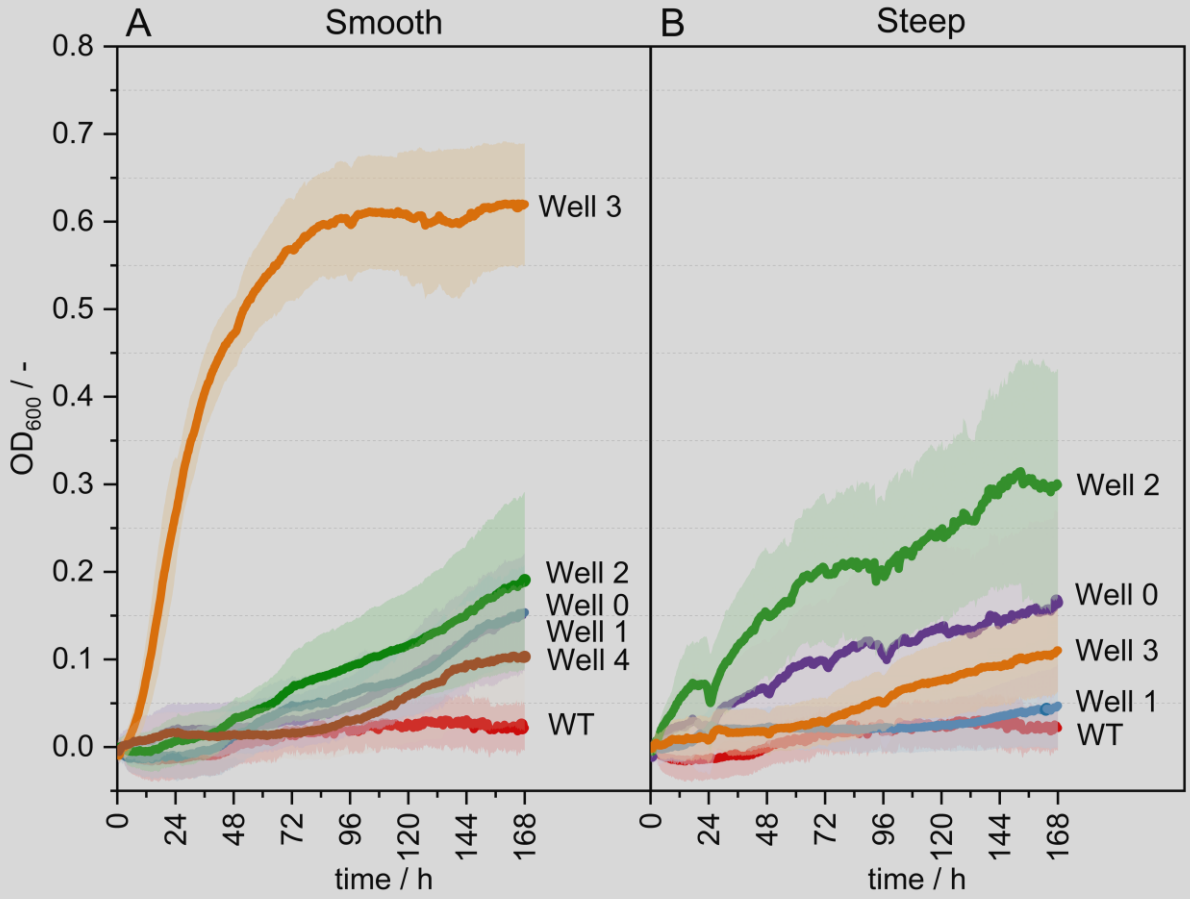

Figure 39: Growth dynamics of evolved C. oleaginosum strains under smooth and steep substrate gradients. Optical density (OD_{600}) was monitored over 168 h for strains isolated from different wells of the microfluidic evo.S chip. (A) Growth profiles of strains obtained from the smooth gradient chip. (B) Growth profiles of strains obtained from the steep gradient chip. The wild-type strain (WT) is shown for comparison. Lines represent mean OD_{600} values and shaded areas indicate the standard deviation of biological sextuplicates (n = 6) and are set to zero at t =0.

Under smooth gradient conditions, strains from wells 0 to 3 exhibited increasing OD_{600} values, with the highest value (~0.6) observed for well 3 after 72 h. Strains from wells 0–2 showed lower OD_{600} values. Under steep gradient conditions, OD_{600} values remained below 0.3 for all strains. No growth was detected for strains from wells 4 and 5. The wild type remained below OD_{600} = 0.025. For further analysis, two isolates were selected: Smooth 3 (well 3, smooth gradient) and Steep 2 (well 2, steep gradient). Growth rates were determined as μmax = 0.297 h^{-1} (Smooth 3), μmax = 0.295 h^{-1} (Steep 2), and μmax = 0.119 h^{-1} (WT). Substrate consumption was analyzed over 11 days (Figure S40), and carbon consumption normalized to OD_{600} change was calculated (Figure S41).

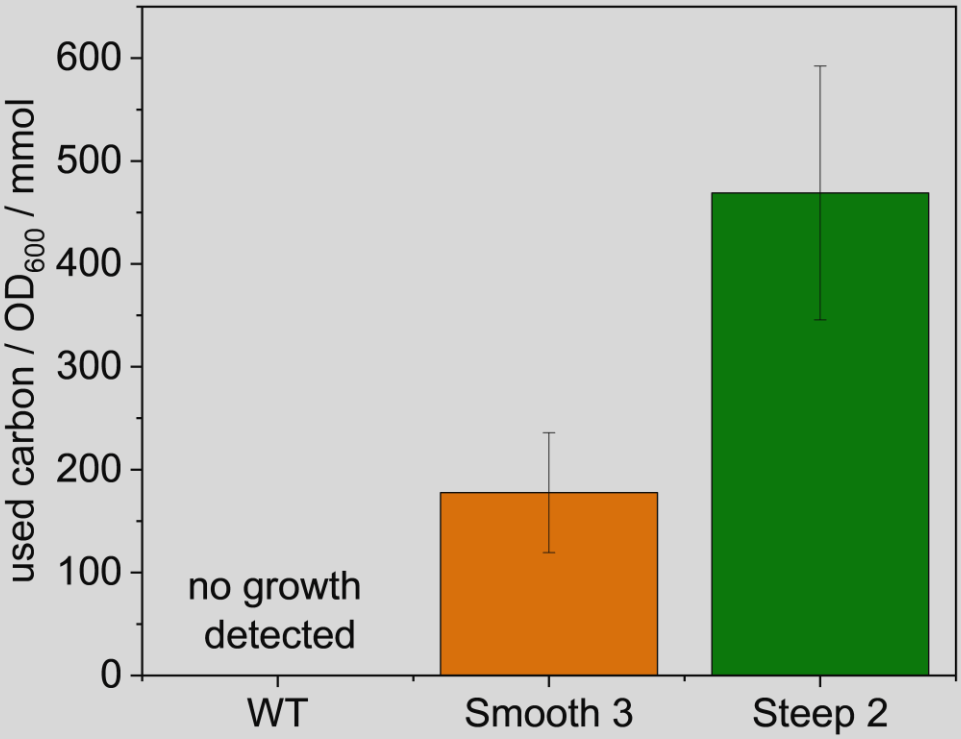

Figure 40: The amount of consumed carbon normalized to the change in OD_{600} is shown for the non-adapted wild type (WT) and for adapted cultures isolated from the smooth gradient chip (Smooth 3) and the steep gradient chip (Steep 2). No growth was detected for the WT under the tested conditions, and therefore no carbon consumption per OD_{600} increase could be determined. Bars represent mean values of technical triplicates (n = 3), and error bars indicate the standard deviation.

The normalized carbon consumption is shown in Figure 40, with the WT exhibiting the highest carbon consumption per OD_{600} increase. Both adapted strains showed lower values, with Smooth 3 displaying the lowest carbon requirement. Metabolite concentrations after 168 h were statistically analyzed (Figure 41, Table S12).

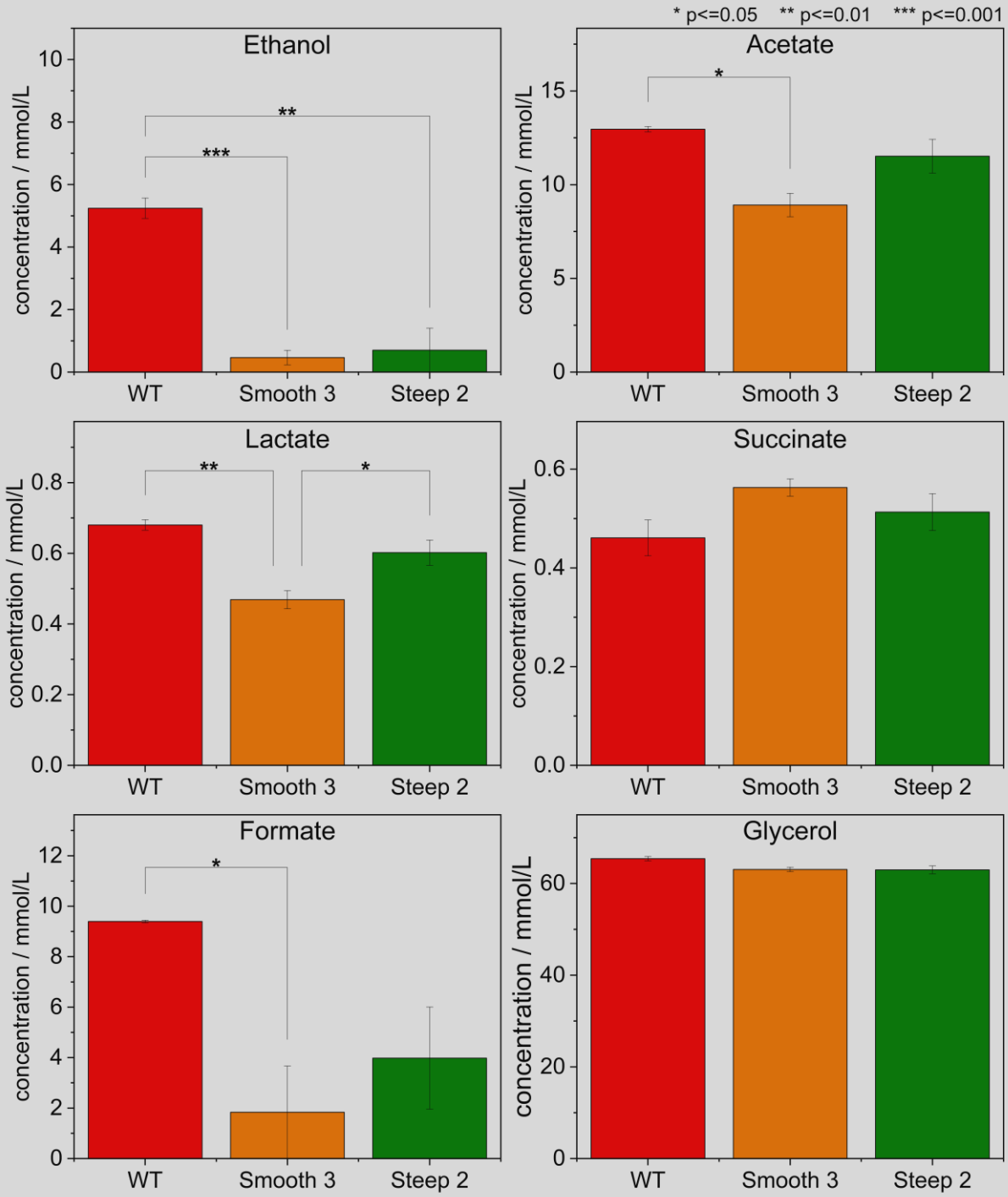

Figure 41: Statistical analysis (Tukey test) of the metabolite concentrations in cultures of the adapted C. oleaginosum strains Smooth 3 and Steep 2 after 168 h cultivation in main-flow medium in a 96-well plate in comparison to a non-adapted wild type (WT) strain in biological triplicates (n = 3). Mean values, standard deviation, standard error of the mean and 95 % confidence intervals from the conducted tukey test for end concentrations of the metabolic screening are represented in Table S12.

Significant differences were observed for ethanol, acetate, lactate and formate. Ethanol concentrations were significantly reduced in both adapted strains compared to WT ($p \leq 0.001$; $p \leq 0.01$). Formate levels were also reduced ($p \leq 0.01$), with the lowest values observed for Smooth 3. Lactate was significantly lower in Smooth 3 compared to WT ($p \leq 0.01$) and to Steep 2 ($p \leq 0.05$). Acetate showed moderate reduction ($p \leq 0.05$). No significant differences were observed for glycerol and succinate.

Chapter 6: 4 Discussion

The strong reduction in biomass formation in medium Y-EALS and the absence of measurable CDW in medium Y-EALS+F (Figure 36) showed that the mixture of anaerobic fungal fermentation intermediates imposed a substantial physiological burden on *C. oleaginosum*. The fact that formate alone did not support growth and that its addition to the mixed-substrate medium abolished detectable biomass formation identifies formate as a major limiting factor under the tested conditions. Notably, this severe phenotype occurred although the concentrations of the individual compounds were selected with reference to published first-toxicity thresholds, indicating that the mixed-substrate context itself substantially intensified stress. Because organism-specific toxicity data for *C. oleaginosum* ATCC 20509 are not yet available, toxicity thresholds reported for *S. cerevisiae* were utilized as orientation. The observed phenotype is consistent with a combined effect of weak-acid stress, altered carbon-regulatory responses to non-preferred substrates, and the central metabolic role of formate in growth and energy metabolism [238-243]. Given the severe growth limitation on a substrate mixture that is nevertheless highly relevant for lignocellulose-based bioprocesses, adaptive laboratory evolution in the microfluidic evo.S chip was a rational strategy. The cultivations in the chip setup without additional stressors demonstrated that *C. oleaginosum* can be maintained and propagated under continuous-flow conditions, with growth occurring mainly in the wells and low-flow inlet regions (Figure 37). The recovery of growth after temporary air-bubble formation and the spatial growth pattern observed in the device are in line with the previously described robustness and growth behavior of the platform, confirming its applicability for yeast adaptation experiments [236]. The gradient experiments further showed that on-chip biomass accumulation and improved planktonic fitness are not necessarily equivalent. Although the steep gradient chip exhibited more pronounced turbidity development than the smooth gradient chip, especially between days 7 and 14 (Figure 38), isolates obtained from the smooth gradient performed substantially better after transfer to agitated liquid cultures (Figure 39). This discrepancy suggests that the steep gradient may have favored phenotypes that were advantageous in the structured microfluidic environment but less beneficial in homogeneous planktonic cultivation. One plausible explanation is the selection of surface-associated or biofilm-like growth states. Fungal biofilms are known to enhance persistence under stress through extracellular matrix formation, altered metabolism, and localized protection, but these traits do not necessarily translate into improved growth in well-mixed systems [244]. In contrast, the smooth gradient likely imposed a more gradual selective pressure, thereby favoring more stable fitness gains in liquid culture. This interpretation is consistent with previous work showing that the dynamics and steepness of environmental change strongly influence adaptive trajectories and the balance between transient protection and robust growth improvement [46,236,245]. The off-chip characterization of the evolved isolates supports this view. Among all tested strains, the isolate recovered from well 3 of the smooth gradient chip showed the strongest phenotype, reaching OD_{600} values of approximately 0.6 within 72 h, whereas the best-performing steep-gradient isolate reached only around OD_{600} = 0.3 after 168 h (Figure 39). The wild type, in contrast, remained near baseline throughout the assay. Both evolved strains exhibited markedly higher maximum specific growth rates than the wild type, yet as expected, they still remained below the growth rates reported for *C. oleaginosum* under favorable conditions. Thus, the observed adaptation represents a substantial improvement specifically for the inhibitor-rich mixed-substrate medium rather than a return to fully optimal growth behavior [190]. The metabolic data indicate that adaptation improved not only tolerance but also the efficiency with which the available substrates were converted into biomass. The near absence of wild-type growth, despite the presence of carbon sources that were readily consumed by the adapted strains (Figure 40), points to poor coupling between substrate uptake and biomass formation under mixed-stress conditions. Weak acids such as formate and acetate can enter cells in their undissociated form and increase the energetic demand for pH homeostasis, thereby diverting carbon from biomass formation toward maintenance functions; in addition, formic acid stress has been associated with oxidative stress and suppression of biosynthetic pathways [226,243].

In contrast, both evolved strains, and particularly Smooth 3, displayed a clearly more growth-coupled phenotype. Together with the lower residual concentrations of ethanol, lactate, and formate, this suggests that smooth-gradient adaptation resulted not merely in increased tolerance but in improved substrate assimilation. The fact that the clearest differences were observed for ethanol, lactate, and formate, whereas glycerol and succinate remained largely unchanged and acetate was only moderately affected (Figure 41), further suggests that adaptation primarily improved the handling of selected components of the mixture rather than causing a global increase in uptake of all available carbon sources. Enhanced handling of formate is a particularly plausible contributor to this phenotype, because improved formate detoxification and oxidation have been shown to simultaneously increase resistance to formic and acetic acid while improving cellular viability and energy status [238]. An additional noteworthy observation is that crude glycerol, although supplied as an auxiliary carbon source, remained largely unconsumed by both the wild type and the adapted strains. This indicates that glycerol was not a preferred substrate in the presence of the anaerobic fungal fermentation intermediates, despite its established suitability as a carbon source for oleaginous yeasts under defined conditions. Carbon source utilization in yeasts is strongly influenced by hierarchical regulation and catabolite repression, which favor substrates that can be exploited with lower immediate regulatory and energetic costs [239]. At the same time, substrate preferences in oleaginous yeasts are highly context dependent and can shift substantially with feedstock composition and the presence of co-occurring stressors, including combinations of lignocellulosic hydrolysates and crude glycerol [41]. The preferential depletion of ethanol and formate therefore suggests that these intermediates provided a more immediate metabolic benefit under the tested conditions; for formate, such a benefit is plausible because it occupies a central position in one-carbon and energy metabolism [241]. In contrast, glycerol metabolism may have been deprioritized under a selection regime that primarily favored survival and growth on inhibitory mixed substrates rather than lipid accumulation.

Chapter 6: 5 Conclusion

This study presents the first successful microfluidic ALE of the oleaginous yeast *C. oleaginosum* ATCC 20509 to enable growth on inhibitor-rich fermentation intermediates derived from anaerobic fungal degradation of lignocellulosic biomass. Initial experiments demonstrated that mixtures of typical anaerobic fungal metabolites severely impair growth of the wild-type strain, with formate exerting a particularly strong inhibitory effect despite being present at sub-toxic concentrations, highlighting the relevance of synergistic stress interactions. By applying microfluidic ALE using the evo.S chip under continuous flow for two weeks, *C. oleaginosum* was rapidly adapted to these challenging conditions. The applied gradient profile strongly influenced the adaptive outcome: while steep gradients resulted in visually pronounced on-chip biomass formation, smooth gradients yielded strains with substantially improved and stable planktonic growth. The best-performing smooth-gradient isolate reached OD_{600} values of approximately 0.6–0.7 (μ_{max} of 0.297 h^{-1}), compared to only moderate improvement for the steep-gradient isolate and near-baseline growth of the wild type. Metabolic analysis revealed that improved growth was accompanied by enhanced utilization of ethanol and formate, whereas glycerol remained largely unconsumed, indicating a regulated metabolic preference for stress-related fermentation intermediates. Notably, the smooth-gradient strain exhibited a markedly improved carbon-to-biomass conversion, demonstrating that adaptation resulted in a fundamental metabolic improvement rather than mere stress tolerance. Overall, this work establishes microfluidic ALE as an effective non-GMO strategy to tailor oleaginous yeasts for growth on complex, inhibitor-rich substrates and provides a promising basis for integrating anaerobic fungal biomass deconstruction with sustainable single-cell oil production.

Once the yeast had been adapted toward the fungal metabolite environment, the dissertation reached its final and most integrative question: what happens when both systems are brought together in practice? The seventh chapter addresses this question directly.

3.3.2 Feasibility of linking anaerobic fungal fermentations with oleaginous yeast lipid production

The seventh chapter represents the integrative endpoint of the dissertation. Its purpose is to evaluate whether the upstream and downstream modules developed in the preceding studies can actually be linked in a consecutive cultivation concept. At this stage, the work no longer focuses on one organism group in isolation. Instead, it examines the interface itself: the fungal broth as an upstream output, the oleaginous yeast as a downstream upgrading organism, and the physiological consequences of bringing both together.

This chapter is therefore where the cumulative structure of the dissertation becomes fully visible. The fungal platform has already been characterized, its cultivation environment clarified, and its redox physiology expanded. The yeast platform has been benchmarked under reactor conditions, tested on industrial side streams, and adapted toward fungal metabolites. Chapter 7 now asks whether these individual advances are sufficient to make the overall “straw-to-oil” process technically plausible.

Its particular value within the dissertation lies in the fact that it identifies the **remaining incompatibility** not as a vague problem, but as a concrete biological and chemical barrier. The coupling turns out to be possible in principle, yet more challenging than initially assumed, because broth-derived inhibitory effects interfere with yeast growth. This makes chapter 7 not only the integrative conclusion of the dissertation, but also the point at which the next generation of research questions becomes visible.

Chapter 7: Assessing the Feasibility of Linking Anaerobic Fungal Fermentations with Downstream Cultivation of the Oleaginous Yeast *Cutaneotrichosporon oleaginosum*

Chapter 7: 1 Introduction

The transition toward sustainable biotechnological production systems requires microbial platforms that can efficiently convert complex biomass into industrially relevant products. In this context, anaerobic gut fungi (*Neocallimastigomycota*) have emerged as promising biocatalysts for lignocellulosic biomass conversion. These strictly anaerobic fungi inhabit the digestive tracts of herbivorous animals and are among the primary colonizers of ingested plant material. Their rich repertoire of carbohydrate-active enzymes enables efficient deconstruction of recalcitrant plant biomass and release of fermentable sugars and mixed fermentation products, including acetate, formate, ethanol, lactate, and hydrogen [11,13,246]. Owing to this capacity, anaerobic fungi have attracted growing interest as upstream biocatalysts for biomass valorization and renewable bioprocessing [247].

A particularly attractive downstream partner in such systems is the group of oleaginous organisms, especially oleaginous yeast, which are commonly defined as microorganisms capable of accumulating more than 20% of their cell dry weight as lipids, typically as triacylglycerols [33]. Among them, *Cutaneotrichosporon oleaginosum* has emerged as a particularly promising microbial cell factory because of its rapid growth, broad substrate spectrum, inhibitor tolerance, and high lipid accumulation capacity [35,188]. Under optimized conditions, this yeast can accumulate lipids well above 60% of its dry cell weight; recent process studies report lipid contents of 65–75% under optimized cultivation conditions, and literature reviews report maxima of up to 85% of dry cell weight [248,249]. In addition, *C. oleaginosum* can utilize diverse carbon sources, including lignocellulosic hydrolysates, acetate-rich media, and industrial side streams, to produce plant-oil-like single-cell oils [35,249]. These microbial lipids are attractive as renewable feedstocks for biofuels, oleochemicals, and food- or cosmetic-related applications [250]. Despite these promising characteristics, direct co-cultivation of lignocellulose-degrading anaerobic fungi and lipid-producing yeasts is challenging because their physiological optima and oxygen requirements differ fundamentally. A practical alternative is consecutive cultivation, in which the individual process steps are temporally separated but functionally coupled through the transfer of soluble fungal products. Biphasic concepts based on anaerobic fungal hydrolysates have already been proposed for downstream microbial bioproduction, underlining the suitability of modular process designs for lignocellulose-based biorefineries [246,251].

Within this framework, anaerobic gut fungi are attractive upstream organisms because they convert complex plant biomass into soluble metabolites, whereas oleaginous yeasts such as *C. oleaginosum* can funnel a broad range of carbon substrates into lipid biosynthesis. Establishing a functional coupling between both systems could therefore enable a new microbial platform in which lignocellulosic biomass is first depolymerized and fermented by anaerobic fungi and the resulting metabolite mixture is subsequently transferred to an oleaginous yeast for downstream cultivation. Such a platform would combine biological depolymerization with microbial upgrading and could form the basis of a scalable and more sustainable biotechnological process toward microbial lipid production.

The objective of this study is to evaluate the feasibility of a consecutive cultivation strategy linking anaerobic gut fungi with the oleaginous yeast *C. oleaginosum* as conceptual prerequisite for an integrated bioprocess. Specifically, this work characterizes the metabolite profiles generated by different anaerobic fungal strain combinations and assesses three complementary strategies for downstream establishment of *C. oleaginosum*: a conventional process without further modifications, an approach employing an adaptive laboratory evolution (ALE)-derived yeast strain, and a process based on anaerobic fungal cultivation in the presence of maleic acid. Furthermore, the study identifies a dilution-based process adjustment as a critical step for creating a compatible interface between the fungal and yeast stages, thereby enabling conditioned consecutive cultivation.

Chapter 7: 2 Material and Methods

Chapter 7: 2.1 Microbial strains

The anaerobic gut fungal strains *Aestipascuomyces dupliciliberans* A252, *Caecomyces churrovis* PP313, *Khyollomyces ramosus* X2152, *Orpinomyces joyonii* W212, *Pecoramyces ruminantium* SA222, and *Neocallimastix cameroonii* G341 were used in this study. The oleaginous yeasts used as downstream organisms were *Cutaneotrichosporon oleaginosum* ATCC 20509 and *Cutaneotrichosporon oleaginosum* Smooth 3 (Schulz et al., manuscript in preparation).

Chapter 7: 2.2 Culture media

Separate media formulations were used for the anaerobic gut fungi and the oleaginous yeast to accommodate their distinct physiological requirements. Fungal strains were cultivated in a bicarbonate-buffered medium under strictly anoxic conditions at near-neutral pH, whereas the yeasts if not stated otherwise were cultivated in a nitrogen-limited mineral salt medium at acidic pH.

Chapter 7: 2.2.1 Anaerobic gut fungal cultivation medium

Anaerobic gut fungi were cultivated in a modified minimal medium based on the formulation described by Schulz et al. [14]. The medium consisted, per liter, of 150 mL salt solution 1 (3 g/L K_2HPO_4), 150 mL salt solution 2 (3 g/L KH_2PO_4, 6 g/L $(NH_4)_2SO_4$, 6 g/L NaCl, 0.6 g/L $MgSO_4 \cdot 7H_2O$, and 0.6 g/L $CaCl_2 \cdot 2H_2O$), 2 mL zoospore inducer solution (0.5 g/L hemin chloride dissolved in 50% ethanol and 50% 0.05 M NaOH), 2 mL resazurin solution (1 g/L resazurin sodium salt), 6 g $NaHCO_3$, 1 g L-cysteine hydrochloride monohydrate, and 10 mL trace element solution. The trace element solution contained manganese(II) chloride tetrahydrate, nickel(II) chloride hexahydrate, sodium molybdate dihydrate, boric acid, iron(II) sulfate heptahydrate, cobalt(II) chloride hexahydrate, sodium selenite pentahydrate, sodium metavanadate, zinc sulfate, and copper(II) sulfate pentahydrate dissolved in 0.2 M HCl. The medium was prepared with demineralized water, rendered anaerobic by flushing with CO_2, and adjusted to pH 6.9. Wheat straw particles (1 mm) were used as the standard solid carbon source at 5 g/L. Immediately before inoculation, 0.5 mL of sterile vitamin solution (0.01 mg/L thiamine hydrochloride, 0.652 g/L panthothenic acid hemicalium salt, 0.6 g/L nicotinic acid, 0.02 g/L cyanocobalamin, 0.2 g/L biotin, 0.012 g/L pyridoxine hydrochloride, 0.05 g/L folic acid, and 0.05 g/L P-aminobenzoic acid 0.2 g/L riboflavin) and 0.5 mLof an antibiotic mix (50 g/L ampicillin sodium salt, 50 g/L streptomycin sulfate, 50 g/L penicillin sodium) were added.

Chapter 7: 2.2.2 Oleaginous yeast cultivation medium

Yeasts were cultivated if not stated otherwise in mineral salt medium described by Schulz et al. [42]. The medium consisted of a mineral salt solution (8.99 g/L potassium dihydrogen phosphate, 0.12 g/L disodium hydrogen phosphate, 0.1 g/L sodium citrate dihydrate, 0.1 g/L yeast extract, 0.2 g/L magnesium sulfate heptahydrate, and 4.72 g/L ammonium sulfate) supplemented with 7.7% (v/v) sterile-filtered trace element solution (4 g/L calcium chloride dihydrate, 0.55 g/L iron(II) sulfate dihydrate, 0.475 g/L citric acid, 0.1 g/L zinc sulfate heptahydrate, 0.075 g/L manganese(II) sulfate monohydrate, and 100 µL/L sulfuric acid, 96%), 7.7% (v/v) autoclaved salt solution (10 g/L yeast extract and 20 g/L magnesium sulfate heptahydrate), and 7.7% (v/v) autoclaved glucose solution.

Chapter 7: 2.3 Inoculum preparation

Due to the distinct physiological requirements of the two organism groups, inoculum preparation followed separate procedures. For anaerobic gut fungi, inocula were obtained from actively maintained transfer cultures cultivated under strictly anaerobic conditions. In contrast, *Cutaneotrichosporon oleaginosum* inocula were generated by reactivating frozen cryostocks on agar plates followed by liquid precultivation.

Chapter 7: 2.3.1 Anaerobic gut fungal inoculum

Anaerobic gut fungal precultures were derived from working cultures maintained in 7-day batch cycles. For routine propagation, 5 mL of an actively growing culture were transferred weekly into freshly prepared 100 mL serum bottles containing 50 mL of the medium described in Section 2.2.1 and supplemented with 1 mm wheat straw particles at 5 g/L. The medium was anaerobized with CO_2, adjusted to pH 6.9, supplemented with trace elements, vitamins, and antibiotics, and incubated at 39 °C. These regularly subcultured transfer cultures served as inoculum sources for the subsequent experiments, which were initiated with 5 mL of the respective fungal culture.

Chapter 7: 2.3.2 Oleaginous yeast inoculum

Cryostocks of *C. oleaginosum* ATCC 20509 and *C. oleaginosum* Smooth 3 were prepared from 150 µL pure glycerol and 850 µL of a yeast suspension containing 20 g/L biomass and were stored at -80 °C. For reactivation, cryostocks were streaked onto YM agar plates containing 10 g/L glucose, 3 g/L yeast extract, 3 g/L malt extract, 5 g/L peptone, and 15 g/L agar at pH 7 and incubated for 7 days. A single colony was then transferred to 250 mL baffled Erlenmeyer flasks containing 50 mL of the nitrogen-limited liquid medium described in Section 2.2.2. Precultures were incubated for 4 days at 20 °C and 130 rpm. Subsequently, 1 mL of the first preculture was transferred to fresh medium and incubated for an additional 4 days under identical conditions before use as inoculum for the main cultures.

Chapter 7: 2.4 Experimental design

Chapter 7: 2.4.1 Mixed-strain cultivation of anaerobic gut fungi

To evaluate potential interactions between anaerobic gut fungal strains, the six strains described in Section 2.1 were cultivated as single-strain controls and in multi-strain combinations. In total, 63 unique culture configurations were examined, comprising six single-strain cultures, 15 two-strain combinations, 20 three-strain combinations, 15 four-strain combinations, six five-strain combinations, and one six-strain consortium, as summarized in Table 11. All cultures were established in 100 mL serum bottles containing the anaerobic gut fungi medium described in Section 2.2.1 and supplemented with 1 mm wheat straw particles (5 g/L) as solid carbon source. Actively growing precultures served as inocula. To ensure comparability across all culture configurations, the total inoculum volume was kept constant at 5 mL per bottle and divided equally among the strains included in the respective setup. Cultures were incubated anaerobically for 7 days at 39 °C, and all configurations were prepared in triplicate. At the cultivation endpoint, fermentation pressure was determined and gas and liquid samples were collected for the analysis of hydrogen and soluble fermentation metabolites, respectively, as described in the analytical methods section.

Table 11: Overview of the 63 unique mono- and mixed-strain culture configurations generated from the six anaerobic gut fungal strains used in this study, grouped according to the number of strains present in each combination. Strain abbreviations: A, Aestipascuomyces dupliciliberans A252; G, Neocallimastix cameroonii G341; P, Caecomyces churrovis PP313; S, Pecoramyces ruminantium SA222; W, Orpinomyces joyonii W212; X, Khyollomyces ramosus X2152.

Number of different strains contained	Combinations
1	A, G, P, S, W, X
2	AG, AP, AS, AW, AX, GP, GS, GW, GX, PS, PW, PX, SW, SX, WX
3	AGP, AGS, AGW, AGX, APS, APW, APX, ASW, ASX, AWX, GPS, GPW, GPX, GSW, GSX, GWX, PSW, PSX, PWX, SWX
4	AGPS, AGPW, AGPX, AGSW, AGSX, AGWX, APSW, APSX, APWX, AWSX, GPSW, GPSX, GPWX, GSWX, PSWX
5	AGPSW, AGPSX, AGPWX, AGSWX, APSWX, GPSWX
6	AGPSWX

Chapter 7: 2.4.2 Consecutive cultivation experiment

Consecutive cultivation experiments were performed according to the cultivation procedures described above for anaerobic gut fungi and oleaginous yeast strains. In the first stage, the selected fungal consortium AG, comprising *A. dupliciliberans* A252 and *N. cameroonii* G341, was cultivated anaerobically in standard gut fungal medium containing wheat straw (1 mm, 5 g L^{-1}) as solid substrate. Yeast inocula were prepared separately from reactivated cryostocks by two-step precultivation. At the end of the fungal phase, headspace pressure was recorded using the serum-bottle pressure determination method described below. The fungal cultures were subsequently aerated by mixing with air, adjusted to pH 4.0 with 4 M phosphoric acid, and inoculated with the respective *C. oleaginosum* strain to initiate the yeast phase. All cultivation variants were carried out in biological triplicate (n = 3). pH was monitored daily, and samples were collected at 24 h intervals for HPLC analysis as described in the analytical methods section.

Three consecutive cultivation variants were investigated. In the first variant, the parental *C. oleaginosum* ATCC 20509 strain was inoculated directly into the transferred fungal culture without further modification beyond aeration and pH adjustment. In the second (ALE-based) variant, the parental strain was replaced by the adaptive laboratory evolution (ALE)-derived *C. oleaginosum* strain Smooth 3, which had previously been selected for improved growth on metabolite mixtures representative of anaerobic fungal fermentation products (Schulz et al., manuscript in preparation). In the third (maleic-acid-based) variant, the fungal phase was conducted in a modified bicarbonate-free fungal medium in which the sodium bicarbonate buffer system was replaced by Bis-Tris (6 g L^{-1}) and maleic acid (4 g L^{-1}), based on findings from a separate cultivation study on anaerobic gut fungi (Schulz et al., manuscript in preparation). All subsequent process steps were performed as described for the first variant.

Chapter 7: 2.4.3 Dilution experiment in YM medium

YM broth was prepared according to Wickerham's formulation (10 g L^{-1} glucose, 5 g L^{-1} peptone, 3 g L^{-1} yeast extract, and 3 g L^{-1} malt extract), supplemented with 10 g L^{-1} NaCl and adjusted to pH 4.0 by dropwise addition of 4 M phosphoric acid [252]. The ALE-derived *C. oleaginosum* strain was cultivated for 24 h in 50 mL culture volume under three conditions, each performed in biological triplicate: YM medium supplemented with 5 mL sterile water (=control), YM medium supplemented with 5 mL untreated fungal broth, and YM medium supplemented with 5 mL centrifuged fungal broth. The added volume corresponded to a 1:10 dilution of the fungal broth in the final culture volume. Growth was determined with optical density measurement at 600 nm and HPLC as described in the analytical section.

Chapter 7: 2.5 Analytics

Chapter 7: 2.5.1 Headspace pressure

Headspace pressure was measured at the end of each cultivation as an indirect indicator of gas formation and metabolic activity in the sealed serum bottles. To minimize temperature-dependent fluctuations, measurements were performed with the bottles maintained at cultivation temperature (39 °C). A sterile BD Microlance™ cannula was inserted through the butyl rubber stopper and connected via neoprene tubing (Watson-Marlow) and a 0.22 µm sterile filter (Minisart NML, Sartorius) to either a vacuum gauge (G 1111-VAC, Greisinger) or a digital barometer (GDH 14 AN, Greisinger). Pressure values are reported as overpressure relative to ambient atmospheric pressure (Δp, bar). Measurements were taken immediately prior to gas sampling.

Chapter 7: 2.5.2 Headspace gas composition

Headspace gas composition was analyzed at the end of each cultivation using a 3000 Micro GC System (INFICON Holding AG) equipped with a thermal conductivity detector (TCD). Prior to sampling, serum bottles were equilibrated at 39 °C in a thermostated water bath (ONE 10, Memmert GmbH + Co. KG) to minimize temperature-dependent variability in gas solubility and pressure. A gas sample of 3–5 mL was withdrawn through the butyl rubber stopper using a sterile syringe and introduced into the µGC system, which aspirated the sample at 10 mL min^{-1} by means of its internal vacuum pump. Gas separation was performed using a two-channel configuration. Channel A consisted of a PLOTU pre-column coupled to an Rt-Molsieve 5 Å main column (Agilent Technologies) for the determination of hydrogen (H_2), nitrogen (N_2), and oxygen (O_2), using helium as carrier and reference gas at an operating pressure of 1.72 bar. Channel B was equipped with an Rt-Q-Bond column (Agilent Technologies) for the analysis of carbon dioxide (CO_2) at an operating pressure of 1.38 bar. The injection system, valves, and columns were maintained at 80 °C throughout the analysis. Gas concentrations were quantified by peak area integration following calibration with a seven-point standard gas mixture covering the expected concentration ranges of hydrogen and carbon dioxide.

Chapter 7: 2.5.3 Soluble metabolite analysis

Extracellular metabolites were quantified at the end of each cultivation by high-performance liquid chromatography (HPLC). For sample preparation, 2 mL of culture broth were withdrawn from each serum bottle through the butyl rubber stopper using a sterile BD Microlance™ cannula and transferred to 2 mL microcentrifuge tubes. Samples were centrifuged for 10 min at 13,000 rpm in a Heraeus™ Pico 17 centrifuge (Thermo Fisher Scientific) to remove suspended particles and residual fungal biomass. Subsequently, 1 mL of the clarified supernatant was filtered through a 0.22 µm cellulose acetate syringe filter (Restek) and transferred to chromatography vials (Brown Chromatography Supplies) sealed with Teflon-lined caps. Analyses were performed on an Agilent 1100 HPLC system equipped with a Rezex ROA Organic Acid H^+ (8%) guard column (50 × 7.8 mm) and the corresponding analytical column (300 × 7.8 mm, 8 µm; Phenomenex Ltd.). The mobile phase consisted of 5 mM sulfuric acid (H_2SO_4) at a flow rate of 0.5 mL min^{-1}, and the total run time was 40 min. The column compartment and refractive index detector (RID) were maintained at 50 °C. In addition, a variable wavelength detector (VWD) set to 220 nm was used for compound-specific absorbance detection. Quantification was based on external calibration curves prepared from analytical standards of acetate, ethanol, succinate, formate, lactate and malate in a concentration range of 0.1–10 g L^{-1}. Peak areas were integrated using the instrument software, and metabolite concentrations were calculated by linear regression of the respective calibration curves.

Chapter 7: 3 Results and discussion

Establishing a consecutive cultivation platform linking anaerobic gut fungi with *C. oleaginosum* requires more than the simple sequential use of two microorganisms; it depends on the interplay between fungal substrate conversion, metabolite formation, and the physiological compatibility of the resulting broth with downstream yeast cultivation. The results are therefore discussed in a stepwise framework. First, anaerobic fungal strain combinations were compared to identify upstream cultures with high total soluble product formation, pronounced formation of yeast-relevant carbon sources such as acetate, and a balanced metabolite spectrum suitable for downstream transfer to *C. oleaginosum*. Second, these cultures were evaluated in three direct-transfer consecutive yeast cultivation strategies, including a conventional unmodified setup, the use of the ALE-derived yeast strain Smooth 3, and a maleic-acid-based fungal cultivation approach. Finally, a dilution experiment in YM medium was conducted to clarify whether the observed limitation originated primarily from insufficient nutrient availability or from inhibitory components present in the fungal broth.

The initial screening of mono- and mixed-strain anaerobic gut fungal cultures revealed pronounced differences in overall product formation after 7 d of cultivation on wheat straw. As shown in Figure 42, the product spectrum was dominated by the soluble fermentation products ethanol, acetate, and formate, whereas lactate and succinate were only minor components and citrate and malate were negligible across most configurations. Hydrogen was consistently detected, but contributed only a comparatively small fraction to the total quantified products. This overall profile is in line with the characteristic fermentative metabolism of anaerobic gut fungi, in which lignocellulose-derived carbon is primarily converted into acetate, formate, ethanol, and other reduced end products, while reducing equivalents are partially released as molecular hydrogen [13,246].

Among the individual strains, *C. churrovis* PP313 showed the highest total product formation, followed by strains *A. dupliciliberans* A252, *K. ramosus* X2152, and *P. ruminantium* SA222, whereas *O. joyonii* W212 displayed the lowest overall conversion efficiency (Figure 42, upper left panel). Most pairwise combinations produced intermediate total product levels and did not exceed the best-performing monoculture. Nevertheless, selected two-strain combinations, particularly *A. dupliciliberans* A252 + *N. cameroonii* G341, *N. cameroonii* G341 + *P. ruminantium* SA222, *C. churrovis* PP313 + *K. ramosus* X2152, and *P. ruminantium* SA222 + *K. ramosus* X2152, retained comparatively high product titers (Figure 42, upper right panel). Within the three-strain combinations, the response remained strongly composition-dependent: while several consortia remained at moderate levels, combinations such as *C. churrovis* PP313 + *O. joyonii* W212 + *K. ramosus* X2152, *P. ruminantium* SA222 + *O. joyonii* W212 + *K. ramosus* X2152, *C. churrovis* PP313 + *P. ruminantium* SA222 + *K. ramosus* X2152, and *C. churrovis* PP313 + *P. ruminantium* SA222 + *O. joyonii* W212 showed the highest total product formation within this group (Figure 42, middle left panel). In contrast, the four-strain, five-strain, and six-strain consortia exhibited a clear decline in total product formation and converged toward a comparatively narrow range of lower endpoint values (Figure 42, middle right and lower panels). These results indicate that fungal consortium performance was determined more by strain composition than by the absolute number of strains present. Increasing community complexity did not lead to additive or synergistic enhancement of substrate conversion; rather, the progressive decline observed in the higher-order consortia suggests non-additive interactions, likely caused by competition for substrate colonization, overlapping functional roles, or altered metabolic partitioning within the consortium. At the same time, the fact that selected two- and three-strain combinations still performed relatively well indicates that limited functional complementarity may occur in specific strain constellations.

Because the strains used in this study were isolated from different host animals, natural co-occurrence or ecological adaptation to each other cannot be assumed. Therefore, the observed behavior of mixed cultures should not be interpreted as reflecting naturally established fungal communities. In the present dataset, no unusual metabolite or species-specific marker compound was detected among the quantified fermentation products. Instead, differences between culture configurations were primarily quantitative and reflected shifts in the relative formation of common metabolites such as acetate, formate, ethanol, and hydrogen. One possible explanation for the reduced performance of higher-order consortia is that increasing community complexity may enhance competition for substrate colonization and alter metabolic partitioning. In addition, the strict anaerobic lifestyle of gut fungi makes them highly sensitive to oxygen, and it cannot be fully excluded that subtle differences in oxygen exposure during handling may have contributed to performance differences in more complex consortia. However, no similar effects were observed in comparable experiments by Schulz et al. (2025) [14].

In other fungal systems, direct confrontation and cocultivation markedly remodel the secondary metabolite spectrum and can activate otherwise silent biosynthetic pathways [253,254]. This possibility is particularly relevant for anaerobic gut fungi, which possess unexpectedly rich biosynthetic potential for nonribosomal peptides, polyketides, and related natural products [98]. The decline observed in the four- to six-strain consortia may therefore reflect not only competition for substrate colonization and niche overlap, but also chemically mediated interference that becomes more probable as additional strains are combined. From the perspective of downstream process design, this finding is highly relevant, because successful consecutive cultivation requires upstream cultures that generate sufficiently high concentrations of soluble, assimilable products rather than maximally complex fungal communities. In this context, the consistent formation of acetate is particularly promising, as *C. oleaginosum* is known to utilize acetate-containing and otherwise compositionally diverse feed streams for lipid production [35,188].

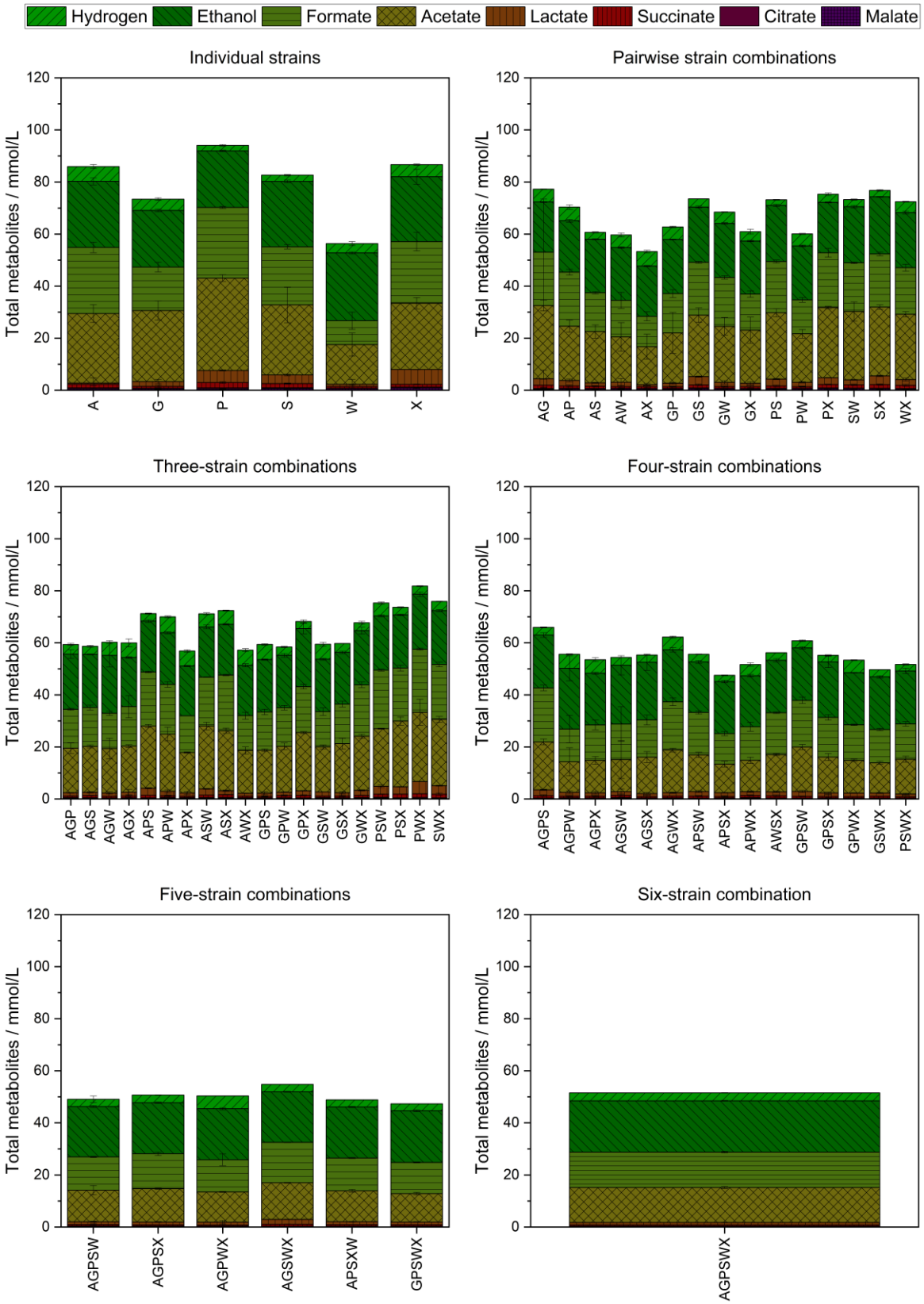

Figure 42: Endpoint fermentation product profiles of individual anaerobic gut fungal strains and mixed-strain consortia cultivated on wheat straw (5 g L-1) for 7 d. Stacked bars show the mean endpoint levels of hydrogen and extracellular metabolites (ethanol (also added with hemin solution), formate, acetate, lactate, succinate, citrate, and malate) for all 63 unique culture configurations, grouped according to the number of strains present in each consortium. Error bars indicate the standard deviation of total quantified products (n = 3). Strain abbreviations: A, A. dupliciliberans A252; G, N. cameroonii G341; P, C. churrovis PP313; S, P. ruminantium SA222; W, O. joyonii W212; X, K. ramosus X2152.

Based on the data presented in Figure 42, the pairwise consortium AG was selected for the subsequent consecutive cultivation experiments. AG combined comparatively high overall product formation with a balanced metabolite profile and thus represented a suitable upstream culture for transfer to the yeast stage. Moreover, selecting a two-strain consortium allowed the use of a biologically more tractable system than the more complex higher-order consortia while still accounting for potential interstrain effects. The pronounced acetate formation in AG was considered particularly relevant for downstream processing.

Following selection of the AG consortium as the upstream culture, the three consecutive cultivation variants were evaluated using pH development and extracellular metabolite profiles as indicators of a successful transfer to the yeast stage. As shown by the pH profiles in Figure 43 the measured pH remained close to 4.0 throughout the 192 h observation period in all three consecutive-cultivation variants. However, this apparent similarity should not be interpreted as evidence of identical buffering conditions. In the conventional and ALE-based setups, the fungal broth originated from bicarbonate-buffered anaerobic cultures, and adjustment to the yeast-stage pH caused visible CO_2 outgassing. As a consequence, the original CO_2/HCO_3^- buffer equilibrium was effectively disrupted before or during transfer to the yeast phase. Only the maleic-acid/buffer-exchange variant therefore entered the second stage with a defined non-bicarbonate buffer system. The stable pH observed in the conventional and ALE-based variants is thus best interpreted as an indication of limited net proton turnover rather than preserved bicarbonate buffering [125,255].

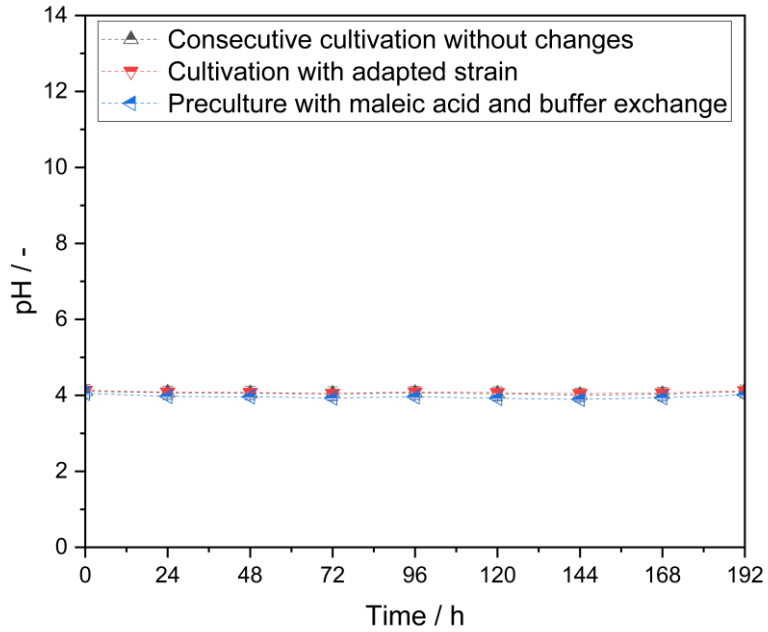

Figure 43: Time-resolved pH profiles during consecutive cultivation based on the selected anaerobic gut fungal consortium AG. Symbols indicate pH values measured over 192 h following the transition from the fungal to the yeast stage for three process variants: conventional consecutive cultivation without further modification, consecutive cultivation using the ALE-derived C. oleaginosum strain Smooth 3, and consecutive cultivation based on fungal precultures grown with maleic acid and buffer exchange. All cultivations were performed in biological triplicate (n=3).

The HPLC data in Figure 44 support this interpretation. In both the conventional and ALE-based variants, the total soluble metabolite pool remained broadly stable over time and no pronounced depletion pattern indicative of yeast growth was observed. Instead, the most visible trend was a gradual decrease in ethanol accompanied by an increase in acetate, while formate remained largely unchanged. This suggests that some limited oxidative reshaping of the transferred broth may have occurred after aeration, but not a productive downstream conversion associated with yeast growth. The maleic-acid/buffer-exchange variant showed a clearly different metabolite distribution already at the first sampling point, with lower total soluble products and relatively larger fractions of lactate, succinate, and malate. Because this altered pattern was present from the start and persisted over time, it is best interpreted as an upstream effect of the modified fungal cultivation chemistry rather than a consequence of improved chemical conversion of the yeast.

Even so, this variant is informative from a process-design perspective because it demonstrates that the composition of the transferred broth can be shifted substantially by engineering the fungal stage itself. Rather than treating incompatibility exclusively downstream, these data suggest that AGF cultivation conditions may be used to steer metabolite output and possibly suppress stress-associated broth components before transfer. Given the strong condition dependence of AGF metabolism and the association of extracellular malate and citrate with stress or lysis, harvest timing and upstream medium design are likely to be key levers for establishing a yeast-compatible interface. The mechanistic basis of that fungal cultivation strategy is the subject of a separate forthcoming study, but the general observation itself is fully consistent with the strong condition-dependence of AGF metabolite formation described previously [14].

The central result of the direct-transfer experiments is therefore that authentic fungal broth was markedly more restrictive than the defined metabolite mixture used during ALE. This distinction is important. Because Smooth 3 had already been adapted to growth on fungal metabolite mixtures at pH 4, neither acidity alone nor the mere presence of acetate, ethanol, lactate, succinate, and formate can fully explain the failure of direct transfer. Instead, the data are most consistent with the presence of additional inhibitory components or missing compounds in the transferred fungal broth. This point should be emphasized because Smooth 3 had already been adapted under pH 4 conditions on a defined mixture of the major AGF metabolites. Accordingly, the failure of direct transfer cannot be attributed to pH 4 alone and is also not readily explained by the presence of acetate, ethanol, lactate, succinate, and formate per se. In other oleaginous yeasts, low concentrations of some organic acids can even be tolerated or partially stimulatory, whereas inhibitory behavior emerges strongly as a function of concentration, mixture composition, and physiological context [48]. The authentic AGF broth therefore appears to contain an additional inhibitory layer that was absent from the defined ALE medium.

Two observations from the recent AGF physiology study by Schulz et al. reinforce this interpretation. First, a room-temperature shock applied to fungal precultures reduced the metabolic performance of the subsequent generation after transfer, showing that stress in one cultivation stage can propagate into the next. Second, the same study interpreted extracellular malate and citrate—both normally intracellular metabolites—as indicators of cellular stress or lysis under challenging cultivation conditions [14]. This is consistent with the idea that stressed or aging AGF cultures can release additional soluble factors during stress or lysis that remain biologically active after transfer. The present dataset does not identify those compounds directly, but it fits this model more closely than a simple nutrient-limitation explanation.

This hypothesis is also biologically plausible in light of AGF secondary metabolism. Anaerobic gut fungi are now recognized as an underexplored reservoir of natural products, with biosynthetic genes for nonribosomal peptides, polyketides, and related metabolites that may regulate microbial community membership in the herbivore gut [98]. In filamentous fungi more broadly, secondary metabolism is tightly linked to stress, development, and intermicrobial competition, and mixed-culture or stress-related conditions are well known to activate otherwise silent biosynthetic pathways [256-258]. From a process perspective, such compounds are unwanted inhibitors. From a discovery perspective, however, they may be highly valuable. Fungal interaction metabolites have historically yielded major pharmaceuticals, including β-lactam antibiotics, cyclosporin A from *Tolypocladium inflatum*, and pneumocandin-derived echinocandins from *Glarea lozoyensis*, the precursor family of caspofungin [259-262]. In that sense, the same broth components that presently limit process integration may ultimately represent a second value stream of AGF biotechnology, namely the discovery of new antimicrobial or otherwise bioactive molecules.

Although low pH is not a sufficient explanation for the failure of Smooth 3, it likely intensified the inhibitory burden of the authentic fungal broth. At acidic pH, weak organic acids such as acetate and formate are present to a greater extent in their undissociated form, which facilitates passive influx into yeast cells and promotes intracellular acidification, ATP-consuming proton export, and oxidative or energetic stress [129,226,263]. In biomass-derived media, inhibitor mixtures generally act in a combinatorial rather than purely additive manner, meaning that weak acids can amplify the effects of other toxic compounds even when they are not solely responsible for growth failure [264]. Thus, the most consistent interpretation is that the authentic AGF broth imposed a multifactorial stress regime: Smooth 3 could tolerate the defined core metabolites at pH 4, but not the full chemical complexity of the transferred fungal broth without further conditioning.

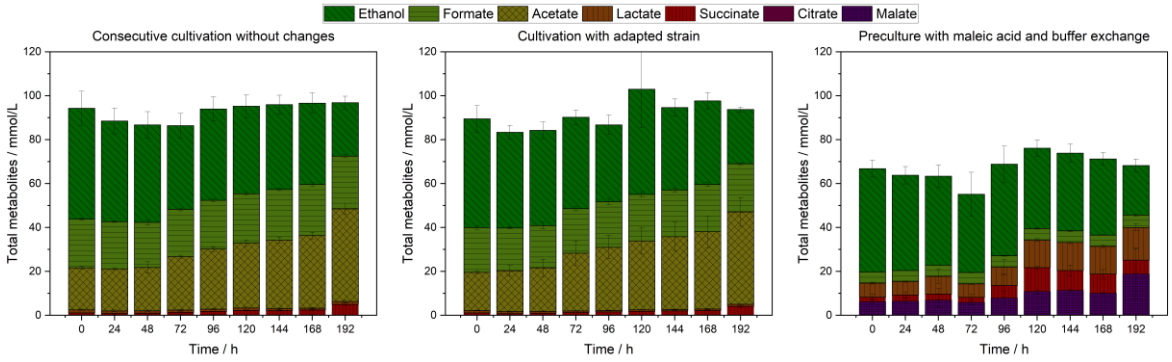

Figure 44: Time-resolved extracellular metabolite profiles during consecutive cultivation based on the selected anaerobic gut fungal consortium AG (A. dupliciliberans A252 + N. cameroonii G341). Stacked bars show the concentrations of quantified soluble metabolites (ethanol, formate, acetate, lactate, succinate, citrate, and malate), with total bar height representing the sum of the displayed metabolites. Three process variants were compared: conventional consecutive cultivation without further modification with C. oleaginosum (left), consecutive cultivation using the ALE-derived C. oleaginosum strain Smooth 3 (middle), and consecutive cultivation based on fungal precultures grown with maleic acid and buffer exchange with C. oleaginosum (right). Samples were collected over 192 h following transition from the fungal to the yeast stage. In the right panel, acetate is not displayed because the corresponding HPLC signal produced an unrealistically large apparent value and would otherwise have obscured the visualization of the remaining metabolites. Error bars indicate standard deviation (n = 3).

The decisive advance came from the dilution experiment. When the fungal broth was diluted 1:10 into nutrient-rich YM medium and supplied to Smooth 3, measurable yeast growth was observed in both fungal-broth-containing conditions (Figure 45). This changes the interpretation of the whole study. The system was not fundamentally incompatible; rather, direct transfer was too chemically restrictive, whereas conditioned transfer enabled downstream establishment. In this sense, the YM-supported transfer constitutes a proof-of-principle consecutive cultivation linking anaerobic gut fungal fermentation broth with downstream growth of an oleaginous yeast. Previous AGF integration studies had primarily focused on conceptual biphasic schemes or on bacterial partners such as *Clostridium acetobutylicum* [246,251]; the present study extends that concept to an oleaginous yeast platform. At the same time, growth in the broth-containing cultures reached only about 60–65% of the water control, demonstrating that dilution reduced but did not abolish the inhibitory load. Operationally, this result is important because it converts the study from a purely negative direct-transfer outcome into a successful conditioned-transfer proof of concept. To our knowledge, this represents the first demonstration that authentic AGF fermentation broth can support downstream growth of an oleaginous yeast when the broth interface is appropriately conditioned. The remaining growth penalty after 1:10 dilution also implies that the inhibitory effect is not trivial: either comparatively potent soluble inhibitors are present, or individually tolerable compounds become inhibitory in the authentic broth matrix through combinatorial effects, a phenomenon that is well known for lignocellulosic inhibitor mixtures [48,129,264].

The comparison between untreated and centrifuged fungal broth further clarifies the nature of that load. If growth inhibition had been driven mainly by particulate material, such as suspended fungal biomass or straw-associated components, centrifugation should have improved performance. However, growth was nearly identical in untreated and centrifuged broth, indicating that the dominant inhibitory fraction was already present in the soluble phase. This finding narrows the list of candidate inhibitors. Compounds that remain after simple clarification include weak acids, aromatic compounds, secreted peptides, and low-molecular-weight secondary metabolites, whereas intact hyphal biomass or coarse straw particles are less likely to account for the residual inhibition. In fungal systems, such soluble interaction products are commonly generated during cocultivation or stress and can remain bioactive without continued cell contact [253,254,265]. Consequently, further optimization should prioritize characterization and mitigation of the liquid-phase inhibitor fraction rather than biomass removal alone. The corresponding HPLC data in Figure 45 showed that both broth-containing conditions remained dominated by acetate, formate, and ethanol over the first 24 h, again consistent with partial relief of inhibition rather than full metabolic takeover by the yeast. In combination with the direct-transfer data, this strongly suggests that the key process bottleneck lies in soluble broth chemistry, not in simple oxygen transition, pH alone, or particulate carryover. This conclusion is also compatible with the known physiology of *C. oleaginosum*, which is generally robust toward complex waste streams and organic acids, but still responds strongly to feedstock-specific inhibitor cocktails and their concentration-dependent interactions [35,41,188].

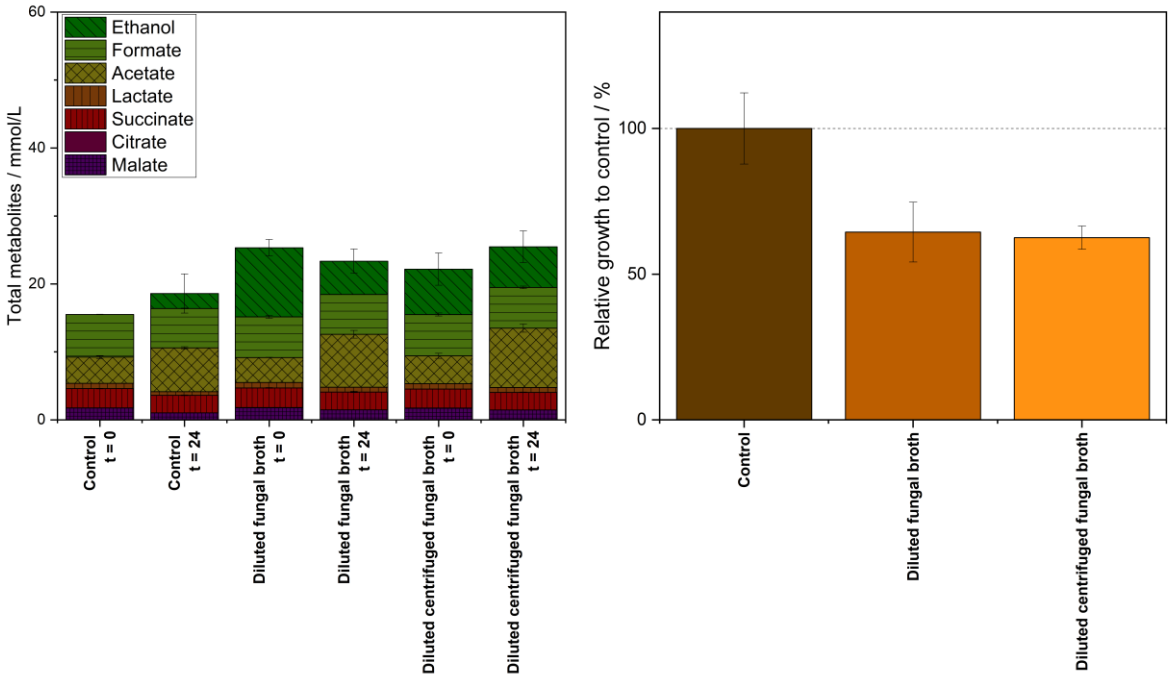

Figure 45: Dilution experiment in YM medium using the ALE-derived C. oleaginosum strain Smooth 3. Left panel: stacked bars show HPLC-quantified extracellular metabolite profiles at 0 and 24 h for the YM water control and for cultures supplemented with 5 mL untreated or centrifuged anaerobic fungal broth, corresponding to a 1:10 dilution in the final 50 mL culture volume. Right panel: relative growth normalized to the water control based on optical density measurements at 600 nm. Error bars indicate standard deviation (n=3).

Chapter 7: 4 Conclusion

This study evaluated the feasibility of coupling anaerobic gut fungal fermentation with downstream cultivation of *Cutaneotrichosporon oleaginosum* as a prerequisite for future microbial lipid production in a consecutive cultivation process. The initial screening of mono- and mixed-strain fungal cultures showed that fermentation performance depended strongly on strain composition rather than consortium size. While selected two- and three-strain combinations retained comparatively high product formation, increasing community complexity did not improve substrate conversion and instead resulted in lower overall metabolite yields, identifying strain selection as a key design parameter for establishing an efficient upstream fungal stage. Using the selected AG consortium as upstream culture, none of the three tested direct-transfer consecutive cultivation strategies enabled robust downstream establishment of *C. oleaginosum*. Neither the conventional setup, nor the use of the ALE-derived strain Smooth 3, nor the maleic-acid/buffer-exchange variant resulted in the broad metabolite depletion expected for productive yeast growth. Instead, the transferred fungal broths remained metabolically stable over time, indicating that the main limitation was not the lack of carbon sources but insufficient physiological compatibility of the authentic fungal broth with the yeast stage. The subsequent dilution experiment in nutrient-rich YM medium showed that this incompatibility was not absolute. Growth of the ALE-derived strain could be partially restored after 1:10 dilution, demonstrating that fungal fermentation broth can, in principle, support downstream cultivation of an oleaginous yeast once the inhibitory burden is reduced. This dilution-assisted transfer therefore constitutes a conditioned proof of principle for AGF–yeast consecutive cultivation. However, the persistent growth penalty relative to the control, together with the negligible effect of broth centrifugation, indicates that the dominant limitation was mainly associated with soluble inhibitory components rather than particulate fungal biomass. In combination with the acetate- and formate-rich metabolite mixture and the broader chemical complexity of authentic fungal broth, these results point to a chemically and physiologically challenging broth interface as the main bottleneck of the current process configuration. Overall, the present work demonstrates that linking anaerobic gut fungal fermentations with downstream cultivation of an oleaginous yeast is conceptually possible, but not yet operationally robust under direct broth-transfer conditions. Future process development should therefore focus on targeted conditioning of the fungal broth, improved control of the fungal harvest state, and identification or mitigation of soluble inhibitory compounds in order to establish a stable and scalable interface between the fungal and yeast stages. Such optimization will be essential before robust downstream bioconversion and lipid formation can be evaluated in an integrated process in which lignocellulosic substrates are first converted by anaerobic fungi and subsequently upgraded by *C. oleaginosum*.

Viewed as a whole, the seven chapters of this dissertation form a coherent progression from **substrate deconstruction** to **process integration**. The first three chapters establish anaerobic gut fungi as a biologically and mechanistically interpretable upstream platform. The fourth and fifth chapters define a robust and scalable downstream lipid-production platform with oleaginous yeasts. The sixth chapter begins to engineer the compatibility between both systems at the strain level, and the seventh chapter evaluates the practical consequences of bringing them together.

The reader should therefore understand the dissertation not as a sequence of loosely connected chapters, but as a gradually constructed argument. Each chapter answers one necessary question, and each answer creates the basis for the next question. The red thread running through all chapters is the transformation of a broad sustainability-oriented idea—using lignocellulosic residues as renewable feedstock for microbial oil production—into a set of experimentally grounded process principles. In that sense, the cumulative structure of this dissertation mirrors the development of the bioprocess itself: from biological possibility, through mechanistic understanding, toward technological realization.

4. Final Conclusions and Future Perspectives

Taken together, the results of this dissertation show that a biologically integrated **"straw-to-oil"** concept is scientifically sound, but that its successful implementation depends on mastering three distinct yet interdependent challenges: first, the controlled conversion of lignocellulosic material into a reproducible fungal metabolite platform; second, the robust and economically realistic production of microbial lipids from low-cost and chemically complex substrates; and third, the engineering of the biological interface between both systems. The central conclusion is therefore not merely that anaerobic gut fungi and oleaginous yeasts can each perform valuable conversions in isolation, but that they define complementary process modules whose coupling is possible in principle, yet considerably more demanding than a simple sequential use of two organisms would suggest.

A first major outcome of this work is that anaerobic gut fungi can no longer be regarded simply as difficult-to-handle rumen organisms with interesting enzyme systems; rather, they emerge as **genuine primary biocatalysts for lignocellulose conversion** whose operating window can be defined far more precisely than before. Across the six strains investigated, the work demonstrates that fungal performance is shaped by a combination of temperature, substrate identity, substrate concentration, gas atmosphere, inorganic carbon availability, and cultivation mode. The data show that the frequently used "standard" conditions of AGF cultivation conceal important physiological variation: while overall growth-related activity was usually highest around 39 °C, hydrogen optima were strain specific; straw particle size had only limited influence on total metabolite output, yet partly enhanced hydrogen formation; glucose and cellobiose were readily metabolized, whereas xylose often triggered stress-like responses; and increasing sugar concentrations reproducibly shifted metabolism toward formate and lactate, indicating overflow-like reallocation of reducing equivalents. These results substantially deepen the process understanding of AGF cultivation and make clear that fungal metabolite spectra are not fixed properties of a species, but controllable outputs of defined cultivation conditions. Equally important, the strong performance of several kitchen and agro-industrial residues as substrates broadens the feedstock perspective beyond wheat straw alone and highlights the wider residue-processing potential of this organism group.

A second key conclusion concerns the **fundamental cultivation requirements of AGF**. By decoupling headspace composition, buffer chemistry, bicarbonate availability, pH, and nitrogen supply, this dissertation shows that the traditional CO_2/HCO_3^- bottle system masks two central facts: first, the gas atmosphere is an active determinant of metabolic performance; and second, bicarbonate serves a physiological role beyond simple pH stabilization. The increased hydrogen production under N_2 headspace, together with the loss of sustained growth in bicarbonate-free but externally pH-stable media, reveals that AGF metabolism is strongly conditioned by inorganic carbon availability and by the physicochemical environment in which hydrogenosomal fermentation takes place. The restoration of activity at low, strain-specific bicarbonate threshold concentrations, the inability of alternative carboxylic acids to substitute for bicarbonate, and the identification of a pH optimum around 6.4 collectively establish a far more mechanistic cultivation framework than previously available. In practical terms, these findings are highly consequential: they mean that future AGF process development cannot rely on empirical medium recipes alone, but must explicitly account for gas-phase effects, inorganic carbon supply, and pH control as primary process variables. The OD_{750}-based biomass quantification method established in this work further contributes to this framework by improving the comparability of growth-related data in a culture system where morphology and particle association have long impeded straightforward biomass assessment.

A third central outcome is that **AGF redox metabolism appears to be broader** than expected from conventional product balances alone. The bioelectrochemical experiments indicate that historical deficits in electron recovery are unlikely to arise solely from medium chemistry or analytical incompleteness. Instead, the reproducible ferricyanide-dependent current signals observed in the eCuvette system provide the first evidence that an anaerobic gut fungus is capable of mediated extracellular electron transfer. This is an important conceptual extension of the known metabolic repertoire of *Neocallimastigomycota*. Although the immediate biotechnological implications remain to be clarified, this result opens an entirely new line of thought: AGF may not only be optimized through substrate and culture engineering, but potentially also through redox engineering, electro-fermentation, or the strategic use of extracellular electron acceptors. At the very least, the findings underscore that future AGF research should treat electron disposal as an explicit design parameter rather than a passive consequence of fermentation.

On the downstream side, this dissertation demonstrates that oleaginous yeasts can be developed into a **robust lipid-production platform under production-relevant conditions**, provided that both nutrient limitation and substrate complexity are addressed systematically. The comparative reactor benchmark shows that nitrogen limitation remains the most effective route to high lipid titres, whereas phosphate limitation can decouple lipid productivity from biomass formation and therefore constitutes a strategically relevant alternative when nitrogen-rich feedstocks are used. This distinction is more than a physiological curiosity; it provides a concrete process-engineering tool for future feedstock-flexible lipid production. In other words, the results show that the choice of nutrient limitation regime should depend on the intended substrate class and process objective rather than on tradition alone. In parallel, the work with untreated crude glycerol demonstrates that lipid production from industrial side streams does not necessarily require detoxification if the process is designed intelligently. The stepwise feeding strategy established here did not simply improve an existing cultivation; it **solved a central bottleneck by reducing the inhibitor-to-biomass ratio** during the vulnerable early growth phase. The fact that this principle remained effective during long-term repeated-batch operation in transition scale, while lipid quality stayed remarkably stable, is one of the strongest indications in the dissertation that process engineering can convert a biologically problematic waste stream into a robust production feedstock.

The work on adaptive laboratory evolution provides a sixth and particularly important conclusion: **the compatibility between fungal fermentation products and oleaginous yeast metabolism is not fixed, but can be actively improved**. The strong growth inhibition of wild-type *Cutaneotrichosporon oleaginosum* on representative AGF metabolite mixtures, especially in the presence of formate, initially appeared to represent a major barrier to process integration. However, the microfluidic ALE strategy developed here showed that even complex inhibitory mixtures can be used as selection environments to obtain improved, non-GMO strains. The best isolates displayed significantly enhanced growth and uptake of ethanol, lactate, and formate, indicating that strain-level adaptation is a realistic and powerful lever for narrowing the physiological gap between upstream and downstream modules. This is a decisive result for future process design. It shows that successful coupling of fungal and yeast bioprocesses will not depend solely on optimizing the fungal broth, but also on tailoring the downstream organism to the actual chemical landscape generated upstream.

At the same time, the preliminary results of the ongoing consecutive-cultivation experiments underline the current **critical compatibility barrier** of the whole concept. The direct use of fungal fermentation broths by the oleaginous yeast proved more difficult than initially anticipated. While the metabolite composition is, in principle, well suited to act as a carbon platform, the experiments suggest that an inhibitory factor present in the fungal broth prevents efficient downstream growth unless dilution is applied. The current working hypothesis is that this effect is associated with a compound formed intracellularly and released into the medium, rather than being caused exclusively by the major quantified fermentation products. This observation is highly significant because it changes the focus of future integration work. The central challenge is no longer simply whether AGF can produce suitable metabolites and whether yeasts can use them, but whether the total broth chemistry can be made compatible with downstream physiology. The practical implication is clear: successful process coupling will require not only carbon matching, but also targeted broth conditioning, toxin identification, and possibly selective removal, dilution, adsorption, or controlled release strategies. In this sense, the final experiments of the dissertation do not weaken the “straw-to-oil” concept; rather, they identify the exact point at which future work must intervene to make it operational.

From these conclusions, several future perspectives follow directly. On the AGF side, future work should prioritize the identification of the physiological role of bicarbonate, the molecular basis of strain-specific metabolite distributions, and the regulation of electron disposal. More detailed transcriptomic, proteomic, and metabolomic studies—especially under defined headspace and bicarbonate conditions—would be particularly valuable for distinguishing between carbon fixation, redox balancing, and stress adaptation functions. Likewise, the newly observed extracellular electron transfer capability should be followed by mechanistic studies addressing mediator specificity, possible endogenous redox shuttles, and the potential of electrochemical control over fungal metabolism. From an engineering perspective, future AGF cultivation will benefit from moving beyond static serum-bottle systems toward better-defined reactor environments with improved gas handling, controlled headspace-to-liquid transfer, and more reproducible inoculation strategies. Methods for long-term preservation and standardized inoculum preparation remain particularly important, as they represent a practical bottleneck for broader implementation.

For the yeast platform, the next logical step is to connect process engineering with targeted physiological improvement. The reactor studies presented here clearly show that optimization of nutrient limitation, feeding strategy, and substrate adaptation can dramatically alter lipid productivity and process robustness. Future work should therefore investigate fungal metabolite mixtures not only as direct feedstocks, but also in combination with co-substrates such as crude glycerol, which may improve both redox balance and economic feasibility. In parallel, the most promising non-GMO adapted isolates should be studied under controlled bioreactor conditions to determine whether their improvements in shake-flask cultures translate into stable and productive performance at scale. Additional work is also needed on downstream implications, particularly whether inhibitor-rich feedstocks alter lipid class distribution, extraction behavior, or final oil quality under industrially relevant operation.

Most importantly, the future of this research lies in the **deliberate engineering of the interface** between both biological systems. The final goal should not be seen as the simple sequential use of two unrelated organisms, but as the development of a coordinated conversion chain in which the AGF stage is tuned for downstream compatibility and the yeast stage is tuned for upstream reality. To reach that goal, the inhibitory component(s) in fungal broths must be identified and their mode of action resolved. Once this is achieved, several technically realistic strategies become possible: controlled broth dilution, partial detoxification, selective adsorption, membrane-based separation, adaptation against real fungal supernatants rather than synthetic metabolite mixtures, and optimization of fungal cultivation specifically toward more yeast-compatible broth compositions. In addition, a broader techno-economic and life-cycle perspective will ultimately be necessary to define whether hydrogen, fungal metabolites, microbial lipids, or combinations thereof provide the most attractive use of the biomass carbon. Such analyses should include not only product yields and reactor performance, but also feedstock availability, process energy demand, and downstream recovery costs.

In summary, this dissertation does not merely provide isolated findings on anaerobic fungi or oleaginous yeasts. It establishes a coherent process logic for a future upcycling platform in which lignocellulosic side streams are first unlocked by AGF and subsequently converted into microbial lipids by yeasts. It demonstrates that the upstream and downstream modules can each be made substantially more robust and more mechanistically understood than before. At the same time, it identifies the coupling step itself as the decisive frontier of future development. The most important overall conclusion is therefore that the “straw-to-oil” concept is biologically plausible and technologically promising, but its realization will depend on mastering the chemical and physiological interface between biomass deconstruction and lipid production. By defining both the opportunities and the bottlenecks with this degree of clarity, the present work provides a solid basis for future scientific progress and for the eventual biotechnological implementation of anaerobic fungi-yeast process chains.

5. List of references

1. Abbass, K.; Qasim, M.Z.; Song, H.; Murshed, M.; Mahmood, H.; Younis, I. A review of the global climate change impacts, adaptation, and sustainable mitigation measures. *Environ Sci Pollut Res Int* **2022**, *29*, 42539-42559, doi:10.1007/s11356-022-19718-6.
2. Geissdoerfer, M.; Savaget, P.; Bocken, N.M.P.; Hultink, E.J. The Circular Economy – A new sustainability paradigm? *Journal of Cleaner Production* **2017**, *143*, 757-768, doi:10.1016/j.jclepro.2016.12.048.
3. Grossmann, L. Sustainable media feedstocks for cellular agriculture. *Biotechnol Adv* **2024**, *73*, 108367, doi:10.1016/j.biotechadv.2024.108367.
4. Qaseem, M.F.; Shaheen, H.; Wu, A.-M. Cell wall hemicellulose for sustainable industrial utilization. *Renewable and Sustainable Energy Reviews* **2021**, *144*, doi:10.1016/j.rser.2021.110996.
5. Leong, H.Y.; Chang, C.K.; Khoo, K.S.; Chew, K.W.; Chia, S.R.; Lim, J.W.; Chang, J.S.; Show, P.L. Waste biorefinery towards a sustainable circular bioeconomy: a solution to global issues. *Biotechnol Biofuels* **2021**, *14*, 87, doi:10.1186/s13068-021-01939-5.
6. Mesa, J.A.; Sierra-Fontalvo, L.; Ortegon, K.; Gonzalez-Quiroga, A. Advancing circular bioeconomy: A critical review and assessment of indicators. *Sustainable Production and Consumption* **2024**, *46*, 324-342, doi:10.1016/j.spc.2024.03.006.
7. Rahmati, S.; Doherty, W.; Dubal, D.; Atanda, L.; Moghaddam, L.; Sonar, P.; Hessel, V.; Ostrikov, K. Pretreatment and fermentation of lignocellulosic biomass: reaction mechanisms and process engineering. *Reaction Chemistry & Engineering* **2020**, *5*, 2017-2047, doi:10.1039/d0re00241k.
8. Ochsenreither, K.; Gluck, C.; Stressler, T.; Fischer, L.; Syldatk, C. Production Strategies and Applications of Microbial Single Cell Oils. *Front Microbiol* **2016**, *7*, 1539, doi:10.3389/fmicb.2016.01539.
9. Himmel, M.E.; Ding, S.Y.; Johnson, D.K.; Adney, W.S.; Nimlos, M.R.; Brady, J.W.; Foust, T.D. Biomass recalcitrance: engineering plants and enzymes for biofuels production. *Science* **2007**, *315*, 804-807, doi:10.1126/science.1137016.
10. Scheller, H.V.; Ulvskov, P. Hemicelluloses. *Annu Rev Plant Biol* **2010**, *61*, 263-289, doi:10.1146/annurev-arplant-042809-112315.
11. Lankiewicz, T.S.; Choudhary, H.; Gao, Y.; Amer, B.; Lillington, S.P.; Leggieri, P.A.; Brown, J.L.; Swift, C.L.; Lipzen, A.; Na, H.; et al. Lignin deconstruction by anaerobic fungi. *Nat Microbiol* **2023**, *8*, 596-610, doi:10.1038/s41564-023-01336-8.
12. Polizeli, M.L.; Rizzatti, A.C.; Monti, R.; Terenzi, H.F.; Jorge, J.A.; Amorim, D.S. Xylanases from fungi: properties and industrial applications. *Appl Microbiol Biotechnol* **2005**, *67*, 577-591, doi:10.1007/s00253-005-1904-7.
13. Haitjema, C.H.; Solomon, K.V.; Henske, J.K.; Theodorou, M.K.; O'Malley, M.A. Anaerobic gut fungi: Advances in isolation, culture, and cellulolytic enzyme discovery for biofuel production. *Biotechnol Bioeng* **2014**, *111*, 1471-1482, doi:10.1002/bit.25264.
14. Schulz, K.E.; Scholz, D.; Sikiric, A.R.; Rambow, D.; Neumann, A.; Ochsenreither, K. Anaerobic gut fungi as biocatalysts: metabolic and physiological analysis of anaerobic gut fungi under diverse cultivation conditions. *Front Microbiol* **2025**, *16*, 1662047, doi:10.3389/fmicb.2025.1662047.
15. Samrot, A.V.; Rajalakshmi, D.; Sathiyasree, M.; Saigeetha, S.; Kasipandian, K.; Valli, N.; Jayshree, N.; Prakash, P.; Shobana, N. A Review on Biohydrogen Sources, Production Routes, and Its Application as a Fuel Cell. *Sustainability* **2023**, *15*, doi:10.3390/su151612641.
16. Naik, S.N.; Goud, V.V.; Rout, P.K.; Dalai, A.K. Production of first and second generation biofuels: A comprehensive review. *Renewable and Sustainable Energy Reviews* **2010**, *14*, 578-597, doi:10.1016/j.rser.2009.10.003.

17. Egerer, J.; Farhang-Damghani, N.; Grimm, V.; Runge, P. The industry transformation from fossil fuels to hydrogen will reorganize value chains: Big picture and case studies for Germany. *Applied Energy* **2024**, *358*, doi:10.1016/j.apenergy.2023.122485.
18. Röper, K.; Kunz, N.; Gast, L. Renewable hydrogen in industrial production: A bibliometric analysis of current and future applications. *International Journal of Hydrogen Energy* **2025**, *98*, 687-696, doi:10.1016/j.ijhydene.2024.12.034.
19. Teke, G.M.; Anye Cho, B.; Bosman, C.E.; Mapholi, Z.; Zhang, D.; Pott, R.W.M. Towards industrial biological hydrogen production: a review. *World J Microbiol Biotechnol* **2023**, *40*, 37, doi:10.1007/s11274-023-03845-4.
20. Stabel, M.; Haack, K.; Lubbert, H.; Greif, M.; Gorenflo, P.; Aliyu, H.; Ochsenreither, K. Metabolic shift towards increased biohydrogen production during dark fermentation in the anaerobic fungus Neocallimastix cameroonii G341. *Biotechnol Biofuels Bioprod* **2022**, *15*, 96, doi:10.1186/s13068-022-02193-z.
21. Boxma, B.; de Graaf, R.M.; van der Staay, G.W.; van Alen, T.A.; Ricard, G.; Gabaldon, T.; van Hoek, A.H.; Moon-van der Staay, S.Y.; Koopman, W.J.; van Hellemond, J.J.; et al. An anaerobic mitochondrion that produces hydrogen. *Nature* **2005**, *434*, 74-79, doi:10.1038/nature03343.
22. Gruninger, R.J.; Puniya, A.K.; Callaghan, T.M.; Edwards, J.E.; Youssef, N.; Dagar, S.S.; Fliegerova, K.; Griffith, G.W.; Forster, R.; Tsang, A.; et al. Anaerobic fungi (phylum Neocallimastigomycota): advances in understanding their taxonomy, life cycle, ecology, role and biotechnological potential. *FEMS Microbiol Ecol* **2014**, *90*, 1-17, doi:10.1111/1574-6941.12383.
23. Hanafy, R.A.; Dagar, S.S.; Griffith, G.W.; Pratt, C.J.; Youssef, N.H.; Elshahed, M.S. Taxonomy of the anaerobic gut fungi (*Neocallimastigomycota*): a review of classification criteria and description of current taxa. *Int J Syst Evol Microbiol* **2022**, *72*, doi:10.1099/ijsem.0.005322.
24. Meili, C.H.; Jones, A.L.; Arreola, A.X.; Habel, J.; Pratt, C.J.; Hanafy, R.A.; Wang, Y.; Yassin, A.S.; TagElDein, M.A.; Moon, C.D.; et al. Patterns and determinants of the global herbivorous mycobiome. *Nat Commun* **2023**, *14*, 3798, doi:10.1038/s41467-023-39508-z.
25. Marvin-Sikkema, F.D.; Richardson, A.J.; Stewart, C.S.; Gottschal, J.C.; Prins, R.A. Influence of hydrogen-consuming bacteria on cellulose degradation by anaerobic fungi. *Appl Environ Microbiol* **1990**, *56*, 3793-3797, doi:10.1128/aem.56.12.3793-3797.1990.
26. Haitjema, C.H.; Gilmore, S.P.; Henske, J.K.; Solomon, K.V.; de Groot, R.; Kuo, A.; Mondo, S.J.; Salamov, A.A.; LaButti, K.; Zhao, Z.; et al. A parts list for fungal cellulosomes revealed by comparative genomics. *Nat Microbiol* **2017**, *2*, 17087, doi:10.1038/nmicrobiol.2017.87.
27. Lillington, S.P.; Chrisler, W.; Haitjema, C.H.; Gilmore, S.P.; Smallwood, C.R.; Shutthanandan, V.; Evans, J.E.; O'Malley, M.A. Cellulosome Localization Patterns Vary across Life Stages of Anaerobic Fungi. *mBio* **2021**, *12*, e0083221, doi:10.1128/mBio.00832-21.
28. Solomon, K.V.; Haitjema, C.H.; Henske, J.K.; Gilmore, S.P.; Borges-Rivera, D.; Lipzen, A.; Brewer, H.M.; Purvine, S.O.; Wright, A.T.; Theodorou, M.K.; et al. Early-branching gut fungi possess a large, comprehensive array of biomass-degrading enzymes. *Science* **2016**, *351*, 1192-1195, doi:10.1126/science.aad1431.
29. Good, N.E.; Winget, G.D.; Winter, W.; Connolly, T.N.; Izawa, S.; Singh, R.M. Hydrogen ion buffers for biological research. *Biochemistry* **1966**, *5*, 467-477, doi:10.1021/bi00866a011.
30. Papanikolaou, S.; Aggelis, G. Lipids of oleaginous yeasts. Part I: Biochemistry of single cell oil production. *European Journal of Lipid Science and Technology* **2011**, *113*, 1031-1051, doi:10.1002/ejlt.201100014.
31. Athenaki, M.; Gardeli, C.; Diamantopoulou, P.; Tchakouteu, S.S.; Sarris, D.; Philippoussis, A.; Papanikolaou, S. Lipids from yeasts and fungi: physiology, production and analytical considerations. *J Appl Microbiol* **2018**, *124*, 336-367, doi:10.1111/jam.13633.
32. Ageitos, J.M.; Vallejo, J.A.; Veiga-Crespo, P.; Villa, T.G. Oily yeasts as oleaginous cell factories. *Appl Microbiol Biotechnol* **2011**, *90*, 1219-1227, doi:10.1007/s00253-011-3200-z.
33. Salvador Lopez, J.M.; Vandeputte, M.; Van Bogaert, I.N.A. Oleaginous yeasts: Time to rethink the definition? *Yeast* **2022**, *39*, 553-606, doi:10.1002/yea.3827.

34. Abeln, F.; Chuck, C.J. The history, state of the art and future prospects for oleaginous yeast research. *Microbial Cell Factories* **2021**, *20*, doi:10.1186/s12934-021-01712-1.
35. Di Fidio, N.; Minonne, F.; Antonetti, C.; Raspolli Galletti, A.M. *Cutaneotrichosporon oleaginosus*: A Versatile Whole-Cell Biocatalyst for the Production of Single-Cell Oil from Agro-Industrial Wastes. *Catalysts* **2021**, *11*, doi:10.3390/catal11111291.
36. Awad, D.; Bohnen, F.; Mehlmer, N.; Brueck, T. Multi-Factorial-Guided Media Optimization for Enhanced Biomass and Lipid Formation by the Oleaginous Yeast *Cutaneotrichosporon oleaginosus*. *Front Bioeng Biotechnol* **2019**, *7*, 54, doi:10.3389/fbioe.2019.00054.
37. Morales-Palomo, S.; Tomas-Pejo, E.; Gonzalez-Fernandez, C. Phosphate limitation as crucial factor to enhance yeast lipid production from short-chain fatty acids. *Microb Biotechnol* **2023**, *16*, 372-380, doi:10.1111/1751-7915.14197.
38. Vitousek, P.M.; Porder, S.; Houlton, B.Z.; Chadwick, O.A. Terrestrial phosphorus limitation: mechanisms, implications, and nitrogen-phosphorus interactions. *Ecol Appl* **2010**, *20*, 5-15, doi:10.1890/08-0127.1.
39. Elser, J.J. Phosphorus: a limiting nutrient for humanity? *Curr Opin Biotechnol* **2012**, *23*, 833-838, doi:10.1016/j.copbio.2012.03.001.
40. Wang, Y.; Zhang, S.; Zhu, Z.; Shen, H.; Lin, X.; Jin, X.; Jiao, X.; Zhao, Z.K. Systems analysis of phosphate-limitation-induced lipid accumulation by the oleaginous yeast *Rhodosporidium toruloides*. *Biotechnol Biofuels* **2018**, *11*, 148, doi:10.1186/s13068-018-1134-8.
41. Passoth, V.; Brandenburg, J.; Chmielarz, M.; Martin-Hernandez, G.C.; Nagaraj, Y.; Muller, B.; Blomqvist, J. Oleaginous yeasts for biochemicals, biofuels and food from lignocellulose-hydrolysate and crude glycerol. *Yeast* **2023**, *40*, 290-302, doi:10.1002/yea.3838.
42. Schulz, K.E.; Hegmann, P.; Dreher, B.; Schreidl, M.; Ochsenreither, K.; Neumann, A. Adapted Feeding Strategies Enable Efficient Growth and Lipid Accumulation Using Untreated Crude Glycerol in Transition Scale with *Cutaneotrichosporon oleaginosum* ATCC 20509. *Fermentation* **2026**, *12*, doi:10.3390/fermentation12030154.
43. Klein, M.; Swinnen, S.; Thevelein, J.M.; Nevoigt, E. Glycerol metabolism and transport in yeast and fungi: established knowledge and ambiguities. *Environ Microbiol* **2017**, *19*, 878-893, doi:10.1111/1462-2920.13617.
44. Signori, L.; Ami, D.; Posteri, R.; Giuzzi, A.; Mereghetti, P.; Porro, D.; Branduardi, P. Assessing an effective feeding strategy to optimize crude glycerol utilization as sustainable carbon source for lipid accumulation in oleaginous yeasts. *Microb Cell Fact* **2016**, *15*, 75, doi:10.1186/s12934-016-0467-x.
45. Hirasawa, T.; Maeda, T. Adaptive Laboratory Evolution of Microorganisms: Methodology and Application for Bioproduction. *Microorganisms* **2022**, *11*, doi:10.3390/microorganisms11010092.
46. Zoheir, A.E.; Stolle, C.; Rabe, K.S. Microfluidics for adaptation of microorganisms to stress: design and application. *Appl Microbiol Biotechnol* **2024**, *108*, 162, doi:10.1007/s00253-024-13011-x.
47. Sitepu, I.; Selby, T.; Lin, T.; Zhu, S.; Boundy-Mills, K. Carbon source utilization and inhibitor tolerance of 45 oleaginous yeast species. *J Ind Microbiol Biotechnol* **2014**, *41*, 1061-1070, doi:10.1007/s10295-014-1447-y.
48. Huang, C.; Wu, H.; Liu, Z.J.; Cai, J.; Lou, W.Y.; Zong, M.H. Effect of organic acids on the growth and lipid accumulation of oleaginous yeast *Trichosporon fermentans*. *Biotechnol Biofuels* **2012**, *5*, 4, doi:10.1186/1754-6834-5-4.
49. Lyu, Q.; Dar, R.A.; Baganz, F.; Smoliński, A.; Rasmey, A.-H.M.; Liu, R.; Zhang, L. Effects of Lignocellulosic Biomass-Derived Hydrolysate Inhibitors on Cell Growth and Lipid Production During Microbial Fermentation of Oleaginous Microorganisms—A Review. *Fermentation* **2025**, *11*, doi:10.3390/fermentation11030121.
50. Declerck, L.; Bouchon, F.; Demeester, W.; Guidi, C.; De Mey, M. Accelerated adaptive laboratory evolution: A tool for evolutionary biotechnology. *Biotechnol Adv* **2026**, *86*, 108741, doi:10.1016/j.biotechadv.2025.108741.

51. Wang, G.; Li, Q.; Zhang, Z.; Yin, X.; Wang, B.; Yang, X. Recent progress in adaptive laboratory evolution of industrial microorganisms. *J Ind Microbiol Biotechnol* **2023**, *50*, doi:10.1093/jimb/kuac023.
52. Maza, D.D.; Barros, J.M.; Guillamón, J.M.; Aybar, M.J.; Viñarta, S.C. Valorization of Sugarcane Vinasse and Crude Glycerol for Single-Cell Oils Production by *Rhodotorula glutinis* R4: A Preliminary Approach to the Integration of Biofuels Industries for Sustainable Biodiesel Feedstock. *Fermentation* **2024**, *10*, doi:10.3390/fermentation10040178.
53. Petricevic, O.; Teece, D.J. The structural reshaping of globalization: Implications for strategic sectors, profiting from innovation, and the multinational enterprise. *Journal of International Business Studies* **2019**, *50*, 1487-1512, doi:10.1057/s41267-019-00269-x.
54. Abel, G.J.; Barakat, B.; Kc, S.; Lutz, W. Meeting the Sustainable Development Goals leads to lower world population growth. *Proc Natl Acad Sci U S A* **2016**, *113*, 14294-14299, doi:10.1073/pnas.1611386113.
55. Yang, M.; Chen, L.; Wang, J.; Msigwa, G.; Osman, A.I.; Fawzy, S.; Rooney, D.W.; Yap, P.-S. Circular economy strategies for combating climate change and other environmental issues. *Environmental Chemistry Letters* **2022**, *21*, 55-80, doi:10.1007/s10311-022-01499-6.
56. De Guzman, R.; Schiller, J. Air pollution and its impact on cancer incidence, cancer care and cancer outcomes. *BMJ Oncol* **2025**, *4*, e000535, doi:10.1136/bmjonc-2024-000535.
57. Wu, Z.; Prakash, B.; Shi, Y. Synthesizing lignin-based gelators to prepare oleogels used as green and fossil-free greases. *Int J Biol Macromol* **2025**, *305*, 141074, doi:10.1016/j.ijbiomac.2025.141074.
58. Ringseis, R.; Eder, K. Up to date evidence about the suitability of filamentous fungi as a feed source for broilers. *Arch Anim Nutr* **2025**, *79*, 73-94, doi:10.1080/1745039X.2025.2495619.
59. Balchandani, S.; Gracida-Alvarez, U.R.; Hawkins, T.R.; Benavides, P.T. Greenhouse Gas Emissions Associated with Pretreatment Techniques Utilized for Biosugar Production. *ACS Sustain Chem Eng* **2025**, *13*, 7469-7480, doi:10.1021/acssuschemeng.5c00873.
60. Ho, Y.W.; Abdullah, N.; Jalaludin, S. Penetrating Structures of Anaerobic Rumen Fungi in Cattle and Swamp Buffalo. *Microbiology* **1988**, *134*, 177-181, doi:10.1099/00221287-134-1-177.
61. Jin, W.; Cheng, Y.F.; Mao, S.Y.; Zhu, W.Y. Isolation of natural cultures of anaerobic fungi and indigenously associated methanogens from herbivores and their bioconversion of lignocellulosic materials to methane. *Bioresour Technol* **2011**, *102*, 7925-7931, doi:10.1016/j.biortech.2011.06.026.
62. Hsin, K.T.; Lee, H.; Huang, Y.C.; Lin, G.J.; Lin, P.Y.; Lin, Y.J.; Chen, P.Y. Lignocellulose degradation in bacteria and fungi: cellulosomes and industrial relevance. *Front Microbiol* **2025**, *16*, 1583746, doi:10.3389/fmicb.2025.1583746.
63. Krauss, J.; Zverlov, V.V.; Schwarz, W.H. In vitro reconstitution of the complete *Clostridium thermocellum* cellulosome and synergistic activity on crystalline cellulose. *Appl Environ Microbiol* **2012**, *78*, 4301-4307, doi:10.1128/AEM.07959-11.
64. Hibbett, D.S.; Binder, M.; Bischoff, J.F.; Blackwell, M.; Cannon, P.F.; Eriksson, O.E.; Huhndorf, S.; James, T.; Kirk, P.M.; Lucking, R.; et al. A higher-level phylogenetic classification of the Fungi. *Mycol Res* **2007**, *111*, 509-547, doi:10.1016/j.mycres.2007.03.004.
65. Orpin, C.G. The occurrence of chitin in the cell walls of the rumen organisms *Neocallimastix frontalis*, *Piromonas communis* and *Sphaeromonas communis*. *J Gen Microbiol* **1977**, *99*, 215-218, doi:10.1099/00221287-99-1-215.
66. Omondi, V.O.; Bosire, G.O.; Onyari, J.M.; Kibet, C.; Mwasya, S.; Onyonyi, V.N.; Getahun, M.N. Multi-omics analyses reveal rumen microbes and secondary metabolites that are unique to livestock species. *mSystems* **2024**, *9*, e0122823, doi:10.1128/msystems.01228-23.
67. Cheng, Y.F.; Jin, W.; Mao, S.Y.; Zhu, W.Y. Production of Citrate by Anaerobic Fungi in the Presence of Co-culture Methanogens as Revealed by (1)H NMR Spectrometry. *Asian-Australas J Anim Sci* **2013**, *26*, 1416-1423, doi:10.5713/ajas.2013.13134.

68. Kwon, M.; Song, J.; Ha, J.K.; Park, H.-S.; Chang, J. Analysis of Functional Genes in Carbohydrate Metabolic Pathway of Anaerobic Rumen Fungus *Neocallimastix frontalis* PMA02. *Asian-Australasian Journal of Animal Sciences* **2009**, *22*, 1555-1565, doi:10.5713/ajas.2009.80371.
69. Wilken, S.E.; Monk, J.M.; Leggieri, P.A.; Lawson, C.E.; Lankiewicz, T.S.; Seppala, S.; Daum, C.G.; Jenkins, J.; Lipzen, A.M.; Mondo, S.J.; et al. Experimentally Validated Reconstruction and Analysis of a Genome-Scale Metabolic Model of an Anaerobic *Neocallimastigomycota* Fungus. *mSystems* **2021**, *6*, doi:10.1128/mSystems.00002-21.
70. Boxma, B.; Voncken, F.; Jannink, S.; van Alen, T.; Akhmanova, A.; van Weelden, S.W.; van Hellemond, J.J.; Ricard, G.; Huynen, M.; Tielens, A.G.; et al. The anaerobic chytridiomycete fungus *Piromyces sp.* E2 produces ethanol via pyruvate:formate lyase and an alcohol dehydrogenase E. *Mol Microbiol* **2004**, *51*, 1389-1399, doi:10.1046/j.1365-2958.2003.03912.x.
71. Stabel, M.; Schweitzer, T.; Haack, K.; Gorenflo, P.; Aliyu, H.; Ochsenreither, K. Isolation and Biochemical Characterization of Six Anaerobic Fungal Strains from Zoo Animal Feces. *Microorganisms* **2021**, *9*, doi:10.3390/microorganisms9081655.
72. McLeod, M.J.; Barwell, S.A.E.; Holyoak, T.; Thorne, R.E. A structural perspective on the temperature dependent activity of enzymes. *Structure* **2025**, *33*, 924-934 e922, doi:10.1016/j.str.2025.02.013.
73. Matsushita, K.; Azuma, Y.; Kosaka, T.; Yakushi, T.; Hoshida, H.; Akada, R.; Yamada, M. Genomic analyses of thermotolerant microorganisms used for high-temperature fermentations. *Biosci Biotechnol Biochem* **2016**, *80*, 655-668, doi:10.1080/09168451.2015.1104235.
74. Chen, Y.J.; Shi, R.C.; Xiang, Y.C.; Fan, L.; Tang, H.; He, G.; Zhou, M.; Feng, X.Z.; Tan, J.D.; Huang, P.; et al. Malate initiates a proton-sensing pathway essential for pH regulation of inflammation. *Signal Transduct Target Ther* **2024**, *9*, 367, doi:10.1038/s41392-024-02076-9.
75. Zhao, Y.; Luo, L.; Xu, J.; Xin, P.; Guo, H.; Wu, J.; Bai, L.; Wang, G.; Chu, J.; Zuo, J.; et al. Malate transported from chloroplast to mitochondrion triggers production of ROS and PCD in *Arabidopsis thaliana*. *Cell Res* **2018**, *28*, 448-461, doi:10.1038/s41422-018-0024-8.
76. Pasalari, H.; Gharibi, H.; Darvishali, S.; Farzadkia, M. The effects of different pretreatment technologies on microbial community in anaerobic digestion process: A systematic review. *J Environ Health Sci Eng* **2024**, *22*, 439-453, doi:10.1007/s40201-024-00917-x.
77. Yang, Z.; Zhu, Q.; Zhang, Y.; Jiang, P.; Wang, Y.; Fei, J.; Rong, X.; Peng, J.; Wei, X.; Luo, G. Soil carbon storage and accessibility drive microbial carbon use efficiency by regulating microbial diversity and key taxa in intercropping ecosystems. *Biology and Fertility of Soils* **2024**, *60*, 437-453, doi:10.1007/s00374-024-01804-1.
78. Yaseen, M.; Ahmad, T.; Sablok, G.; Standardi, A.; Hafiz, I.A. Review: role of carbon sources for in vitro plant growth and development. *Mol Biol Rep* **2013**, *40*, 2837-2849, doi:10.1007/s11033-012-2299-z.
79. Schoemaker, H.E.; Mink, D.; Wubbolts, M.G. Dispelling the myths--biocatalysis in industrial synthesis. *Science* **2003**, *299*, 1694-1697, doi:10.1126/science.1079237.
80. Battjes, J.; Grigaitis, P.; Hoving, M.; Visser, T.D.; Stampfl, K.; Miguel, G.A.; van Heerden, J.; Andersen, J.K.; Bruggeman, F.J.; Teusink, B. Mitochondrial efficiency determines Crabtree effect across yeasts. *bioRxiv* **2024**, doi:10.1101/2024.11.01.621473.
81. Nguyen, D.V.; Nguyen, H.T.N. High Carboxyl Content Cellulose Nanofibers from Banana Peel via One-Pot Nitro-Oxidative Fabrication. *Revue des composites et des matériaux avancés* **2023**, *33*, 127-133, doi:10.18280/rcma.330208.
82. Kalogiannis, A.; Diamantis, V.; Eftaxias, A.; Stamatelatou, K. Long-Term Anaerobic Digestion of Seasonal Fruit and Vegetable Waste Using a Leach-Bed Reactor Coupled to an Upflow Anaerobic Sludge Bed Reactor. *Sustainability* **2023**, *16*, doi:10.3390/su16010050.
83. Czubaszek, R.; Wysocka-Czubaszek, A. Anaerobic Co-Digestion of Common Reed and Plant-Based Biowaste from Households. *Energies* **2025**, *18*, doi:10.3390/en18092178.
84. Hernandez-Hosaka, C.; Park, B.R.; Zhao, Y.; Jung, J. Effect of pretreatment and peracetic acid pulping on cellulosic materials converted from spent coffee grounds. *J Food Sci* **2024**, *89*, 9407-9419, doi:10.1111/1750-3841.17416.

85. Lovley, D.R. Electromicrobiology. *Annu Rev Microbiol* **2012**, *66*, 391-409, doi:10.1146/annurev-micro-092611-150104.
86. Marques, H.M. Electron transfer in biological systems. *J Biol Inorg Chem* **2024**, *29*, 641-683, doi:10.1007/s00775-024-02076-8.
87. Shi, L.; Dong, H.; Reguera, G.; Beyenal, H.; Lu, A.; Liu, J.; Yu, H.Q.; Fredrickson, J.K. Extracellular electron transfer mechanisms between microorganisms and minerals. *Nat Rev Microbiol* **2016**, *14*, 651-662, doi:10.1038/nrmicro.2016.93.
88. Stevens, E.; Marco, M.L. Bacterial extracellular electron transfer in plant and animal ecosystems. *FEMS Microbiol Rev* **2023**, *47*, doi:10.1093/femsre/fuad019.
89. Sydow, A.; Krieg, T.; Mayer, F.; Schrader, J.; Holtmann, D. Electroactive bacteria--molecular mechanisms and genetic tools. *Appl Microbiol Biotechnol* **2014**, *98*, 8481-8495, doi:10.1007/s00253-014-6005-z.
90. Niman, C.M.; Sukenik, N.; Dang, T.; Nwachukwu, J.; Thirumurthy, M.A.; Jones, A.K.; Naaman, R.; Santra, K.; Das, T.K.; Paltiel, Y.; et al. Bacterial extracellular electron transfer components are spin selective. *J Chem Phys* **2023**, *159*, doi:10.1063/5.0154211.
91. Kamra, D.N.S., B. . Anaerobic Gut Fungi. In *Developments in Fungal Biology and Applied Mycology*; 2017; pp. 125-134.
92. Kovacs, E.; Szucs, C.; Juhasz-Erdelyi, A.; Bagi, Z.; Kovacs, K.L. Anaerobic fungi: effective warriors in lignocellulosic biomass degradation and fermentation. *FEMS Microbiol Ecol* **2025**, *101*, doi:10.1093/femsec/fiaf108.
93. Saye, L.M.G.; Navaratna, T.A.; Chong, J.P.J.; O'Malley, M.A.; Theodorou, M.K.; Reilly, M. The Anaerobic Fungi: Challenges and Opportunities for Industrial Lignocellulosic Biofuel Production. *Microorganisms* **2021**, *9*, doi:10.3390/microorganisms9040694.
94. Gemünde, A.; Gail, J.; Holtmann, D. Redox mediator interaction with *Cupriavidus necator* – spectroelectrochemical online analysis. *Electrochemistry Communications* **2024**, *162*, doi:10.1016/j.elecom.2024.107705.
95. Gemünde, A.; Gail, J.; Janek, J.; Holtmann, D. e-Cuvettes parallelize electrochemical and photometric measurements in cuvettes and facilitate applications in bio-electrochemistry. *Biosensors and Bioelectronics: X* **2023**, *14*, doi:10.1016/j.biosx.2023.100378.
96. Hansen, E.B. Redox reactions in food fermentations. *Current Opinion in Food Science* **2018**, *19*, 98-103, doi:10.1016/j.cofs.2018.03.004.
97. Butkovich, L.V.; Swift, C.L.; Clendinen, C.S.; Olson, H.M.; Purvine, S.O.; Vining, O.B.; O'Malley, M.A. Untargeted GC-MS Metabolic Profiling of Anaerobic Gut Fungi Reveals Putative Terpenoids and Strain-Specific Metabolites. *Metabolites* **2025**, *15*, doi:10.3390/metabo15090578.
98. Swift, C.L.; Louie, K.B.; Bowen, B.P.; Olson, H.M.; Purvine, S.O.; Salamov, A.; Mondo, S.J.; Solomon, K.V.; Wright, A.T.; Northen, T.R.; et al. Anaerobic gut fungi are an untapped reservoir of natural products. *Proc Natl Acad Sci U S A* **2021**, *118*, doi:10.1073/pnas.2019855118.
99. Çakir, S.; Arslan, E. Voltammetry of resazurin at a mercury electrode. *Chemical Papers* **2010**, *64*, doi:10.2478/s11696-010-0007-9.
100. Rabanal-Sanchez, J.; Santiago-Contreras, J. Effects of pH on electrochemical and electronic behaviors of resazurin and initial evaluation of a new square wave voltammetry-based method for bacterial quantification. *Monatshefte für Chemie - Chemical Monthly* **2025**, *157*, 61-72, doi:10.1007/s00706-025-03418-1.
101. Kumara Behera, B.V., A. Material-Balance Calculation of Fermentation Processes. In *Microbial Biomass Process Technologies and Management*; 2017; pp. 257-298.
102. Gizewski, J.K., T.; Dallmann, L.; Li, M.; Holtmann, D. . *Cupriavidus necator* as flexible platform organism for trehalose production. **2025**, doi:10.21203/rs.3.rs-7630680/v1.
103. Gemünde, A.; Ruppert, N.L.; Holtmann, D. Unraveling the Electron Transfer in *Cupriavidus necator* – Insights Into Mediator Reduction Mechanics. *ChemElectroChem* **2024**, *11*, doi:10.1002/celc.202400273.

104. Pratt, C.J.; Meili, C.H.; Jones, A.L.; Jackson, D.K.; England, E.E.; Wang, Y.; Hartson, S.; Rogers, J.; Elshahed, M.S.; Youssef, N.H. Anaerobic fungi in the tortoise alimentary tract illuminate early stages of host-fungal symbiosis and Neocallimastigomycota evolution. *Nat Commun* **2024**, *15*, 2714, doi:10.1038/s41467-024-47047-4.
105. Akin, D.E.; Borneman, W.S. Role of rumen fungi in fiber degradation. *J Dairy Sci* **1990**, *73*, 3023-3032, doi:10.3168/jds.S0022-0302(90)78989-8.
106. Miller, T.L.; Wolin, M.J. A Serum Bottle Modification of the Hungate Technique for Cultivating Obligate Anaerobes. *Applied Microbiology* **1974**, *27*, 985-987, doi:10.1128/am.27.5.985-987.1974.
107. Rees, E.M.R.; Lloyd, D.; Williams, A.G. The effects of differing concentrations of CO2 and O2 on the fermentative metabolism of the rumen fungi Neocallimastix patriciarum and Neocallimastix frontalis L2. *Canadian Journal of Microbiology* **1998**, *44*, 819-824, doi:10.1139/w98-080.
108. Leggieri, P.A.; Kerdman-Andrade, C.; Lankiewicz, T.S.; Valentine, M.T.; O'Malley, M.A. Non-destructive quantification of anaerobic gut fungi and methanogens in co-culture reveals increased fungal growth rate and changes in metabolic flux relative to mono-culture. *Microb Cell Fact* **2021**, *20*, 199, doi:10.1186/s12934-021-01684-2.
109. Mountfort, D.O.; Asher, R.A.; Bauchop, T. Fermentation of Cellulose to Methane and Carbon Dioxide by a Rumen Anaerobic Fungus in a Triculture with Methanobrevibacter sp. Strain RA1 and Methanosarcina barkeri. *Appl Environ Microbiol* **1982**, *44*, 128-134, doi:10.1128/aem.44.1.128-134.1982.
110. Mountfort, D.O.; Asher, R.A. Production and regulation of cellulase by two strains of the rumen anaerobic fungus Neocallimastix frontalis. *Appl Environ Microbiol* **1985**, *49*, 1314-1322, doi:10.1128/aem.49.5.1314-1322.1985.
111. Schulte-Schulze-Berndt, A.; Krabiell, K. Nitrogen generation by pressure swing adsorption based on carbon molecular sieves. *Gas Separation & Purification* **1993**, *7*, 253-257, doi:10.1016/0950-4214(93)80026-s.
112. Marcinek, A.; Guderian, J.; Bathen, D. Process intensification of the high-purity nitrogen production in twin-bed Pressure Swing Adsorption plants. *Adsorption* **2021**, *27*, 937-952, doi:10.1007/s10450-020-00291-8.
113. Bozorg, M.; Addis, B.; Piccialli, V.; Ramírez-Santos, Á.A.; Castel, C.; Pinnau, I.; Favre, E. Polymeric membrane materials for nitrogen production from air: A process synthesis study. *Chemical Engineering Science* **2019**, *207*, 1196-1213, doi:10.1016/j.ces.2019.07.029.
114. Kruger, A.; Wiechert, J.; Gatgens, C.; Polen, T.; Mahr, R.; Frunzke, J. Impact of CO(2)/HCO(3)(-) Availability on Anaplerotic Flux in Pyruvate Dehydrogenase Complex-Deficient Corynebacterium glutamicum Strains. *J Bacteriol* **2019**, *201*, doi:10.1128/JB.00387-19.
115. Zhu, L.W.; Zhang, L.; Wei, L.N.; Li, H.M.; Yuan, Z.P.; Chen, T.; Tang, Y.L.; Liang, X.H.; Tang, Y.J. Collaborative regulation of CO2 transport and fixation during succinate production in Escherichia coli. *Sci Rep* **2015**, *5*, 17321, doi:10.1038/srep17321.
116. Orpin, C.G. Studies on the rumen flagellate Neocallimastix frontalis. *J Gen Microbiol* **1975**, *91*, 249-262, doi:10.1099/00221287-91-2-249.
117. Verhaart, M.R.; Bielen, A.A.; van der Oost, J.; Stams, A.J.; Kengen, S.W. Hydrogen production by hyperthermophilic and extremely thermophilic bacteria and archaea: mechanisms for reductant disposal. *Environ Technol* **2010**, *31*, 993-1003, doi:10.1080/09593331003710244.
118. Bauchop, T.; Mountfort, D.O. Cellulose fermentation by a rumen anaerobic fungus in both the absence and the presence of rumen methanogens. *Appl Environ Microbiol* **1981**, *42*, 1103-1110, doi:10.1128/aem.42.6.1103-1110.1981.
119. Teunissen, M.J.; Kets, E.P.; Op den Camp, H.J.; Huis in't Veld, J.H.; Vogels, G.D. Effect of coculture of anaerobic fungi isolated from ruminants and non-ruminants with methanogenic bacteria on cellulolytic and xylanolytic enzyme activities. *Arch Microbiol* **1992**, *157*, 176-182, doi:10.1007/BF00245287.

120. Li, Y.; Sun, M.; Li, Y.; Cheng, Y.; Zhu, W. Co-cultured methanogen improved the metabolism in the hydrogenosome of anaerobic fungus as revealed by gas chromatography-mass spectrometry analysis. *Asian-Australas J Anim Sci* **2020**, *33*, 1948-1956, doi:10.5713/ajas.19.0649.
121. Elleuche, S.; Poggeler, S. Carbonic anhydrases in fungi. *Microbiology (Reading)* **2010**, *156*, 23-29, doi:10.1099/mic.0.032581-0.
122. Martin, R.; Pohlers, S.; Muhlschlegel, F.A.; Kurzai, O. CO(2) sensing in fungi: at the heart of metabolic signaling. *Curr Genet* **2017**, *63*, 965-972, doi:10.1007/s00294-017-0700-0.
123. Klengel, T.; Liang, W.J.; Chaloupka, J.; Ruoff, C.; Schroppel, K.; Naglik, J.R.; Eckert, S.E.; Mogensen, E.G.; Haynes, K.; Tuite, M.F.; et al. Fungal adenylyl cyclase integrates CO2 sensing with cAMP signaling and virulence. *Curr Biol* **2005**, *15*, 2021-2026, doi:10.1016/j.cub.2005.10.040.
124. Mogensen, E.G.; Janbon, G.; Chaloupka, J.; Steegborn, C.; Fu, M.S.; Moyrand, F.; Klengel, T.; Pearson, D.S.; Geeves, M.A.; Buck, J.; et al. Cryptococcus neoformans senses CO2 through the carbonic anhydrase Can2 and the adenylyl cyclase Cac1. *Eukaryot Cell* **2006**, *5*, 103-111, doi:10.1128/EC.5.1.103-111.2006.
125. McNamara, D.P.; Whitney, K.M.; Goss, S.L. Use of a physiologic bicarbonate buffer system for dissolution characterization of ionizable drugs. *Pharm Res* **2003**, *20*, 1641-1646, doi:10.1023/a:1026147620304.
126. Krieg, B.J.; Taghavi, S.M.; Amidon, G.L.; Amidon, G.E. In vivo predictive dissolution: transport analysis of the CO2 , bicarbonate in vivo buffer system. *J Pharm Sci* **2014**, *103*, 3473-3490, doi:10.1002/jps.24108.
127. Michl, J.; Park, K.C.; Swietach, P. Evidence-based guidelines for controlling pH in mammalian live-cell culture systems. *Commun Biol* **2019**, *2*, 144, doi:10.1038/s42003-019-0393-7.
128. Youssef, N.H.; Couger, M.B.; Struchtemeyer, C.G.; Liggenstoffer, A.S.; Prade, R.A.; Najar, F.Z.; Atiyeh, H.K.; Wilkins, M.R.; Elshahed, M.S. The genome of the anaerobic fungus Orpinomyces sp. strain C1A reveals the unique evolutionary history of a remarkable plant biomass degrader. *Appl Environ Microbiol* **2013**, *79*, 4620-4634, doi:10.1128/AEM.00821-13.
129. Ullah, A.; Orij, R.; Brul, S.; Smits, G.J. Quantitative analysis of the modes of growth inhibition by weak organic acids in Saccharomyces cerevisiae. *Appl Environ Microbiol* **2012**, *78*, 8377-8387, doi:10.1128/AEM.02126-12.
130. Carmelo, V.; Santos, H.; Sa-Correia, I. Effect of extracellular acidification on the activity of plasma membrane ATPase and on the cytosolic and vacuolar pH of Saccharomyces cerevisiae. *Biochim Biophys Acta* **1997**, *1325*, 63-70, doi:10.1016/s0005-2736(96)00245-3.
131. Mollapour, M.; Phelan, J.P.; Millson, S.H.; Piper, P.W.; Cooke, F.T. Weak acid and alkali stress regulate phosphatidylinositol bisphosphate synthesis in Saccharomyces cerevisiae. *Biochem J* **2006**, *395*, 73-80, doi:10.1042/BJ20051765.
132. Unden, G.; Bongaerts, J. Alternative respiratory pathways of Escherichia coli: energetics and transcriptional regulation in response to electron acceptors. *Biochim Biophys Acta* **1997**, *1320*, 217-234, doi:10.1016/s0005-2728(97)00034-0.
133. Kruger, A.; Geisler, V.; Lemma, E.; Theis, F.; Lenger, R. Bacterial fumarate respiration. *Archives of Microbiology* **1992**, *158*, 311-314, doi:10.1007/bf00245358.
134. Crow, V.L.; Pritchard, G.G. Purification and properties of pyruvate kinase from Streptococcus lactis. *Biochim Biophys Acta* **1976**, *438*, 90-101, doi:10.1016/0005-2744(76)90225-4.
135. Otsuka, K.i. Cis-trans Isomerase: Isomerisation from Maleic Acid to Fumaric Acid. . *Agricultural and Biological Chemistry* **1961**, *25*, 726-730, doi:10.1080/00021369.1961.10857869.
136. Nagaraja, T.G.; Lechtenberg, K.F. Acidosis in feedlot cattle. *Vet Clin North Am Food Anim Pract* **2007**, *23*, 333-350, viii-ix, doi:10.1016/j.cvfa.2007.04.002.
137. Leggieri, P.A.; Blair, E.M.; Lankiewicz, T.S.; O'Malley, M.A. Continuous culture of anaerobic fungi enables growth and metabolic flux tuning without use of genetic tools. *Bioresour Technol* **2024**, *391*, 129854, doi:10.1016/j.biortech.2023.129854.

138. Di Lonardo, D.P.; van der Wal, A.; Harkes, P.; de Boer, W. Effect of nitrogen on fungal growth efficiency. *Plant Biosystems - An International Journal Dealing with all Aspects of Plant Biology* **2020**, *154*, 433-437, doi:10.1080/11263504.2020.1779849.
139. Ratledge, C. Fatty acid biosynthesis in microorganisms being used for Single Cell Oil production. *Biochimie* **2004**, *86*, 807-815, doi:10.1016/j.biochi.2004.09.017.
140. Mata, T.M.; Martins, A.A.; Caetano, N.S. Microalgae for biodiesel production and other applications: A review. *Renewable and Sustainable Energy Reviews* **2010**, *14*, 217-232, doi:10.1016/j.rser.2009.07.020.
141. Koreti, D.; Kosre, A.; Jadhav, S.K.; Chandrawanshi, N.K. A comprehensive review on oleaginous bacteria: an alternative source for biodiesel production. *Bioresour Bioprocess* **2022**, *9*, 47, doi:10.1186/s40643-022-00527-1.
142. Gu, D.; Andreev, K.; Dupre, M.E. Major Trends in Population Growth Around the World. *China CDC Wkly* **2021**, *3*, 604-613, doi:10.46234/ccdcw2021.160.
143. Vasudevan, P.T.; Briggs, M. Biodiesel production--current state of the art and challenges. *J Ind Microbiol Biotechnol* **2008**, *35*, 421, doi:10.1007/s10295-008-0312-2.
144. Ward, O.P.; Singh, A. Omega-3/6 fatty acids: Alternative sources of production. *Process Biochemistry* **2005**, *40*, 3627-3652, doi:10.1016/j.procbio.2005.02.020.
145. Xu, J.; Du, W.; Zhao, X.; Liu, D. Renewable microbial lipid production from Oleaginous Yeast: some surfactants greatly improved lipid production of *Rhodosporidium toruloides*. *World J Microbiol Biotechnol* **2016**, *32*, 107, doi:10.1007/s11274-016-2076-6.
146. Liang, M.H.; Jiang, J.G. Advancing oleaginous microorganisms to produce lipid via metabolic engineering technology. *Prog Lipid Res* **2013**, *52*, 395-408, doi:10.1016/j.plipres.2013.05.002.
147. Pérez-Rivero, C.; López-Gómez, J.P. Unlocking the Potential of Fermentation in Cosmetics: A Review. *Fermentation* **2023**, *9*, doi:10.3390/fermentation9050463.
148. Wierzchowska, K.; Roszko, M.; Derewiaka, D.; Szulc, K.; Zieniuk, B.; Nowak, D.; Fabiszewska, A. Yeast lipids as a sustainable source of nutrients in dairy products analogs. *Food Bioscience* **2024**, *62*, doi:10.1016/j.fbio.2024.105321.
149. Kyle, D.J.; Ratledge, C. *Industrial Applications of Single Cell Oils*; 1992.
150. Leesing, R.; Siwina, S.; Ngernyen, Y.; Fiala, K. Innovative approach for co-production of single cell oil (SCO), novel carbon-based solid acid catalyst and SCO-based biodiesel from fallen *Dipterocarpus alatus* leaves. *Renewable Energy* **2022**, *185*, 47-60, doi:10.1016/j.renene.2021.11.120.
151. Khan, N.; Sudhakar, K.; Mamat, R. Role of Biofuels in Energy Transition, Green Economy and Carbon Neutrality. *Sustainability* **2021**, *13*, doi:10.3390/su132212374.
152. Chi, Z.; Zheng, Y.; Ma, J.; Chen, S. Oleaginous yeast *Cryptococcus curvatus* culture with dark fermentation hydrogen production effluent as feedstock for microbial lipid production. *International Journal of Hydrogen Energy* **2011**, *36*, 9542-9550, doi:10.1016/j.ijhydene.2011.04.124.
153. Klug, L.; Daum, G. Yeast lipid metabolism at a glance. *FEMS Yeast Res* **2014**, *14*, 369-388, doi:10.1111/1567-1364.12141.
154. Bao, R.; Wu, X.; Liu, S.; Xie, T.; Yu, C.; Lin, X. Efficient Conversion of Fructose-Based Biomass into Lipids with Trichosporon fermentans Under Phosphate-Limited Conditions. *Appl Biochem Biotechnol* **2018**, *184*, 113-123, doi:10.1007/s12010-017-2536-y.
155. Aziz, M.M.A.; Kassim, K.A.; Shokravi, Z.; Jakarni, F.M.; Liu, H.Y.; Zaini, N.; Tan, L.S.; Islam, A.B.M.S.; Shokravi, H. Two-stage cultivation strategy for simultaneous increases in growth rate and lipid content of microalgae: A review. *Renewable and Sustainable Energy Reviews* **2020**, *119*, doi:10.1016/j.rser.2019.109621.
156. Nasseri, A.T.; Rasoul-Ami, S.; Morowvat, M.H.; Ghasemi, Y. Single Cell Protein: Production and Process. *American Journal of Food Technology* **2011**, *6*, 103-116, doi:10.3923/ajft.2011.103.116.
157. Mordenti, A.L.; Giaretta, E.; Campidonico, L.; Parazza, P.; Formigoni, A. A Review Regarding the Use of Molasses in Animal Nutrition. *Animals (Basel)* **2021**, *11*, doi:10.3390/ani11010115.

158. Tiessen, H. Phosphorus in the global environment. In *The Ecophysiology of Plant-Phosphorus Interactions*; Plant Ecophysiology; 2008; pp. 1-7.
159. Larsen, S. Phosphorus - a limiting factor in future food production. *Netherlands Journal of Agricultural Science* **1974**, *22*, 270-274, doi:10.18174/njas.v22i4.17211.
160. Wu, S.; Hu, C.; Jin, G.; Zhao, X.; Zhao, Z.K. Phosphate-limitation mediated lipid production by *Rhodosporidium toruloides*. *Bioresour Technol* **2010**, *101*, 6124-6129, doi:10.1016/j.biortech.2010.02.111.
161. Maltsev, Y.; Kulikovskiy, M.; Maltseva, S. Nitrogen and phosphorus stress as a tool to induce lipid production in microalgae. *Microb Cell Fact* **2023**, *22*, 239, doi:10.1186/s12934-023-02244-6.
162. Gorte, O.; Kugel, M.; Ochsenreither, K. Optimization of carbon source efficiency for lipid production with the oleaginous yeast *Saitozyma podzolica* DSM 27192 applying automated continuous feeding. *Biotechnol Biofuels* **2020**, *13*, 181, doi:10.1186/s13068-020-01824-7.
163. Gujjari, P.; Suh, S.O.; Coumes, K.; Zhou, J.J. Characterization of oleaginous yeasts revealed two novel species: *Trichosporon cacaoliposimilis sp. nov.* and *Trichosporon oleaginosus sp. nov. Mycologia* **2011**, *103*, 1110-1118, doi:10.3852/10-403.
164. Moon, N.J.; Hammond, E.G.; Glatz, B.A. Conversion of Cheese Whey and Whey Permeate to Oil and Single-Cell Protein. *Journal of Dairy Science* **1978**, *61*, 1537-1547, doi:10.3168/jds.S0022-0302(78)83762-X.
165. Ratledge, C. Biotechnology as Applied to the Oils and Fats Industry. *Fette, Seifen, Anstrichmittel* **2006**, *86*, 379-389, doi:10.1002/lipi.19840861002.
166. Hassan, M.; Blanc, P.J.; Pareilleux, A.; Goma, G. Selection of fatty acid auxotrophs from the oleaginous yeast *Cryptococcus curvatus* and production of cocoa butter equivalents in batch culture. *Biotechnology Letters* **1994**, *16*, 819-824, doi:10.1007/bf00133960.
167. Moreton, R.S. Yeast lipid estimation by enzymatic and nuclear magnetic resonance methods. *Appl Environ Microbiol* **1989**, *55*, 3009-3011, doi:10.1128/aem.55.11.3009-3011.1989.
168. Schulze, I.; Hansen, S.; Grosshans, S.; Rudszuck, T.; Ochsenreither, K.; Syldatk, C.; Neumann, A. Characterization of newly isolated oleaginous yeasts - *Cryptococcus podzolicus*, *Trichosporon porosum* and *Pichia segobiensis*. *AMB Express* **2014**, *4*, 24, doi:10.1186/s13568-014-0024-0.
169. Gorte, O.; Nazarova, N.; Papachristou, I.; Wustner, R.; Leber, K.; Syldatk, C.; Ochsenreither, K.; Frey, W.; Silve, A. Pulsed Electric Field Treatment Promotes Lipid Extraction on Fresh Oleaginous Yeast *Saitozyma podzolica* DSM 27192. *Front Bioeng Biotechnol* **2020**, *8*, 575379, doi:10.3389/fbioe.2020.575379.
170. Qian, X.; Zhou, X.; Chen, L.; Zhang, X.; Xin, F.; Dong, W.; Zhang, W.; Ochsenreither, K.; Jiang, M. Bioconversion of volatile fatty acids into lipids by the oleaginous yeast *Apiotrichum porosum* DSM27194. *Fuel* **2021**, *290*, doi:10.1016/j.fuel.2020.119811.
171. Kourist, R.; Bracharz, F.; Lorenzen, J.; Kracht, O.N.; Chovatia, M.; Daum, C.; Deshpande, S.; Lipzen, A.; Nolan, M.; Ohm, R.A.; et al. Genomics and Transcriptomics Analyses of the Oil-Accumulating Basidiomycete Yeast *Trichosporon oleaginosus*: Insights into Substrate Utilization and Alternative Evolutionary Trajectories of Fungal Mating Systems. *mBio* **2015**, *6*, e00918, doi:10.1128/mBio.00918-15.
172. Aliyu, H.; Gorte, O.; Neumann, A.; Ochsenreither, K. Global Transcriptome Profile of the Oleaginous Yeast *Saitozyma podzolica* DSM 27192 Cultivated in Glucose and Xylose. *J Fungi (Basel)* **2021**, *7*, doi:10.3390/jof7090758.
173. Qian, X.; Lei, H.; Zhou, X.; Zhang, L.; Cui, W.; Zhou, J.; Xin, F.; Dong, W.; Jiang, M.; Ochsenreither, K. Engineering *Scheffersomyces segobiensis* for palmitoleic acid-rich lipid production. *Microb Biotechnol* **2024**, *17*, e14301, doi:10.1111/1751-7915.14301.
174. Beopoulos, A.; Nicaud, J.M.; Gaillardin, C. An overview of lipid metabolism in yeasts and its impact on biotechnological processes. *Appl Microbiol Biotechnol* **2011**, *90*, 1193-1206, doi:10.1007/s00253-011-3212-8.

175. Huang, X.F.; Shen, Y.; Luo, H.J.; Liu, J.N.; Liu, J. Enhancement of extracellular lipid production by oleaginous yeast through preculture and sequencing batch culture strategy with acetic acid. *Bioresour Technol* **2018**, *247*, 395-401, doi:10.1016/j.biortech.2017.09.096.
176. Palmonari, A.; Cavallini, D.; Sniffen, C.J.; Fernandes, L.; Holder, P.; Fagioli, L.; Fusaro, I.; Biagi, G.; Formigoni, A.; Mammi, L. Short communication: Characterization of molasses chemical composition. *J Dairy Sci* **2020**, *103*, 6244-6249, doi:10.3168/jds.2019-17644.
177. Schoeters, F.; Thoré, E.S.J.; De Cuyper, A.; Noyens, I.; Goossens, S.; Lybaert, S.; Meers, E.; Van Miert, S.; de Souza, M.F. Microalgal cultivation on grass juice as a novel process for a green biorefinery. *Algal Research* **2023**, *69*, doi:10.1016/j.algal.2022.102941.
178. Li, Y.-h.; Li, H.-b.; Xu, X.-y.; Xiao, S.-y.; Wang, S.-q.; Xu, S.-c. Fate of nitrogen in subsurface infiltration system for treating secondary effluent. *Water Science and Engineering* **2017**, *10*, 217-224, doi:10.1016/j.wse.2017.10.002.
179. Khan, S.; Das, P.; Thaher, M.I.; AbdulQuadir, M.; Mahata, C.; Al Jabri, H. Utilization of nitrogen-rich agricultural waste streams by microalgae for the production of protein and value-added compounds. *Current Opinion in Green and Sustainable Chemistry* **2023**, *41*, doi:10.1016/j.cogsc.2023.100797.
180. Calin, M.; Raut, I.; Arsene, M.L.; Capra, L.; Gurban, A.M.; Doni, M.; Jecu, L. Applications of Fungal Strains with Keratin-Degrading and Plant Growth Promoting Characteristics. *Agronomy* **2019**, *9*, doi:10.3390/agronomy9090543.
181. Panasiuk, R.; Amarowicz, R.; Kostyra, H.; Sijtsma, L. Determination of α-amino nitrogen in pea protein hydrolysates: a comparison of three analytical methods. *Food Chemistry* **1998**, *62*, 363-367, doi:10.1016/s0308-8146(97)00164-7.
182. Wasserman, A.E. Whey Utilization. IV. Availability of Whey Nitrogen for the Growth of *Saccharomyces Fragilis*. *Journal of Dairy Science* **1960**, *43*, 1231-1234, doi:10.3168/jds.S0022-0302(60)90309-X.
183. Petersen, K.S.; Maki, K.C.; Calder, P.C.; Belury, M.A.; Messina, M.; Kirkpatrick, C.F.; Harris, W.S. Perspective on the health effects of unsaturated fatty acids and commonly consumed plant oils high in unsaturated fat. *Br J Nutr* **2024**, *132*, 1039-1050, doi:10.1017/S0007114524002459.
184. Ratledge, C.; Cohen, Z. Microbial and algal oils: Do they have a future for biodiesel or as commodity oils? *Lipid Technology* **2008**, *20*, 155-160, doi:10.1002/lite.200800044.
185. Ratledge, C.; Wynn, J.P. The biochemistry and molecular biology of lipid accumulation in oleaginous microorganisms. *Adv Appl Microbiol* **2002**, *51*, 1-51, doi:10.1016/s0065-2164(02)51000-5.
186. Masri, M.A.; Garbe, D.; Mehlmer, N.; Brück, T.B. A sustainable, high-performance process for the economic production of waste-free microbial oils that can replace plant-based equivalents. *Energy & Environmental Science* **2019**, *12*, 2717-2732, doi:10.1039/c9ee00210c.
187. Dujon, B.A.; Louis, E.J. Genome Diversity and Evolution in the Budding Yeasts (*Saccharomycotina*). *Genetics* **2017**, *206*, 717-750, doi:10.1534/genetics.116.199216.
188. Bracharz, F.; Beukhout, T.; Mehlmer, N.; Bruck, T. Opportunities and challenges in the development of *Cutaneotrichosporon oleaginosus* ATCC 20509 as a new cell factory for custom tailored microbial oils. *Microb Cell Fact* **2017**, *16*, 178, doi:10.1186/s12934-017-0791-9.
189. Duman-Özdamar, Z.E. Engineering Oleaginous Yeasts for a Bio-Based Future. Wageningen University, 2025.
190. Meesters, P.A.E.P.; Huijberts, G.N.M.; Eggink, G. High-cell-density cultivation of the lipid accumulating yeast *Cryptococcus curvatus* using glycerol as a carbon source. *Applied Microbiology and Biotechnology* **1996**, *45*, 575-579, doi:10.1007/s002530050731.
191. Mhlongo, S.I.; Ezeokoli, O.T.; Roopnarain, A.; Ndaba, B.; Sekoai, P.T.; Habimana, O.; Pohl, C.H. The Potential of Single-Cell Oils Derived From Filamentous Fungi as Alternative Feedstock Sources for Biodiesel Production. *Front Microbiol* **2021**, *12*, 637381, doi:10.3389/fmicb.2021.637381.
192. Uğur, Ş.; Zieniuk, B.; Fabiszewska, A. Nutritional and Medicinal Properties of Microbial Oil. *Applied Sciences* **2024**, *14*, doi:10.3390/app14104232.

193. Chilakamarry, C.R.; Sakinah, A.M.M.; Zularisam, A.W.; Pandey, A. Glycerol waste to value added products and its potential applications. *Syst Microbiol Biomanuf* **2021**, *1*, 378-396, doi:10.1007/s43393-021-00036-w.
194. Awogbemi, O.; Desai, D.A. Recent advances in purification technologies for biodiesel-derived crude glycerol. *International Journal of Ambient Energy* **2025**, *46*, doi:10.1080/01430750.2025.2533373.
195. Abdul Raman, A.A.; Tan, H.W.; Buthiyappan, A. Two-Step Purification of Glycerol as a Value Added by Product From the Biodiesel Production Process. *Front Chem* **2019**, *7*, 774, doi:10.3389/fchem.2019.00774.
196. Liu, Y.; Zhong, B.; Lawal, A. Recovery and utilization of crude glycerol, a biodiesel byproduct. *RSC Adv* **2022**, *12*, 27997-28008, doi:10.1039/d2ra05090k.
197. Elgharbawy, A.S.; Sadik, W.A.; Sadek, O.M.; Kasaby, M.A. A Review on Biodiesel Feedstocks and Production Technologies. *Journal of the Chilean Chemical Society* **2021**, *66*, 5098-5109, doi:10.4067/s0717-97072021000105098.
198. European Biodiesel Board (EBB). *EBB Statistical Report 2023*; European Biodiesel Board (EBB): 2023.
199. Almeida, E.L.; Olivo, J.E.; Andrade, C.M.G. Production of Biofuels from Glycerol from the Biodiesel Production Process—A Brief Review. *Fermentation* **2023**, *9*, doi:10.3390/fermentation9100869.
200. Johnson, D.T.; Taconi, K.A. The glycerin glut: Options for the value-added conversion of crude glycerol resulting from biodiesel production. *Environmental Progress* **2007**, *26*, 338-348, doi:10.1002/ep.10225.
201. Yu, Z.; Chang, Z.; Lu, Y.; Xiao, H. Metabolic engineering of *Saccharomyces cerevisiae* for glycerol utilization. *FEMS Yeast Res* **2023**, *23*, doi:10.1093/femsyr/foad014.
202. Ram, S.; Tyagi, R.; Drogui, P. Effect of Sludge Concentration and Crude Glycerol Matrix as a Substrate on the Production of Single-Cell Oil by Oleaginous Yeast *Yarrowia lipolytica* SKY7. *Fermentation* **2018**, *4*, doi:10.3390/fermentation4020024.
203. Poontawee, R.; Limtong, S. Feeding Strategies of Two-Stage Fed-Batch Cultivation Processes for Microbial Lipid Production from Sugarcane Top Hydrolysate and Crude Glycerol by the Oleaginous Red Yeast *Rhodosporidiobolus fluvialis*. *Microorganisms* **2020**, *8*, doi:10.3390/microorganisms8020151.
204. Karamerou, E.E.; Theodoropoulos, C.; Webb, C. Evaluating feeding strategies for microbial oil production from glycerol by *Rhodotorula glutinis*. *Eng Life Sci* **2017**, *17*, 314-324, doi:10.1002/elsc.201600073.
205. Lowry, O.; Rosebrough, N.; Farr, A.L.; Randall, R. Protein Measurement with the Folin Phenol Reagent. *Journal of Biological Chemistry* **1951**, *193*, 265-275, doi:10.1016/s0021-9258(19)52451-6.
206. Yemm, E.W.; Willis, A.J. The estimation of carbohydrates in plant extracts by anthrone. *Biochem J* **1954**, *57*, 508-514, doi:10.1042/bj0570508.
207. Hidalgo, P.; Toro, C.; Ciudad, G.; Navia, R. Advances in direct transesterification of microalgal biomass for biodiesel production. *Reviews in Environmental Science and Bio/Technology* **2013**, *12*, 179-199, doi:10.1007/s11157-013-9308-0.
208. SolÓRzano, L. Determination of ammonia in natural waters by the phenolhypochlorite method. *Limnology and Oceanography* **2003**, *14*, 799-801, doi:10.4319/lo.1969.14.5.0799.
209. Hartmann, L.; Martin, M.C.; Neumann, A.; Holtmann, D.; Ochsenreither, K. Understanding the Role of pH Regulation and Neutralizing Agents in Organic Acid Production and Growth of *Aspergillus oryzae*. *Biotechnol Bioeng* **2026**, *123*, 116-133, doi:10.1002/bit.70091.
210. Kumar, L.R.; Yellapu, S.K.; Yan, S.; Tyagi, R.D.; Drogui, P. Elucidating the effect of impurities present in different crude glycerol sources on lipid and citric acid production by *Yarrowia lipolytica* SKY7. *Journal of Chemical Technology & Biotechnology* **2020**, *96*, 227-240, doi:10.1002/jctb.6531.

211. Agyeman-Duah, E.; Kumar, S.; Gangwar, B.; Ujor, V.C. Glycerol Utilization as a Sole Carbon Source Disrupts the Membrane Architecture and Solventogenesis in *Clostridium beijerinckii* NCIMB 8052. *Fermentation* **2022**, *8*, doi:10.3390/fermentation8070339.
212. Pham, N.; Reijnders, M.; Suarez-Diez, M.; Nijsse, B.; Springer, J.; Eggink, G.; Schaap, P.J. Genome-scale metabolic modeling underscores the potential of *Cutaneotrichosporon oleaginosus* ATCC 20509 as a cell factory for biofuel production. *Biotechnol Biofuels* **2021**, *14*, 2, doi:10.1186/s13068-020-01838-1.
213. Sara, M.; Brar, S.K.; Blais, J.F. Lipid production by *Yarrowia lipolytica* grown on biodiesel-derived crude glycerol: optimization of growth parameters and their effects on the fermentation efficiency. *RSC Advances* **2016**, *6*, 90547-90558, doi:10.1039/c6ra16382c.
214. Duman-Ozdamar, Z.E.; Martins Dos Santos, V.A.P.; Hugenholtz, J.; Suarez-Diez, M. Tailoring and optimizing fatty acid production by oleaginous yeasts through the systematic exploration of their physiological fitness. *Microb Cell Fact* **2022**, *21*, 228, doi:10.1186/s12934-022-01956-5.
215. Chopra, J.; Sen, R. Process optimization involving critical evaluation of oxygen transfer, oxygen uptake and nitrogen limitation for enhanced biomass and lipid production by oleaginous yeast for biofuel application. *Bioprocess Biosyst Eng* **2018**, *41*, 1103-1113, doi:10.1007/s00449-018-1939-7.
216. Abeln, F.; Chuck, C.J. Achieving a high-density oleaginous yeast culture: Comparison of four processing strategies using *Metschnikowia pulcherrima*. *Biotechnol Bioeng* **2019**, *116*, 3200-3214, doi:10.1002/bit.27141.
217. Bayrock, D.P.; Ingledew, W.M. Inhibition of yeast by lactic acid bacteria in continuous culture: nutrient depletion and/or acid toxicity? *J Ind Microbiol Biotechnol* **2004**, *31*, 362-368, doi:10.1007/s10295-004-0156-3.
218. Donzella, S.; Serra, I.; Fumagalli, A.; Pellegrino, L.; Mosconi, G.; Lo Scalzo, R.; Compagno, C. Recycling industrial food wastes for lipid production by oleaginous yeasts *Rhodosporidiobolus azoricus* and *Cutaneotrichosporon oleaginosum*. *Biotechnol Biofuels Bioprod* **2022**, *15*, 51, doi:10.1186/s13068-022-02149-3.
219. Ratledge, C.; Wynn, J.P. Oils from Microorganisms. In *Bailey's Industrial Oil and Fat Products*; 2020; pp. 1-34.
220. Wan, Z.; Hu, H.; Liu, K.; Qiao, Y.; Guo, F.; Wang, C.; Xin, F.; Zhang, W.; Jiang, M. Engineering industrial yeast for improved tolerance and robustness. *Crit Rev Biotechnol* **2024**, *44*, 1461-1477, doi:10.1080/07388551.2024.2326677.
221. Karras, T.; Thrän, D. The Costs of Straw in Germany: Development of Regional Straw Supply Costs between 2010 and 2020. *Waste and Biomass Valorization* **2024**, *15*, 5369-5385, doi:10.1007/s12649-024-02528-x.
222. Brandenburg, J.; Blomqvist, J.; Shapaval, V.; Kohler, A.; Sampels, S.; Sandgren, M.; Passoth, V. Oleaginous yeasts respond differently to carbon sources present in lignocellulose hydrolysate. *Biotechnol Biofuels* **2021**, *14*, 124, doi:10.1186/s13068-021-01974-2.
223. Chaves, S.R.; Rego, A.; Martins, V.M.; Santos-Pereira, C.; Sousa, M.J.; Corte-Real, M. Regulation of Cell Death Induced by Acetic Acid in Yeasts. *Front Cell Dev Biol* **2021**, *9*, 642375, doi:10.3389/fcell.2021.642375.
224. Pyne, M.E.; Bagley, J.A.; Narcross, L.; Kevvai, K.; Exley, K.; Davies, M.; Wang, Q.; Whiteway, M.; Martin, V.J.J. Screening non-conventional yeasts for acid tolerance and engineering *Pichia occidentalis* for production of muconic acid. *Nat Commun* **2023**, *14*, 5294, doi:10.1038/s41467-023-41064-5.
225. Sahana, G.R.; Balasubramanian, B.; Joseph, K.S.; Pappuswamy, M.; Liu, W.-C.; Meyyazhagan, A.; Kamyab, H.; Chelliapan, S.; Joseph, B.V. A review on ethanol tolerance mechanisms in yeast: Current knowledge in biotechnological applications and future directions. *Process Biochemistry* **2024**, *138*, 1-13, doi:10.1016/j.procbio.2023.12.024.

226. Zeng, L.; Si, Z.; Zhao, X.; Feng, P.; Huang, J.; Long, X.; Yi, Y. Metabolome analysis of the response and tolerance mechanisms of *Saccharomyces cerevisiae* to formic acid stress. *Int J Biochem Cell Biol* **2022**, *148*, 106236, doi:10.1016/j.biocel.2022.106236.
227. Stellner, N.I.; Rerop, Z.S.; Mehlmer, N.; Masri, M.; Ringel, M.; Bruck, T.B. Expanding the genetic toolbox for *Cutaneotrichosporon oleaginosus* employing newly identified promoters and a novel antibiotic resistance marker. *BMC Biotechnol* **2023**, *23*, 40, doi:10.1186/s12896-023-00812-7.
228. Cui, Y.; Blackburn, J.W.; Liang, Y. Fermentation optimization for the production of lipid by *Cryptococcus curvatus*: Use of response surface methodology. *Biomass and Bioenergy* **2012**, *47*, 410-417, doi:10.1016/j.biombioe.2012.09.017.
229. Depree, J.; Emerson, G.W.; Sullivan, P.A. The cell wall of the oleaginous yeast *Trichosporon cutaneum*. *J Gen Microbiol* **1993**, *139*, 2123-2133, doi:10.1099/00221287-139-9-2123.
230. Ringel, M.; Paper, M.; Willing, M.; Schneider, M.; Melcher, F.; Stellner, N.I.; Bruck, T. Sustainable Lipid Production with *Cutaneotrichosporon oleaginosus*: Insights into Metabolism, Feedstock Valorization and Bioprocess Development. *Microorganisms* **2025**, *13*, doi:10.3390/microorganisms13091988.
231. Zheng, Y.; Chi, Z.; Ahring, B.K.; Chen, S. Oleaginous yeast *Cryptococcus curvatus* for biofuel production: Ammonia's effect. *Biomass and Bioenergy* **2012**, *37*, 114-121, doi:10.1016/j.biombioe.2011.12.022.
232. Teixeira, I.R.; Carvalho, G.S.; Barbosa, L.S.; Dos Santos Franca, J.; de Almeida Medeiros, R.M.; Andrade, B.B.; de Souza, C.O.; da Silva, J.B.A.; de Jesus Assis, D.; Cardoso, L.G. Valorization of crude glycerol by microorganisms: A bibliographic and technological survey. *Mar Pollut Bull* **2026**, *222*, 118712, doi:10.1016/j.marpolbul.2025.118712.
233. Amin, M.; Tahir, F.; Akbar, I.; Alessa, A.H.; Alsaigh, A.A.; Liu, C.-G.; Xin, F.; Chi, Z.; Syafiuddin, A.; Mehmood, M.A.; et al. Towards Environmental Sustainability: Employing Adaptive Laboratory Evolution to Develop Elite Algae Strains for Industrial and Environmental Applications. *Current Pollution Reports* **2025**, *11*, doi:10.1007/s40726-025-00346-w.
234. Liu, Q.; Zhang, B.; Hu, M.; Bao, J. Simultaneous enhancement of lignin-derived inhibitor tolerance and lipid accumulation of oleaginous yeast *Trichosporon cutaneum* by adaptive evolution. *Process Biochemistry* **2024**, *137*, 20-29, doi:10.1016/j.procbio.2023.12.010.
235. European Union. Directive (EU) 2018/350 of 8 March 2018 amending Directive 2001/18/EC as regards the environmental risk assessment of genetically modified organisms. **2018**, 30-45.
236. Zoheir, A.E.; Spath, G.P.; Niemeyer, C.M.; Rabe, K.S. Microfluidic Evolution-On-A-Chip Reveals New Mutations that Cause Antibiotic Resistance. *Small* **2021**, *17*, e2007166, doi:10.1002/smll.202007166.
237. Fuchs, T.; Melcher, F.; Rerop, Z.S.; Lorenzen, J.; Shaigani, P.; Awad, D.; Haack, M.; Prem, S.A.; Masri, M.; Mehlmer, N.; et al. Identifying carbohydrate-active enzymes of *Cutaneotrichosporon oleaginosus* using systems biology. *Microb Cell Fact* **2021**, *20*, 205, doi:10.1186/s12934-021-01692-2.
238. Du, C.; Li, Y.; Xiang, R.; Yuan, W. Formate Dehydrogenase Improves the Resistance to Formic Acid and Acetic Acid Simultaneously in *Saccharomyces cerevisiae*. *Int J Mol Sci* **2022**, *23*, doi:10.3390/ijms23063406.
239. Hedbacker, K.; Carlson, M. SNF1/AMPK pathways in yeast. *Front Biosci* **2008**, *13*, 2408-2420, doi:10.2741/2854.
240. Liu, Z.; Oyetunde, T.; Hollinshead, W.D.; Hermanns, A.; Tang, Y.J.; Liao, W.; Liu, Y. Exploring eukaryotic formate metabolisms to enhance microbial growth and lipid accumulation. *Biotechnol Biofuels* **2017**, *10*, 22, doi:10.1186/s13068-017-0708-1.
241. Oizel, K.; Tait-Mulder, J.; Fernandez-de-Cossio-Diaz, J.; Pietzke, M.; Brunton, H.; Lilla, S.; Dhayade, S.; Athineos, D.; Blanco, G.R.; Sumpton, D.; et al. Formate induces a metabolic switch in nucleotide and energy metabolism. *Cell Death Dis* **2020**, *11*, 310, doi:10.1038/s41419-020-2523-z.

242. Pietzke, M.; Meiser, J.; Vazquez, A. Formate metabolism in health and disease. *Mol Metab* **2020**, *33*, 23-37, doi:10.1016/j.molmet.2019.05.012.
243. Warnecke, T.; Gill, R.T. Organic acid toxicity, tolerance, and production in *Escherichia coli* biorefining applications. *Microb Cell Fact* **2005**, *4*, 25, doi:10.1186/1475-2859-4-25.
244. Wang, D.; Zeng, N.; Li, C.; Li, Z.; Zhang, N.; Li, B. Fungal biofilm formation and its regulatory mechanism. *Heliyon* **2024**, *10*, e32766, doi:10.1016/j.heliyon.2024.e32766.
245. Tan, Y.S.; Zhang, R.K.; Liu, Z.H.; Li, B.Z.; Yuan, Y.J. Microbial Adaptation to Enhance Stress Tolerance. *Front Microbiol* **2022**, *13*, 888746, doi:10.3389/fmicb.2022.888746.
246. Henske, J.K.; Wilken, S.E.; Solomon, K.V.; Smallwood, C.R.; Shutthanandan, V.; Evans, J.E.; Theodorou, M.K.; O'Malley, M.A. Metabolic characterization of anaerobic fungi provides a path forward for bioprocessing of crude lignocellulose. *Biotechnol Bioeng* **2018**, *115*, 874-884, doi:10.1002/bit.26515.
247. Hooker, C.A.; Lee, K.Z.; Solomon, K.V. Leveraging anaerobic fungi for biotechnology. *Curr Opin Biotechnol* **2019**, *59*, 103-110, doi:10.1016/j.copbio.2019.03.013.
248. Schneider, M.; Melcher, F.; Fimmen, R.; Mertens, J.; Garbe, D.; Paper, M.; Ringel, M.; Bruck, T. Influence of process parameters on single-cell oil production by *Cutaneotrichosporon oleaginosus* using response surface methodology. *Biotechnol Biofuels Bioprod* **2025**, *18*, 115, doi:10.1186/s13068-025-02717-3.
249. Rerop, Z.S.; Stellner, N.I.; Graban, P.; Haack, M.; Mehlmer, N.; Masri, M.; Brück, T.B. Bioconversion of a Lignocellulosic Hydrolysate to Single Cell Oil for Biofuel Production in a Cost-Efficient Fermentation Process. *Fermentation* **2023**, *9*, doi:10.3390/fermentation9020189.
250. Szczepanska, P.; Hapeta, P.; Lazar, Z. Advances in production of high-value lipids by oleaginous yeasts. *Crit Rev Biotechnol* **2022**, *42*, 1-22, doi:10.1080/07388551.2021.1922353.
251. Brown, J.L.; Perisin, M.A.; Swift, C.L.; Benyamin, M.; Liu, S.; Singan, V.; Zhang, Y.; Savage, E.; Pennacchio, C.; Grigoriev, I.V.; et al. Co-cultivation of anaerobic fungi with *Clostridium acetobutylicum* bolsters butyrate and butanol production from cellulose and lignocellulose. *J Ind Microbiol Biotechnol* **2023**, *49*, doi:10.1093/jimb/kuac024.
252. Wickerham, L.J. *Taxonomy of yeasts*; U.S. Department of Agriculture: Washington, DC, 1951; pp. 1–56.
253. Schroeckh, V.; Scherlach, K.; Nutzmann, H.W.; Shelest, E.; Schmidt-Heck, W.; Schuemann, J.; Martin, K.; Hertweck, C.; Brakhage, A.A. Intimate bacterial-fungal interaction triggers biosynthesis of archetypal polyketides in *Aspergillus nidulans*. *Proc Natl Acad Sci U S A* **2009**, *106*, 14558-14563, doi:10.1073/pnas.0901870106.
254. Wang, G.; Ran, H.; Fan, J.; Keller, N.P.; Liu, Z.; Wu, F.; Yin, W.B. Fungal-fungal cocultivation leads to widespread secondary metabolite alteration requiring the partial loss-of-function VeA1 protein. *Sci Adv* **2022**, *8*, eabo6094, doi:10.1126/sciadv.abo6094.
255. Garbacz, G.; Kolodziej, B.; Koziolek, M.; Weitschies, W.; Klein, S. An automated system for monitoring and regulating the pH of bicarbonate buffers. *AAPS PharmSciTech* **2013**, *14*, 517-522, doi:10.1208/s12249-013-9933-5.
256. Brakhage, A.A. Regulation of fungal secondary metabolism. *Nat Rev Microbiol* **2013**, *11*, 21-32, doi:10.1038/nrmicro2916.
257. Keller, N.P. Fungal secondary metabolism: regulation, function and drug discovery. *Nat Rev Microbiol* **2019**, *17*, 167-180, doi:10.1038/s41579-018-0121-1.
258. Netzker, T.; Fischer, J.; Weber, J.; Mattern, D.J.; Konig, C.C.; Valiante, V.; Schroeckh, V.; Brakhage, A.A. Microbial communication leading to the activation of silent fungal secondary metabolite gene clusters. *Front Microbiol* **2015**, *6*, 299, doi:10.3389/fmicb.2015.00299.
259. Yang, X.; Feng, P.; Yin, Y.; Bushley, K.; Spatafora, J.W.; Wang, C. Cyclosporine Biosynthesis in Tolypocladium inflatum Benefits Fungal Adaptation to the Environment. *mBio* **2018**, *9*, doi:10.1128/mBio.01211-18.
260. Chen, L.; Yue, Q.; Li, Y.; Niu, X.; Xiang, M.; Wang, W.; Bills, G.F.; Liu, X.; An, Z. Engineering of *Glarea lozoyensis* for exclusive production of the pneumocandin B0 precursor of the antifungal

drug caspofungin acetate. *Appl Environ Microbiol* **2015**, *81*, 1550-1558, doi:10.1128/AEM.03256-14.

261. Mroczynska, M.; Brillowska-Dabrowska, A. Review on Current Status of Echinocandins Use. *Antibiotics (Basel)* **2020**, *9*, doi:10.3390/antibiotics9050227.
262. Conrado, R.; Gomes, T.C.; Roque, G.S.C.; De Souza, A.O. Overview of Bioactive Fungal Secondary Metabolites: Cytotoxic and Antimicrobial Compounds. *Antibiotics (Basel)* **2022**, *11*, doi:10.3390/antibiotics11111604.
263. Henriques, S.F.; Mira, N.P.; Sa-Correia, I. Genome-wide search for candidate genes for yeast robustness improvement against formic acid reveals novel susceptibility (Trk1 and positive regulators) and resistance (Haa1-regulon) determinants. *Biotechnol Biofuels* **2017**, *10*, 96, doi:10.1186/s13068-017-0781-5.
264. Piotrowski, J.S.; Zhang, Y.; Bates, D.M.; Keating, D.H.; Sato, T.K.; Ong, I.M.; Landick, R. Death by a thousand cuts: the challenges and diverse landscape of lignocellulosic hydrolysate inhibitors. *Front Microbiol* **2014**, *5*, 90, doi:10.3389/fmicb.2014.00090.
265. Ding, C.; Wu, X.; Auckloo, B.N.; Chen, C.T.; Ye, Y.; Wang, K.; Wu, B. An Unusual Stress Metabolite from a Hydrothermal Vent Fungus *Aspergillus sp*. WU 243 Induced by Cobalt. *Molecules* **2016**, *21*, 105, doi:10.3390/molecules21010105.
266. Wang, R.; Wang, J.; Xu, R.; Fang, Z.; Liu, A. Oil Production by the Oleaginous Yeast *Lipomyces starkeyi* using Diverse Carbon Sources. *BioResources* **2014**, *9*, doi:10.15376/biores.9.4.7027-7040.
267. Dobrowolski, A.; Mitula, P.; Rymowicz, W.; Mironczuk, A.M. Efficient conversion of crude glycerol from various industrial wastes into single cell oil by yeast *Yarrowia lipolytica*. *Bioresour Technol* **2016**, *207*, 237-243, doi:10.1016/j.biortech.2016.02.039.
268. Saran, S.; Mathur, A.; Dalal, J.; Saxena, R.K. Process optimization for cultivation and oil accumulation in an oleaginous yeast *Rhodosporidium toruloides* A29. *Fuel* **2017**, *188*, 324-331, doi:10.1016/j.fuel.2016.09.051.

6. List of publications

6.1 Encompassed peer-reviewed publications in this dissertation:

- **Schulz K. E.**, Scholz D., Sikirić A. R., Rambow D., Neumann A., Ochsenreither K. *Anaerobic gut fungi as biocatalysts: metabolic and physiological analysis of anaerobic gut fungi under diverse cultivation conditions.* **Frontiers in Microbiology** (2025), 16, 1662047. https://doi.org/10.3389/fmicb.2025.1662047
- **Schulz K. E.**, Hegmann P., Dreher B., Regenauer L., Delso Muniesa C., Frey W., Ochsenreither K., Neumann A. *Phosphate Versus Nitrogen Limitation: A Reactor-Scale Process Comparison for Single-Cell Oil Production in Oleaginous Yeasts.* **Fermentation** (2026), 12(4), 172. https://doi.org/10.3390/fermentation12040172
- **Schulz K. E.**, Hegmann P., Dreher B., Schreidl M., Ochsenreither K., Neumann A. *Adapted Feeding Strategies Enable Efficient Growth and Lipid Accumulation Using Untreated Crude Glycerol in Transition Scale with Cutaneotrichosporon oleaginosum ATCC 20509.* **Fermentation** (2026), 12(3), 154. https://doi.org/10.3390/fermentation12030154

6.2 Submitted publications included in this dissertation:

- **Schulz K. E.**, Baron Diaz D., Holtmann D. *Ferricyanide-dependent current production by Neocallimastix cameroonii G341 in a miniaturized anaerobic bioelectrochemical system.* Submitted to **FEMS Microbiology Letters**
- **Schulz K. E.**, Pfau A., Tarhan T., van Almsick C., Scholz D., Sikirić A. R., Neumann A., Ochsenreither K. *Beyond Carbon Dioxide: Decoupling Headspace and Buffering Reveals a Bicarbonate Requirement for Anaerobic Gut Fungi Growth.* Submitted to **Fungal Biology and Biotechnology**
- **Schulz K. E.**, Stolle C., Schwendemann A. R. M., Holtmann D., Rabe K. S. *Microfluidic adaptive laboratory evolution of the oleaginous yeast Cutaneotrichosporon oleaginosum.* Submitted to **Applied Microbiology and Biotechnology**

6.3 Published peer-reviewed publications not included in this dissertation:

- Grünberger A., Schepp E., Lang S., **Schulz K. E.**, Baron Diaz D., Sivanesapillai A., Diepold A., Stolle C., Rabe K., Ulber R. et al.
  Exploitation of Biodiversity in Bioeconomy: Examples, Opportunities, and Challenges.
  Advances in Biochemical Engineering/Biotechnology (2025). Book chapter.
  https://doi.org/10.1007/10_2025_288
- Lamparter T., Babian J., Fröhlich K., Mielke M., Weber N., Wunsch N., Zais F., **Schulz K.**, Aschmann V., Spohrer N. et al.
  The involvement of type IV pili and the phytochrome CphA in gliding motility, lateral motility and photophobotaxis of the cyanobacterium Phormidium lacuna.
  PLOS ONE (2022). https://doi.org/10.1371/journal.pone.0249509

6.4 Submitted publications not included in this disseratation:

- **Schulz K. E.**, Fischbach D., Frey W., Ochsenreither K., Neumann A.
  Microwave-Assisted Wet Route Downstream Processing for Single Cell Oil from Oleaginous Yeast Using Environment-Friendly Green Solvents.
  Submitted to **Journal of Cleaner Chemical Engineering** (2026).

6.5 Planed publications not included in this dissertation:

- **Schulz K. E.**, Delso Muniesa C., Fischbach D. F., Frey W., Ochsenreither K., Neumann A.
  Variability of Oil Extractability in Oleaginous Yeasts

6.6 Conference Contributions:

- **Schulz K. E.**, Ochsenreither K., Neumann A.
  From straw to oil – Establishment of a biobased upcycling process of hemi- and lignocellulosic biomass.
  VAAM – Jahrestagung 2023, 10.09.2023 – 13.09.2023, Göttingen
- **Schulz K. E.**, Ochsenreither K., Neumann A.
  Usage of lignocellulosic materials for H_2 production by anaerobic gut fungi.
  VAAM – Jahrestagung 2024, 02.06.2024 – 05.06.2024, Würzburg
- **Schulz K. E.**, Ochsenreither K., Neumann A.
  From straw to oil – Establishment of a biobased upcycling process of hemi- and lignocellulosic biomass.
  IAFC 2024, 15.10.2024 – 17.10.2024, Online
- **Schulz K. E.**, Ochsenreither K., Neumann A.
  Phosphate limited production of single cell oils with unconventional yeast.
  VAAM – Jahrestagung 2025, 23.03.2025 – 26.03.2025, Bochum

7. List of figures

Figure 1: Total amount of metabolites produced after 7 days of cultivation of the tested strains in serum bottles with CO2 atmosphere and bicarbonate buffer on the carbon source wheat straw (n = 3). ***38***
Figure 2: Effect of 24 h preculture room temperature shock to the metabolic activity of the next generation (n = 1). ***39***
Figure 3: Statistical comparison for evaluation of significant differences in metabolite production based on particle size. All six tested strains are combined (n = 12)..... ***40***
Figure 4: Produced metabolites with the different used soluble C-sources and residual concentration per experiment (n = 3). ***43***
Figure 5: Hydrogen per gram carbon source produced...... ***44***
Figure 6: General overview of anaerobic gut fungi metabolic pathways and the succession in production of metabolites with increasing concentrations of soluble carbon source based on growth experiments with the six chosen fungal strains and data from Wilken et al, 2021 [69]. ***45***
Figure 7: Statistical analysis of the produced metabolites after 7 days of incubation with the Tukey test for all conducted batch and fed batch fermentations in pairwise comparison (n = 18). ***46***
Figure 8: Relative consumption of solid carbon sources tested in comparison to wheat straw (n = 3)..... ***47***
Figure 9: New growth form of O. joyonii emerged after prolonged cultivation on the soluble carbon source glucose. For comparison a standard slide with 26 mm x 76 mm was used. A: View from above, small holes/ channels are visible; B: View from the bottom; C: Slices of the biomass showing a shift in color with the bright sight showing the upper side and the purple side the lower side; D: Biomass cut in half; E and F: Microscopic pictures of the structure in bright field..... ***48***
Figure 10: Electron recovery (%) of six anaerobic gut fungal species cultivated on different carbon sources and substrate concentrations, based on published data from Schulz et al. (n = 3) [14]. Stacked bars represent the relative contributions of individual fermentation products (hydrogen, ethanol, formate, acetate, lactate, succinate, citrate, and malate) to total electron recovery. Error bars indicate standard deviation of biological triplicates...... ***60***
Figure 11: Screening of redox mediators for extracellular electron transfer in the eCuvette platform. Current density normalized to the initial mediator concentration (µA mM^{-1} cm^{-2}) is shown over time for cultures supplied with ferricyanide (FEC), methyl red (MR), methyl viologen (MV), phenazine ethosulfate (PES), phenazine methosulfate (PMS), resazurin (RES) and riboflavin (RF), alongside a mediator-free control. All experiments were conducted under anaerobic conditions at 39 °C. A temporary temperature switch off (indicated by dashed lines) after (24 h) was introduced to assess the biological contribution to current generation and the capacity for recovery upon reinstating cultivation temperature (29 h). Data represent single experiments (n = 1). ***62***
Figure 12: Chronoamperometric current density profiles of anaerobic gut fungal cultures cultivated in the eCuvette platform with methyl viologen (MV) or ferricyanide (FEC) as redox mediators. Shown are biological replicates for cultures with mediator (Cells + MV, Cells + FEC), corresponding biotic controls lacking mediator (Cells w/o MV, Cells w/o FEC), and abiotic controls containing mediator but no cells (MV abiotic control, FEC abiotic control). Current density (µA cm^{-2}) is plotted against elapsed time since inoculation. A pronounced and reproducible current response is observed in the presence of ferricyanide and cells, whereas methyl viologen and all control conditions show no sustained positive current generation, confirming mediator-specific and fungus-dependent electron transfer. ***63***

Figure 13: Cyclic voltammograms of the two mediators used in the second eCuvette experiments, methyl viologen (blue) and ferricyanide (black), recorded under anaerobic conditions. Current is normalized for better comparison, and potentials are reported versus Ag/AgCl (3 M KCl). The voltammograms confirm the characteristic redox behavior of both mediators within the applied potential window and indicate their electrochemical integrity in the experimental medium. ***64***

Figure 14: Experimental workflow used to systematically disentangle cultivation variables in anaerobic gut fungi (AGF). Starting from conventional CO_2/HCO_3^--based cultivation, the study sequentially evaluated (i) headspace composition (CO_2 vs. N_2), (ii) non-carbonate buffer systems, (iii) minimal bicarbonate requirements, (iv) substitution by structurally diverse carboxylic acids, (v) pH optima using a dual-buffer strategy, and (vi) an OD_{750}-based biomass proxy, which was subsequently applied in an initial (vii) nitrogen-variation experiment. Core readouts included headspace pressure, µGC gas analysis, HPLC metabolite profiling, and OD_{750} where indicated..... ***79***

Figure 15: Atmospheric screening: influence of headspace gas composition (CO_2 vs. N_2) on metabolite production of six anaerobic gut fungal strains after 7 days of cultivation. All cultures were grown in identical bicarbonate-buffered medium and initiated at the same pH (7.5) to control for pH shifts associated with CO_2 removal under N_2. Cultivations were performed in biological triplicates across three independent weekly batches (n = 9). Error bars represent standard deviation. Hydrogen production was consistently higher under N_2 headspace across all strains..... ***80***

Figure 16: Post-sterilization pH values of the indicated buffer systems after anaerobization under 100% N_2 and autoclaving (121 °C, 20 min) across the tested concentration range (0.5-10 g L^{-1}; n = 3). Red lines denote the predefined acceptance window for pH stability (6.9 ± 0.1). Sodium hydrogen carbonate exhibits a concentration-dependent alkaline shift following N_2 treatment, whereas several non-carbonate buffer systems maintain pH values within the target range..... ***83***

Figure 17: Total metabolite production (mmol per bottle) of N. cameroonii cultivated with chemically stable, bicarbonate-free buffer systems after N_2 anaerobization and autoclaving. Only buffer–concentration combinations maintaining post-sterilization pH 6.9 ± 0.1 were evaluated. Limited metabolic activity was observed during the first cultivation cycle (shown above); however, no sustained hydrogen production or metabolite formation was detected after transfer into fresh medium in the subsequent week. Data represent biological triplicates (n = 3); error bars indicate standard deviation. For ACES-containing samples, apparent succinate signals reflect chromatographic co-elution; a representative fixed background value (0.2 mmol L^{-1}) is shown. The numbers on the X-Axis indicate the concentration of the buffer in mM. ***84***

Figure 18: Strain-specific restoration of metabolic activity by sodium hydrogen carbonate under a 100% N_2 atmosphere. Total metabolite production (mmol L^{-1}) of polycentric anaerobic gut fungal strains (A. dupliciliberans, N. cameroonii, O. joyonii, and P. ruminantium) is shown for the second cultivation cycle across increasing sodium hydrogen carbonate concentrations (0-3 g L^{-1}). Carbonate-free conditions (0 g L^{-1} $NaHCO_3$) resulted in negligible hydrogen formation, whereas sodium hydrogen carbonate supplementation restored hydrogen production in a strain-specific, concentration-dependent manner. Data represent biological triplicates (n = 3); error bars indicate standard deviation. The numbers on the X-Axis indicate the concentration of NaHCO3 in g L-1..... ***86***

Figure 19: Metabolite production by A. dupliciliberans under a 100% N_2 atmosphere in media with structurally diverse carboxylic acids. Stacked bars show the individual and total concentrations of quantified metabolites (hydrogen, ethanol, formate, acetate, lactate, succinate, citrate, and malate) after seven days of cultivation in bicarbonate-free medium supplemented with 4 g L^{-1} of the indicated carboxylic acid; the control contained 4 g L^{-1} sodium hydrogen carbonate. Values were corrected for compound-specific background and co-elution artefacts identified by independent standard measurements. None of the tested carboxylic acids restored the bicarbonate-supported hydrogen production observed in the control. Maleic acid yielded the highest metabolite accumulation among the tested carboxylic acids; however, acetate is not shown for this condition because maleic acid can isomerize and generate an interfering HPLC signal, preventing reliable acetate quantification. Data represent biological triplicates (n = 3); error bars indicate standard deviation..... ***88***

Figure 20: Total metabolite production by four polycentric anaerobic gut fungal strains under a 100 % N2 atmosphere at initial pH between 5.8 and 7. Cultures were grown with Bis-Tris (6 g L^{-1}) as the primary buffer and 0.5 g L^{-1} $NaHCO_3$ as a minimal inorganic carbon supplement. Data represent biological triplicates (n = 3); error bars indicate standard deviation. ***89***

Figure 21: Comparison of measured and calculated OD_{750} values for fungal biomass after activated carbon-based inter-device normalization. In the six upper panels, green circles show the OD_{750} values experimentally measured for fungal biomass suspensions of known dry weight concentration (0.005–0.5 g L^{-1}) on Photometer 2 (GENESYS™ 30), whereas black diamonds show the OD_{750} values calculated for the same biomass concentrations from the activated carbon-based normalization function. The two lower panels show the activated carbon calibration curves measured on Photometer 1 and Photometer 2, which were used to derive the normalization function. Measured data represent mean values of ten technical replicates; error bars indicate standard deviation..... ***92***

Figure 22: Impact of ammonium sulfate concentration on biomass formation and metabolic output. A: Biomass (OD_{750}-derived dry mass); B: OD_{750} values; C: Total metabolites (mmol L^{-1}) of Caecomyces churrovis PP313 with varying ammonium sulfate concentrations. No major differences in biomass accumulation or hydrogen production were observed across the tested nitrogen range, indicating non-limiting nitrogen conditions. Data represent biological triplicates; error bars indicate standard deviation..... ***93***

Figure 23: Temporal profiles of ammonium and phosphate concentrations during nitrogen-limited, phosphate-limited and nutrient-replete ("unlimited") bioreactor cultivations, shown as mean values across all duplicates of the four strains (n = 8). Dotted lines indicate trends for visual guidance only. ***106***

Figure 24: Final cell dry weight (CDW) concentrations after 144 h of bioreactor cultivation under nitrogen-limited, phosphate-limited and nutrient-replete ("unlimited") conditions for C. oleaginosum, S. podzolica, S. segobiensis and A. porosum. Bars represent mean values ± standard deviation of biological duplicates (n = 2). Statistical differences between nutrient regimes within each strain were evaluated using Tukey test. Statistical significance was tested at three predefined levels ($p \leq 0.05$, ** $p \leq 0.01$, and *** $p \leq 0.001$). However, only one comparison reached statistical significance and is therefore indicated in the graph as ***. The absence of additional * or ** annotations is intentional and indicates that all remaining comparisons did not meet any of the tested significance thresholds ($p > 0.05$).....* ***107***

Figure 25: Average relative biomass composition of all oleaginous yeasts at the end of cultivation (144 h) under nutrient-replete ("unlimited"), phosphate-limited, and nitrogen-limited conditions measured in duplicate (n = 8). Strain-specific endpoint compositions are shown below (n = 2). ***108***

*Figure 26: Final lipid titres (g L−1) obtained after 144 h of bioreactor cultivation under nitrogen-limited, phosphate-limited and nutrient-replete ("unlimited") conditions for all tested oleaginous yeast strains. Bars represent mean values ± standard deviation of biological duplicates (n = 2). Statistical differences between nutrient regimes within each strain were evaluated using Tukey test. Significance levels are indicated as * p ≤ 0.05, ** p ≤ 0.01, and *** p ≤ 0.001. .....**110***
*Figure 27: Fatty acid profiles after 144 h of cultivation under nitrogen-limited, phosphate-limited and nutrient-replete (unlimited) conditions. Fatty acids were quantified as fatty acid methyl esters by gas chromatography. The total lipid titre (g L−1) is indicated in the center of each diagram (n = 3).....**113***
*Figure 28: Simulated trends in time of relative biomass-related variable B(t); the change in the abstract dilution term V(t); the change in inhibitor-related concentration C(t); and the behavior of relative inhibition index R(t). All axes are displayed linearly. The conceptual illustration shown does not aim to predict kinetics but serves to visualize the qualitative dependency between initial biomass and effective inhibitor burden per cell. All used formulas are further explained in Section 2. .....**130***
*Figure 29: Cultivation parameters pH, temperature, stirrer speed, OD600, cell dry weight and ammonium concentration of 2.5 L stirred tank fermentations of references with (A) CG without adapted feeding, (B) pure glycerol, and of (C,D) with CG with adapted feeding of the strain C. oleaginosum. CG 1 was used. Dotted lines were added only for visual orientation (n = 1). **132***
*Figure 30: Gas analytics and glycerol concentration of 2.5 L stirred tank fermentations of references with (A) CG without adapted feeding, (B) pure glycerol, and of (C,D) with CG with adapted feeding of the strain C. oleaginosum. Crude glycerol 1 (CG 1) was used. The cumulative curves represent the total carbon dioxide emitted and the total oxygen consumed, which increase continuously over the course of the cultivation. In contrast, the carbon transfer rate and oxygen transfer rate are shown as peak-shaped profiles reflecting the instantaneous metabolic activity of the culture. Carbon dioxide–related parameters are shown in black, whereas oxygen-related parameters are shown in red. Dotted lines were added only for visual orientation (n = 1). **133***
*Figure 31: Relative endpoint biomass composition of 2.5 L stirred tank fermentations with C. oleaginosum after 144 h of fermentation time. For protein determination of the reference fermentation with CG not enough biomass was produced. The used CG batch was CG 1 (n = 1).....**134***
*Figure 32: Fatty acid profile of endpoint biomass produced in 2.5 L stirred tank fermentations with C. oleaginosum using CG 1, pure glycerol and adapted feeding with CG 1 (n = 1). **135***
*Figure 33: Cultivation parameters pH, temperature, stirrer speed, dissolved oxygen tension, glycerol concentration, cell dry weight, ammonium concentration and optical density at 600 nm of transition-scale fermentations with C. oleaginosum and separation in repeated batches. CG 1 was used for the initial batch and repeated batch 1 and CG 2 for repeated batch 2 and repeated batch 3. Dotted lines were added only for visual orientation (n = 1). Inoculum for initial fermentation was 1% (v/v), for repeated batch 1 and 2 it was 5% (v/v) and for repeated batch 3 it was 60% (v/v). **136***
*Figure 34: Endpoint biomass composition of the 19 L transition-scale fermentations with C. oleaginosum. CG 1 was used for the initial batch and repeated batch 1 and CG 2 was used for repeated batch 2 and repeated batch 3. Inoculum for initial fermentation was 1% (v/v), for repeated batch 1 and 2 it was 5% (v/v) and for repeated batch 3 it was 60% (v/v) (n = 1). .**138***
*Figure 35: Fatty acid profile of the biomass of the endpoint of the 19 L transition-scale fermentations with C. oleaginosum. CG 1 was used for the initial batch and repeated batch 1, and CG 2 was used for repeated batch 2 and repeated batch 3. Inoculum for initial fermentation was 1% (v/v), for repeated batch 1 and 2 it was 5% (v/v) and for repeated batch 3 it was 60% (v/v) (n = 1).....**139***

Figure 36: Relative amount of cell dry weight after 21 days of cultivation at 30 °C with 130 rpm of C. oleaginosum ATCC 20509 in designated media compositions (n = 1)......***150***
Figure 37: Cultivation of C. oleaginosum in the microfluidic evo.S chip. A) mineral salt medium with glucose (medium Y-G2) was supplied only via the main-flow inlet and C. oleaginosum cells were inoculated into well 0. B) The chip (n=1) was photographed daily during the one-week cultivation to document the growth of the cells via the increase in turbidity. Arrows indicate turbidity in areas of the inlets with lower flow velocities. In addition, the waste bottle was documented photographically at the end of the microfluidic cultivation after 7 days. Please note that after 7 days the chip was removed from the chamber and photographed on a black background to improve the contrast......***151***
Figure 38: Adaptation of C. oleaginosum to stress-relative intermediates using the microfluidic evo.S chip. A) Increasing concentrations of the stress-relative intermediates continuously supplied to the main-flow through co-flows resulted in a concentration gradient across the interconnected growth wells 0-5 (n = 1). B) A smooth and steep gradient profile were implemented on separate chips, both ranging from 6.25% to 100% fraction of maximum intermediate concentration in anaerobic fungi mineral salt medium. C) Photographs of the chips after 7 days and 14 days adaptation. Dotted outline around the growth wells was added for visual purposes. Arrows show turbidity indicating growth. ***152***
Figure 39: Growth dynamics of evolved C. oleaginosum strains under smooth and steep substrate gradients. Optical density (OD_{600}) was monitored over 168 h for strains isolated from different wells of the microfluidic evo.S chip. (A) Growth profiles of strains obtained from the smooth gradient chip. (B) Growth profiles of strains obtained from the steep gradient chip. The wild-type strain (WT) is shown for comparison. Lines represent mean OD_{600} values and shaded areas indicate the standard deviation of biological sextuplicates (n = 6) and are set to zero at t =0......***153***
Figure 40: The amount of consumed carbon normalized to the change in OD_{600} is shown for the non-adapted wild type (WT) and for adapted cultures isolated from the smooth gradient chip (Smooth 3) and the steep gradient chip (Steep 2). No growth was detected for the WT under the tested conditions, and therefore no carbon consumption per OD_{600} increase could be determined. Bars represent mean values of technical triplicates (n = 3), and error bars indicate the standard deviation......***154***
Figure 41: Statistical analysis (Tukey test) of the metabolite concentrations in cultures of the adapted C. oleaginosum strains Smooth 3 and Steep 2 after 168 h cultivation in main-flow medium in a 96-well plate in comparison to a non-adapted wild type (WT) strain in biological triplicates (n = 3). Mean values, standard deviation, standard error of the mean and 95 % confidence intervals from the conducted tukey test for end concentrations of the metabolic screening are represented in Table S12......***155***
Figure 42: Endpoint fermentation product profiles of individual anaerobic gut fungal strains and mixed-strain consortia cultivated on wheat straw (5 g L-1) for 7 d. Stacked bars show the mean endpoint levels of hydrogen and extracellular metabolites (ethanol (also added with hemin solution), formate, acetate, lactate, succinate, citrate, and malate) for all 63 unique culture configurations, grouped according to the number of strains present in each consortium. Error bars indicate the standard deviation of total quantified products (n = 3). Strain abbreviations: A, A. dupliciliberans A252; G, N. cameroonii G341; P, C. churrovis PP313; S, P. ruminantium SA222; W, O. joyonii W212; X, K. ramosus X2152......***168***

Figure 43: Time-resolved pH profiles during consecutive cultivation based on the selected anaerobic gut fungal consortium AG. Symbols indicate pH values measured over 192 h following the transition from the fungal to the yeast stage for three process variants: conventional consecutive cultivation without further modification, consecutive cultivation using the ALE-derived C. oleaginosum strain Smooth 3, and consecutive cultivation based on fungal precultures grown with maleic acid and buffer exchange. All cultivations were performed in biological triplicate (n=3). ***169***

Figure 44: Time-resolved extracellular metabolite profiles during consecutive cultivation based on the selected anaerobic gut fungal consortium AG (A. dupliciliberans A252 + N. cameroonii G341). Stacked bars show the concentrations of quantified soluble metabolites (ethanol, formate, acetate, lactate, succinate, citrate, and malate), with total bar height representing the sum of the displayed metabolites. Three process variants were compared: conventional consecutive cultivation without further modification with C. oleaginosum (left), consecutive cultivation using the ALE-derived C. oleaginosum strain Smooth 3 (middle), and consecutive cultivation based on fungal precultures grown with maleic acid and buffer exchange with C. oleaginosum (right). Samples were collected over 192 h following transition from the fungal to the yeast stage. In the right panel, acetate is not displayed because the corresponding HPLC signal produced an unrealistically large apparent value and would otherwise have obscured the visualization of the remaining metabolites. Error bars indicate standard deviation (n = 3). ***171***

Figure 45: Dilution experiment in YM medium using the ALE-derived C. oleaginosum strain Smooth 3. Left panel: stacked bars show HPLC-quantified extracellular metabolite profiles at 0 and 24 h for the YM water control and for cultures supplemented with 5 mL untreated or centrifuged anaerobic fungal broth, corresponding to a 1:10 dilution in the final 50 mL culture volume. Right panel: relative growth normalized to the water control based on optical density measurements at 600 nm. Error bars indicate standard deviation (n=3). ***173***

8. List of tables

Table 1: Redox mediators evaluated in the electrochemical screening, including the applied working electrode potentials (mV vs. Ag/AgCl, 3 M KCl) and the corresponding final concentrations in the e-Cuvette. ***58***
Table 2: Composition of the anaerobic gut fungus medium (based on in Schulz et al.) and assessment of intrinsic redox-active components. Listed are the individual medium constituents, their redox activity, and their final electron acceptor capacities in Emmol L^{-1} where applicable [14]. ***61***
Table 3: Volumetric lipid production rates (g L−1 h−1) and specific lipid production rates (g gCDW−1 h−1) calculated during the nutrient-limitation phase (N or P below detection limit in media until 144 h) for all tested oleaginous yeast strains under nitrogen- and phosphate-limited conditions (n = 3). ***111***
Table 4: General composition analysis of applied untreated non-sterilized crude glycerol (CG) batches received from industry. Protein content, carbohydrate content and lipid content were determined as percentual value while glycerol concentration is shown in g/L. The ammonium content of crude glycerol 2 (CG 2) was below the detection level of 0.01. ..... ***128***
Table 5: Key performance indicators μMax, YX/S and Pv of fermentations in a 2.5 L scale. Maximum growth rates represent apparent values calculated from biomass data obtained at 24 h sampling intervals, reflecting averaged kinetics rather than instantaneous specific growth rates. ***134***
Table 6: Key performance indicators of C. oleaginosum fermentations in a transition scale. The reported μ values should be interpreted as operational performance indicators rather than physiological maximum growth rates, as their calculation is constrained by sampling resolution. CG 1 was used for the initial batch and repeated batch 1 and CG 2 for repeated batch 2 and repeated batch 3. ..... ***136***
Table 7: Concentration of carbon sources used for the main-flow and co-flows for microfluidic adaptation in the smooth gradient chip. For soluble carbon source composition see Table 9. ..... ***148***
Table 8: Concentration of carbon sources used for the main-flow and co-flows for the microfluidic adaptation in the steep gradient chip. For soluble carbon source composition see
Table 9: Composition of soluble carbon sources supplied to the anaerobic fungi mineral salt medium in the main- and co-flow channels of the smooth and steep gradient microfluidic chips. Carbon source concentrations are given as absolute values (mmol/L) and represent defined fractions of the maximum concentration applied within the respective gradient setup. In the smooth gradient chip, co-flow channels were supplied with stepwise increasing concentrations (6.25–100% of the maximum concentration), whereas in the steep gradient chip, the maximum concentration was applied from co-flow channel 2 onward to generate an abrupt concentration increase. The main-flow channel contained the baseline concentration (6.25% of maximum) in both gradient configurations. ***148***
Table 10: Comparison of concentrations of individual compounds in medium Y-EALS and Y-EALS+F and respective literature values for toxicity for the conventional yeast Saccharomyces cerevisiae. ***150***
Table 11: Overview of the 63 unique mono- and mixed-strain culture configurations generated from the six anaerobic gut fungal strains used in this study, grouped according to the number of strains present in each combination. Strain abbreviations: A, Aestipascuomyces dupliciliberans A252; G, Neocallimastix cameroonii G341; P, Caecomyces churrovis PP313; S, Pecoramyces ruminantium SA222; W, Orpinomyces joyonii W212; X, Khyollomyces ramosus X2152. ..... ***163***

9. List of abbreviations

AGF — Anaerobic gut fungi
ALE — Adaptive laboratory evolution
CA — Chronoamperometry
CAZymes — Carbohydrate-active enzymes
C/N — Carbon-to-nitrogen ratio
C/P — Carbon-to-phosphorus ratio
CDW — Cell dry weight
CG — Crude glycerol
CTR — Carbon transfer rate
CV — Cyclic voltammetry
DET — Direct electron transfer
DOT — Dissolved oxygen tension
EET — Extracellular electron transfer
e-mol — Electron equivalent
FAME — Fatty acid methyl ester
HPLC — High-performance liquid chromatography
MET — Mediated electron transfer
OD_{600} — Optical density at 600 nm
OD_{750} — Optical density at 750 nm
OTR — Oxygen transfer rate
PDMS — Polydimethylsiloxane
pO_2 — Dissolved oxygen tension
PKS/NRPS — Polyketide synthase / non-ribosomal peptide synthetase
RID — Refractive index detector
RQ — Respiratory quotient
SCO — Single-cell oil
TC — Total carbon
TCD — Thermal conductivity detector
TN — Total nitrogen
VWD — Variable wavelength detector
WT — Wild type
µGC — Micro gas chromatography

10. Supplementary Information

10.1 Chapter 1: Anaerobic gut fungi as biocatalysts: metabolic and physiological analysis of anaerobic gut fungi under diverse cultivation conditions

Table S1: Overview of gathered data from the temperature screening. Growth temperature range is defined by the minimal and maximal temperature where hydrogen was produced.

Organism	Growth temperature range / °C	Optimum temperature metabolites / °C	Most metabolites produced / mmol/L	Optimum temperature hydrogen / °C	Hydrogen produced / mmol/L	Hydrogen mmol / g straw
K. ramosus	35 - 41	39	68 ± 05	37	4.10 ± 0.29	0.82 ± 0.06
P. ruminantium	35 - 42	39	60 ± 03	41	2.56 ± 0.16	0.51 ± 0.03
C. churrovis	35 - 41	37	50 ± 09	39	2.36 ± 0.31	0.47 ± 0.06
O. joyonii	35 - 42	39	73 ± 03	41	4.65 ± 0.58	0.93 ± 0.12
N. cameroonii	35 - 42	39	77 ± 08	41	4.37 ± 0.36	0.87 ± 0.07
A. dupliciliberans	37 - 41	39	78 ± 06	39	6.54 ± 0.24	1.31 ± 0.05

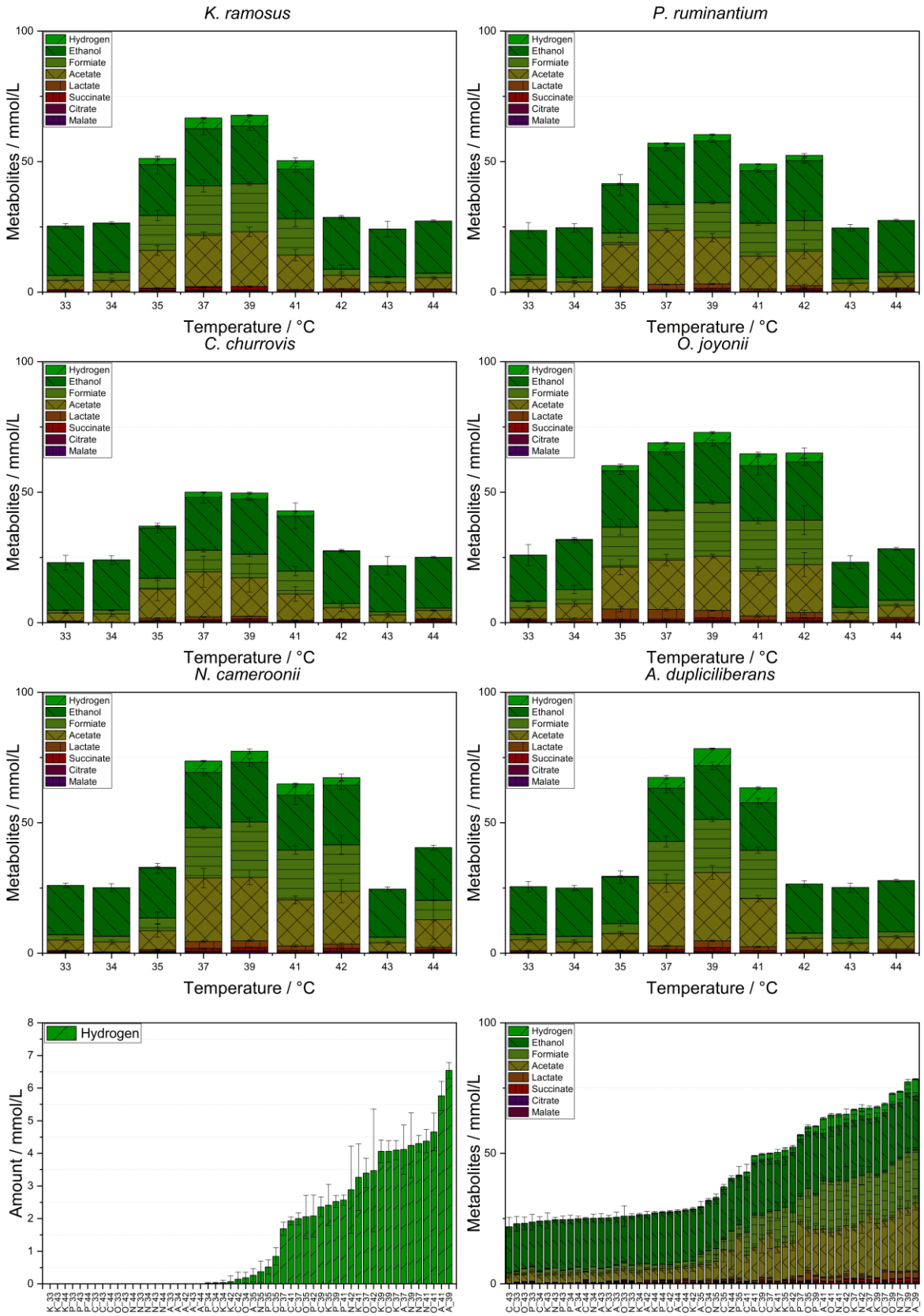

Figure S1: Metabolites produced at different temperatures for the tested strains.

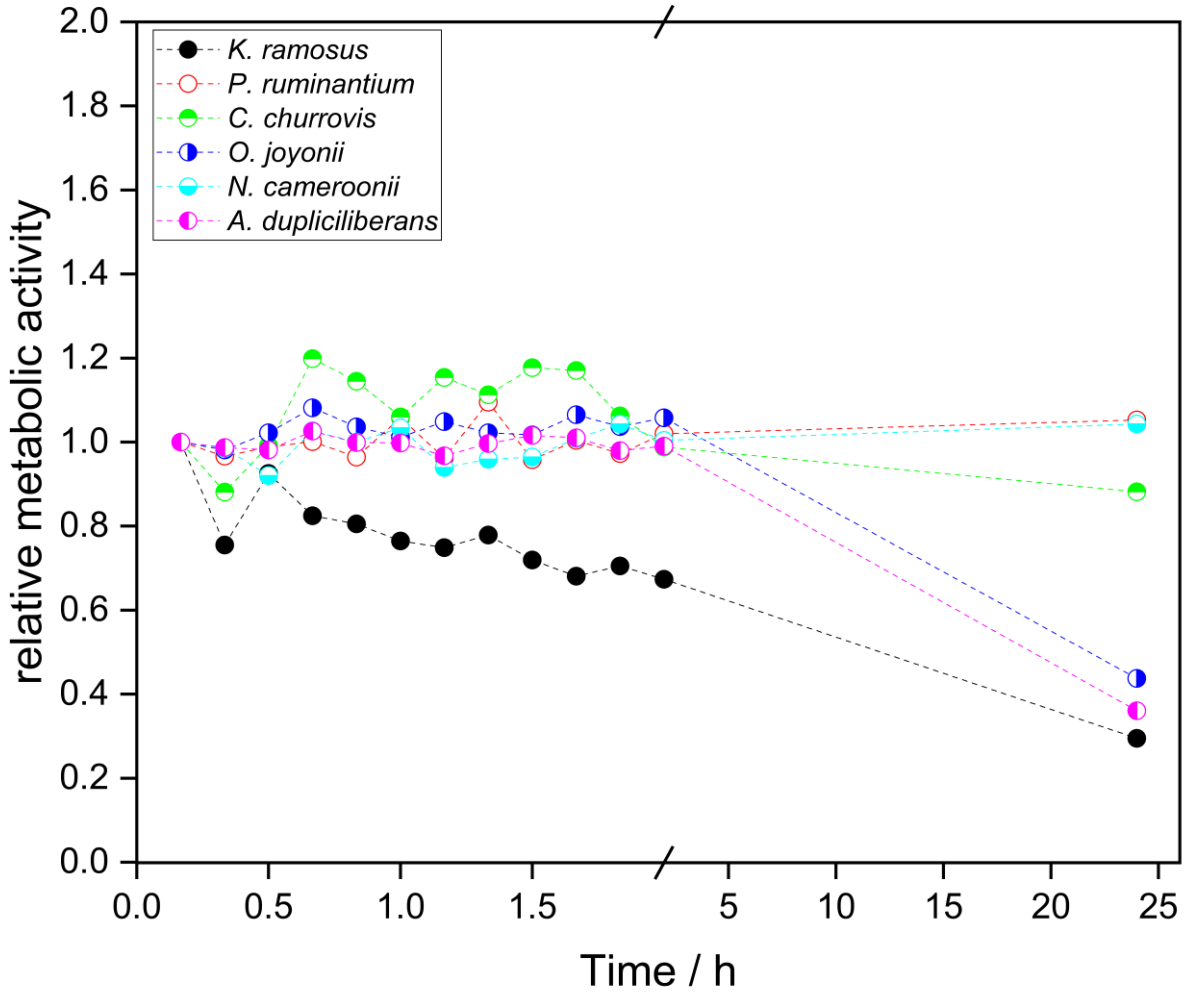

Figure S2: Relative metabolic activity of the next generation after temperature shock at room temperature.

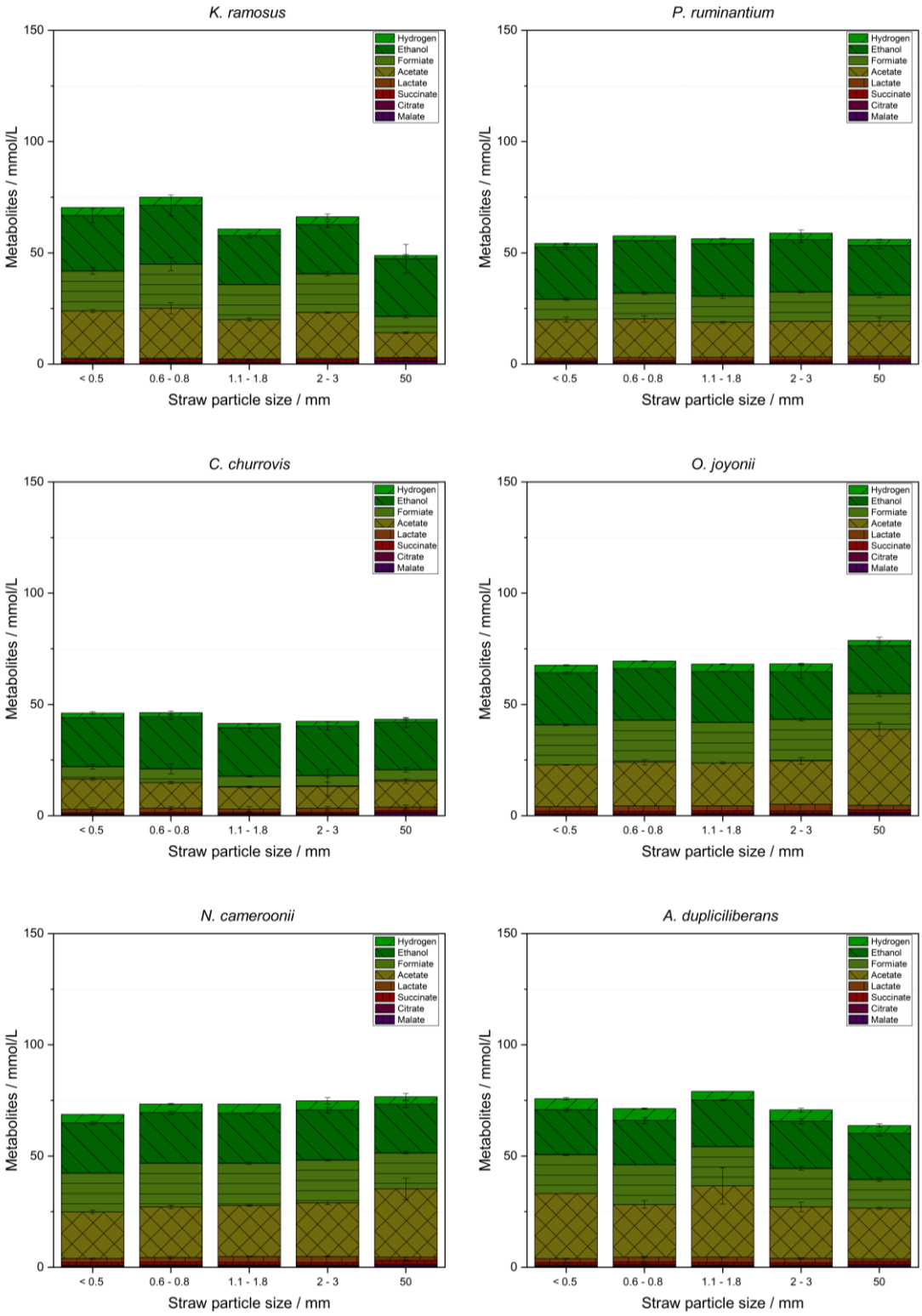

Figure S3: Total metabolite amount produced with different substrate particle sizes.

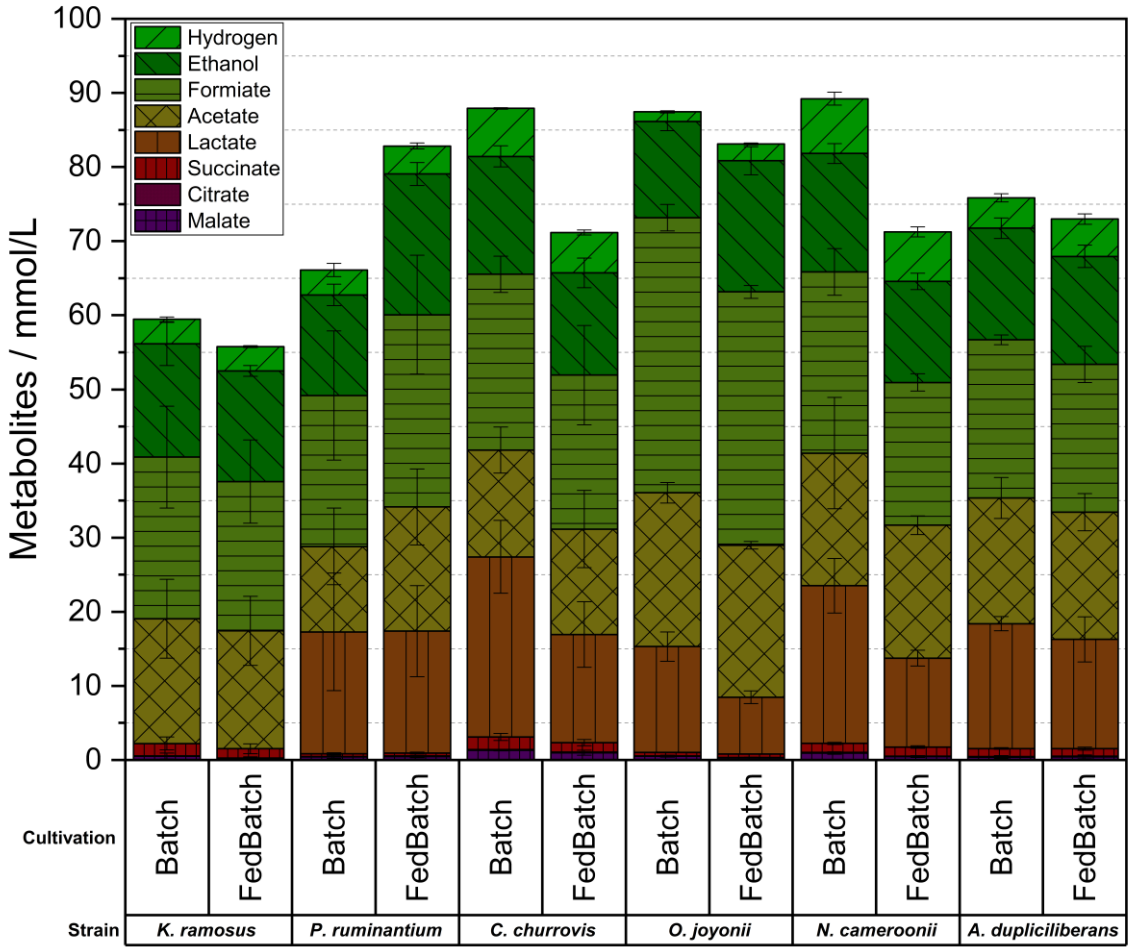

Figure S4: Amount of produced metabolites in batch and fed batch approach.

Table S2: Mean values, standard deviation, standard error of the mean and 95 % confidance intervals from the conducted tukey test for particle sizes.

Substrate	Particle size	Mean value	Standard deviation	*Standard Error of the Mean*	*95 % - Confidence Intervals Lower boundary*	*95 % - Confidence Intervals Upper boundary*
Citrate	≤ 0.5	0.25417	0.08246	0.03367	0.1881768	0.3201632
	0.6 - 0.8	0.28947	0.17579	0.07177	0.1488008	0.4301392
	1.1 - 1.8	0.26607	0.05896	0.02407	0.2188928	0.3132472
	2-3	0.25057	0.05081	0.02074	0.2099196	0.2912204
	50	0.2643	0.06906	0.02819	0.2090476	0.3195524
Malate	≤ 0.5	0.57963	0.03453	0.0141	0.551994	0.607266
	0.6 - 0.8	0.6154	0.04983	0.02034	0.5755336	0.6552664
	1.1 - 1.8	0.63677	0.05183	0.02116	0.5952964	0.6782436
	2-3	0.60723	0.05321	0.02172	0.5646588	0.6498012
	50	1.0531	0.13715	0.05599	0.9433596	1.1628404
Succinate	≤ 0.5	1.0811	0.34931	0.14261	0.8015844	1.3606156
	0.6 - 0.8	1.11593	0.27554	0.11249	0.8954496	1.3364104
	1.1 - 1.8	1.04377	0.34216	0.13968	0.7699972	1.3175428
	2-3	1.06573	0.25682	0.10485	0.860224	1.271236
	50	1.29113	0.33012	0.13477	1.0269808	1.5552792
Lactate	≤ 0.5	1.40303	0.57845	0.23615	0.940176	1.865884
	0.6 - 0.8	1.70063	0.65751	0.26843	1.1745072	2.2267528
	1.1 - 1.8	1.7082	0.76397	0.31189	1.0968956	2.3195044
	2-3	1.93413	0.89153	0.36396	1.2207684	2.6474916
	50	1.26813	0.61486	0.25102	0.7761308	1.7601292
Formiate	≤ 0.5	14.27893	5.44744	2.22391	9.9200664	18.6377936
	0.6 - 0.8	15.64993	5.57351	2.27537	11.1902048	20.1096552
	1.1 - 1.8	14.57273	5.3802	2.19646	10.2676684	18.8777916
	2-3	15.16483	5.43222	2.2177	10.818138	19.511522
	50	11.59613	4.51575	1.84355	7.982772	15.209488
Acetate	≤ 0.5	20.2293	5.22345	2.13246	16.0496784	24.4089216
	0.6 - 0.8	19.5867	4.57241	1.86668	15.9280072	23.2453928
	1.1 - 1.8	19.6175	7.47534	3.0518	13.635972	25.599028
	2-3	18.8414	5.27326	2.1528	14.621912	23.060888
	50	21.00663	9.84474	4.0191	13.129194	28.884066
Hydrogen	≤ 0.5	3.23537	1.23943	0.50599	2.2436296	4.2271104
	0.6 - 0.8	3.39433	1.24363	0.50771	2.3992184	4.3894416
	1.1 - 1.8	3.12527	0.83986	0.34287	2.4532448	3.7972952
	2-3	3.55627	0.98757	0.40317	2.7660568	4.3464832
	50	2.4492	0.91816	0.37484	1.7145136	3.1838864
Ethanol	≤ 0.5	22.72843	1.55003	0.6328	21.488142	23.968718
	0.6 - 0.8	23.1525	2.0715	0.84569	21.4949476	24.8100524
	1.1 - 1.8	22.22543	0.86774	0.35425	21.5311	22.91976
	2-3	22.1032	0.79597	0.32495	21.466298	22.740102
	50	22.28167	1.84565	0.75348	20.8048492	23.7584908

Table S3: Mean values, standard deviation and standard error of the mean from the conducted tukey test for batch vs. fedbatch.

Substrate	Feeding	Mean value	Standard deviation	*Standard Error of the Mean*	*95 % - Confidence Intervals Lower boundary*	*95 % - Confidence Intervals Upper boundary*
Citrate	Batch	0.05937	0.0084	0.00343	0.0526472	0.0660928
	FedBatch	0.064	0.01363	0.00556	0.0531024	0.0748976
Malate	Batch	0.68327	0.3747	0.15297	0.3834488	0.9830912
	FedBatch	0.4745	0.27246	0.11123	0.2564892	0.6925108
Succinate	Batch	1.0883	0.57664	0.23541	0.6268964	1.5497036
	FedBatch	0.9346	0.40594	0.16572	0.6097888	1.2594112
Lactate	Batch	15.52047	8.42591	3.43986	8.7783444	22.2625956
	FedBatch	10.91193	6.15546	2.51296	5.9865284	15.8373316
Formiate	Batch	24.79383	6.2265	2.54196	19.8115884	29.7760716
	FedBatch	23.36633	5.81654	2.37459	18.7121336	28.0205264
Acetate	Batch	16.39443	3.14064	1.28216	13.8813964	18.9074636
	FedBatch	17.0818	2.0993	0.85704	15.4020016	18.7615984
Hydrogen	Batch	4.32937	2.24023	0.91457	2.5368128	6.1219272
	FedBatch	4.40713	1.61121	0.65777	3.1179008	5.6963592
Ethanol	Batch	14.7894	1.2527	0.51141	13.7870364	15.7917636
	FedBatch	15.60677	2.21379	0.90377	13.8353808	17.3781592

10.2 Chapter 2: Ferricyanide-dependent current production by *Neocallimastix cameroonii* G341 in a miniaturized anaerobic bioelectrochemical system

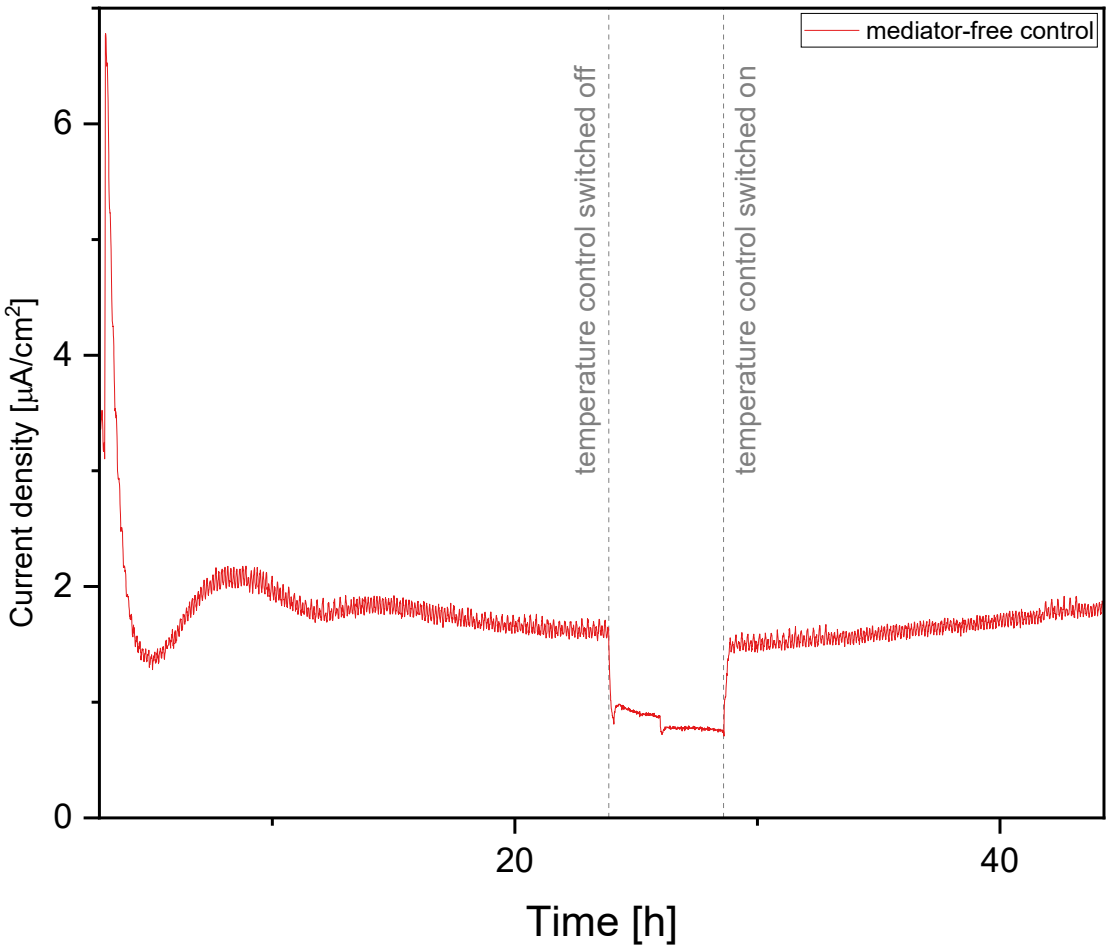

Figure S5: Zoom-in from Figure 2. Chronoamperometric current density profiles of anaerobic gut fungal culture cultivated in the eCuvette system. Current density (µA cm⁻²) is plotted against elapsed time since inoculation. A pronounced and reproducible current response is measured 5 hours after inoculation even in the sample without added exogenous mediators.

10.3 Chapter 3: Beyond Carbon Dioxide: Decoupling Headspace and Buffering Reveals a Bicarbonate Requirement for Anaerobic Gut Fungi Growth

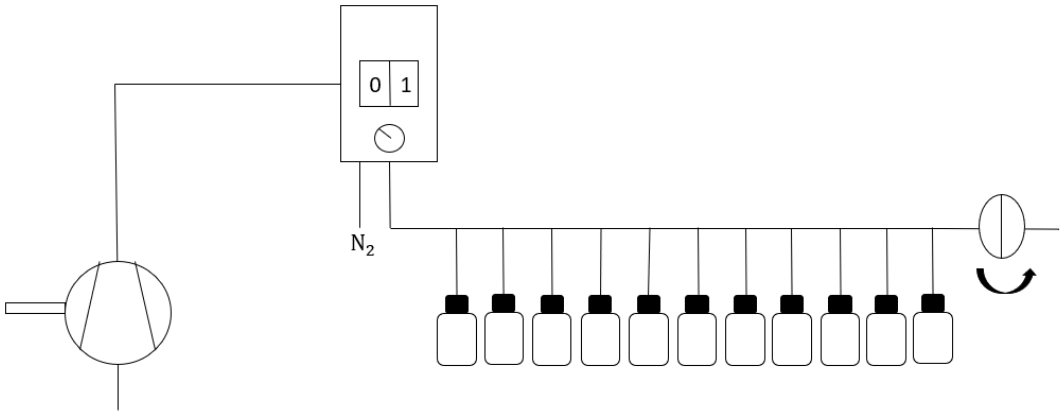

Figure S6: Schematic representation of the custom-built anaerobization station used for N_2-based cultivation. The system enables sequential evacuation and nitrogen overpressure cycles of sealed serum bottles to establish anaerobic conditions prior to incubation.

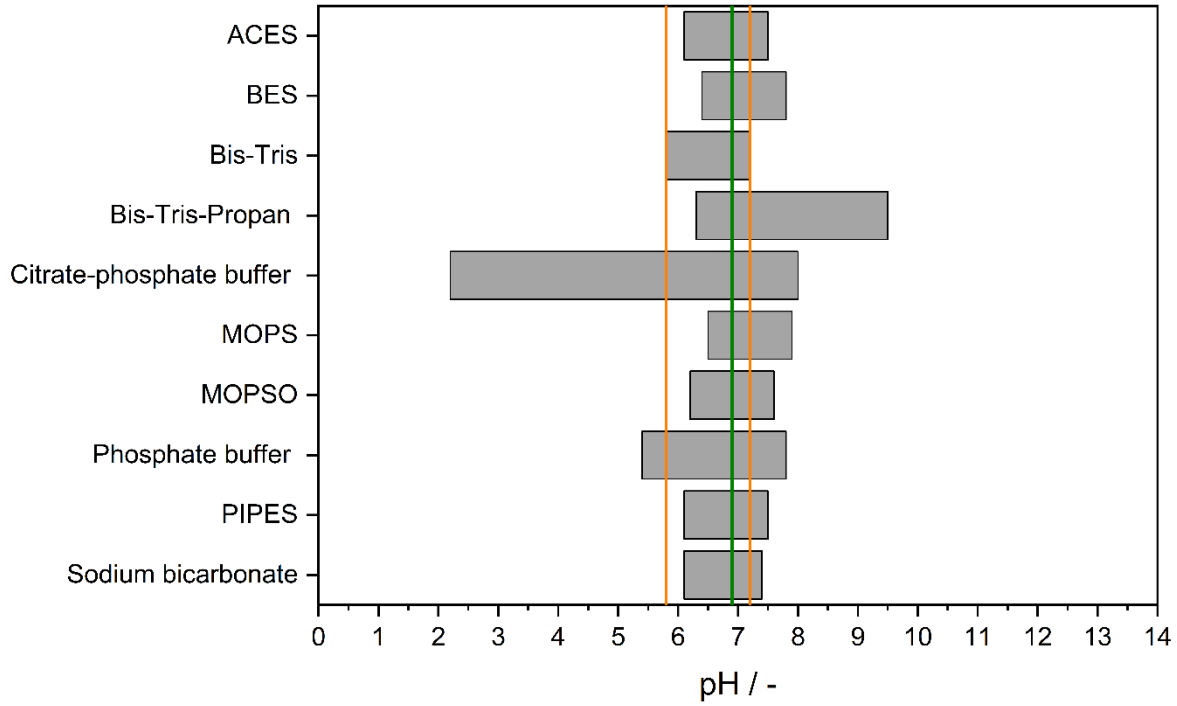

Figure S7: Buffering ranges of the selected non-carbonate buffer systems across the investigated concentration series. Orange lines indicate the physiological rumen pH range, and the green line denotes the commonly reported pH optimum for anaerobic gut fungi cultivation.

Table S4: Overview of buffer–concentration combinations evaluated in the initial buffer screening under N_2 atmosphere. Numbers indicate experimental conditions used for subsequent biological evaluation. Only buffer systems maintaining post-sterilization pH values within the defined stability range (6.9 ± 0.1) were selected for further cultivation experiments.

Concentration [g/L]	0,5	1,0	2,0	4,0	6,0	8,0	10
ACES		1	2	3	4	5	6
BES				7	8	9	10
Bis-Tris			11	12	13	14	15
Bis-Tris-Propan				16	17		
Citrate-phosphate buffer					18		
MOPS	19	20	21	22	23	24	25
MOPSO		26	27	28	29	30	31
Phosphate buffer		32	33	34	35	36	37
PIPES					38		
Sodium bicarbonate		39					

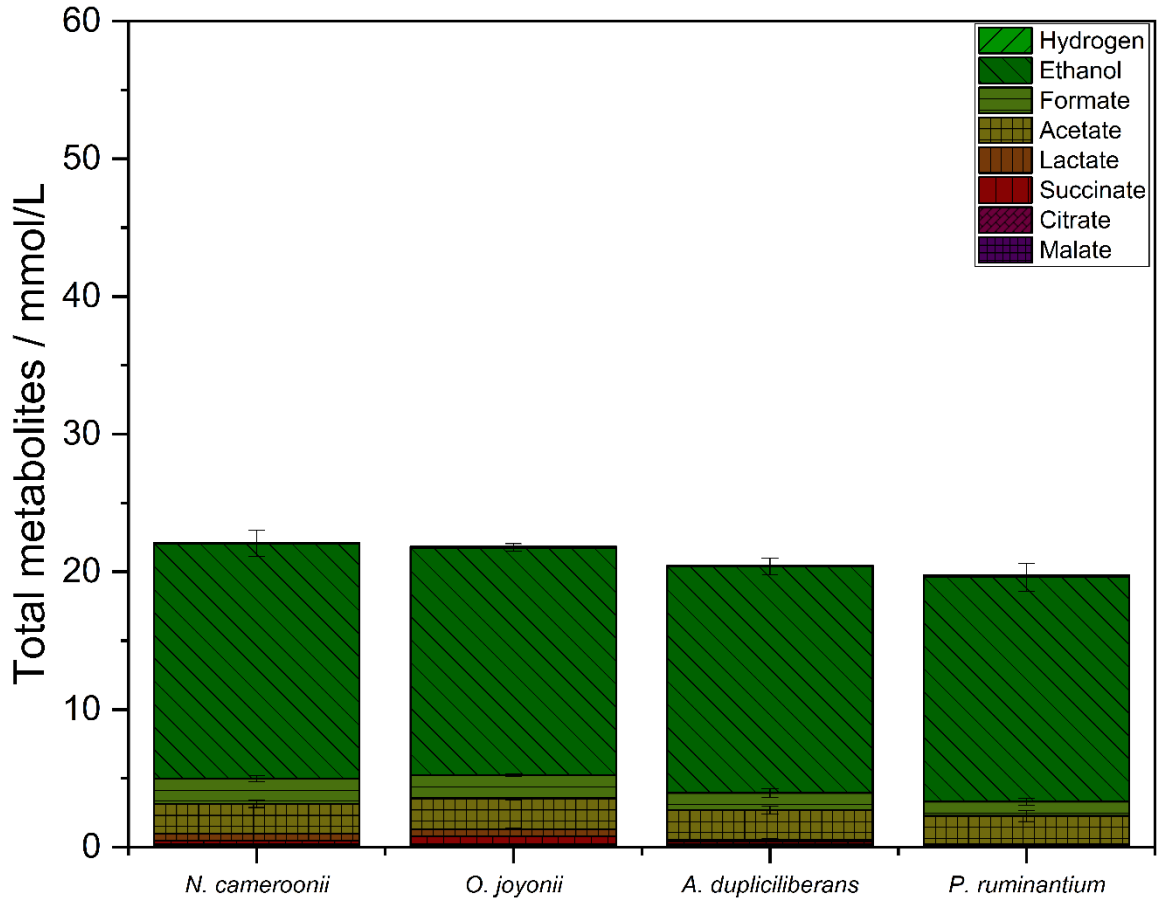

Figure S8: Sodium control experiment for bicarbonate supplementation. NaCl was added at concentrations equivalent to the molar Na^+ contribution of the respective $NaHCO_3$ treatment to discriminate between bicarbonate-specific effects and potential sodium-associated influences on growth. Growth performance was assessed by hydrogen production and metabolite formation under 100% N_2 atmosphere. No growth was detected.

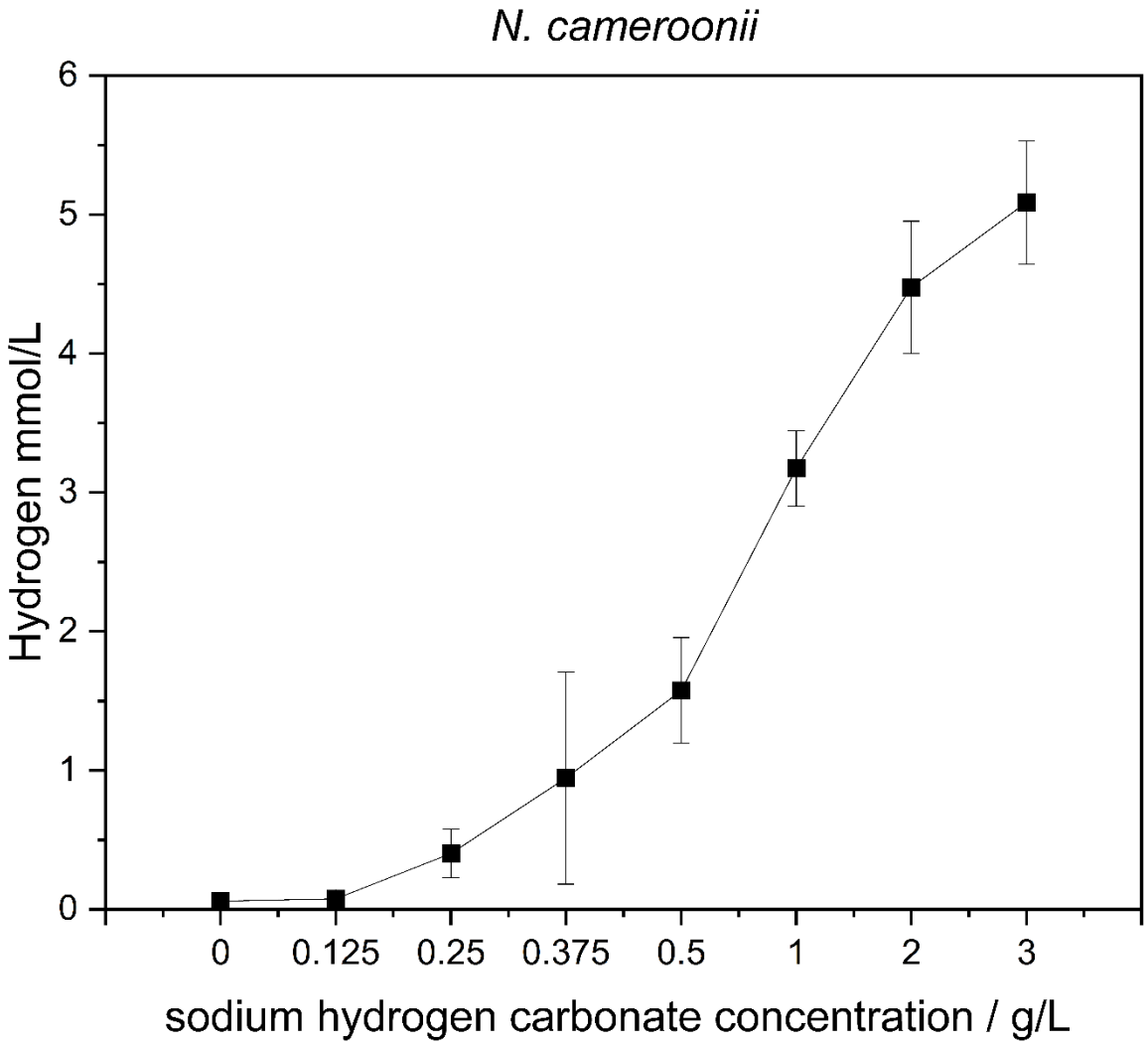

Figure S9: Hydrogen production of N. cameroonii during the minimal sodium carbonate experiment under 100% N_2 atmosphere with increasing sodium hydrogen carbonate concentrations (0–3 g L^{-1}). Hydrogen formation is shown separately as exemplary to highlight plateau like behavior. H_2 production increased strongly between 0.25 and 2 g L^{-1} $NaHCO_3$ and showed smaller incremental gains between 2 and 3 g L^{-1}, indicating an approach toward saturation rather than a fully resolved plateau within the tested concentration range. Data represent biological triplicates (n = 3); error bars indicate standard deviation.

10.4 Chapter 4: Phosphate Versus Nitrogen Limitation: A Reactor-Scale Process Comparison for Single-Cell Oil Production in Oleaginous Yeasts

Methods – 2.16 Influence of antifoam on analytical measurements

The influence of the antifoam agent Contraspum A 4050 on oxygen transfer was assessed under reactor-scale conditions using a 2.5 L stirred-tank bioreactor (Minifors, Infors HT) equipped with a VisiFerm DO Arc 225 H0 probe (Hamilton). Oxygen transfer measurements were performed using a standard dynamic gassing-out approach, in which dissolved oxygen was depleted by nitrogen flushing and re-saturated by switching to air aeration. Dissolved oxygen recovery was recorded at 3 s intervals using BlueVis software (version 4.64.96).

Contraspum A 4050 was added stepwise to final concentrations ranging from 0 to 1000 µL per 1.2 L working volume in increments of 100 µL. Each concentration was measured in triplicate. Oxygen transfer rates were calculated from the temporal increase in dissolved oxygen concentration, and maximum OTR values were determined from consecutive measurement intervals for graphical evaluation.

The influence of Contraspum A 4050 on optical density measurements was evaluated by adding defined antifoam concentrations (250–2000 µL L^{-1}) to nitrogen-limited cultivation medium and recording absorbance spectra between 230 and 1000 nm. Potential interference with fatty acid methyl ester (FAME) analysis was assessed by subjecting pure antifoam to the transesterification and gas chromatographic analysis protocol.

Table S5: Initial nitrogen and phosphorus concentrations in the mineral salt solutions used for nitrogen-limited, phosphate-limited and nutrient-replete cultivations (unlimited), excluding yeast extract.

Mineral salt solution	Nitrogen amount [mmol/L]	Phosphorus amount [mmol/L]
Nitrogen limited media	7.57	15.22
Phosphate limited media	160.43	1.74
Unlimited media	160.43	15.22

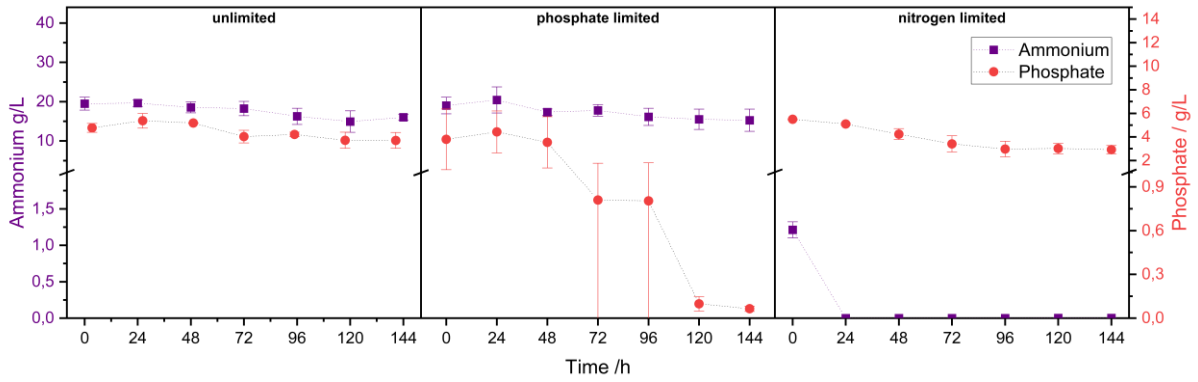

Figure S10: Temporal profiles of ammonium and phosphate concentrations during nitrogen-limited, phosphate-limited and nutrient-replete cultivations of Cutaneotrichosporon oleaginosum, shown as mean values (n = 2). Dotted lines indicate trends for visual guidance only.

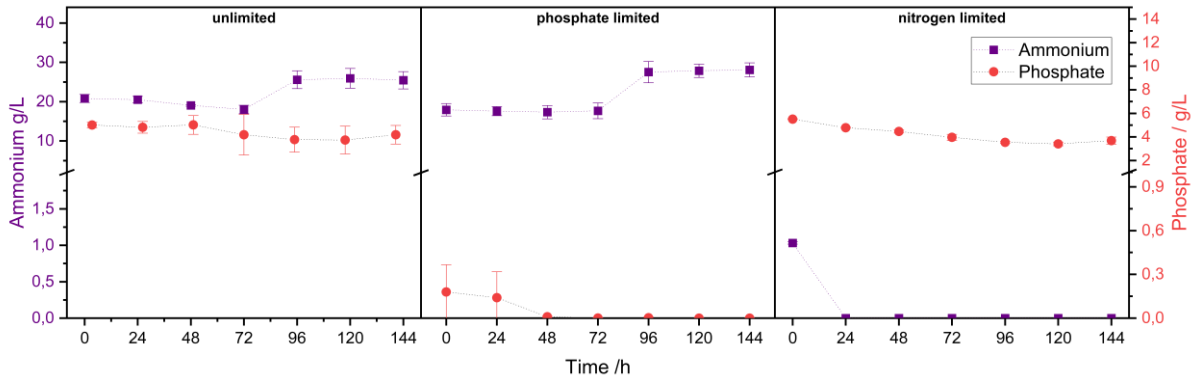

Figure S11: Temporal profiles of ammonium and phosphate concentrations during nitrogen-limited, phosphate-limited and nutrient-replete cultivations of Saitozyma podzolica, shown as mean values (n = 2). Dotted lines indicate trends for visual guidance only.

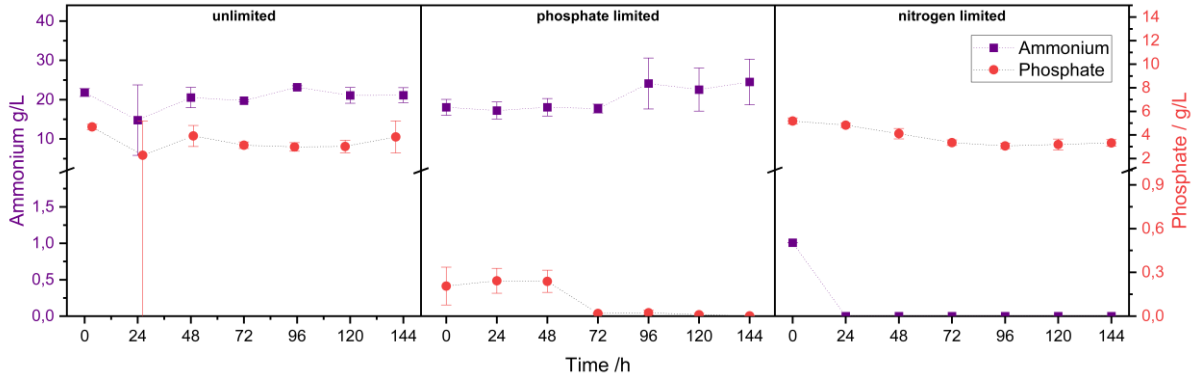

Figure S12: Temporal profiles of ammonium and phosphate concentrations during nitrogen-limited, phosphate-limited and nutrient-replete cultivations of Scheffersomyces segobiensis, shown as mean values (n = 2). Dotted lines indicate trends for visual guidance only

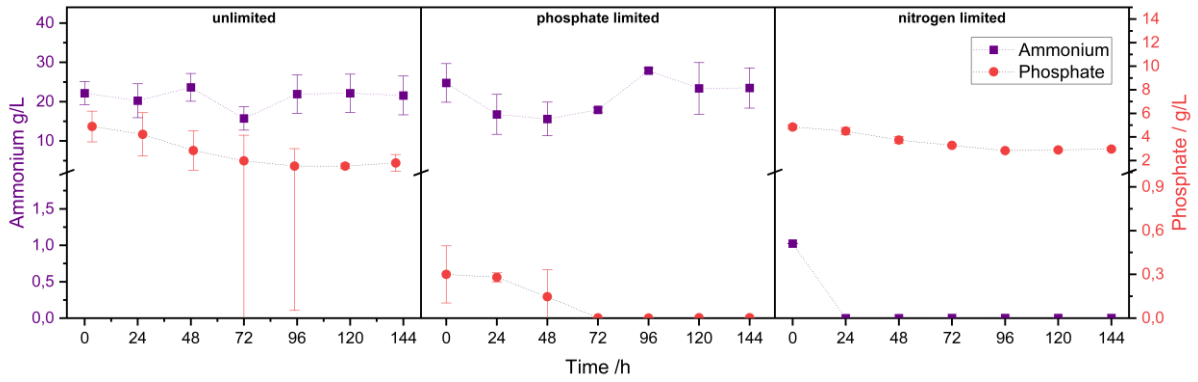

Figure S13: Temporal profiles of ammonium and phosphate concentrations during nitrogen-limited, phosphate-limited and nutrient-replete cultivations of Apiotrichum porosum, shown as mean values (n = 2). Dotted lines indicate trends for visual guidance only.

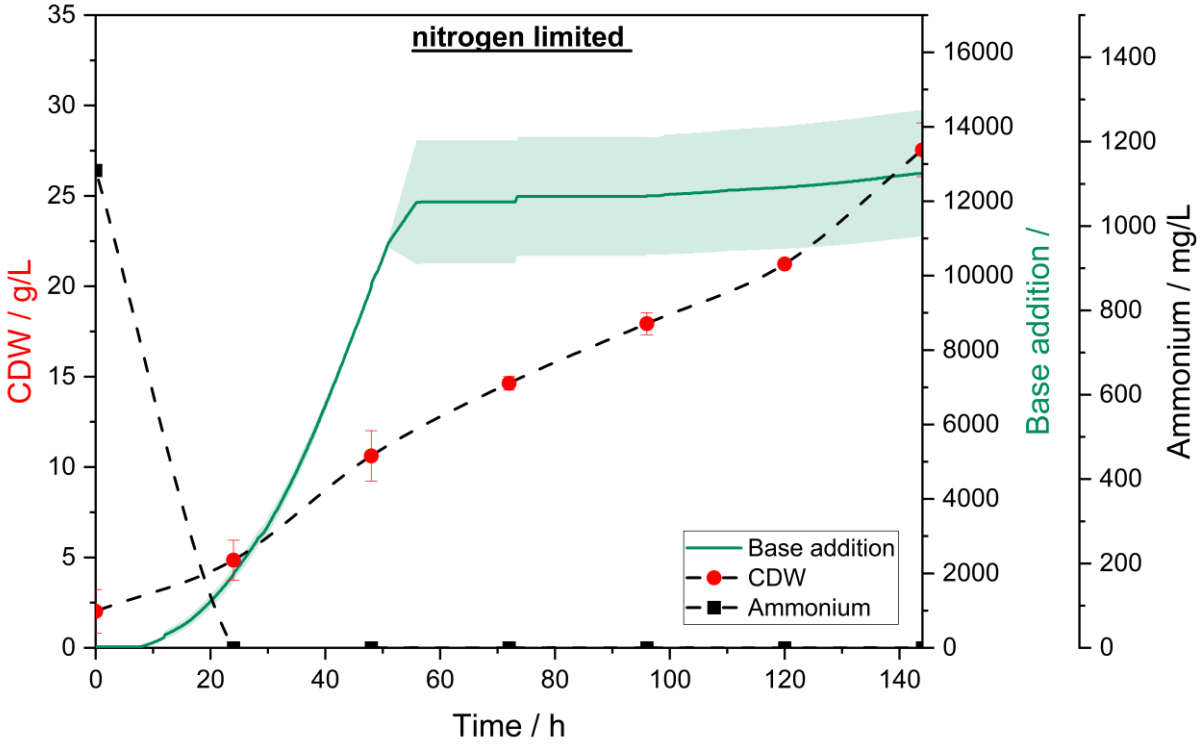

Figure S14: Correlation between cumulative base addition and ammonium depletion during nitrogen-limited cultivation of Cutaneotrichosporon oleaginosum (n = 2). Dotted lines indicate trends for visual guidance only.

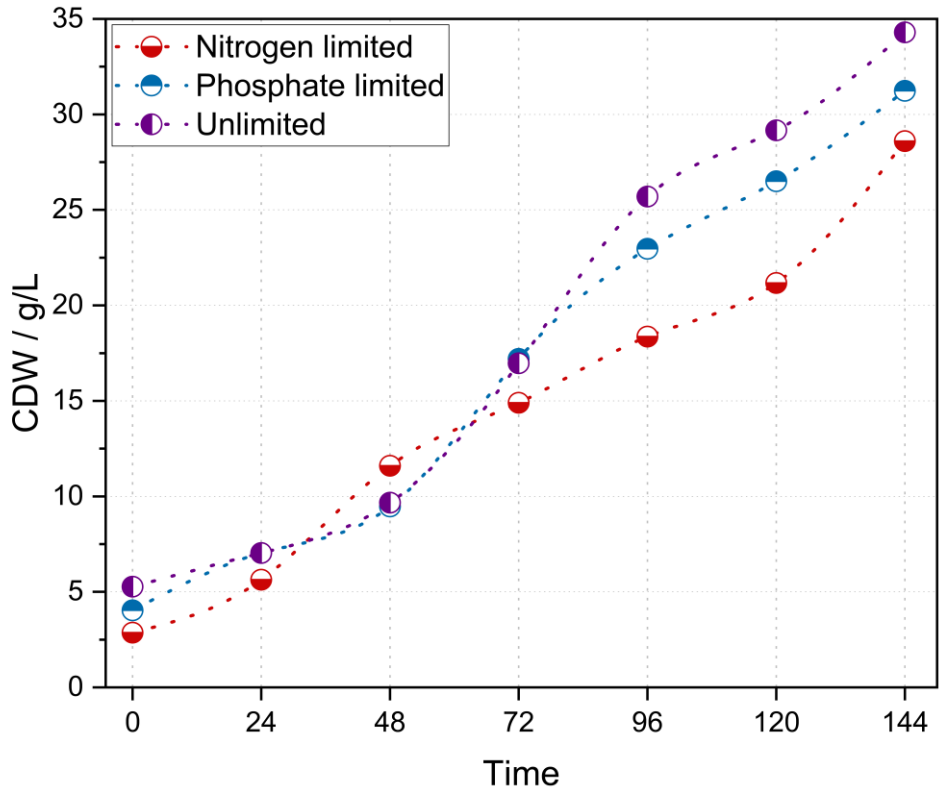

Figure S15: Representative cultivation profiles of Cutaneotrichosporon oleaginosum under nitrogen-limited, phosphate-limited and nutrient-replete conditions. Dotted lines indicate trends for visual guidance only.

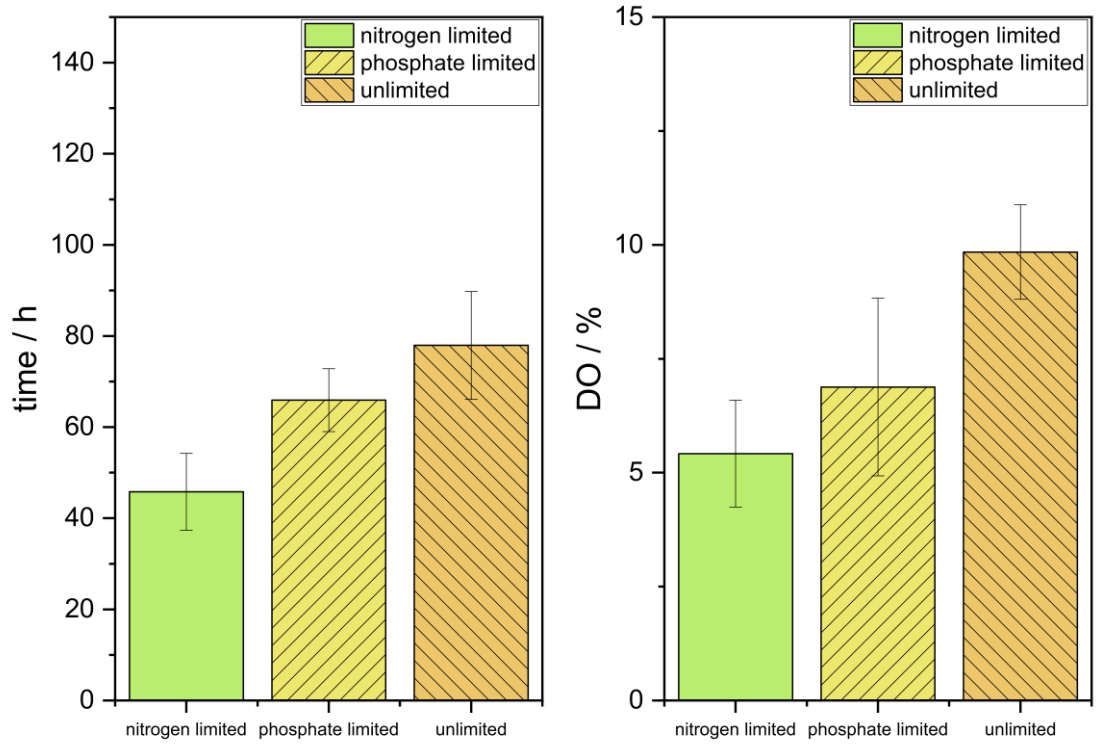

Figure S16: Time to minimum dissolved oxygen concentration and minimum dissolved oxygen levels during bioreactor cultivations, shown as mean values across all tested oleaginous yeast strains (n = 5).

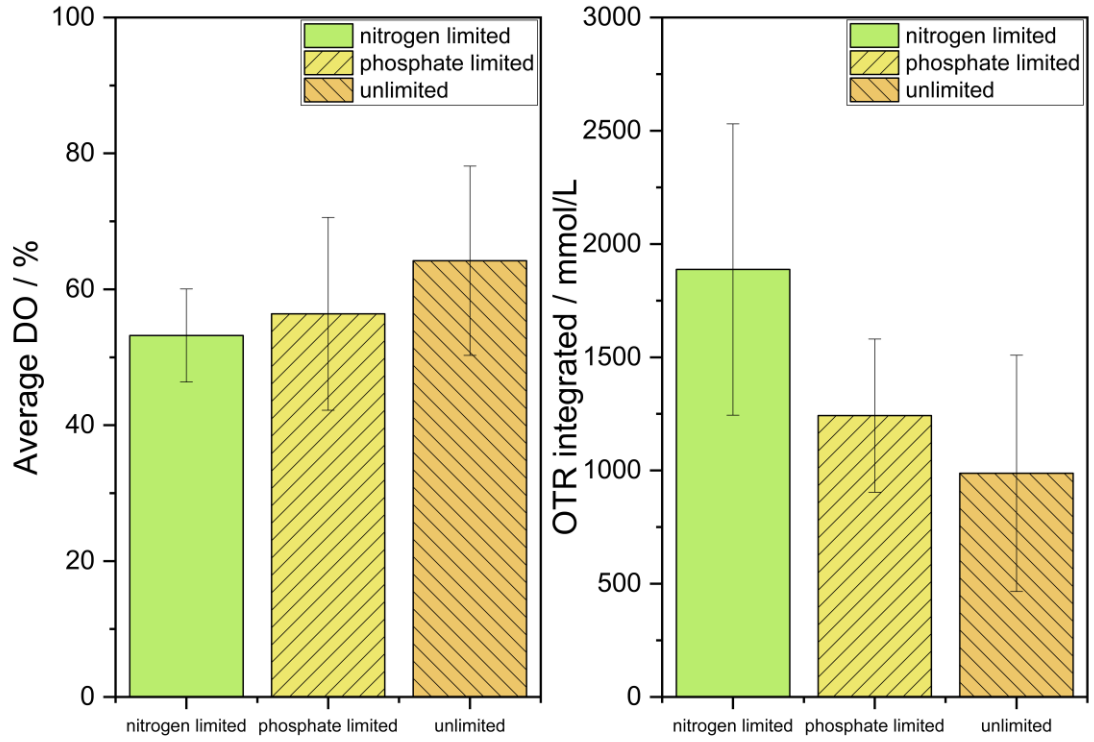

Figure S17: Average dissolved oxygen profiles and cumulative oxygen consumption during bioreactor cultivations under nitrogen-limited, phosphate-limited and nutrient-replete conditions (n = 6–8).

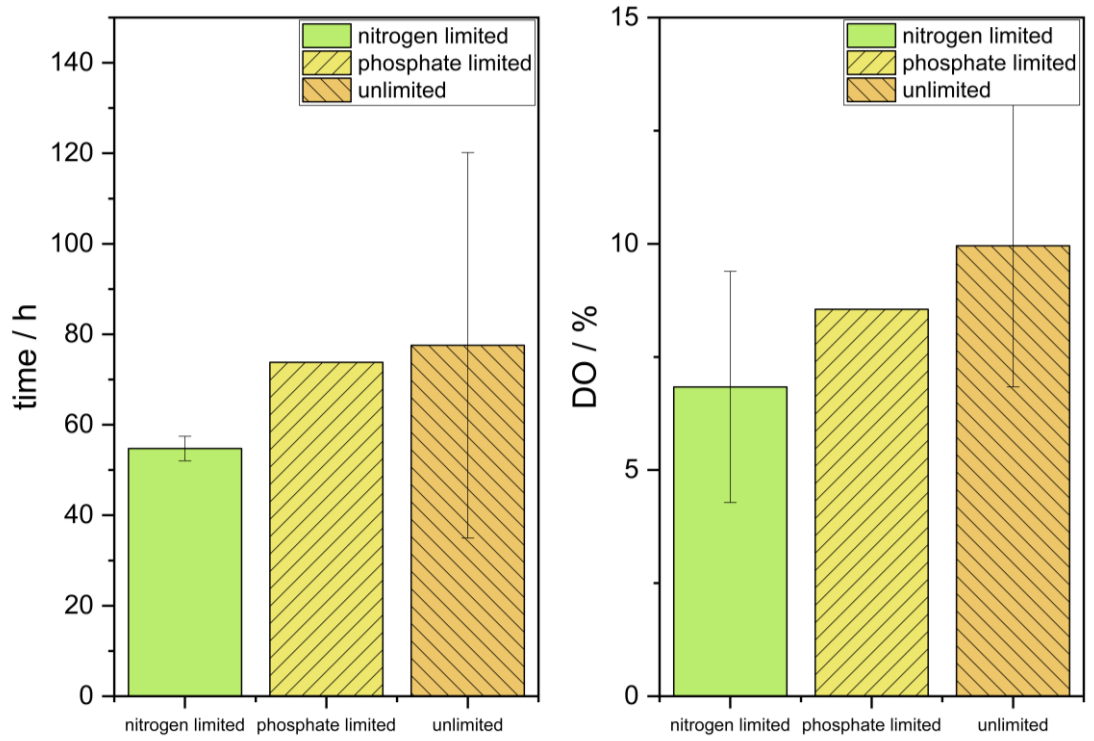

Figure S18: Time to minimum dissolved oxygen concentration and minimum dissolved oxygen levels during cultivation of Cutaneotrichosporon oleaginosum (n = 2). Phosphate-limited cultivation is shown as a single replicate.

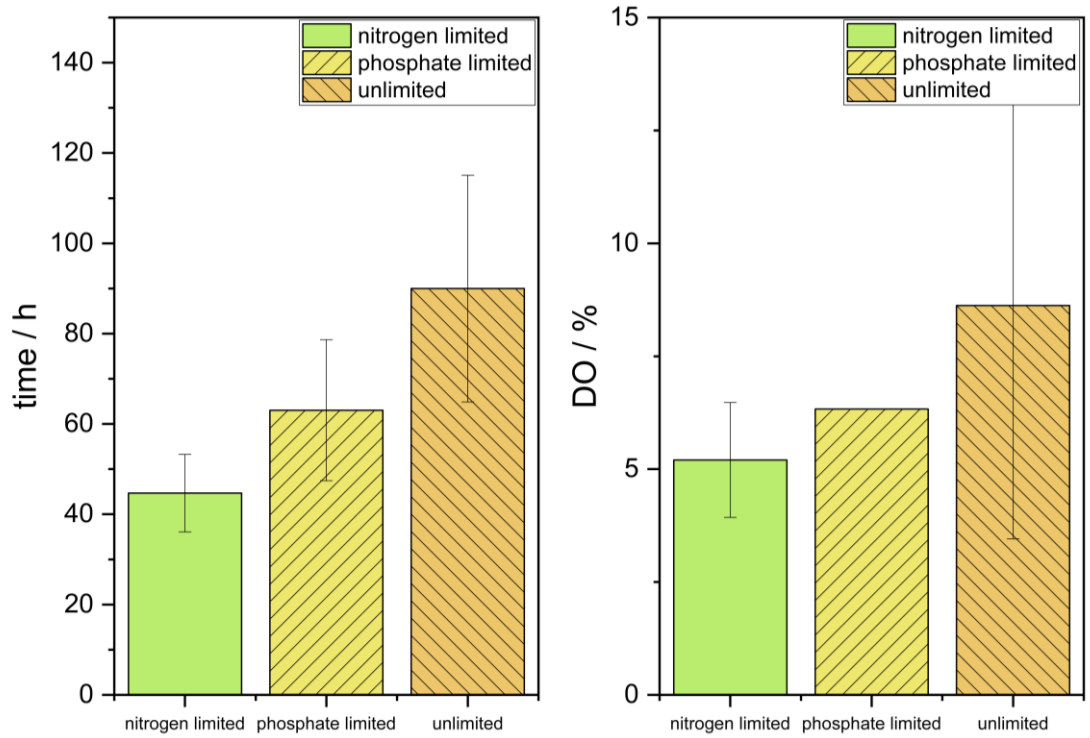

Figure S19: Time to minimum dissolved oxygen concentration and minimum dissolved oxygen levels during cultivation of Saitozyma podzolica (n = 2). Phosphate-limited cultivation is shown as a single replicate.

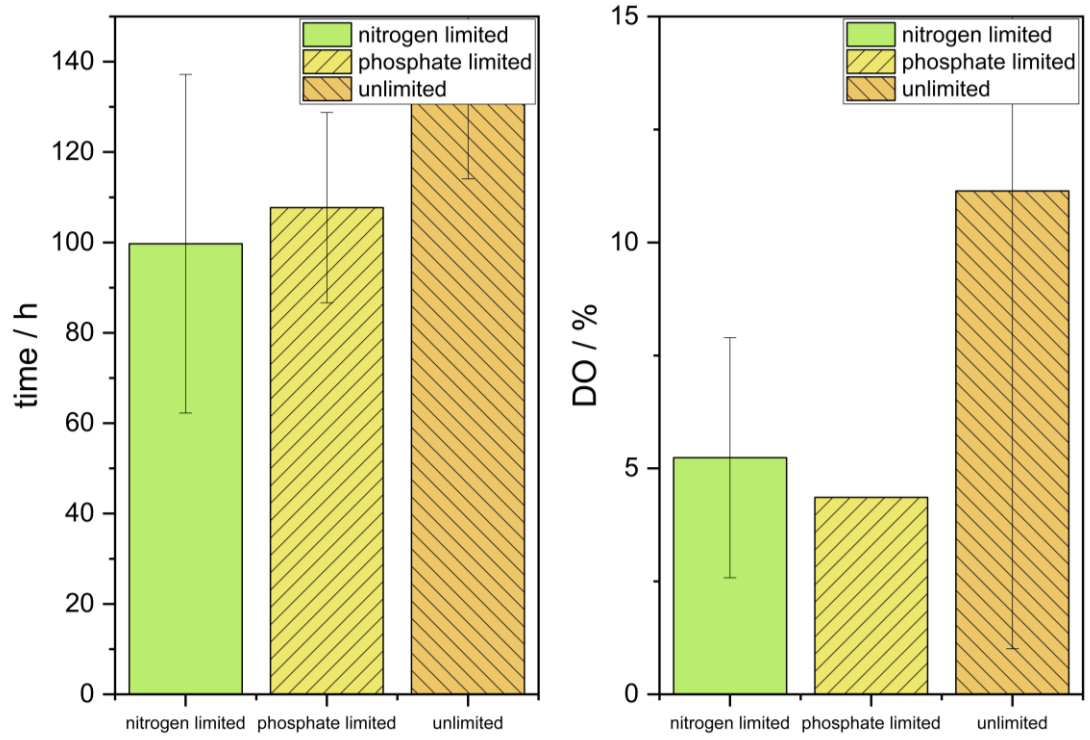

Figure S20: Time to minimum dissolved oxygen concentration and minimum dissolved oxygen levels during cultivation of Scheffersomyces segobiensis (n = 2). Phosphate-limited cultivation is shown as a single replicate.

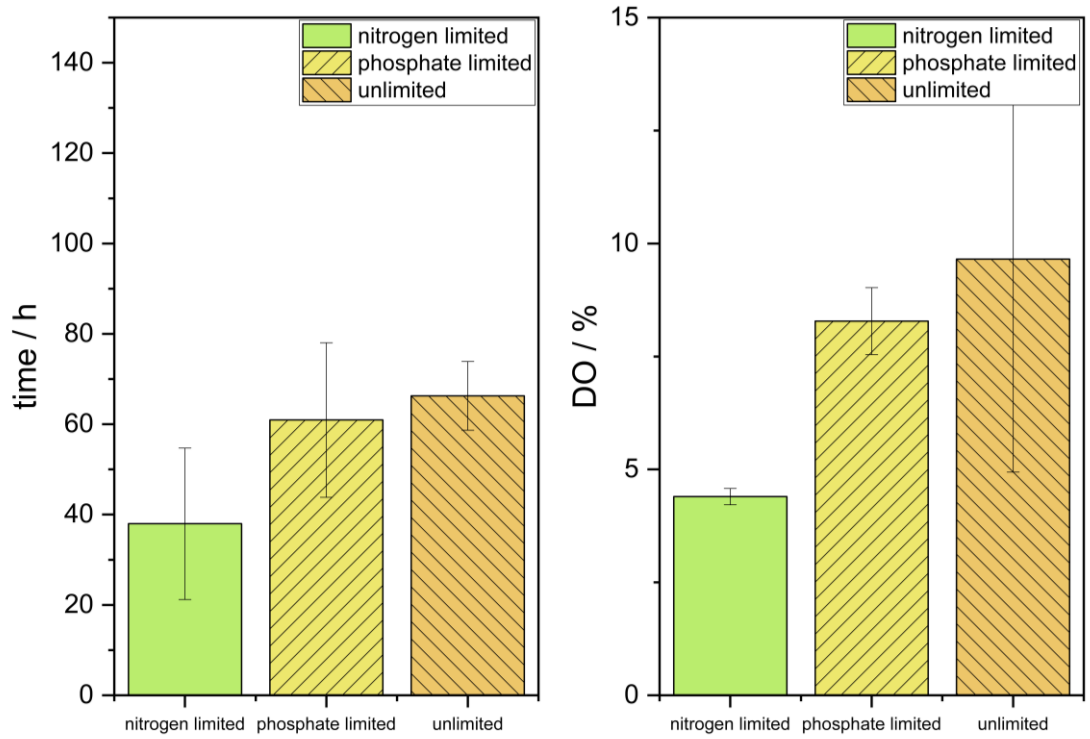

Figure S21: Time to minimum dissolved oxygen concentration and minimum dissolved oxygen levels during cultivation of Apiotrichum porosum (n = 2).

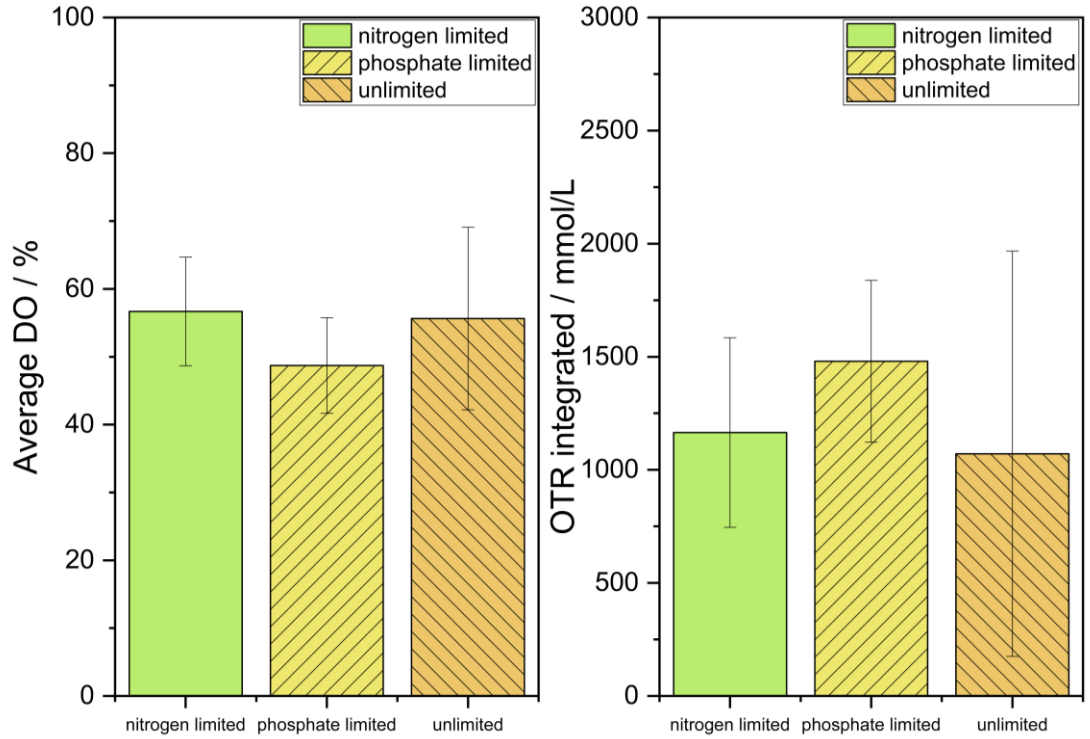

Figure S22: Integrated dissolved oxygen profiles and cumulative oxygen transfer rates during cultivation of Cutaneotrichosporon oleaginosum (n = 2).

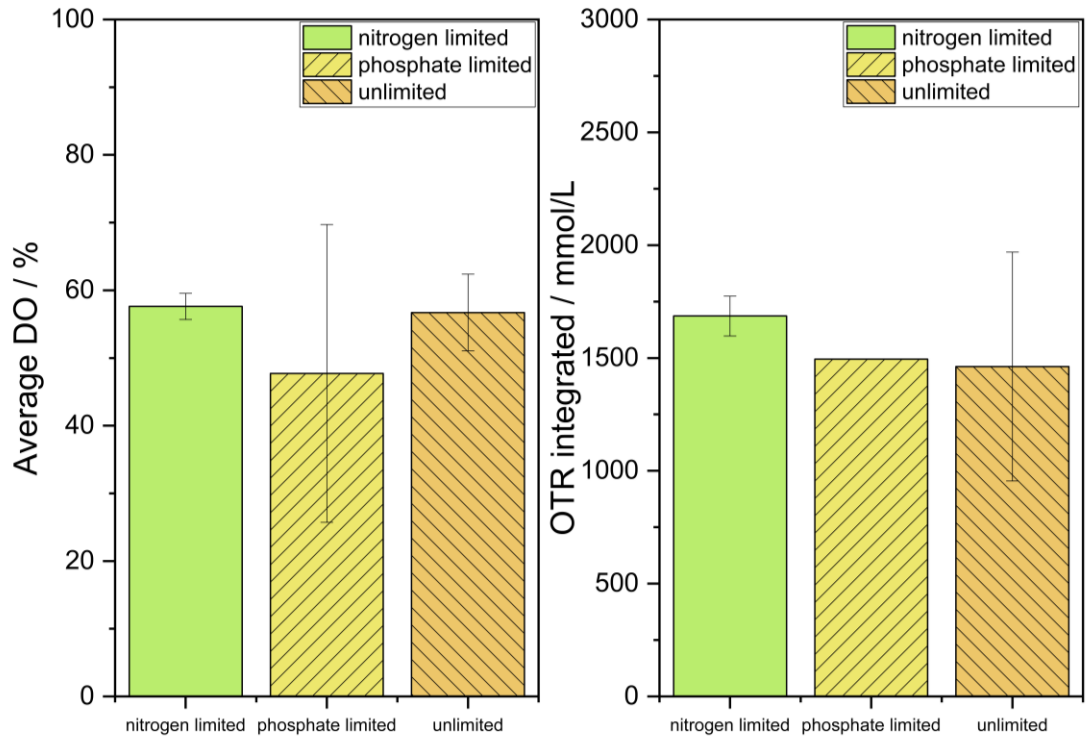

Figure S23: Integrated dissolved oxygen profiles and cumulative oxygen transfer rates during cultivation of Saitozyma podzolica (n = 2). Phosphate-limited cultivation is shown as a single replicate.

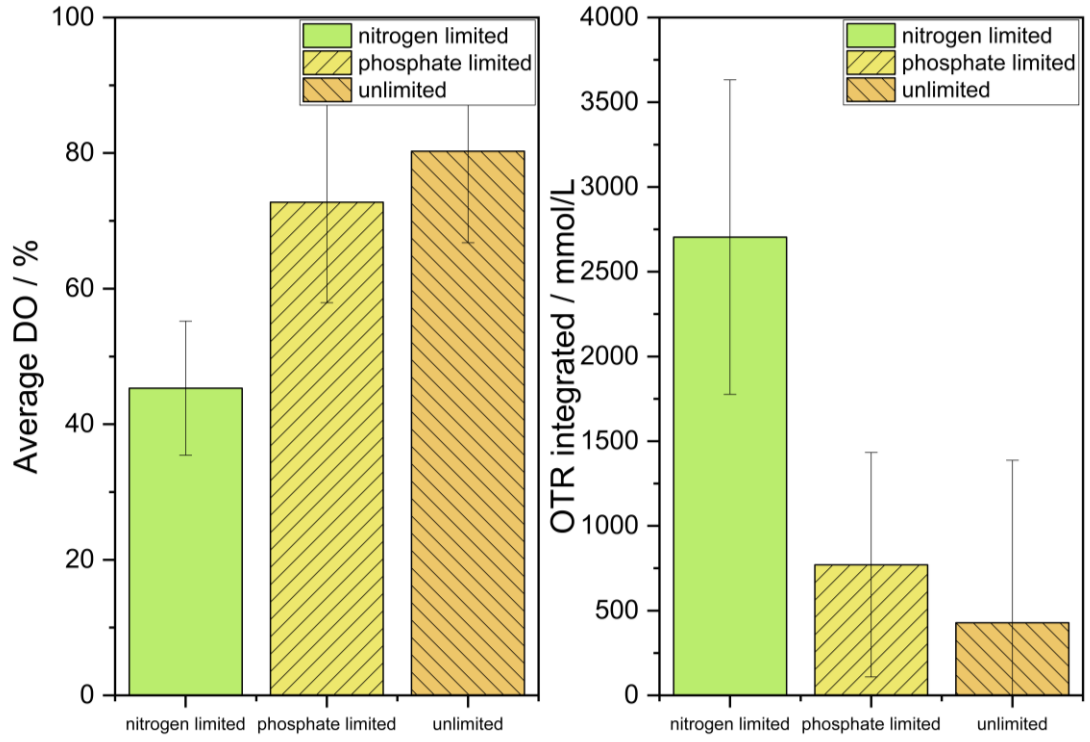

Figure S24: Integrated dissolved oxygen profiles and cumulative oxygen transfer rates during cultivation of Scheffersomyces segobiensis (n = 2).

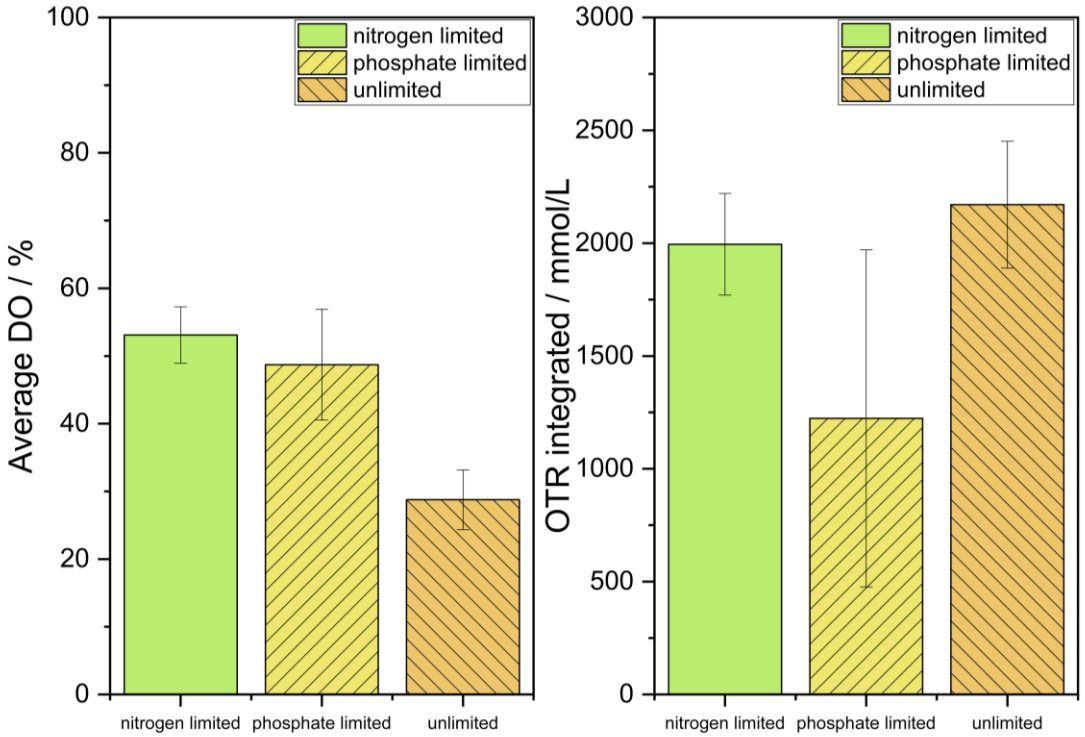

Figure S25: Integrated dissolved oxygen profiles and cumulative oxygen transfer rates during cultivation of Apiotrichum porosum (n = 2).

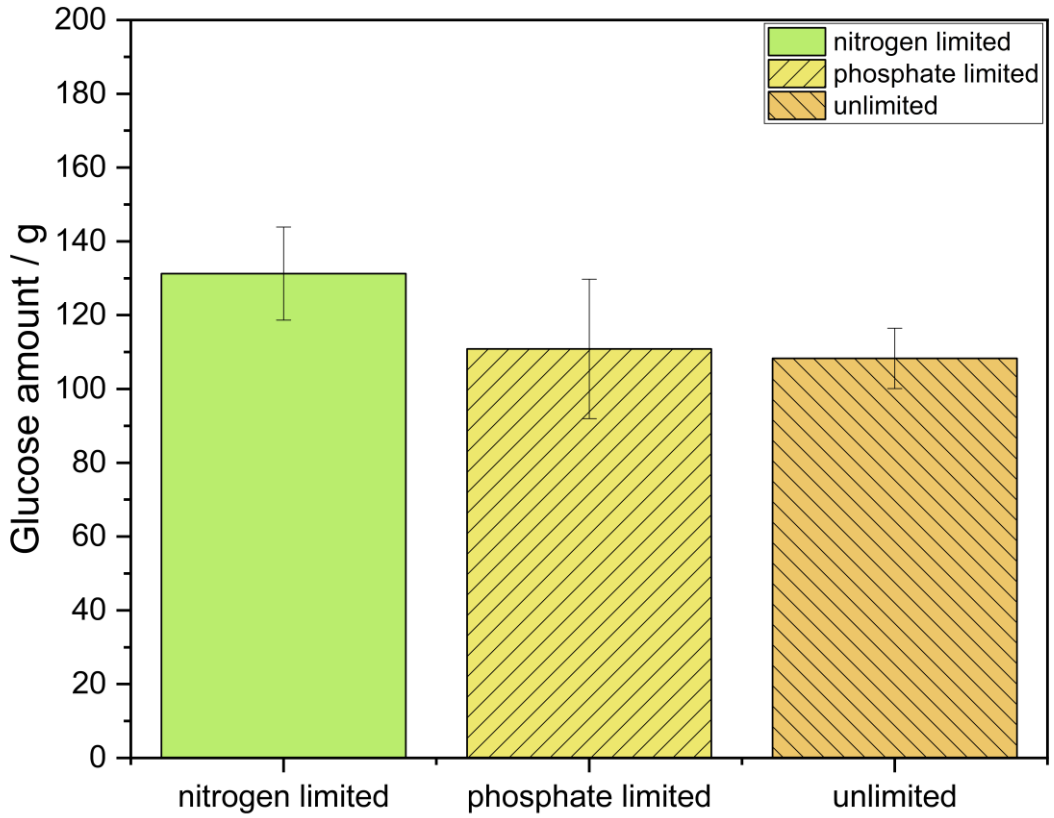

Figure S26: Total glucose consumption during bioreactor cultivations under nitrogen-limited, phosphate-limited and nutrient-replete conditions (1.2 L working volume; n = 6).

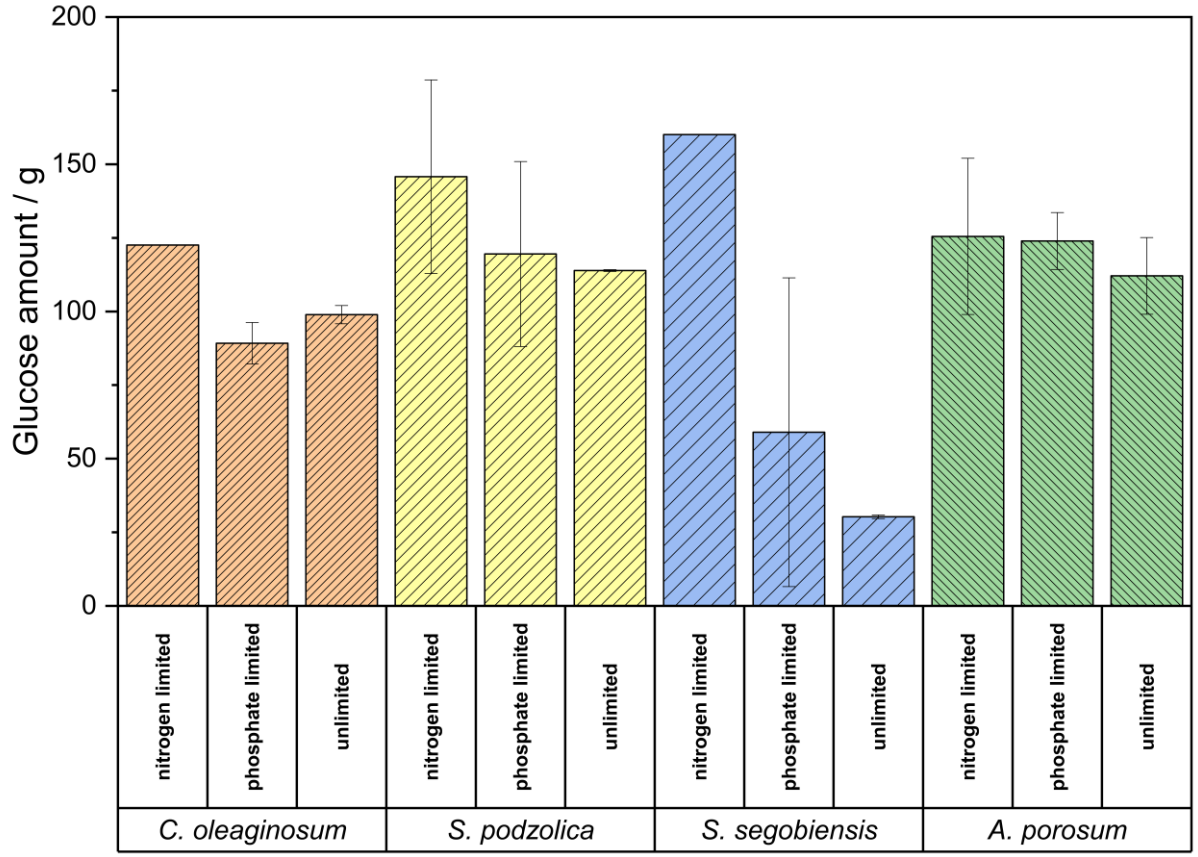

Figure S27: Strain-specific glucose consumption during bioreactor cultivations under nitrogen-limited, phosphate-limited and nutrient-replete conditions.

Table S6: Lipid yield on glucose for all tested oleaginous yeast strains under nitrogen-limited, phosphate-limited and nutrient-replete conditions.

Strain	Condition	Lipid / Glucose [g/g]
C. oleaginosum	nitrogen limited	0.076
	phosphate limited	0.068
	unlimited	0.022
S. podzolica	nitrogen limited	0.071
	phosphate limited	0.044
	unlimited	0.020
S. segobiensis	nitrogen limited	0.009
	phosphate limited	0.057
	unlimited	0.019
A. porosum	nitrogen limited	0.088
	phosphate limited	0.015
	unlimited	0.042

Table S7: Yields of gluconic acid and ethanol per gram of consumed glucose for all tested oleaginous yeast strains under nitrogen-limited, phosphate-limited and nutrient-replete conditions. Gluconic acid formation in C. oleaginosum was additionally confirmed qualitatively using a commercial assay kit (data not shown).

Strain	Condition	Gluconic acid / Glucose [g/g]	Ethanol / Glucose [g/g]
*C. oleaginosum**	nitrogen limited	0.014	0.004
	phosphate limited	0.077	0.003
	unlimited	0.058	0.003
S. podzolica	nitrogen limited	0.147	0.002
	phosphate limited	0.080	0.002
	unlimited	0.056	0.002
S. segobiensis	nitrogen limited	0.011	0.002
	phosphate limited	0.040	0.003
	unlimited	0.047	0.007
A. porosum	nitrogen limited	0.057	0.002
	phosphate limited	0.033	0.002
	unlimited	0.035	0.003

*Qualitatively **but not** quantitively confirmed additionally with an Gluconic acid kit (R-Biopharm) (Data not shown).

Table S8: Comparison of lipid production rates obtained in this study with literature-reported values for selected oleaginous yeasts under nitrogen-limited conditions.

Condition	Organism	Lipid production rate [g/L/h]	Source
Nitrogen limitation	*C. oleaginosum*	0.054 ± 0.004	This study
Phosphate limitation	*C. oleaginosum*	0.035 ± 0.015	This study
unlimited	*C. oleaginosum*	0.012 ± 0.007	This study
Nitrogen limitation	*S. podzolica*	0.060 ± 0.008	This study
Phosphate limitation	*S. podzolica*	0.031 ± 0.005	This study
unlimited	*S. podzolica*	0.013 ± 0.006	This study
Nitrogen limitation	*S. segobiensis*	0.008 ± 0.001	This study
Phosphate limitation	*S. segobiensis*	0.020 ± 0.003	This study
unlimited	*S. segobiensis*	0.003 ± 0.003	This study
Nitrogen limitation	*A. porosum*	0.064 ± 0.001	This study
Phosphate limitation	*A. porosum*	0.011 ± 0.012	This study
unlimited	*A. porosum*	0.027 ± 0.009	This study
Nitrogen limitation	*C. oleaginosum*	0.023	[175]
Nitrogen limitation	*L. starkeyi*	0.026	[266]
Nitrogen limitation	*S. segobiensis*	0.031	[173]
Nitrogen limitation	*A. porosum*	0.053	[170]
Nitrogen limitation	*S. podzolica*	0.060	[162]
Nitrogen limitation	*Y. lipolytica*	0.066	[267]
Nitrogen limitation	*R. toruloides*	0.260	[268]

Table S9: Chemical properties (average unsaturation (AU), Cetane number (CN), Iodine value (IV), kinematic viscosity (KV), specific gravity (SG) and heating value (HV)) of determined fatty acid profiles calculated after Qian et al. [170].

Condition	*AU*	*CN*	*IV*	*KV*	*SG*	*HV*
Nitrogen limited *C. oleaginosum*	0.80	57.53	72.38	4.70	0.87	39.95
Phosphate limited *C. oleaginosum*	0.52	59.44	51.04	4.88	0.87	39.44
unlimited *C. oleaginosum*	1.01	56.17	87.50	4.57	0.87	40.30
Nitrogen limited *S. podzolica*	0.84	57.29	74.98	4.68	0.87	40.01
Phosphate limited *S. podzolica*	0.43	59.98	44.97	4.93	0.87	39.30
unlimited *S. podzolica*	0.87	57.04	77.77	4.65	0.87	40.07
Nitrogen limited *S. segobiensis*	1.00	56.21	87.05	4.58	0.87	40.29
Phosphate limited *S. segobiensis*	0.62	58.75	58.75	4.82	0.87	39.62
unlimited *S. segobiensis*	0.82	57.42	73.54	4.69	0.87	39.97
Nitrogen limited *A. porosum*	0.88	56.99	78.35	4.65	0.87	40.09
Phosphate limited *A. porosum*	0.98	56.31	85.96	4.58	0.87	40.27
unlimited *A. porosum*	0.83	57.32	74.66	4.68	0.87	40.00
Biodiesel*	-	52-70	<120	4.0-5.0	0.86-0.90	33-41
Petrol diesel*	-	40-50	<120	2.0-3.0	0.83-0.86	42.6

*Values from Qian et al. [170]

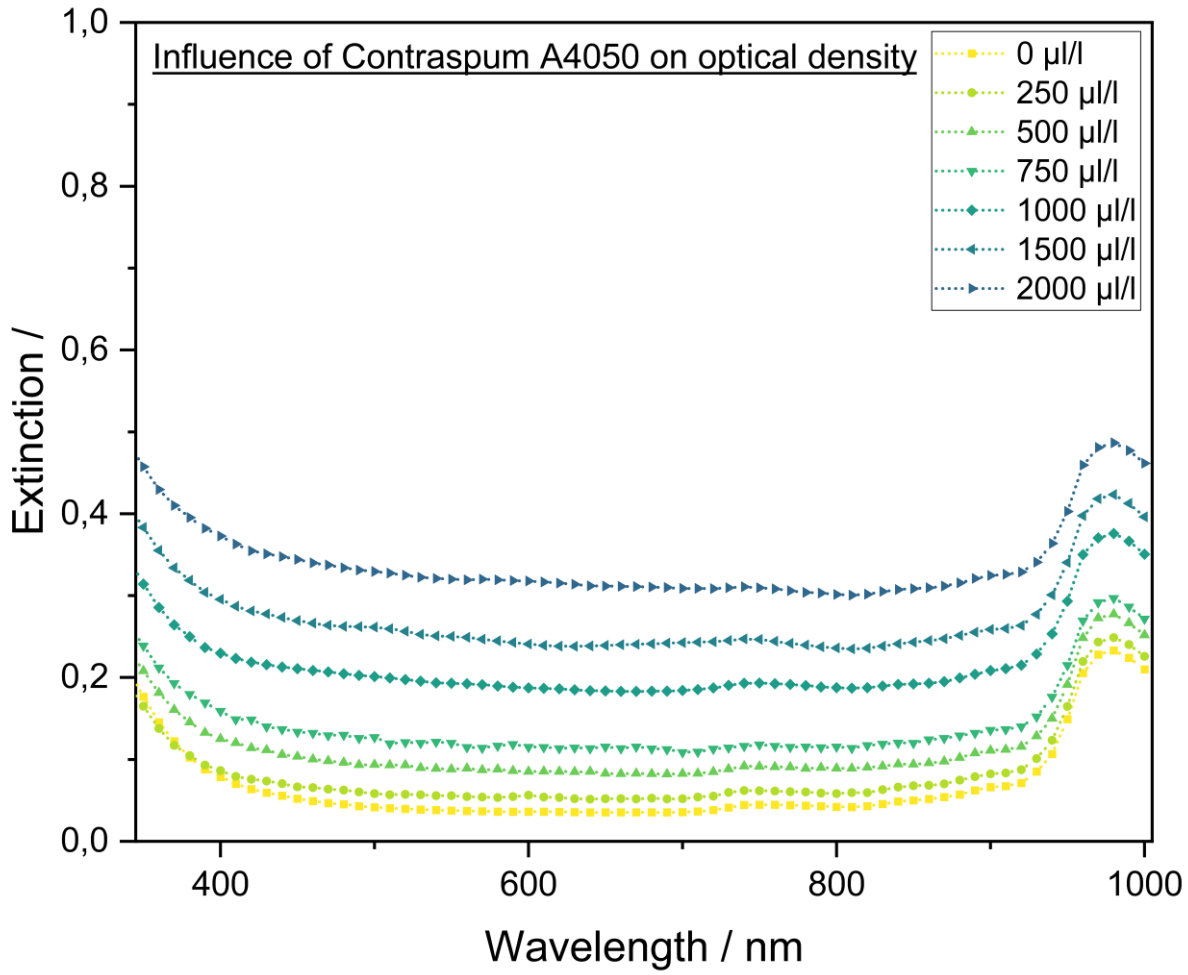

Figure S28: Effect of increasing Contraspum A 4050 concentrations on optical density measurements. Dotted lines indicate trends for visual guidance only.

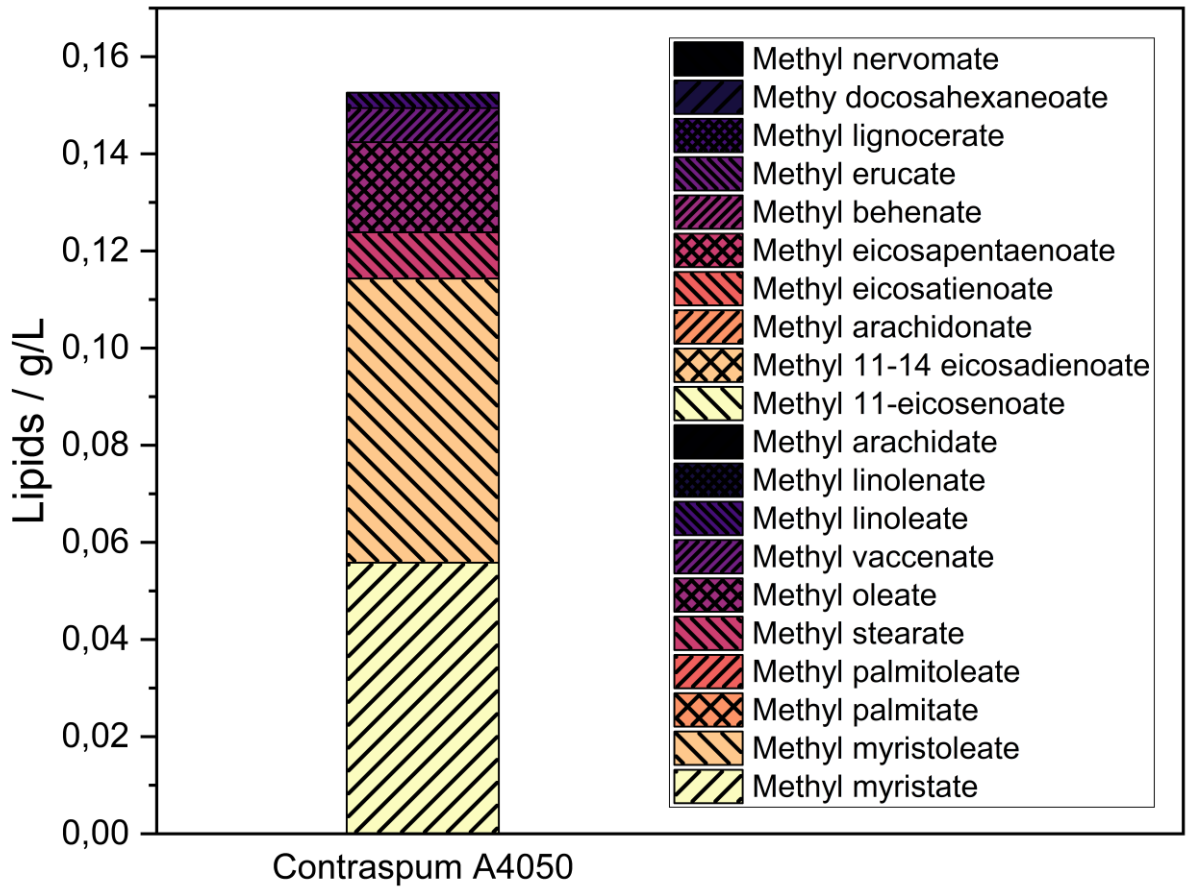

Figure S29: Fatty acid methyl ester signal obtained from pure Contraspum A 4050 subjected to the transesterification and gas chromatographic analysis protocol.

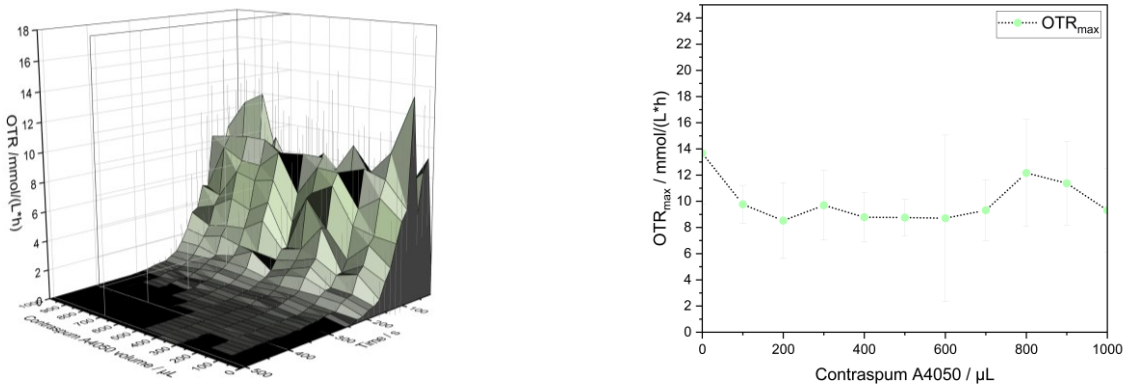

Figure S30: Effect of increasing Contraspum A 4050 concentrations on oxygen transfer rate measurements. Dotted lines indicate trends for visual guidance only.

10.5 Chapter 5: Adapted Feeding Strategies Enable Efficient Growth and Lipid Accumulation Using Untreated Crude Glycerol in Transition Scale with *Cutaneotrichosporon oleaginosum* ATCC 20509

Table S10: Composition of the lipid profiles of the stir tank fermentations.

Fatty acid methyl ester	Crude glycerol / %	Glycerol / %	Adapted feeding / %
Methyl myristate	0.75	0.44	0.36
Methyl myristoleate	0.00	0.00	0.00
Methyl palmitate	15.55	19.99	21.20
Methyl palmitoleate	0.00	0.69	0.81
Methyl stearate	15.89	9.63	10.59
Methyl oleate	36.66	54.58	53.29
Methyl vaccenate	0.00	0.00	0.00
Methyl linoleate	28.60	11.45	10.54
Methyl linolenate	2.56	1.41	1.45
Methyl arachidate	0.00	0.00	0.00
Methyl 11-eicosenoate	0.00	0.00	0.00
Methyl 11-14 eicosadienoate	0.00	0.00	0.00
Methyl arachidonate	0.00	0.00	0.00
Methyl eicosatienoate	0.00	0.00	0.00
Methyl eicosapentaenoate	0.00	0.00	0.00
Methyl behenate	0.00	0.00	0.00
Methyl erucate	0.00	0.00	0.00
Methy lignocerate	0.00	0.00	0.00
Methy docosahexaneoate	0.00	1.81	1.76
Methyl nervomate	0.00	0.00	0.00

Table S11: Composition of the lipid profiles of the pilot scale fermentations.

Fatty acid methyl ester	Main-Fermentation / %	Repeated batch 1 / %	Repeated batch 2 / %	Repeated batch 3 / %
Methyl myristate	0.53	0.46	0.38	0.35
Methyl myristoleate	0.00	0.00	0.00	0.00
Methyl palmitate	20.78	16.77	16.52	16.79
Methyl palmitoleate	0.42	0.34	0.33	0.29
Methyl stearate	14.61	14.18	13.54	15.26
Methyl oleate	52.88	51.14	51.98	50.91
Methyl vaccenate	0.00	0.00	0.00	0.00
Methyl linoleate	7.88	12.40	12.25	10.49
Methyl linolenate	0.80	1.47	1.35	0.96
Methyl arachidate	0.00	0.00	0.00	0.57
Methyl 11-eicosenoate	0.00	0.00	0.00	0.00
Methyl 11-14 eicosadienoate	0.00	0.00	0.00	0.00
Methyl arachidonate	0.00	0.00	0.00	0.00
Methyl eicosatienoate	0.00	0.00	0.00	0.00
Methyl eicosapentaenoate	0.00	0.00	0.00	0.00
Methyl behenate	0.00	0.00	0.00	0.54
Methyl erucate	0.00	0.00	0.00	0.00
Methy lignocerate	0.00	0.00	0.00	0.00
Methy docosahexaneoate	2.10	3.23	3.66	3.82
Methyl nervomate	0.00	0.00	0.00	0.00

10.6 Chapter 6: Microfluidic adaptive laboratory evolution of the oleaginous yeast *Cutaneotrichosporon oleaginosum*

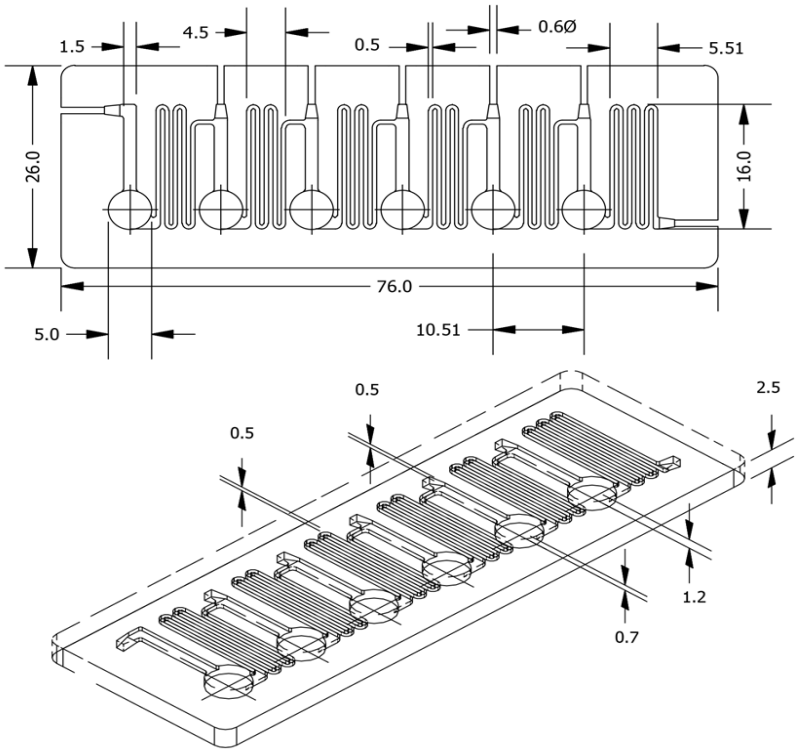

Figure S31: Technical schematic of the microfluidic evo.S chip. Top: plan view showing the overall chip layout and dimensions (26 × 76 × 2.5 mm; H × W × T). Bottom: three-dimensional representation illustrating the internal structure of the cultivation chambers and connecting channels.

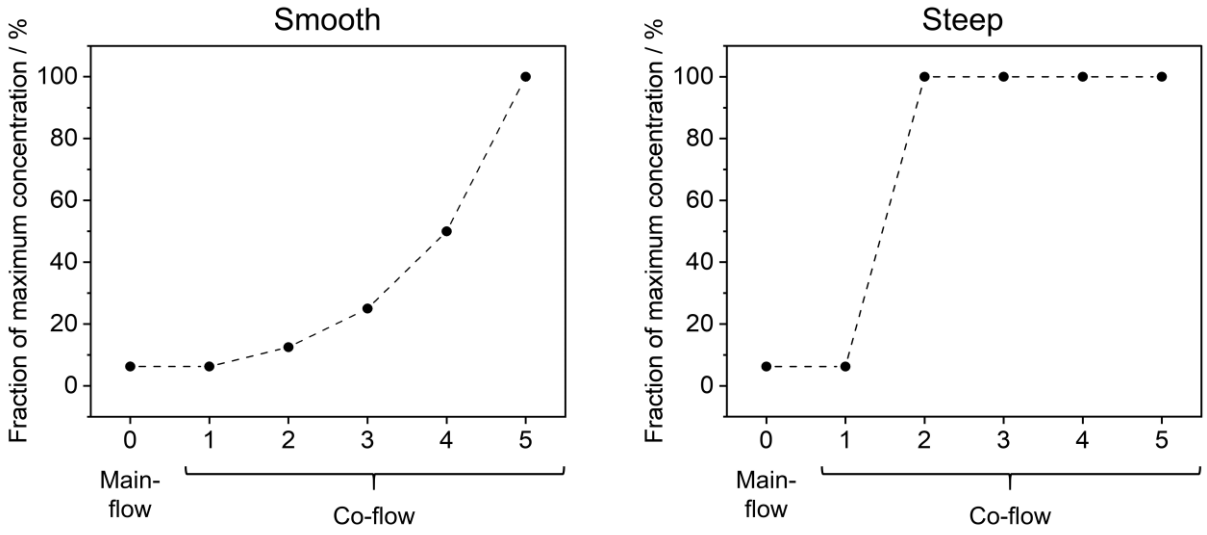

Figure S32: Relative increase of compound mixture concentrations across the microfluidic gradient setups. The fraction of the maximum concentration applied in the main-flow and co-flow channels is shown for the smooth (left) and steep (right) gradient configurations. Concentrations are expressed as a percentage of the maximum concentration used in the experiment. Dashed lines are included solely to guide the eye and do not represent fitted data.

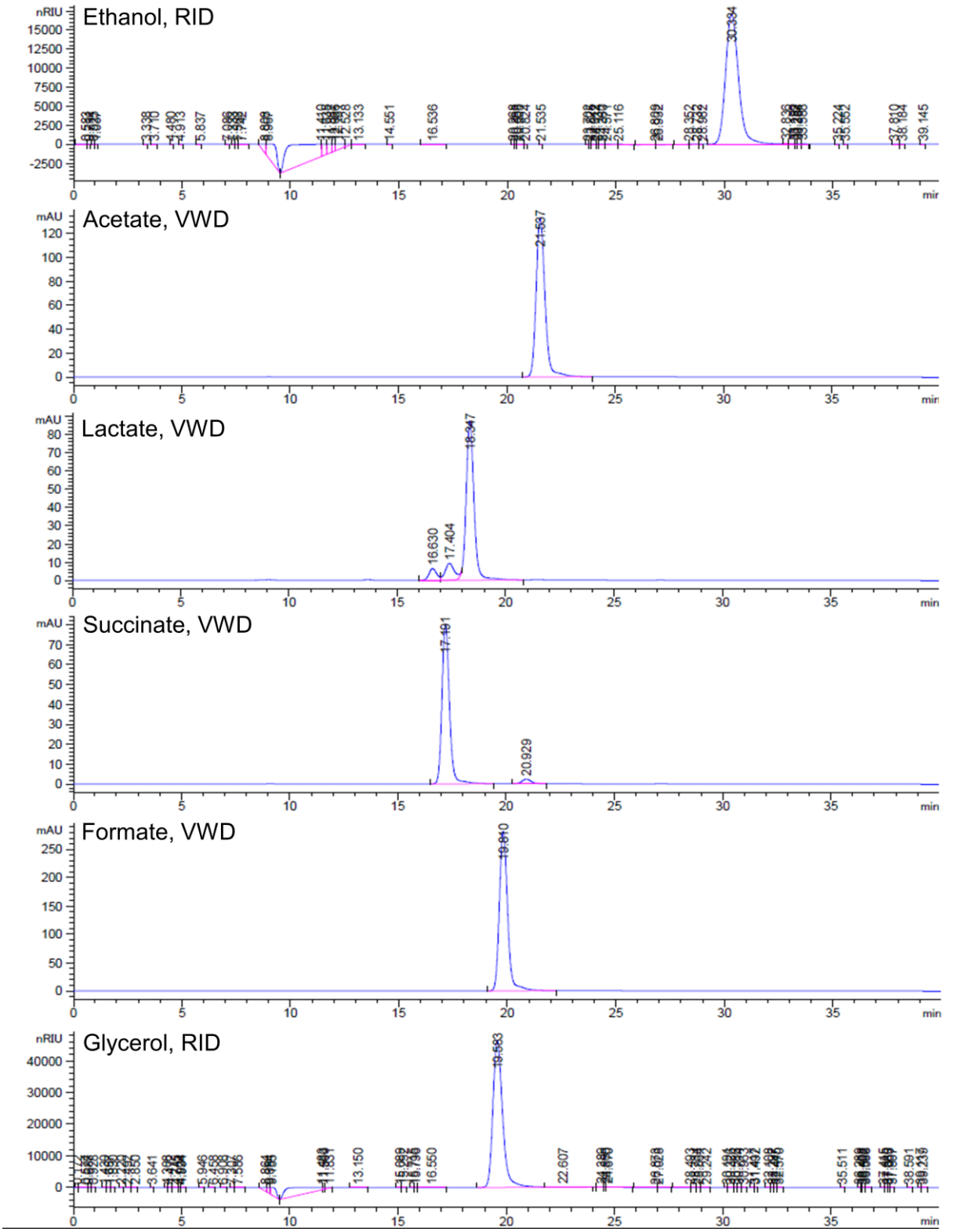

Figure S33: Representative chromatograms of the analyzed carbon sources. Characteristic chromatographic peaks of ethanol, acetate, lactate, succinate, formate, and glycerol are shown together with the respective detection methods. Ethanol and glycerol were detected using a refractive index detector (RID), while acetate, lactate, succinate, and formate were detected using a variable wavelength detector (VWD).

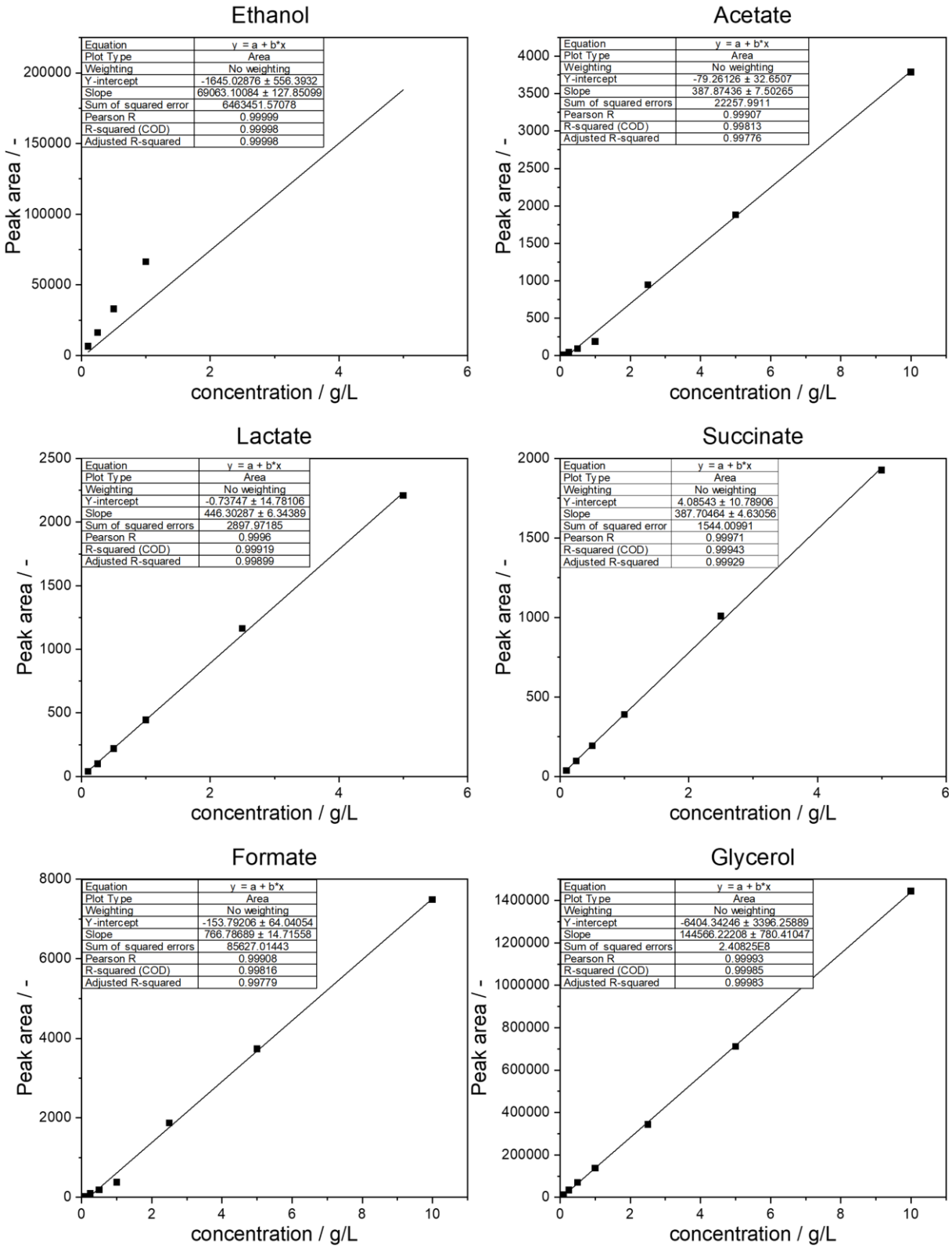

Figure S34: Calibration curves for quantification of the analyzed carbon sources. Calibration curves showing the relationship between peak area and concentration for ethanol, acetate, lactate, succinate, formate, and glycerol used for the determination of carbon concentrations in the samples.

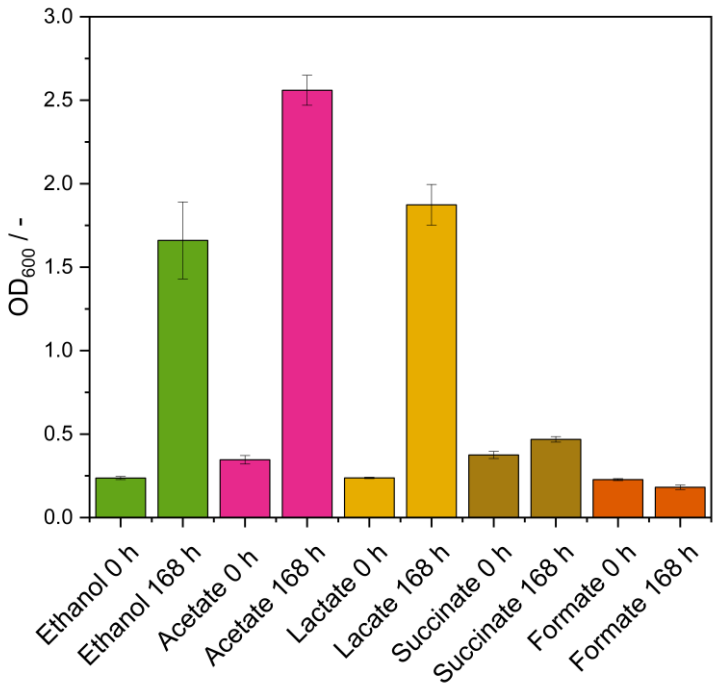

Figure S35: Growth of C. oleaginosum on individual soluble carbon sources. Optical density (OD_{600}) was measured at the start of cultivation (0 h) and after 168 h in Y medium supplemented with individual carbon sources: ethanol (10 mM), acetate (10 mM), lactate (10 mM), succinate (1.2 mM), and formate (10 mM). Cultivations were performed at 30 °C and 130 rpm. Bars represent mean OD_{600} values of biological triplicates (n = 3), and error bars indicate the standard deviation. Growth was observed with ethanol, acetate, lactate, and succinate, whereas no growth occurred in the presence of formate.

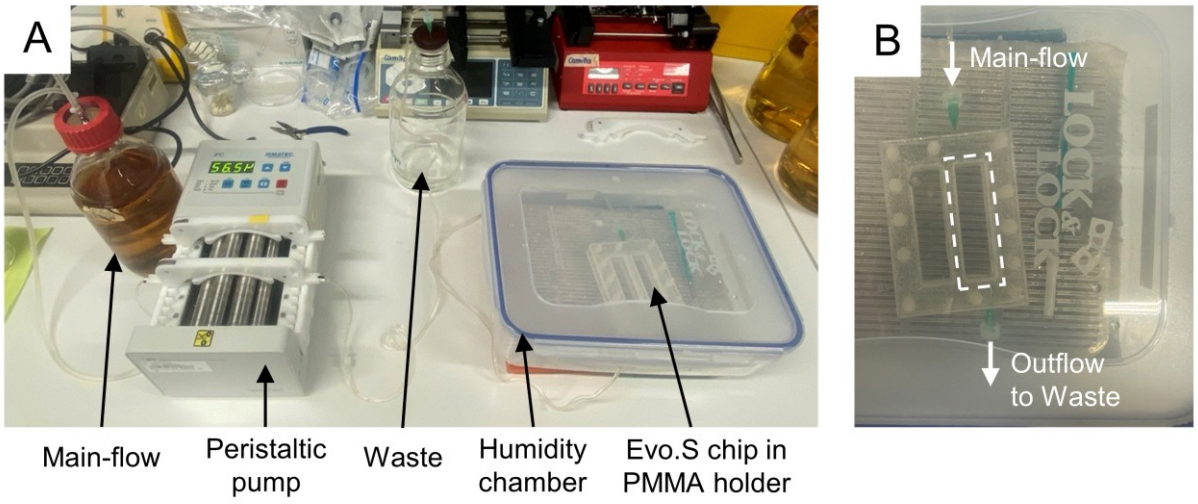

Figure S36: Experimental setup for microfluidic cultivation of C. oleaginosum in the evo.S chip. (A) Overview of the cultivation setup including the main-flow medium reservoir, peristaltic pump, waste container, and the humidity box containing the evo.S chip mounted in a PMMA holder. (B) Close-up of the evo.S chip placed inside the humidity box, showing the main-flow inlet and the outflow connection to waste. The dashed rectangle indicates the chip area used for cultivation.

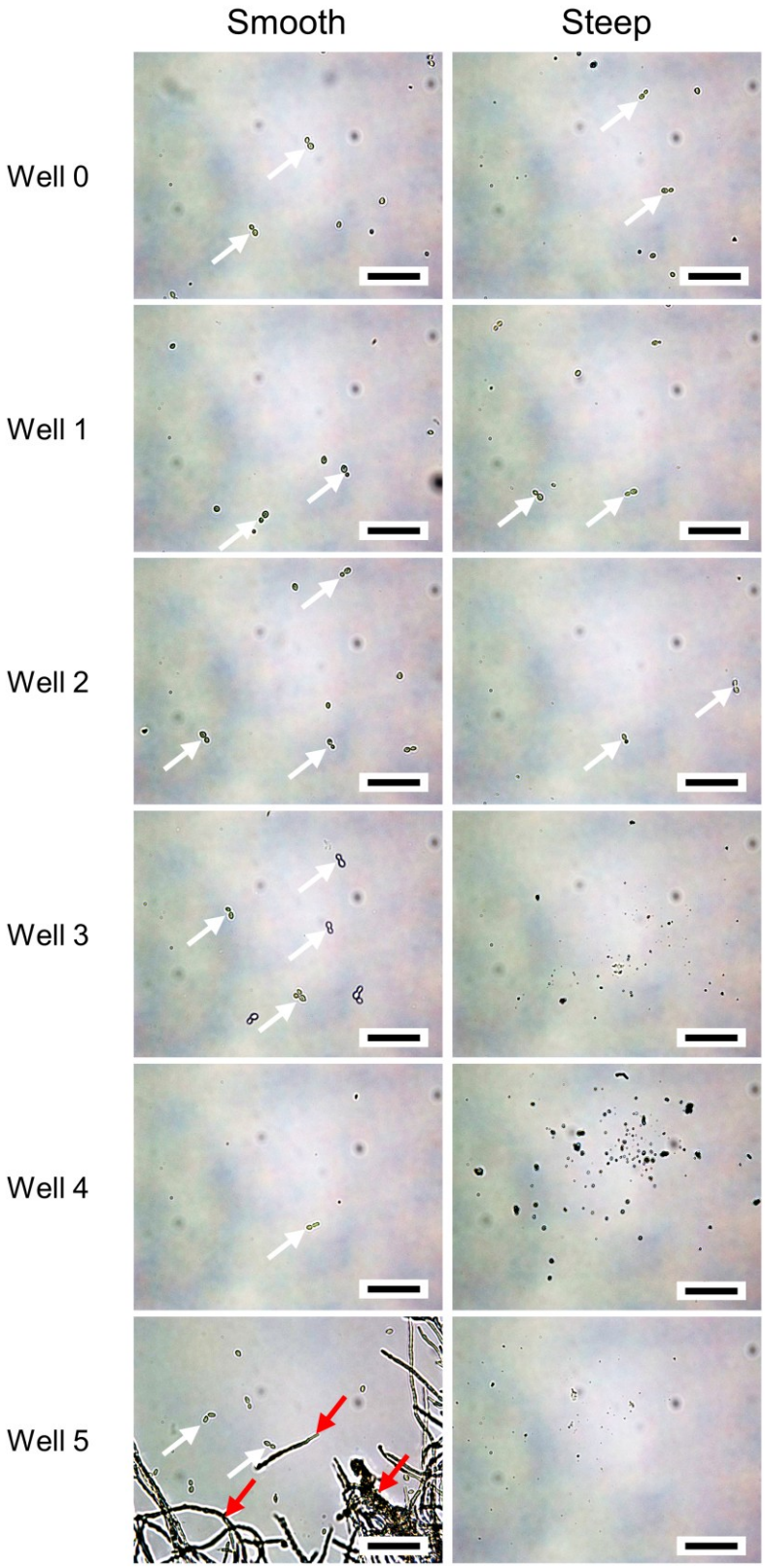

Figure S37: Microscopic observation of C. oleaginosum cells isolated from different wells of the microfluidic gradient chips. Representative micrographs of cultures obtained from wells 0–5 of the smooth (left) and steep (right) gradient configurations. White arrows indicate individual C. oleaginosum cells, while red arrows highlight filamentous fungal contamination observed in the culture from smooth well 5. Scale bars represent 50 µm (n = 1).

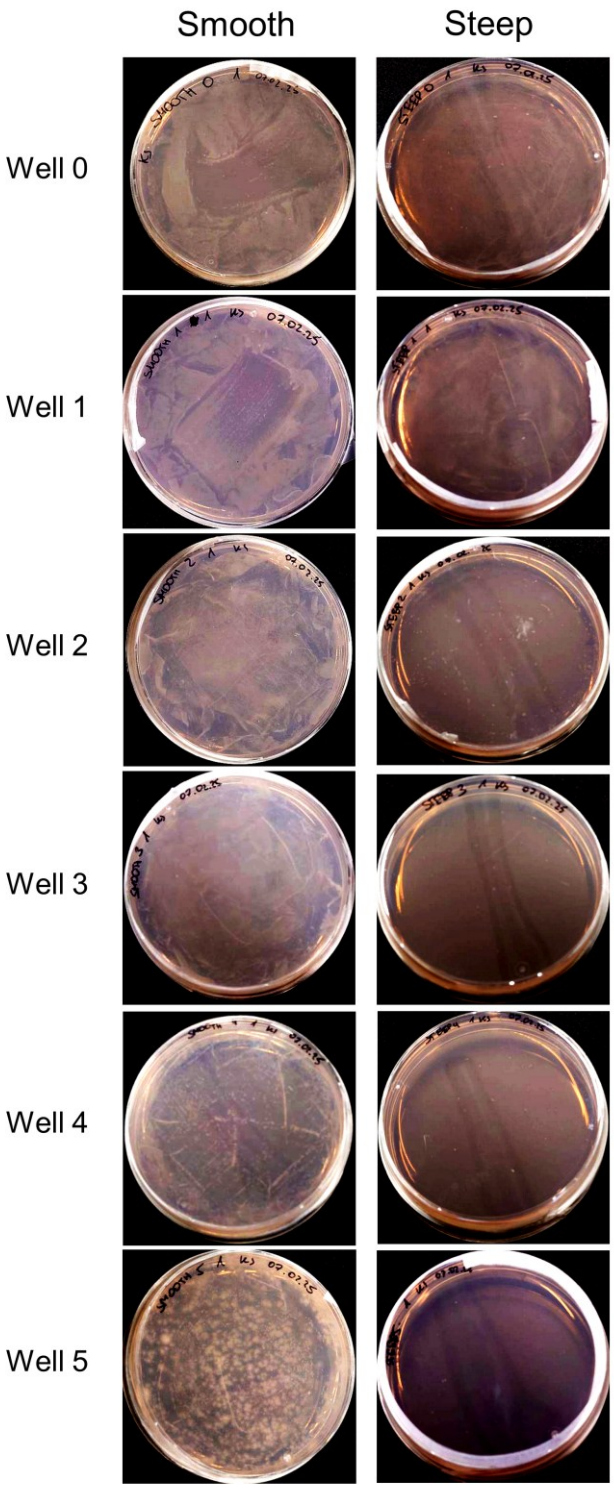

Figure S38: Colony formation of isolates obtained from the microfluidic gradient chips. Cultures recovered from wells 0–5 of the smooth (left) and steep (right) gradient chips were plated on agar plates and incubated for 4 days. Images show representative plates after incubation. Brightness and contrast were adjusted to improve colony visibility (n = 1).

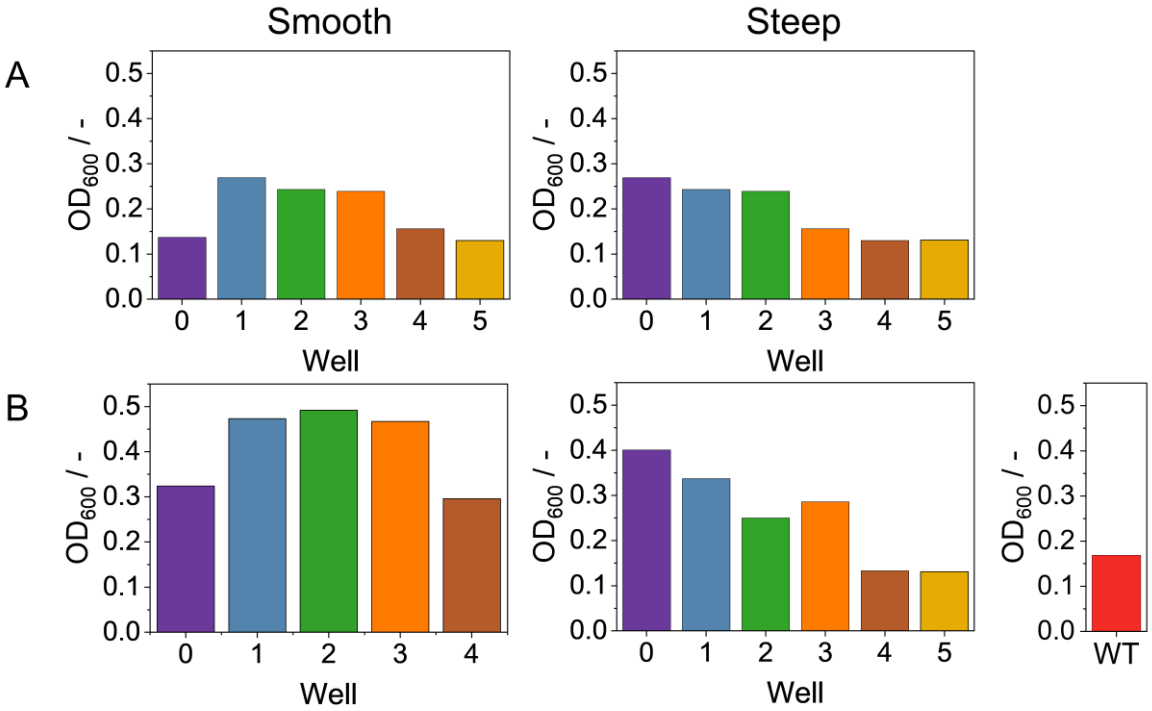

Figure S39: Optical density (OD600) of cultures in main-flow medium. (A) inoculated with cells from wells 0-5 of the smooth and steep gradient chip and incubated for two weeks. (B) inoculated with a single colony from agar plates of biomass from wells 0-5 of the smooth and steep gradient chip and incubated for one week (n = 1).

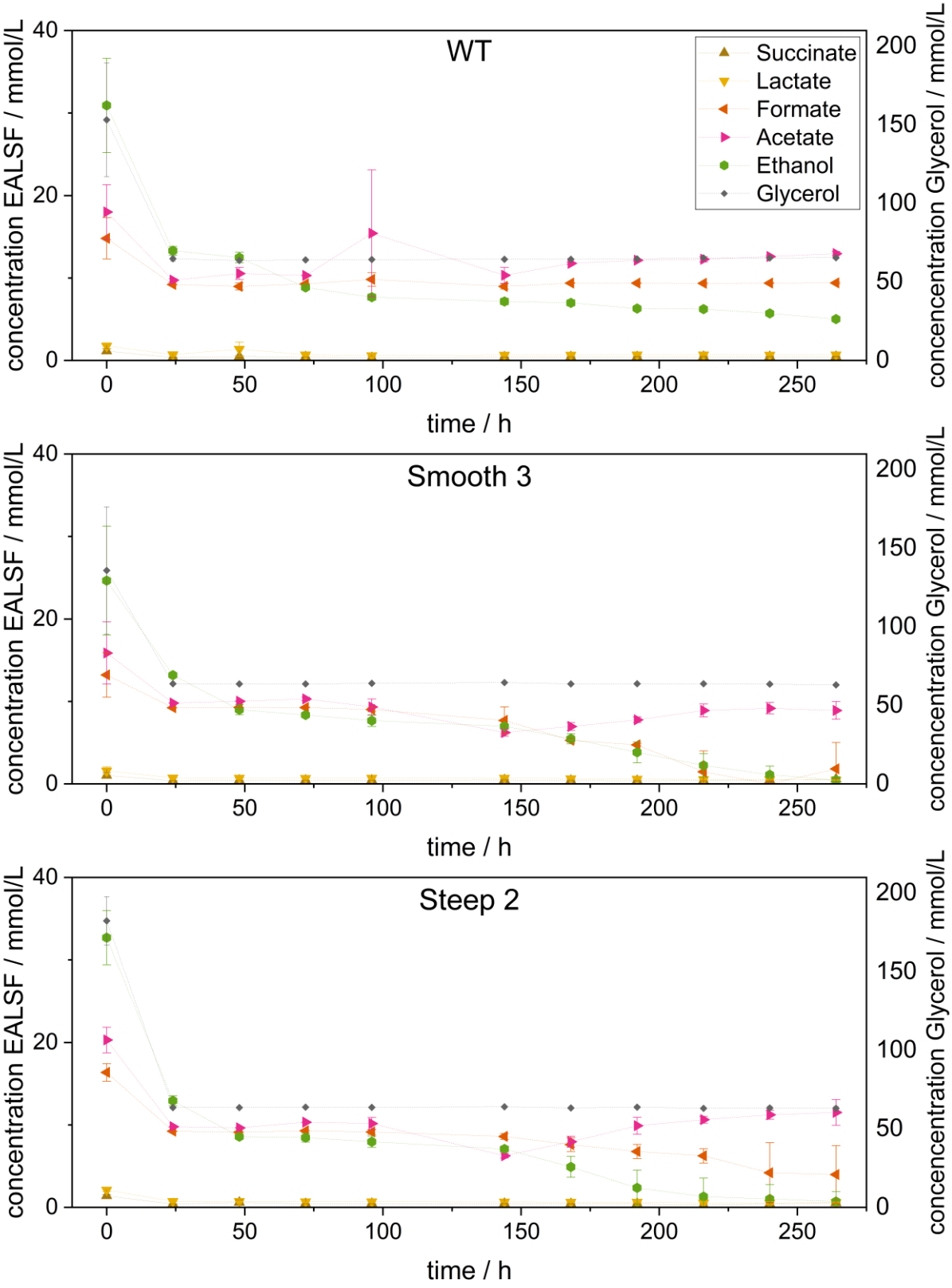

Figure S40: Temporal profiles of extracellular carbon source concentrations during cultivation. Concentrations of ethanol, acetate, lactate, succinate, formate, and glycerol were monitored over a cultivation period of 264 h for the wild type (WT), Smooth 3, and Steep 2. Data represent the mean of three replicates (n = 3), and error bars indicate the standard deviation.

Additional information for Figure S40: Across all three conditions, a pronounced decrease in the measured metabolite concentrations was observed within the first 24 h of cultivation. As this decline occurred before detectable biological activity and was consistently observed across independent experiments, it is unlikely to reflect microbial uptake. Instead, the phenomenon most likely results from physicochemical processes occurring during the initial equilibration phase of the cultivation medium. The medium contains several redox-active components, including cysteine and resazurin, while some metabolites like glycerol may act as a mild reducing agent. In the presence of dissolved oxygen and trace ions, complex chemical interactions may occur during the early incubation period. Under such conditions, partial chemical transformation of metabolites cannot be excluded. As a possible example intermediate could include glycerol-derived carbonyl compounds such as glyceraldehyde or dihydroxyacetone, as well as further oxidized derivatives such as glyceric acid. Such transformations may influence the apparent glycerol concentration determined by refractive index detection (RID). Compounds with altered polarity or refractive properties may generate weaker RID signals compared to glycerol, and certain oxidation products may elute outside the chromatographic window used for metabolite quantification. Consequently, part of the initially observed decrease likely reflects an analytical shift caused by chemical conversion rather than a true biological consumption of glycerol. After approximately 24 h, the system appears to reach a stable chemical equilibrium, as indicated by the nearly constant glycerol concentrations observed thereafter. This stabilization suggests that the initial change primarily reflects medium equilibration processes rather than biologically driven substrate consumption.

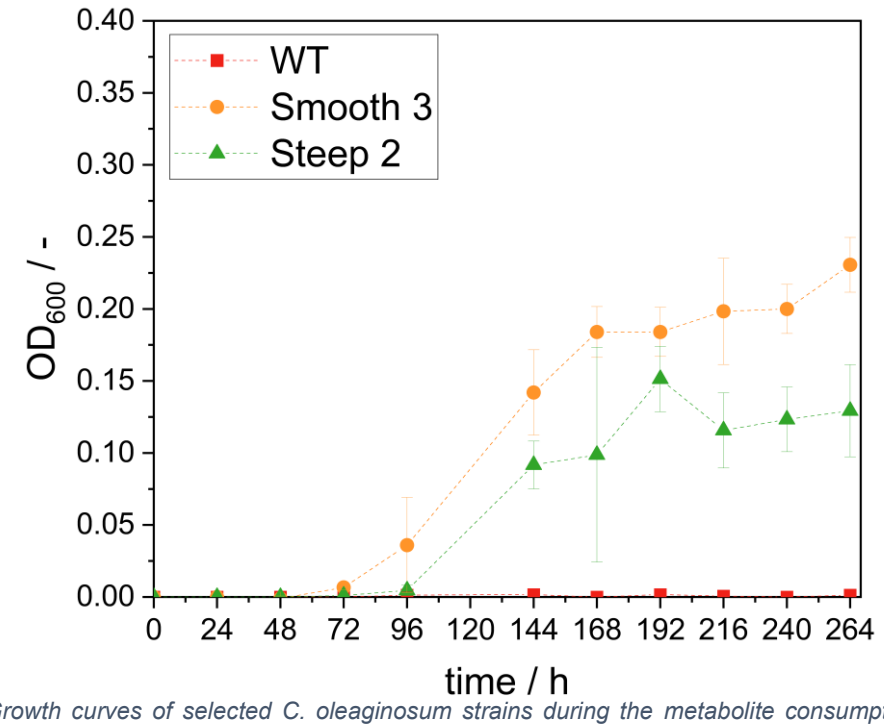

Figure S41: Growth curves of selected C. oleaginosum strains during the metabolite consumption experiment. Optical density (OD_{600}) of the wild type (WT) and the adapted strains Smooth 3 and Steep 2 cultivated under the conditions described in the main text. Data represent the mean of three biological replicates (n = 3), and error bars indicate the standard deviation.

Table S12: Mean values, standard deviation, standard error of the mean and 95 % confidence intervals from the conducted tukey test for end concentrations of the metabolic screening.

Substrate	Strain	Mean value	Standard deviation	*Standard Error of the Mean*	*95 % - Confidence Intervals Lower boundary*	*95 % - Confidence Intervals Upper boundary*
Glycerol	WT	65.4	0.8	0.5	64.5	66.4
	Smooth 3	63.1	0.9	0.5	62.1	64.0
	Steep 2	63.0	1.5	0.9	61.3	64.7
Acetate	WT	13.0	0.2	0.1	12.7	13.2
	Smooth 3	8.9	1.1	0.6	7.7	10.1
	Steep 2	11.5	1.6	0.9	9.7	13.3
Ethanol	WT	30.8	2.4	1.4	28.1	33.4
	Smooth 3	1.2	1.1	0.6	0.0	2.5
	Steep 2	3.7	6.4	3.7	-3.6	11.0
Succinate	WT	0.5	0.1	0.0	0.4	0.5
	Smooth 3	0.6	0.0	0.0	0.5	0.6
	Steep 2	0.5	0.1	0.0	0.4	0.6
Lactate	WT	0.7	0.0	0.0	0.7	0.7
	Smooth 3	0.5	0.0	0.0	0.4	0.5
	Steep 2	0.6	0.1	0.0	0.5	0.7
Formate	WT	9.4	0.1	0.1	9.3	9.5
	Smooth 3	1.8	3.2	1.8	-1.8	5.4
	Steep 2	4.0	3.5	2.0	0.0	7.9

11. Verification of the contribution from the co-authors

Title: Anaerobic gut fungi as biocatalysts: metabolic and physiological analysis of anaerobic gut fungi under diverse cultivation conditions
Journal: Frontiers in Microbiology
Authors: Kevin Edward Schulz, Dominik Scholz, Anto Rafael Sikirić, Daniela Rambow, Anke Neumann, Katrin Ochsenreither

Position in the dissertation:
The content of this publication has been included in Chapter 3.1.1

Contribution of Kevin Edward Schulz: Conceptualization, Formal analysis, Investigation, Methodology, Supervision, Validation, Visualization, Writing – original draft, Writing – review & editing
Contribution of Dominik Scholz: Investigation, Validation, Writing – review & editing,
Contribution of Anto Rafael Sikirić: Investigation, Validation, Writing – review & editing
Contribution of Daniela Rambow: Investigation, Writing – review & editing
Contribution of Anke Neumann: Writing – review & editing, Resources, Supervision
Contribution of Katrin Ochsenreither: Conceptualization, Supervision, Writing – review & editing

Title: Ferricyanide-dependent current production by *Neocallimastix cameroonii* G341 in a miniaturized anaerobic bioelectrochemical system
Journal: FEMS Microbiology Letters
Authors: Kevin Edward Schulz, Daniel Baron Diaz, Dirk Holtmann

Position in the dissertation:
The content of this publication has been included in Chapter 3.1.2

Contribution of Kevin Edward Schulz: Conceptualization, Investigation, Methodology, Validation, Visualization, Writing – original draft
Contribution of Daniel Baron Diaz: Conceptualization, Investigation, Methodology, Validation, Visualization, Writing – original draft
Contribution of Dirk Holtmann: Resources, Funding acquisition, Supervision, Project administration, Writing – review & editing

Title: Beyond Carbon Dioxide: Decoupling Headspace and Buffering Reveals a Bicarbonate Requirement for Anaerobic Gut Fungi Growth
Journal: Springer Nature - Fungal Biology and Biotechnology
Authors: Kevin Edward Schulz, Alisa Pfau, Tuba Tarhan, Charlotte van Almsick, Dominik Scholz, Anto Rafael Sikirić, Anke Neumann, Katrin Ochsenreither

Position in the dissertation:
The content of this publication has been included in Chapter 3.1.3

Contribution of Kevin Edward Schulz: Conceptualization, Formal analysis, Investigation, Methodology, Validation, Supervision, Visualization, Writing – original draft, Writing – review & editing
Contribution of Alisa Pfau: Investigation
Contribution of Tuba Tarhan: Investigation
Contribution of Charlotte van Almsick: Investigation
Contribution of Dominik Scholz: Investigation
Contribution of Anto Rafael Sikirić: Investigation
Contribution of Anke Neumann: Supervision, Writing – review & editing
Contribution of Katrin Ochsenreither: Supervision, Writing – review & editing

Title: Phosphate versus Nitrogen Limitation: A Reactor-Scale Process Comparison for Single-Cell Oil Production in Oleaginous Yeasts
Journal: MDPI Fermentation
Authors: Kevin Edward Schulz, Paula Hegmann, Bastian Dreher, Lena Regenauer, Carlota Delso Muniesa, Wolfgang Frey, Katrin Ochsenreither and Anke Neumann

Position in the dissertation:
The content of this publication has been included in Chapter 3.2.1

Contribution of Kevin Edward Schulz: Conceptualization, Methodology, Formal analysis, Investigation, Validation, Data curation, Visualization, Writing – original draft, Writing – review & editing, Supervision
Contribution of Paula Hegmann: Investigation, Validation
Contribution of Bastian Dreher: Investigation, Validation
Contribution of Lena Regenauer: Investigation, Validation
Contribution of Carlota Delso Muniesa: Writing – review & editing
Contribution of Wolfgang Frey: Writing – review & editing, Project administration, Funding acquisition
Contribution of Katrin Ochsenreither: Writing – review & editing, Supervision, Funding acquisition
Contribution of Anke Neumann: Resources, Writing – review & editing, Supervision, Project administration, Funding acquisition

Title: Adapted Feeding Strategies Enable Efficient Growth and Lipid Accumulation Using Untreated Crude Glycerol in Transition Scale with *Cutaneotrichosporon oleaginosum* ATCC 20509
Journal: MDPI Fermentation
Authors: Kevin Edward Schulz, Paula Hegmann, Bastian Dreher, Marina Schreidl, Katrin Ochsenreither, Anke Neumann

Position in the dissertation:
The content of this publication has been included in Chapter 3.2.2

Contribution of Kevin Edward Schulz: Conceptualization, Formal analysis, Investigation, Methodology, Supervision, Validation, Writing – original draft, Writing – review & editing
Contribution of Paula Hegmann: Investigation
Contribution of Bastian Dreher: Investigation
Contribution of Marina Schreidl: Investigation
Contribution of Katrin Ochsenreither: Conceptualization, Writing – review & editing
Contribution of Anke Neumann: Conceptualization, Supervision, Writing – review & editing

Title: Microfluidic adaptive laboratory evolution of the oleaginous yeast *Cutaneotrichosporon oleaginosum*
Journal: Applied Microbiology and Biotechnology
Authors: Kevin Edward Schulz, Camilla Stolle, Anne Rosa Maria Schwendemann, Dirk Holtmann, Kersten Stefan Rabe

Position in the dissertation:
The content of this publication has been included in Chapter 3.3.1

Contribution of Kevin Edward Schulz: Conceptualization, Investigation, Formal analysis, Visualization, Writing – original draft
Contribution of Camilla Stolle: Conceptualization, Investigation, Formal analysis, Visualization, Writing – original draft
Contribution of Anne Rosa Maria Schwendemann: Investigation, Validation
Contribution of Dirk Holtmann: Resources, Supervision, Writing – review & editing
Contribution of Kersten Stefan Rabe: Conceptualization, Resources, Supervision, Project administration, Writing – review & editing